CYCLIC VOLUMETRIC AND SHEAR STRAIN RESPONSES OF
FINE-GRAINED SOILS

A THESIS SUBMITTED TO
THE GRADUATE SCHOOL OF NATURAL AND APPLIED SCIENCES
OF
MIDDLE EAST TECHNICAL UNIVERSITY

BY

HABİB TOLGA BİLGE

IN PARTIAL FULFILLMENT OF THE REQUIREMENTS
FOR
THE DEGREE OF DOCTOR OF PHILOSOPHY
IN
CIVIL ENGINEERING

MAY 2010

Approval of the thesis:

CYCLIC VOLUMETRIC AND SHEAR STRAIN RESPONSES OF FINE-GRAINED SOILS

submitted by **HABİB TOLGA BİLGE** in partial fulfillment of the requirements for the degree of **Doctor of Philosophy in Civil Engineering Department, Middle East Technical University** by,

Prof. Dr. Canan ÖZGEN
Dean, Graduate School of **Natural and Applied Sciences** _____

Prof. Dr. Güney Özcebe
Head of Department, **Civil Engineering** _____

Prof. Dr. K. Önder Çetin
Supervisor, **Civil Engineering Dept., METU** _____

Examining Committee Members:

Prof. Dr. M. Yener ÖZKAN
Civil Engineering Dept., METU _____

Prof. Dr. K. Önder ÇETİN
Civil Engineering Dept., METU _____

Prof. Dr. A. Orhan EROL
Civil Engineering Dept., METU _____

Prof. Dr. Vedat DOYURAN
Geological Engineering Dept., METU _____

Prof. Dr. Reşat ULUSAY
Geological Engineering Dept., Hacettepe Univ. _____

Date: ___May 04, 2010___

I hereby declare that all information in this document has been obtained and presented in accordance with academic rules and ethical conduct. I also declare that, as required by these rules and conduct, I have fully cited and referenced all material and results that are not original to this work.

Name, Last name: Habib Tolga Bilge

Signature   :

ABSTRACT

CYCLIC VOLUMETRIC AND SHEAR STRAIN RESPONSES OF FINE-GRAINED SOILS

Bilge, Habib Tolga

Ph. D., Department of Civil Engineering

Supervisor: Prof. Dr. K. Önder Çetin

May 2010, 279 pages

Although silt and clay mixtures were mostly considered to be resistant to cyclic loading due to cohesional components of their shear strength, ground failure case histories compiled from fine grained soil profiles after recent earthquakes (e.g. 1994 Northridge, 1999 Adapazarı, 1999 Chi-Chi) revealed that the responses of low plasticity silt and clay mixtures are also critical under cyclic loading. Consequently, understanding the cyclic response of these soils has become a recent challenge in geotechnical earthquake engineering practice. While most of the current attention focuses on the assessment of liquefaction susceptibility of fine-grained soils, it is believed that cyclic strain and strength assessments of silt and clay mixtures need to be also studied as part of complementary critical research components. Inspired by these gaps, a comprehensive laboratory testing program was designed. As part of the

laboratory testing program 64 stress-controlled cyclic triaxial tests, 59 static strain-controlled consolidated undrained triaxial tests, 17 oedometer, 196 soil classification tests including sieve analyses, hydrometer, and consistency tests were performed. Additionally 116 cyclic triaxial test results were compiled from available literature. Based on this data probability-based semi-empirical models were developed to assess liquefaction susceptibility and cyclic-induced shear strength loss, cyclically-induced maximum shear, post-cyclic volumetric and residual shear strains of silt and clay mixtures. Performance comparisons of the proposed model alternatives were studied, and it is shown that the proposed models follow an unbiased trend and produce superior predictions of the observed laboratory test response. Superiority of the proposed alternative models was proven by relatively smaller model errors (residuals).

Keywords: Silt and clay mixtures, triaxial testing, cyclic-induced soil strains, liquefaction susceptibility, post-cyclic shear strength loss.

ÖZ

İNCE DANELİ ZEMİNLERİN TEKRARLI YÜKLER ALTINDAKİ HACİM VE MAKASLAMA BİRİM DEFORMASYON DAVRANIŞI

Bilge, Habib Tolga

Doktora, İnşaat Mühendisliği Bölümü

Tez Yöneticisi: Prof. Dr. K. Önder Çetin

Mayıs 2010, 279 sayfa

Silt ve kil karışımları makaslama dayanımlarına katkı yapan kohezyon bileşeninden ötürü, uzun zaman boyunca tekrarlı yüklere karşı dayanıklı olarak kabul edilmişlerse de, yakın zamanlı depremlerde (örneğin 1994 Northridge, 1999 Adapazarı, 1999 Chi-Chi gibi) ince daneli zemin profillerinden derlenen yenilme vaka örnekleri, düşük plastisiteli silt ve kil karışımlarının da tekrarlı yükler altında sıvılaşma yenilmesine maruz kaldıklarını göstermiştir. Bu sebeple, bu tip zeminlerin tekrarlı yükleme davranışı geoteknik (yer tekniği) deprem mühendisliğinin yakın zamandaki en ilgi çekici konularından biri olmuştur. İnce daneli zeminlerin sıvılaşabilirliği bu ilginin büyük bir kısmını üzerine çekerken, silt ve kil karışımlarının tekrarlı yükleme nedenli birim deformasyon ve dayanımlarının değerlendirilmesinin de çalışılması

gerekli ve tamamlayıcı kritik araştırma konuları olduğuna inanılmaktadır. Bu gereksinim dikkate alınarak ayrıntılı bir laboratuvar deney programı tasarlanmıştır. Bu programın bir bölümü olarak, 64 adet gerilme kontrollü-tekrarlı yüklemeli üç eksenli deney, 59 adet birim deformasyon kontrollü konsolidasyonlu-drenajsız statik üç eksenli deney, 17 odömetre ve elek analizi, hidrometre ve kıvam limitlerinin tayinini içeren 196 zemin sınıflandırma deneyi yapılmıştır. Ek olarak, literatürden 116 tekrarlı yükleme deneyi daha derlenmiştir. Silt ve kil karışımlarındaki sıvılaşabilirlik ve tekrarlı yükleme nedenli dayanım kaybının, en büyük makaslama birim deformasyonunun, tekrarlı yükleme sonrası hacim ve artık makaslama birim deformasyonlarının belirlenmesine yönelik olasılık tabanlı yarı ampirik (görgül) modeller geliştirilmiştir. Önerilen alternatif modellerin performansları karşılaştırmalı olarak çalışılmış ve önerilen modellerin deneylerde gözlenen zemin davranışını tarafsız eğilimlerle ve mevcut yöntemlere oranla daha üstün şekilde tahmin edebildiği gösterilmiştir. Önerilen alternatif modellerin başarısı küçük model hataları (kalıntılar) ile kanıtlanmıştır.

Anahtar Kelimeler: Silt ve kil karışımları, üç eksenli deney, tekrarlı yükleme nedenli zemin birim deformasyonları, sıvılaşma duyarlılığı, tekrarlı yükleme sonrası makaslama dayanımı kaybı.

To My Mother, for her unlimited and unconditional love...

ACKNOWLEDGMENTS

I want to gratefully thank to Dr. Kemal Önder Çetin, without whom I would not be able to complete this dissertation. I wish to express my appreciation for his continuous and unconditional guidance and support at each step of this study. His unlimited assistance, patience and tolerance made my research come into this stage and his continuous intellectual challenges throughout these years contributed to my academic, professional, and personal development, for which I am indebted and miss most of all. My appreciation is not only his being a mentor in academic and professional life, but also treating me as a friend or a brother in the last eight years.

Thanks are also due to the members of my dissertation committee: Dr. M. Yener Özkan and Dr. Vedat Doyuran, for their constructive suggestions and subjective comments throughout this research period.

I owe further thanks to Dr. Orhan Erol for his positive approach and considerable support during my graduate studies in Middle East Technical University.

Similarly, I want to thank Dr. Robb Moss for his considerable support and hospitality during my stay in California Polytechnic State University.

I want to thank my former officemate Dr. Berna Unutmaz for her support and friendship during these years. She was always kind and positive to me, and definitely deserves appreciation for all of her helps during different stages of this study.

I want express my deepest gratitude to my friends Başak Bayraktaroğlu, Doğan Kaygısız, Elif Alp Ulutaş, İbrahim Taşkın, Onur Çelik, Ekim Peker, Gökçe Arslan Kırkgöz, Salih Tileylioğlu, Michael Annuzzi, Sarp Kemaloğlu, Yıldıray Aydın, Baran Özbek, Onur Dulkadiroğlu, Ersan Yıldız, Murat Bozkurt, Can Alpdoğan and Mübin Aral for their continuous support, love, encouragement and help during hard

TABLE OF CONTENTS

LIST OF TABLES

LIST OF FIGURES

xvii

xviii

LIST OF ABBREVIATIONS

Acc : Overall accuracy

$A_{corrected}$: Area of specimen during shear

A_0^* : Area of specimen at the start of shear

B : Pore water pressure ratio coefficient

C_c : Compression index

C_{dyn} : Compression index induced by cyclic loading

CL : Clay of low plasticity

CPT : Cone Penetration Test

CRR : Cyclic resistance ratio

C_r : Recompression index

C_s : Swelling index

CSR : Cyclic stress ratio

d_0 : Initial diameter of specimen

e : Void ratio

e_0 : Initial void ratio

$E_{i,cy}$: Undrained secant moduli after cyclic loading

$E_{i,NC}$	: Undrained secant moduli before cyclic loading
FC	: Fines content in percentage
F_{cyc}	: Cyclic deviator stress
FL	: False liquefiable
FNL	: False non-liquefiable
$F_{st,0}$	: Axial deviatoric load applied in anisotropic consolidation stage
FS_{bc}	: Factory of safety for bearing capacity failure
F_{β}	: F-score
G_s	: Specific gravity
H	: Thickness of fine-grained soil layer
h_0	: Initial height of specimen
h_0^*	: Initial height of specimen at the start of shear
K_0	: Coefficient of earth pressure at rest
LI	: Liquidity index
LL	: Liquid limit
MH	: Silt of high plasticity
ML	: Silt of low plasticity
M_w	: Moment magnitude

$n\,,N$	: Number of loading cycles
N_{60}	: Procedure corrected SPT blow counts
N_{kt}	: Cone factor
$NVES$	: Normalized vertical effective stress
n_q	: Equivalent over consolidation ratio
OCR	: Over consolidation ratio
P	: Precision
p_c	: Mean consolidation stress
PI	: Plasticity index
p'_0	: Initial effective overburden stress
p'_c	: Pre-consolidation pressure
p_e'	: Mean effective stress after cyclic loading
p_i'	: Mean effective stress before cyclic loading
$r_{u,N}$	: Excess pore water pressure ratio at N^{th} loading cycle
q	: Half of deviatoric stress
q_s	: Initial deviatoric stress
q_t	: Cone tip resistance
q_u	: Unconfined compressive strength

R	: Recall
R_f	: Cyclic shear strength
R_k	: Ratio of $E_{i,NC}$ to $E_{i,cy}$
R_q	: Ratio of $s_{u,cy}$ to $s_{u,NC}$
r_u	: Excess pore water pressure ratio
R^2	: Pearson product moment correlation coefficient
S	: Sensitivity ratio
$S_{i,NC}$	: Immediate settlement due to structural loads under static loading conditions
SPT	: Standard Penetration Test
SR	: Stress ratio
SRR	: Stress reversal ratio
s_u	: Undrained shear strength
$s_{u,cy}$	: Post-cyclic residual shear strength
$s_{u,NC}$	: Undrained shear strength before earthquake
$s_{u_{cyc,min}}$	: Minimum cyclic shear strength during cyclic loading
t_{50}	: Time required to complete 50 % consolidation
TL	: True liquefiable

TNL	: True non-liquefiable
u_e	: Excess pore water pressure
u_p	: Excess pore water pressure at peak axial strain
V_0^*	: Volume specimen after consolidation
w_c	: Natural moisture content
β	: Importance of recall to precision
β	: Pore pressure decay constant
χ	: Critical state swelling coefficient
δh_{cons}	: Change in height
δh^*	: Change in height during test
Δs_{cy}	: Total earthquake induced settlement
$\Delta s_{i,cy}$	: Cyclic-induced immediate settlement
Δs_{vr}	: Cyclic-induced recompression settlement
$\Delta \sigma_3$	: Increase in cell pressure
$\Delta \sigma_{bldg}$	: Structure-induced stresses
$\Delta \sigma_{fpsd}$	: Filter paper side drain correction
$\Delta \sigma_{rm}$	: Rubber membrane correction

$\Delta\sigma_{v,cyc}$: Vertically acting stresses due to racking of structure

Δu : Increase in pore water pressure

ΔV_{cons} : Change in volume

ΔV_{pc} : Post-cyclic volume change

ε_a : Axial strain

$\varepsilon_{a,pc}$: Post-cyclic axial strain

ε_p : Cumulative plastic strain

ε_p : Peak axial strain

$\varepsilon_{v,pc}$: Post-cyclic volumetric strain

ϕ' : Peak effective angle of friction angle

γ : Cyclic shear strain

γ_c : Cyclic shear strain

γ_{cyc} : Cyclic shear strain

γ_{fs} : Strain required for monotonic failure

γ_{max} : Maximum double amplitude cyclic shear strain at 20th loading cycle

$\gamma_{max,20}$: Maximum double amplitude cyclic shear strain at 20th loading cycle

$\gamma_{\max,N}$: Maximum cyclic shear strain at N^{th} loading cycle

γ_{res} : Residual shear strain

λ : Critical state compressibility coefficient

η_p : Effective stress ratio at the peak cyclic stress

η_s : Effective stress ratio for initial consolidation condition

η_f : Effective stress for failure condition

$\mu_{residual}$: Mean of residuals

σ_d : Cyclic deviator stress

σ_s : Static shear strength

σ'_0 : Initial effective stress

σ'_1 : Major effective principal stress

σ'_3 : Minor effective principal stress

σ'_1/σ'_3 : Effective stress obliquity

σ_d : Deviatoric stress

σ'_h : Horizontal effective stress

$\sigma_{residual}$: Standard deviation of residuals

σ'_v : Vertical effective stress

σ'_{v0} : Initial effective vertical stress

$\sum lh$: Likelihood value

τ_{cyc} : Cyclic shear stress

τ_{st} : Static shear stress

CHAPTER 1

INTRODUCTION

1.1. RESEARCH STATEMENT

The aim of this research studies includes the development of frameworks for the evaluation of liquefaction susceptibility of fine-grained soils, assessment of cyclic-induced straining problem and post-cyclic shear strength of silt and clay mixtures. Similarly, it is intended to resolve cyclic pore water pressure generation problem which is observed to be a difficult issue. Within this scope, a comprehensive laboratory testing program was designed. As part of the laboratory testing program 64 stress-controlled cyclic triaxial tests, 59 static strain-controlled consolidated undrained triaxial tests, 17 oedometer, 196 soil classification tests including sieve analyses, hydrometer, and consistency tests were performed. Additionally 116 cyclic triaxial test results were compiled from available literature. Based on this data, robust and defensible probabilistically-based semi-empirical models were developed for the assessment of cyclic maximum shear, post-cyclic volumetric and residual shear strain potentials, as well as minimum cyclic shear strength and excess pore water pressure generation response of silt and clay mixtures. Moreover, new criteria were proposed for the purpose of screening out potentially liquefiable fine-grained soils.

1.2. PROBLEM SIGNIFICANCE AND LIMITATIONS OF PREVIOUS STUDIES

Assessment of cyclic response of fine-grained soils is considered to be one of the most challenging topics of geotechnical earthquake engineering profession. Although it is a concept covering a very broad range of problems, this thesis will focus on mostly two major issues: a) evaluation of seismic liquefaction triggering susceptibility and b) assessment of both cyclic strength and straining responses of silt and clay mixtures.

In the early days of the profession, plastic silt and clay mixtures were considered to be resistant to cyclic loading, and most of the research interests focused on understanding liquefaction response of saturated sandy soils after liquefaction-induced ground failure case histories from of 1964 Alaska and Niigata earthquakes. However, after fine-grained soil failure case histories of 1975 Haicheng and 1979 Tangshan earthquakes in China (Wang, 1979), increasing research interest was shown in understanding fine-grained soils' cyclic response. Based upon recommendations of Wang (1979), Chinese Criteria were proposed by Seed and Idriss (1982) to assess liquefaction susceptibility of fine-grained soils. These criteria were continued to be widely used until recently with slight modifications (Finn et al., 1994; Perlea et al., 1999; Andrews and Martin, 2000). Ground failure case histories after 1989 Loma Prieta, 1994 Northridge, 1999 Adapazari and Chi-Chi earthquakes have accelerated research studies on assessing cyclic mobility response of clayey soils, as case histories from these earthquakes highlighted that low plasticity silt and clay mixtures might significantly strain soften, which may in turn cause significant damage to overlying structural systems. Alternative to Chinese Criteria, Seed et al. (2003), Bray and Sancio (2006) and Boulanger and Idriss (2006) proposed new susceptibility criteria based on field observations and laboratory test results. As will be discussed thoroughly in the following chapters, none of these existing criteria can consistently and reliably identify fine-grained soils susceptible to liquefaction.

On a similar path, assessment of cyclic-induced soil straining continued to be another critical aspect of the problem, especially from performance point of view. While there exist semi-empirical procedures (e.g. Tokimatsu and Seed, 1984; Ishihara and Yoshimine, 1992; Cetin et al. 2009, etc.) for the assessment of cyclic straining response of saturated sandy soils, only a limited number of studies is available for silt and clay mixtures. Ohara and Matsuda (1988), Yasuhara et al. (1992 and 2001) and Hyodo et al. (1994) developed constitutive models, on the basis of well known one-dimensional consolidation theory, used for the assessment of cyclically-induced ground settlements in normally- and over-consolidated clayey soils. However, these models require the determination of input parameters through laboratory testing (oedometer and strain-controlled cyclic tests), which will then be used in either 2- or 3-D dynamic numerical analyses. These requirements limit practical use of these constitutive model based assessments. Moreover, other than the work of Hyodo et al. (1994), which attempts to determine residual axial strains, none of these efforts resolve cyclic shear (deviatoric) straining problem.

Estimation of post-cyclic shear strength is a complementary step in performance assessment of fine grained soils subjected to cyclic loading. This topic has drawn relatively more attention, and various studies have been performed since late-60's (e.g., Thiers and Seed, 1968 and 1969; Castro and Christian, 1976; Ansal and Erken, 1989; Yasuhara, 1994, etc.). Based on these early efforts, it was concluded that post-cyclic strength loss may vary in the range of 20 to 80 %. Although these early efforts identified the factors affecting cyclically-induced strength loss, quantification of post-cyclic strength has still remained as a complex task, which needs to be further tackled.

Inspired by these gaps, it is intended to assess cyclic response of fine grained soils on the basis of robust and defensible frameworks composed of the following components: i) evaluation of seismic soil liquefaction triggering susceptibility, ii) assessment of maximum cyclic shear, post-cyclic volumetric and residual shear straining potentials, and iii) prediction of minimum cyclic shear strength.

1.3. SCOPE OF THE STUDY

Following this introduction, an overview available literature focusing on seismic liquefaction triggering susceptibility, prediction of cyclically-induced straining potential, and post-cyclic shear strength of silt and clay mixtures is presented in Chapter 2.

In Chapter 3, details of laboratory testing program, description of the test equipment and testing procedures along with data processing efforts are presented. Database compilation efforts are also discussed within the confines of this chapter.

Chapter 4 is devoted to the discussion of seismic liquefaction triggering susceptibility of fine-grained soils. Based on experimental observations, probabilistically-based models are developed for identifying fine-grained soils prone to cyclic liquefaction and mobility type responses. This chapter is concluded with the performance evaluation of proposed and existing methodologies by introducing comparative statistical metrics.

Chapter 5 begins with the discussion of test results-based behavioral trends and proceeds with detailed presentation of the proposed probabilistically-based semi-empirical models for the assessment of cyclic maximum shear, post-cyclic volumetric and residual shear strain potentials of silt and clay mixtures. As a part of the proposed post-cyclic volumetric straining model, a new cyclic pore water pressure generation model is also introduced.

Chapter 6 deals with the assessment of cyclic shear strength performance of silt and clay mixtures. A simplified procedure is proposed for the prediction of minimum cyclic shear strength. This chapter is concluded by a discussion on potential applications of the proposed procedures.

Finally, a summary of the research, major conclusions, and recommendations for future area of study are presented in Chapter 7.

CHAPTER 2

AN OVERVIEW ON CYCLIC RESPONSE OF SATURATED FINE-GRAINED SOILS

2.1 INTRODUCTION

During earthquakes, shear stresses due to stress wave propagation induce cyclic shear strains leading to rearrangement of soil particles / minerals and generation of excess pore water pressure. This particle rearrangement and elevated pore water pressure reduce the soil stiffness which in turn triggers the vicious cycle of further strain and excess pore water pressure accumulation. Although this mechanism is valid for both saturated cohesionless and cohesive soils, for decades research interest has been mostly focused on the cyclic response of saturated sandy soils; whereas saturated fine-grained soils, i.e. silt and clay mixtures, have been considered to be resistant to cyclic loading. However, ground failure case histories observed at fine-grained soil sites after 1964 Alaska (Idriss, 1985; Boulanger and Idriss, 2004), 1975 Haicheng and 1976 Tangshan (Wang, 1979), 1978 Miyagiken-Oki (Sasaki et al. 1980; Suzuki, 1984), 1985 Mexico City (Seed et al., 1987; Mendoza and Auvinet, 1988), 1989 Loma Prieta (Boulanger et al., 1998), 1994 Northridge (Holzer et al., 1999), 1999 Adapazari (Bray et al., 2001) and 1999 Chi-Chi (Chu et al. 2004)

earthquakes clearly revealed that fine-grained soils are also vulnerable to significant strength loss under cyclic loading. These observations have accelerated research studies in this field. Different aspects of the problem, such as dynamic stiffness reduction, cyclic and post-cyclic strengths, effective stress response, liquefaction susceptibility, straining potential, have continued to be studied by various researchers.

Due to very broad and complex nature of the problem, within the confines of this chapter, it is intended to focus and review available literature on following issues: i) liquefaction susceptibility, ii) cyclically-induced straining potential, and iii) cyclic shear strength. The former issue is arguably one of the most controversial issues in geotechnical earthquake engineering; whereas, the latter two have vital significance from performance-based engineering point of view. In the following chapters, alternative assessment methodologies will also be introduced to resolve these critical problems.

2.2 LIQUEFACTION SUSCEPTIBILITY OF FINE-GRAINED SOILS

Terzaghi and Peck (1948) first used the term "liquefaction" to describe the significant loss of strength of very loose sands resulting in flow failures due to slight disturbance. Later, Mogami and Kubo (1953) referred to this term to define loss in shear strength due to seismically-induced cyclic loading. However, according to Seed (1976), the vital importance of this problem was not been fully understood until the 1964 Great Alaska and Niigata earthquakes. Since these earthquakes, numerous research studies have been performed to better understand the mechanisms behind this phenomenon. Current state-of-the-practice is mainly constituted by the recent works of 1997 NCEER Workshop Proceedings (later summarized by Youd et al. (2001) as a separate paper) and Seed et al. (2003).

As part of the 1997 NCEER Workshop, Robertson and Wride reported that the engineering term of "liquefaction" has been used to define two related, yet different

soil responses during earthquakes: flow liquefaction and cyclic softening. Although these mechanisms are quite different, it is difficult to distinguish them since they can lead to similar consequences.

Robertson and Wride (1997) defined "flow liquefaction" as a phenomenon in which the equilibrium is jeopardized by static or dynamic loading applied to soil deposits with relatively lower residual strength (i.e., shear strength under large strain levels). This mechanism applies to strain softening soils under undrained loading conditions, and it requires in-situ shear stresses to be greater than the ultimate or minimum undrained shear strength of soil. Failures caused by flow liquefaction are often characterized by large and rapid soil displacements which can lead to disastrous consequences.

The other response associated with liquefaction is cyclic softening, which is triggered by cyclic loading. It occurs in soil deposits where static shear stresses are lower than the soil strength. Robertson and Wride (1997) stated that deformations due to cyclic softening develop incrementally. Two engineering terms are used to define the cyclic softening phenomenon, namely cyclic mobility and cyclic liquefaction.

Cyclic mobility is the type of response, during which shear stress reversals do not occur, and zero effective stress state does not develop. Deformations during cyclic loading stabilize, unless the soil is very loose and flow liquefaction is triggered. Both sandy and clayey soils can experience cyclic mobility. On the other hand, cyclic liquefaction involves the occurrence of shear stress reversals and the development of zero shear stress state. Significant soil strains can accumulate during cyclic loading, but they are stabilized when cyclic loading stops. Both sandy and clayey soils can experience cyclic liquefaction; however, due to cohesive strength component of clayey soils at zero effective stress, cyclically-induced strains are generally smaller in amplitude.

7

In their state-of-the-art paper, Seed et al. (2003) summarized major components of seismic soil liquefaction engineering as presented in Table 2.2-1. The primary step of liquefaction engineering involves the determination of soil's potential to liquefaction triggering. Until 1975 Haicheng and 1976 Tangshan earthquakes, only saturated "clean sandy soils" with few percent of fines were considered to be vulnerable to seismic soil liquefaction. However, ground failure case histories after these earthquakes (Wang, 1979) revealed that cohesive fine-grained soils could also liquefy. Case histories from recent earthquakes of 1989 Loma Prieta (Boulanger et al., 1998), 1994 Northridge (Holzer et al., 1999), 1999 Adapazari (Bray et al., 2001, 2004) and 1999 Chi-Chi (Chu et al., 2003, 2008) once again proved that silty and clayey soil layers can exhibit both cyclic mobility and cyclic liquefaction type soil responses. Wang (1979) proposed a methodology to screen potentially liquefiable soils based on observations from 1975 Haicheng and 1976 Tangshan earthquakes. Consistent with the advances in seismic soil liquefaction engineering, susceptibility assessment of fine-grained soils evolved from Chinese Criteria to the methodologies of Seed and Idriss (1982), Andrews and Martin (2000), Bray and Sancio (2006), Boulanger and Idriss (2006). Some widely used criteria will be reviewed in following sections.

Table 2.2-1. Steps of liquefaction engineering

1	Assessment of the likelihood of "triggering" or initiation of soil liquefaction.
2	Assessment of post-liquefaction strength and overall post-liquefaction stability.
3	Assessment of expected liquefaction-induced deformations and displacements.
4	Assessment of the consequences of these deformations and displacements.
5	Implementation (and evaluation) of engineered mitigation, if necessary.

2.2.1 Chinese Criteria

As referred to earlier, Wang (1979) founded his pioneering study on field observations after 1975 Haicheng and 1976 Tangshan earthquakes in China. A database was compiled from sites, where liquefaction was and was not observed. Wang established that any clayey soil mixture containing less than 15-20% particles by weight smaller than 0.005 mm with a w_c / LL ratio greater than 0.9 is susceptible to liquefaction.

Assessing the same database, Seed and Idriss (1982) stated that clayey soils were susceptible to liquefaction only if all of the following conditions are satisfied: i) percent of particles smaller than 0.005 mm is less than 15 %, ii) $LL < 35$, and iii) $w_c / LL > 0.90$. Owing to its origins, these criteria were named as "Chinese Criteria". Later, Koester (1992) noted that the determination of LL by means of fall cone apparatus, widely used in Chinese practice, produced LL values about 4 % higher than values obtained by means of the Casagrande percussion device. A slight reduction in LL is recommended when Chinese Criteria is used as a screening tool. Later, Finn et al. (1994) and Perlea et al. (1999) also proposed slightly modified versions of Chinese Criteria.

Using almost the same database, Andrews and Martin (2000) proposed improved criteria for the identification of soils susceptible to liquefaction. These criteria, as presented in Table 2.2-2, utilized clay content and LL parameters as screening tools. However, size of clay particles was defined as 0.002 mm rather than 0.005 mm, consistent with USCS-based silt and clay definitions. Also critical LL value was reduced to 32, benefiting from the recommendations of Koester (1992).

Table 2.2-2. Liquefaction susceptibility criteria by Andrews and Martin (2000)

	Liquid Limit < 32%	Liquid Limit ≥ 32%
Clay Content (< 0.002 mm) < 10%	Potentially Liquefiable	Further studies required considering plastic non-clay sized grains
Clay Content (< 0.002 mm) ≥ 10%	Further studies required considering non-plastic clay sized grains	Non-Liquefiable

Being a pioneer effort, Chinese Criteria and later its modified versions have been used in practice for over 2 decades. However, these criteria have been subjected to increasing criticisms since mid-90s, as number of case histories and high quality test data increases. Boulanger et al. (1998), Holzer et al. (1999), Chu et al. (2003), Bray et al. (2004) reported liquefaction case histories at fine-grained soil sites, which could not be correctly identified by using any versions of Chinese Criteria. The major limitation of these criteria is related to using percent particle size (0.002 or 0.005 μm) as a screening tool. Recent studies of Seed et al. (2003) and Bray and Sancio (2006) stated that rather than just the amount of "clay-size" minerals, both type and amount of clay minerals are important for cyclic response. Similarly, Boulanger and Idriss (2006) also indicated the importance of mineralogy for distinguishing soil behavior. Besides, it is important to notice that Chinese Criteria were developed based on solely case history data compiled from only two earthquakes (1975 Haicheng and 1976 Tangshan), which produced only a narrow range of peak ground accelerations, and consequently a narrow range of corollary cyclic stress ratios. In simpler terms, this meant that performance of silt and clay mixtures was studied only for certain earthquake loading conditions, which may not be valid for other earthquakes which produce significantly different levels or durations of shaking.

2.2.2 Seed et al. (2003)

Inconsistent with Chinese Criteria, which was developed based on the amount of "clay-size" particles in the soil, recent advances revealed that i) non-plastic fine grained soils can also liquefy, and ii) PI is a major controlling factor in the cyclic response of fine grained soils. Bray et al. (2001) suggested that the use of Chinese Criteria percent "clay-size" definition might be misleading, and rather than percent of clay size material, their activities should be more important. Seed et al. (2003) recommended a set of new criteria inspired from case histories, and results of cyclic tests performed on "undisturbed" fine-grained soils compiled after 1999 Adapazarı and Chi-Chi earthquakes. These criteria classify saturated soils with $PI < 12$ and $LL < 37$ as potentially liquefiable, provided that w_c / LL is greater than 0.8. Similarly, authors also indicated that soils satisfying following conditions of i) $12 < PI < 20$, ii) $37 < LL < 47$ and iii) $w_c / LL > 0.85$, require further testing before giving final decision; whereas soils with $PI > 20$ and $LL > 47$ are considered as not susceptible to soil liquefaction; although it is also recommended to be cautious of sensitivity-induced problems. Figure 2.2-1 schematically presents these criteria and demonstrates these zones.

Although this study is judged to be a major improvement over previous efforts, the basis of these recommendations is still unclear and as presented elsewhere (Pehlivan, 2009), it did not produce favorably unbiased predictions for the database it was claimed to be based on. The proposed criteria seem to be a subjective summary of authors' expert opinion.
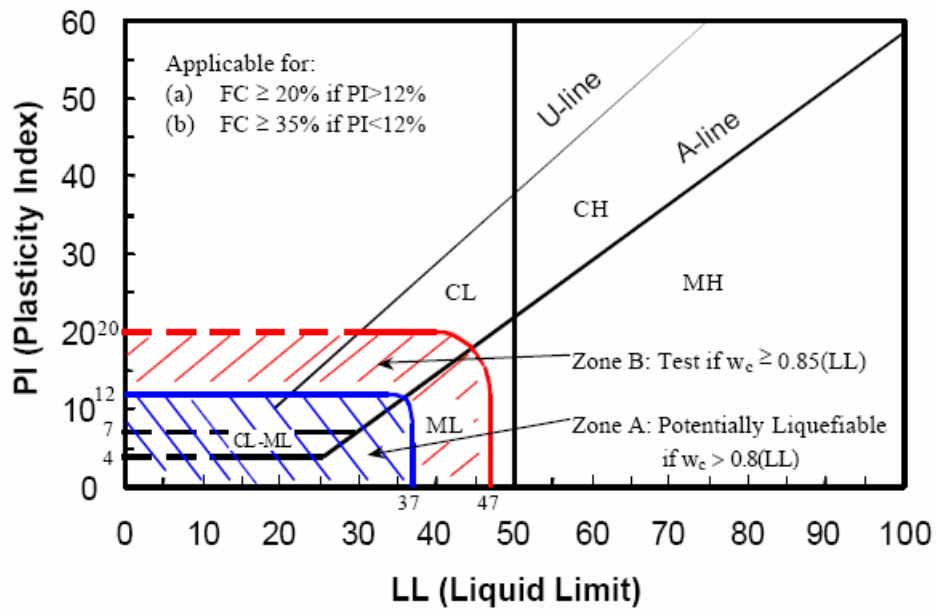
Figure 2.2-1. Criteria for liquefaction susceptibility of fine-grained sediments proposed by Seed et al. (2003)

2.2.3 Bray and Sancio (2006)

Bray and Sancio (2006) proposed their liquefaction susceptibility criteria based on cyclic test results performed on undisturbed fine grained soil specimens retrieved from Adapazarı city. In their testing program, soil samples were mostly isotropically consolidated to a confining stress of 50 kPa, and then CSR levels of 0.3, 0.4, and 0.5 were applied on these specimens. Cyclic loading was continued until 4 % double amplitude axial strain was achieved, which was adopted as their liquefaction triggering criterion. According to authors, soils with $w_c / LL > 0.85$ and $PI < 12$ are susceptible to liquefaction, and further testing is recommended for soils with $w_c / LL > 0.80$ and $12 < PI < 18$; whereas, soils having $PI > 18$ are considered to be non-liquefiable under low effective stress levels owing to their high clay content. The proposed criteria are schematically presented in Figure 2.2-2.
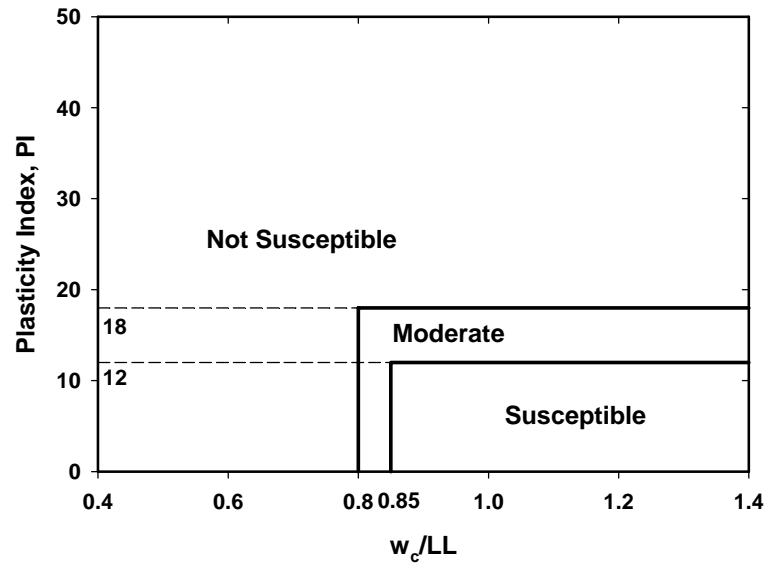
Figure 2.2-2. Criteria for liquefaction susceptibility of fine-grained sediments proposed by Bray and Sancio (2006)

Among all, Bray and Sancio (2006) is the methodology providing the most information on the database used (i.e. tested specimens and test conditions). However, these criteria seem to be specifically developed for a specific scenario which is Adapazarı region and soils subjected to 1999 Kocaeli earthquake, as clearly revealed by the adopted cyclic stress levels and consolidation stress histories. This is believed to be a major limitation of this study. Moreover by excluding *LL* as a screening parameter, these criteria lose its ability to distinguish the behavioral differences exhibited by ML, CL and MH type soils, since for these types of soils, it is possible to have same *PI* and w_c / *LL* values with significantly different *LL* levels.

2.2.4 Boulanger and Idriss (2006)

Another recent attempt was made by Boulanger and Idriss (2006), which was claimed to be based on cyclic laboratory test results and extensive engineering

judgment. As part of this new methodology, cyclic response of fine-grained soils are grouped under "sand-like" and "clay-like" responses, where soils behaving "sand-like" are judged to be liquefiable and have substantially lower values of cyclic resistance ratio (CRR) compared to those classified as to behave "clay-like" as presented in Figure 2.2-3.

Boulanger and Idriss (2006) intended to propose criteria independent of in-situ conditions (i.e. independent of variations of soil's in-situ moisture content). They evaluated; i) hysteretic stress-strain loops (i.e. dissipated energy), ii) existence of zero shear resistance zone, and iii) pore water pressure generation response to distinguish sand- and clay-like soil responses from a limited number of test data compiled from literature. Authors claimed that PI by itself is capable of explaining the difference in above listed responses and consequently it was used as the unique screening parameter.
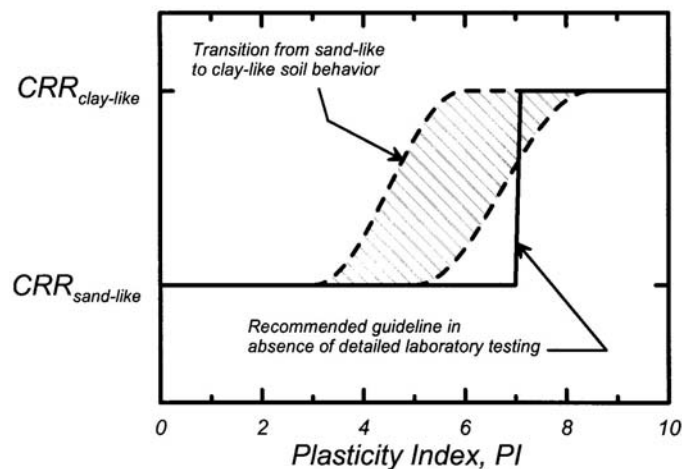
Figure 2.2-3. Criteria for differentiating between sand-like and clay-like sediment behavior proposed by Boulanger and Idriss (2006)

The main drawback of this methodology is the fact that the y-axis of Figure 2.2-3 is not to scale, thus a direct comparison between CRR of "clay-like" and "sand-like"

14

responses is not possible. Moreover, while preparing this plot the authors adopted different CRR definitions. For sand-like soils, cyclic shear stress (τ_{cyc}) was normalized by initial effective vertical stress (σ'_{v0}); whereas for clay-like soils normalization was performed according to undrained shear strength of soil (s_u). Even though, these definitions are frequently used in the literature; it is believed that such schematic comparisons produce misleading and biased conclusions.

2.2.5 Evaluation of Recent Liquefaction Susceptibility Criteria

Although the former three studies are judged to be improvements over earlier efforts, they suffer from one or more of the following issues:

i.   ideally separate assessments of a) identifying liquefiable soils and b) liquefaction triggering were combined into a single assessment; hence if soil layers (in the field) or samples (in the laboratory) liquefy under a unique combination of CSR and number of equivalent loading cycle (or moment magnitude of the earthquake), then they are considered to be potentially liquefiable. These types of combined assessment procedures produce mostly unconservatively-biased classifications of liquefaction susceptible soils.

ii.   judging liquefaction susceptibility of a soil layer or a sample through a unique combination of CSR and number of equivalent loading cycle (or moment magnitude of the earthquake) requires clear definitions of liquefaction triggering. These definitions do not exist, or least to say were not documented.

iii.   liquefaction triggering manifestations are not unique, and they can be listed as surface manifestations in the forms of sand boils, extensive settlements, lateral spreading etc., in the field, or exceedance of threshold r_u or γ_{max} levels in the laboratory. These threshold levels are not uniquely and consistently defined. As discussed elsewhere, depending on the relative density (or consistency for fine-grained soils) and stress states, different

15

threshold levels may need to be adopted (Cetin and Bilge, 2010a). Success rates of existing assessment methodologies for identifying liquefaction susceptible soils depend strongly on these adopted threshold levels.

It is believed that the existing criteria need a re-visit considering their listed limitations and the significance of the problem. For this purpose, new criteria will be attempted to be established as part of this dissertation.

2.3   PREDICTION OF CYCLICALLY-INDUCED SOIL STRAINING

During vertical propagation of seismic shear waves, soil layers are subject to two significantly different forms of straining; i) shear (deviatoric) strain –occurs during undrained loading and involves mostly shape changes, and ii) post-cyclic volumetric (reconsolidation) strain –occurs mostly after undrained cyclic shearing with dissipation of excess pore water pressure and it may involve both shape and volume changes.

Seed et al. (2003) referred to engineering assessment of these strains as the third step soil liquefaction engineering (Table 2.2-1), and it is considered as a very important and also challenging part of design projects. This section is devoted to the review of available earlier efforts on prediction of cyclically-induced straining potential of cohesive soils.

A close inspection on literature reveals that the most of previous efforts have focused on saturated cohesionless soils, considering their significant straining potential. Various researchers, including Tokimatsu and Seed (1984 and 1987), Ishihara and Yoshimine (1992), Shamoto et al. (1998), Zhang et al. (2002) and more recently Cetin et al. (2009), proposed semi-empirical procedures for the assessment of strain potentials of saturated sands with only limited amount of fines content (i.e., $FC \leq 35\%$). On the other hand, there exist only a few attempts aiming to quantify cyclic strains in saturated fine-grained soils.

Pioneering theoretically-based attempts from mid-70's (e.g. Wilson and Greenwood, 1974; Hyde and Brown, 1976; Majidzadeh et al., 1976 and 1978) intended to predict plastic deformation potential for fine-grained subgrade soils under repeated traffic loading. These early efforts were summarized by Li and Selig (1996), in which a new semi-empirical model was also proposed for the prediction of cumulative plastic strains (ε_p) as given in Equation (2 – 1).

$$\varepsilon_p = a \cdot (\sigma_d / \sigma_s)^m \cdot N^b \qquad (2 - 1)$$

where σ_d is the cyclic deviator stress, σ_s is the static shear strength of soil, N is the number of applied loading cycles, and a, b and m are material constants, the values of which were provided by the authors for different types of soils as listed in Table 2.3-1.

Table 2.3-1. Material constants recommended by Li and Selig (1996)

Model Parameters		Soil Classification			
		ML	MH	CL	CH
b	Average	0.10	0.13	0.16	0.18
	Range	0.06-0.17	0.08-0.19	0.08-0.34	0.12-0.27
a	Average	0.64	0.84	1.1	1.2
	Range	-	-	0.3-3.5	0.82-1.5
m	Average	1.7	2.0	2.0	2.4
	Range	1.4-2.0	1.3-4.2	1.0-2.6	1.3-3.9

The model of Li and Selig (1996) and others provide practical solutions for the prediction of cumulative plastic strains due to repetitive traffic loads. However, it is

important to notice that due to significantly different loading conditions (frequency and drainage conditions) these studies cannot be reliably used for the assessment of seismically-induced soil strain problems.

On a separate stream, some researchers have proposed constitutive models founded on one-dimensional consolidation theory for the prediction of seismically-induced ground settlements (i.e. post-cyclic volumetric strain) in normally- and over-consolidated clayey soils.

Ohara and Matsuda (1988) expressed post-cyclic volumetric strain ($\varepsilon_{v,pc}$) as a function of excess pore water pressure ratio (r_u), initial void ratio (e_0) and compression index induced by cyclic loading (C_{dyn}) as given in Equation (2 – 2).

$$\varepsilon_{v,pc} = \frac{C_{dyn}}{1+e_0} \cdot log\left(\frac{1}{1-r_u}\right)$$
(2 - 2)

The relationship between C_{dyn} and over consolidation ratio (OCR) along with compression (C_c) and swelling (C_s) indices were given by Ohara and Matsuda (1988) as presented in Figure 2.3-1. On the other hand, r_u is defined conventionally in terms of the excess pore water pressure (u_e) and initial effective stress (σ'_0) as follows:

$$r_u = \frac{u_e}{\sigma'_0}$$
(2 - 3)

The authors also proposed a model for the prediction of r_u as a function of cyclic shear strain (γ_{cyc}), cycle number (n) and a number of material coefficients (A, B, C, D and E) as given in Equation (2 – 4).

$$r_u = \frac{n}{A \cdot (\gamma_{cyc})^m + \left\{ \dfrac{\gamma_{cyc}}{(B + C \cdot \gamma_{cyc})} \right\} \cdot n} - D - E \cdot \log(\gamma_{cyc}) \qquad (2\text{-}4)$$

This model was developed based on strain-controlled cyclic tests performed on kaolinite clay powder. It is important to notice that determination of these material coefficients requires cyclic testing for each specific material. This requirement reduces the practical use of both r_u and also $\varepsilon_{v,pc}$ models, significantly.
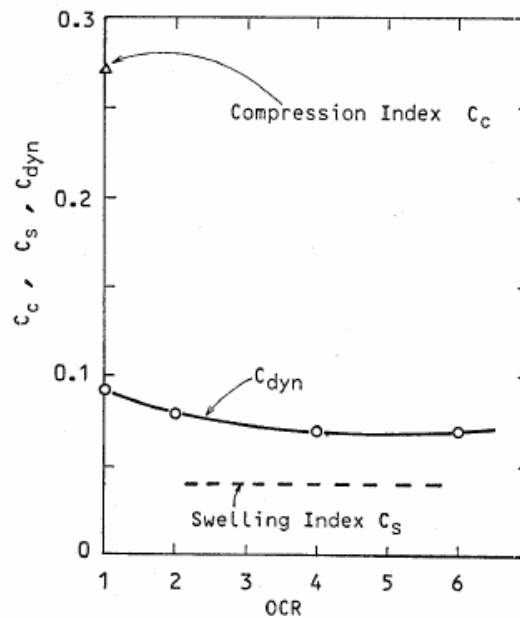
Figure 2.3-1. Relationship between C$_{dyn}$ and OCR (Ohara and Matsuda, 1988)

Using 1-D consolidation theory, a similar methodology was also proposed by Yasuhara and Andersen (1991) for normally-consolidated clays. Later, Yasuhara et al. (1992) modified this study for over-consolidated clays and proposed the following model for the prediction of $\varepsilon_{v,pc}$:

19

$$\varepsilon_{v,pc} = \frac{\alpha \cdot C_r}{1 + e_0} \cdot log\left(\frac{1}{1 - r_u}\right) \qquad (2 - 5)$$

where α is an experimental constant depending on the severity of cyclic loading and C_r is the recompression index. Based on cyclic tests performed on reconstituted Ariake clay (specific gravity (G_s) = 2.58 – 2.65, LL = 115 – 123, and PI = 69 – 72) and Itsukaichi marine clay (G_s = 2.53, LL = 124.2, PI = 72.8), seismically-induced excess pore water pressure and volume change responses were studied by the authors. Yasuhara et al. (1992) stated that the level of $\varepsilon_{v,pc}$ increased significantly when cyclic failure occurred as presented in Figure 2.3-2, and α value of 1.5 fitted well to the observed behavioral trends especially when r_u value exceeded 0.5.
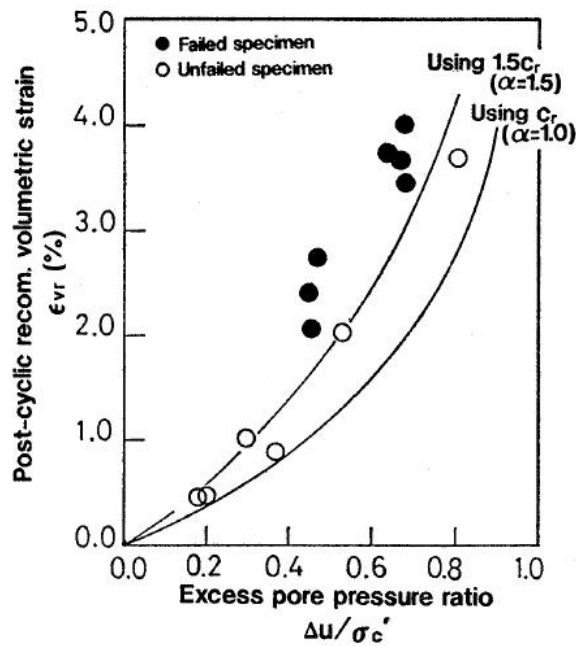

Figure 2.3-2. Relationship between $\varepsilon_{v,pc}$ and r_u (Yasuhara et al., 1992)

As revealed by Figure 2.3-2, the proposed methodology was derived based on limited amount of data. Moreover, Yasuhara et al. (1992) did not address to how to deal with the pore water pressure generation issue, which constituted an integral part of this model.

Later, Yasuhara et al. (2001) proposed a design methodology for the assessment of post-cyclic volumetric settlements (i.e. strains) based on the results of Yasuhara and Andersen (1991), Yasuhara et al. (1992, 1994 and 1997) and Yasuhara and Hyde (1997). The proposed methodology provides design charts in terms of factor of safety for bearing capacity failure (FS_{bc}), PI and earthquake induced - r_u. The authors considered free-field stress conditions and the stress state due to presence of an existing structure (or an embankment) while developing their procedure. For the latter case, which was concluded to be more critical, total earthquake induced settlement (Δs_{cy}) was stated to be the sum of immediate ($\Delta s_{i,cy}$) and recompression settlements (Δs_{vr}) due to dissipation of excess pore pressures as presented in Equation (2 − 6).

$$\Delta s_{cy} = \Delta s_{i,cy} + \Delta s_{vr} = f_1 \cdot S_{i,NC} + f_2 \cdot \left\{ \frac{H}{1+e_0} \right\} \qquad (2\text{ - }6)$$

where H is the thickness of fine-grained soil layer, $S_{i,NC}$ is the immediate settlement due to structural loads under static loading conditions, and e_0 is the initial void ratio; whereas f_1 and f_2 are defined by Equations (2 − 7) and (2 − 8), respectively.

$$f_1 = \frac{R_q}{R_k} \cdot \left[\frac{1 - 1/FS_{bc}}{R_q - 1/FS_{bc}} \right] - 1 \qquad (2\text{ - }7)$$

$$f_2 = 0.225 \cdot C_c \cdot \log(n_q) \qquad (2\text{ - }8)$$

where R_q is the ratio of post-cyclic residual shear strength ($s_{u,cy}$) to undrained shear strength before earthquake ($s_{u,NC}$), R_k is the ratio of undrained secant moduli before ($E_{i,NC}$) and after cyclic loading ($E_{i,cy}$), C_c is the compression index and n_q is the equivalent over consolidation ratio. Yasuhara (1994) and Yasuhara and Hyde (1997) defined R_q and R_k, respectively as follows:

$$R_q = \frac{s_{u,cy}}{s_{u,NC}} = n_q^{\Lambda_0/(1-C_s/C_c)-1} \tag{2-9}$$

$$R_k = \frac{E_{s,cy}}{E_{s,NC}} = \frac{1 - \dfrac{C}{\Lambda} \cdot \ln(n_q)}{n_q} \tag{2-10}$$

where C_s is swelling index and Λ, Λ_0, C and n_q are defined by Equations (2 – 11) to (2 – 14), respectively. In Equations (2 – 18) and (2 – 19), the PI -based expressions of Λ and Λ_0 were given by Ue et al. (1991).

$$\Lambda = 1 - \frac{C_s}{C_c} = 0.815 - 0.002 \cdot PI \tag{2-11}$$

$$\Lambda_0 = \frac{\log\left[\dfrac{(s_u/p')_{OC}}{(s_u/p')_{NC}}\right]}{\log(OCR)} = 0.757 - 3.49 \cdot 10^{-3} \cdot PI + 4 \cdot 10^{-4} \cdot PI^2 \tag{2-12}$$

$$C = \frac{\left[(E/p')_{OC}/(E/p')_{NC}\right] - 1}{\ln(OCR)} \tag{2-13}$$

$$n_q = \frac{1}{1 - \dfrac{u}{p'_0}} \tag{2-14}$$

22

where p'_0 is the initial effective overburden stress and subscripts OC and NC indicates whether the corresponding parameter belongs to over- or normally-consolidated states, respectively.

According to the proposed methodology by using the sets of equations from $(2-6)$ to $(2-14)$, earthquake-induced settlements of structures founded on fine-grained soils can be calculated when following information is available: i) load intensity and the average width and the depth of foundation (required for FS_{bc} calculations), ii) PI, e_0 and thickness of soil layers, iii) soil strength's (s_u), stiffness' (E) and compressibility's (C_c) variation with depth, and iv) magnitude and distribution of earthquake-induced excess pore water pressure.

Among all input parameters, the last one remains as the most challenging, and Yasuhara et al. (2001) recommended performing 2- or 3-D dynamic numerical analysis for the determination of excess pore water pressure distribution within the soil media. Then, the user is referred to the design chart, presented in Figure 2.3-3, for the determination of f_1 and f_2.

Yasuhara et al. (2001) presented a valuable and unique effort for the prediction of cyclically-induced settlements by taking into account the effects of existing structures and various properties of fine-grained soil layers. Yet, the need to perform 2- or 3-D numerical analysis for the prediction of excess pore water pressure contradicts with authors' intention of developing a practical design procedure; since these dynamic analyses are not practical but time-consuming, and require great amount of experience to obtain reliable results.

As clearly presented, most of the attention has focused on the quantification of post-cyclic volumetric (reconsolidation) strains, and cyclic shear strains are not properly referred to. Hyodo et al. (1994) performed a study in normally-consolidated Itsukaichi marine clay having G_s, LL and PI values of 2.532, 124.2 and 72.8, respectively. Specimens were consolidated under different levels of initial static

shear stresses, and stress controlled cyclic triaxial tests were performed under a loading frequency of 0.02 Hz. Based on these test results, Hyodo et al. (1994) proposed a procedure for the prediction of cyclically-induced residual axial strains, which is summarized as follows:

1. Cyclic shear strength (R_f) is determined for the selected initial deviatoric stress (q_s) and number of stress cycles (N) by using Equation (2 – 15).
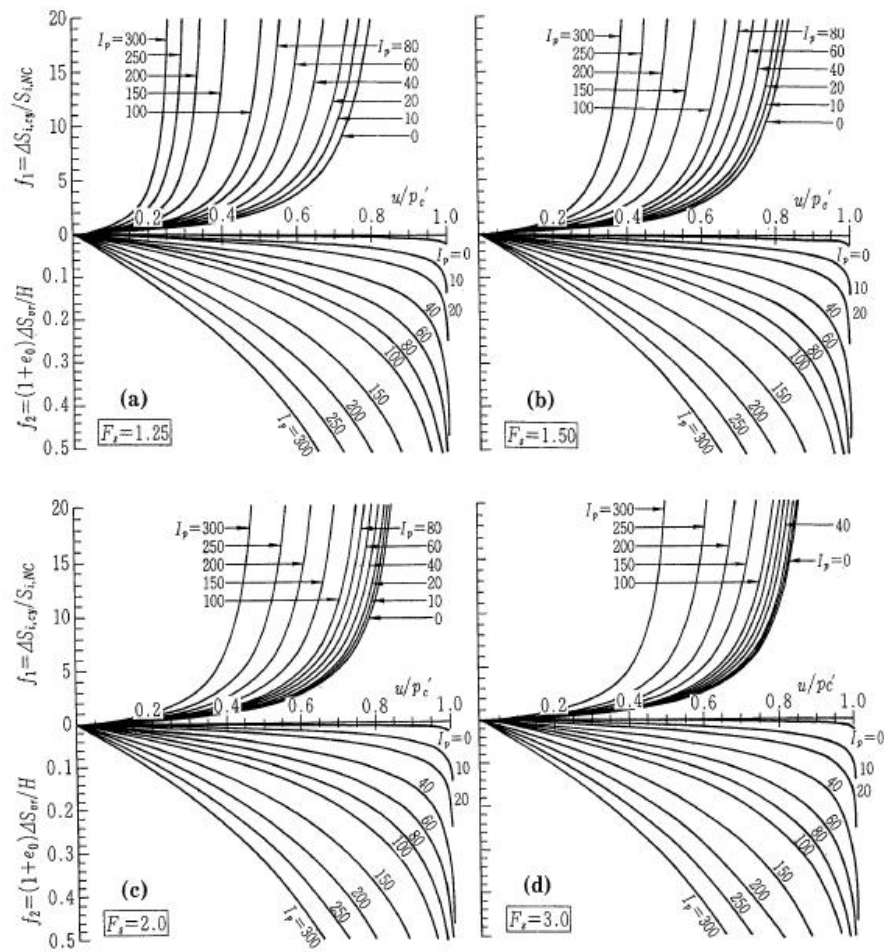
Figure 2.3-3. Design charts of Yasuhara et al. (2001) for prediction of f_1 and f_2

$$R_f = \mathrm{K} \cdot N^{\beta} \qquad (2\text{-}15)$$

where β is a material constant and represents the slope of number of cycles to failure, which was defined as 10 % residual axial strain. For the tested clay, its value was reported as -0.088, and K is defined as follows:

$$\mathrm{K} = 1.0 + 1.5 \cdot \frac{q_s}{p_c} \qquad (2\text{-}16)$$

where p_c is the mean consolidation stress. Then, the relative cyclic shear stress is calculated by dividing the applied stress ratio (R) to R_f.

$$\frac{R}{R_f} = \frac{(q_s + q_{cyc})/p_c}{\mathrm{K} \cdot N^{\beta}} \qquad (2\text{-}17)$$

where q_{cyc} is the applied cyclic deviator stress.

2. The relative effective stress ratio (η^*) is determined by using Equation (2 – 18).

$$\eta^* = \frac{R/R_f}{\left\{ (a_2 - (a_2 - 1) \cdot R/R_f \right\}} \qquad (2\text{-}18)$$

where a_2 is determined experimentally as 6.5 by Hyodo et al. (1994) for Itsukaichi clay.

3. The effective stress ratio (η_p) at the peak cyclic stress of a given stress cycle is calculated by using Equation (2 – 19).

$$\eta_p = \eta^* \cdot (\eta_f - \eta_s) + \eta_s \qquad (2\text{-}19)$$

where η_s and η_f are effective stress ratios for initial consolidation and failure conditions, respectively.

4. The pore pressure at the peak axial strain (u_p) is calculated as follows:

$$u_p = p_c + \frac{q_{cyc}}{3} - \frac{(q_s + q_{cyc})}{\eta_p}$$ (2 - 20)

5. The peak axial strain (ε_p) is evaluated by substituting η_p into the proposed hyperbolic model of authors, which is also given by Equation (2 – 21).

$$\varepsilon_p = \frac{a_1 \cdot \eta_p}{1 - \eta_p / \eta_{ult}}$$ (2 - 21)

where a_1 and η_{ult} are defined as 0.5 and 2.0, respectively for Itsukaichi marine clay based on cyclic test results.

Hyodo et al. (1994) assessed $\varepsilon_{v,pc}$ by adopting a 1-D consolidation theory based solution. However, unlike Ohara and Matsuda (1988) and Yasuhara et al. (1992), Hyodo et al. (1994) directly used recompression index (C_r), and reported that its value for the tested clay is 0.243.

The methodology of Hyodo et al. (1994) is another valuable effort, mostly because it attempted to estimate cyclically-induced shear strains based on residual axial strains. However, this study suffered from several issues. First, presented coefficients are material specific which limits potential use of this methodology for other soils without further advance testing. Moreover, the adopted loading frequency is believed to affect the results significantly, since shear strength of clayey soils is known to be a function of loading rate due to viscous creep. Viscous creep was defined by Mitchell (1976) as the "time dependent shear and / or volumetric strains that develop at a rate controlled by the 'viscous resistance' of the soil structure" of clayey soils. Hence considering the rapid nature of seismic loads, an apparent

increase in strength of cohesive soils can be observed during the course of seismic excitation. The effects of loading rate on both monotonic and cyclic resistance of cohesive soils have been studied by various researchers (e.g. Mitchell, 1976; Vaid et al., 1979; Graham et al., 1983; Lefebvre and Lebouef, 1987; Ansal and Erken, 1989; Zergoun and Vaid, 1994; Zavoral and Campanella, 1994; Sheahan et al., 1996; Lefebvre and Pfendler, 1996 etc.) and later based on the results of those studies, Boulanger and Idriss (2004) stated that cyclic strength of soils increase about 9 % due to a 10 fold increase in the loading rate. Moreover, researchers also pointed out that with increasing plasticity of soil, the effect of loading rate becomes more pronounced.

Zergoun and Vaid (1994) approached the problem from excess pore water pressure point of view. They performed a detailed research to identify factors affecting cyclic pore pressure response. One of their conclusions was regarding the effect of loading rate, which will also be referred to in the following sections. Zergoun and Vaid (1994) pointed out that unless frequency of cyclic loading is sufficiently slow to allow pore water pressure equalization throughout the specimen, pore pressure measurements will be erroneous. Based on consolidation test results, the drained rate of loading is recommended to be adopted as $16 \cdot t_{50}$, i.e. 16 times the time to 50 % consolidation. If such a loading rate is adopted, then frequency of loading will vary in the range of 0.005 Hz to 0.1 Hz. Considering the effect of frequency on cyclic response, and the fact that rapid loading better represents high frequency content of an earthquake; slow loading tests are judged not to be the best option to study seismic response of plastic silt and clay mixtures.

Based on this discussion, due to creep-induced deformations, it can be claimed that in its current form, Hyodo et al. (1994)'s model over-predicts earthquake-induced residual strains even for the selected material.

Very recently, Hyde et al. (2007) studied post-cyclic recompression stiffness and cyclic strength of low plasticity silts. Based on cyclic tests results and 1-D

consolidation theory, the authors proposed an expression in which $\varepsilon_{v,pc}$ was expressed as a function of initial sustained deviator stress ratio (q_s / p'_c), post-cyclic axial strain ($\varepsilon_{a,pc}$) and void ratio (e) of the tested material as follows:

$$\varepsilon_{v,pc} = \frac{1.74}{e^{1.71} \cdot (q_s / p'_c)} \cdot \varepsilon_{a,pc}^{\,0.461} \qquad (2\text{-}22)$$

Hyde et al. (2007) recommended a different approach by modeling $\varepsilon_{v,pc}$ as a function of axial strain rather than as a function of excess pore water pressure. This approach has been used for saturated sandy soils by various researchers (e.g. Tatsuoka et al., 1984; Ishihara and Yoshimine, 1992), but not widely adopted for fine-grained soils, possibly due to absence of tools for predicting resulting axial strains. This, in fact, limits possible extensive use of Hyde et al.'s model.

The most recent study on post-cyclic recompression straining of fine-grained soils was presented by Toufigh and Ouria (2009). Similar to previous efforts, this study also adopted 1-D consolidation theory, but limited itself to one-way (i.e. only in compression) rectangular cyclic loads. Authors also implemented their model into a finite difference based computer code. However, besides its loading scheme related limitations, this model also requires parameters estimated by oedometer testing of undisturbed soil specimen.

Within the confines of this section, the existing studies on the assessment of cyclically-induced straining are summarized. Previous efforts are invaluable and inspiring; however as indicated in previous paragraphs, a robust and practical procedure for the assessment of cyclic softening problem is still needed. For instance, *Guidelines for Analyzing and Mitigating Liquefaction in California* manual recommends using Tokimatsu and Seed (1987) for the prediction of strains in saturated sandy soils; whereas it recommends cyclic testing on undisturbed specimens for the same problem in saturated cohesive fine-grained soils. Thus, inspired by this gap, the main motivation of this study is defined as the development

of practical-to-use semi-empirical models for the assessment of seismically-induced shear (deviatoric or axial) and post-cyclic volumetric (reconsolidation) strain potential of cohesive fine-grained soils. As mentioned in the introduction chapter, an extensive experimental program was designed, which will be introduced in the following chapter.
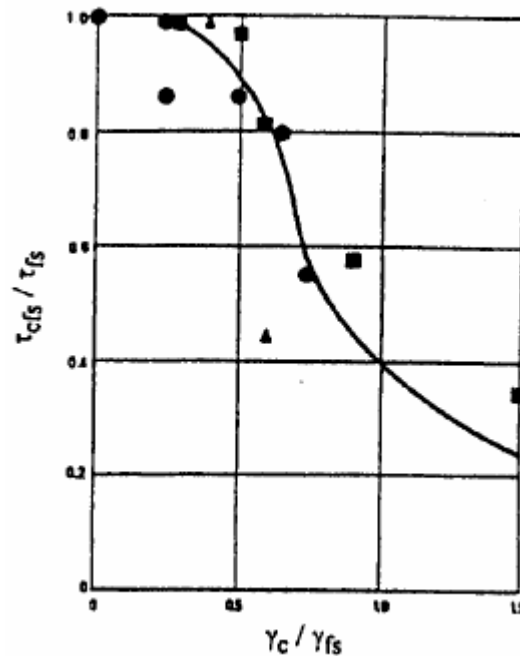
2.4 POST-CYCLIC SHEAR STRENGTH

Similar to cyclic straining problem, post-cyclic shear strength of saturated sandy soils has drawn considerably more interest compared to that of cohesive soils. Yet, since late-60's a few researchers have also focused on cohesive soils.

Depending on the dilatancy properties of soils, the intensity of shaking and also post-cyclic stress path, post-cyclic shear strength may be higher or lower than the initial monotonic shear strength. However, shear strength of most sands decreases as a result of disturbed cementation bonds, re-orientation of particles, and also excess pore pressure buildup during cyclic loading.

In their pioneering study, Thiers and Seed (1969) proposed a chart solution (Figure 2.4-1) where ratio of post-cyclic to initial monotonic shear strength was defined as a function of cyclic shear strain amplitude to shear strain, at which monotonic failure takes place. Figure 2.4-1 reveals that strength loss may reach up to 80 %. However, as long as the level of cyclic shear strain (γ_c) is less than half of the strain required for monotonic failure (γ_{fs}), reduction in shear strength is observed to be less than 10 %. Later, Lee and Focht (1976), Koutsoftas (1978) and Sherif et al. (1977) provided experimental data supporting the findings of Thiers and Seed (1969). Additionally, Sangrey and France (1980) adopted critical state soil mechanics concepts to the resolution of problems involving cyclic response of fined grained soils. Castro and Christian (1976) also investigated post-cyclic shear strength of various types of soils. They underlined that $s_{u,pc}$ predictions based on effective stress based Mohr Coulomb failure criterion might be misleading, since this

approach ignored the possible dilative nature of soil specimens. They also stated that post-cyclic shear strength ($s_{u,pc}$) of clayey soils were very close to their initial monotonic shear strength (s_u). The latter observation is based on results of 4 cyclic tests performed on clayey soils having *PI* and *LI* values varying between 15 to 19 and 0.27 to 0.69, respectively. Thus, it is believed that findings of authors may not be valid for potentially liquefiable fine-grained soils and their statement on the equality of $s_{u,pc}$ and s_u is judged to be potentially unconservative.

Figure 2.4-1. Cyclic shear strain induced reduction in shear strength (Thiers and Seed, 1969)

Van Eekelen and Potts (1978) proposed the following expression relating $s_{u,pc}$ and s_u of clayey soils.

$$\frac{s_{u,pc}}{s_u} = \left(1 - r_u\right)^{\chi/\lambda} \tag{2-23}$$

where χ and λ are the critical state swelling and compressibility coefficients, respectively, and the determination of these values require further oedometer testing.

Using consolidation theory as its theoretical basis, Yasuhara (1994) proposed a framework for estimating post-cyclic shear strength of cohesive soils considering both undrained and drained loading conditions. Based on Yasuhara's conclusions, the decrease in shear strength varies in the range of 10 to 50 % of initial monotonic shear strength. Yasuhara (1994) proposed the closed form solution presented in Equation (2 – 24)

$$\frac{s_{u,cy}}{s_{u,NC}} = \left(OCR\right)_q \cdot \left(\frac{\Lambda_0}{1 - C_s/C_c} - 1\right) \tag{2-24}$$

where $s_{u,cy}$ and $s_{u,NC}$ are the post-cyclic and original monotonic shear strengths, respectively; C_s and C_c are swelling and compressibility indices, respectively; $(OCR)_q$ is the ratio of mean effective stresses before (p_i') and after (p_e') the application of cyclic shear stresses; and Λ_0 is a material constant, determination of which requires additional consolidation testing. Based on the findings of Ue et al. (1991), Yasuhara (1994) proposed the use of following equation for the prediction of $\Lambda_0/(1 - C_s/C_c)$ term;

$$\Lambda_0/(1 - C_s/C_c) = 0.939 - 0.002 \cdot PI \tag{2-25}$$

While this framework is arguably the most complete approach to assess post-cyclic shear strength of cohesive soils, it is judged to suffer from the following limitations. First of all, its applicability to post-liquefaction residual shear strength problems is still questionable due to lack of verification in mostly low plasticity soils. As part of verification attempts, Yasuhara (1994) used clayey soils with *PI* values ranging

from 13 to 320. As expected none of the specimens experienced high r_u levels. Additionally, there is no information on moisture content of specimens, so it is not possible to accurately comment on liquefaction susceptibility of the tested specimens. This is believed to be important to evaluate applicability of this methodology in post-liquefaction stability analysis.

$(OCR)_q$ is another important component of this model; yet its prediction is not trivial. This term has been used by various researchers earlier: Okamura (1971) called this term as "disturbance ratio", Matsui et al. (1980) used the term "equivalent overconsolidation ratio" and Yasuhara et al. (1983) called it as "apparent" or "quasi-overconsolidation ratio". According to definition of Yasuhara, its value depends on cyclically-induced excess pore water pressure ratio. Following simplified expression was proposed for Yasuhara (1994) to predict $(OCR)_q$.

$$(OCR)_q = (OCR)^{1-C_s/C_c} \qquad (2 \text{ - } 26)$$

where OCR is the overconsolidation ratio of the tested specimen. For the sake of producing a practical approach, Yasuhara adopted a relationship given by Ue et al. (1991) for the prediction of C_s/C_c, which is given as follows:

$$C_s/C_c = 0.185 + 0.002 \cdot PI \qquad (2 \text{ - } 27)$$

Expressing the parameters as a function of PI is a very practical approach; yet in turn, the success of Yasuhara's method strongly depends on Ue et al. (1991)'s correlations. Performance of these correlations is believed to be questionable since database of Ue et al. (1991) involves significant amount of data scatter as presented by Figures 2.4-2 and 2.4-3, which are used as input to Equations (2 – 25) and (2 – 27), respectively. Considering the fact that very same equations were also used as part of post-cyclic settlement prediction model of Yasuhara et al. (2001), users need to be cautious and aware of its limitations
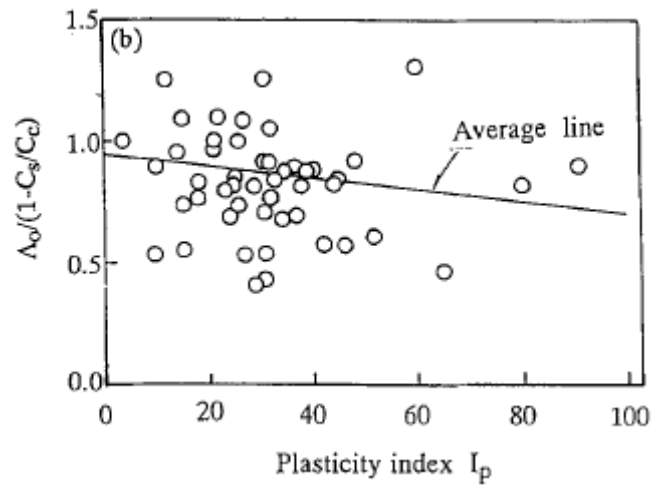
Figure 2.4-2. Database used for the development of Equation (2 – 25) (Ue et al., 1991)
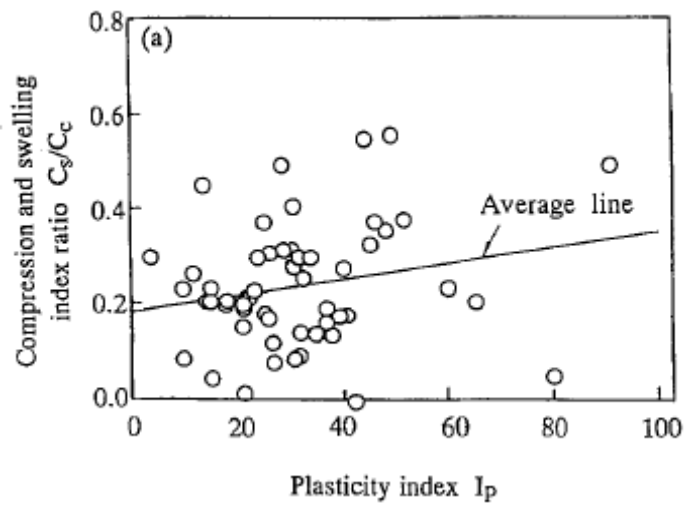
Figure 2.4-3. Database used for the development of Equation (2 – 27) (Ue et al., 1991)

33

CHAPTER 3

LABORATORY TESTING PROGRAM

AND

DATABASE COMPILATION EFFORTS

3.1 INTRODUCTION

This chapter is devoted to the discussion of laboratory testing details, and the presentation of results and additional data compiled from available literature, which are all used in the development of probabilistically-based semi-empirical models.

Within the confines of this experimental program, undisturbed fine-grained soil specimens, sampled from variety of locations in Adapazarı and Ordu cities of Turkey were used. Samples were retrieved from various depths (varying from 2.5 to 7 meters) by large diameter thin wall Shelby tubes. Besides monotonic and cyclic triaxial tests, simple index tests were also performed to determine Atterberg limits, specific gravity (G_s) and moisture content of each sample, and grain size distribution of some representative samples. Moreover, oedometer tests were also performed to determine the consolidation stress history of representative samples. After

explanation of applied testing procedures and presentation of test results, this chapter proceeds with detailed information on data compilation efforts from available literature.

3.2 SOIL INDEX TESTING

For cohesive fine-grained soils, physically meaningful index properties include Atterberg limits, specific gravity and grain size distribution. As revealed by findings of previous studies (e.g. Seed et al., 2003; Bray and Sancio, 2006), it is believed that Atterberg limits (along with moisture content) of specimens are the most important index properties affecting cyclic response of silts and clay mixtures. Hence for each specimen, liquid limit (LL), plastic limit (PL) and plasticity index (PI) were determined in accordance with "ASTM D4318 Standard Test Method for Liquid Limit, Plastic Limit and Plasticity Index of Soils" (ASTM, 1998). Figure 3.2-1 summarizes the Atterberg limits of the tested specimens on USCS Plasticity Chart. As revealed by this figure, various types of specimens, ranging from ML to CH, were tested as part of this laboratory testing program. Moreover, the spread of LL and PI of tested materials are also presented in Figures 3.2-2 and 3.2-3, respectively.
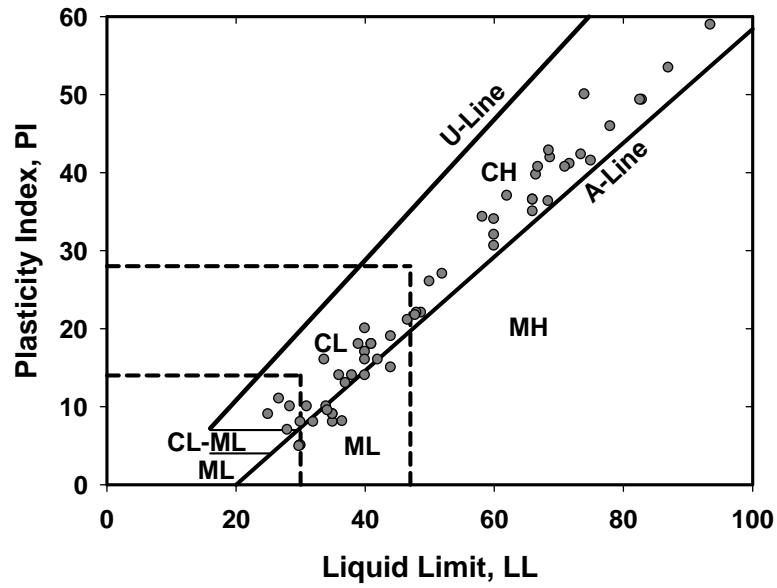
Figure 3.2-1. Summary of test data on USCS Plasticity Chart
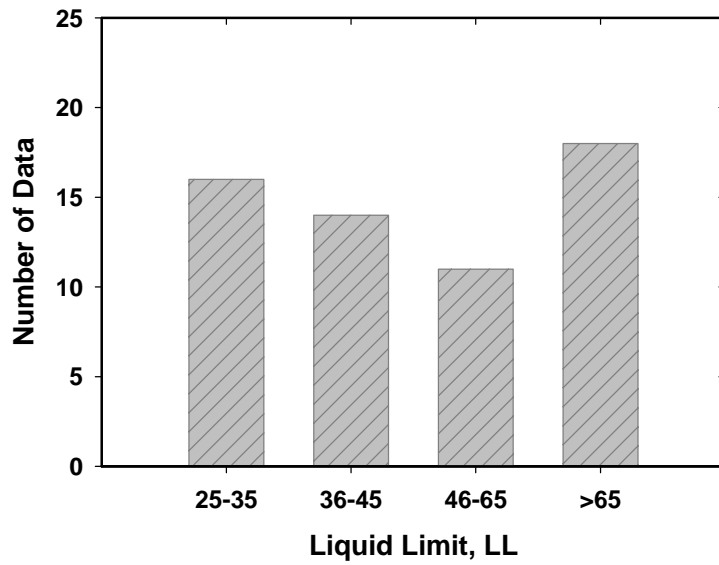
Figure 3.2-2. Histogram of LL values
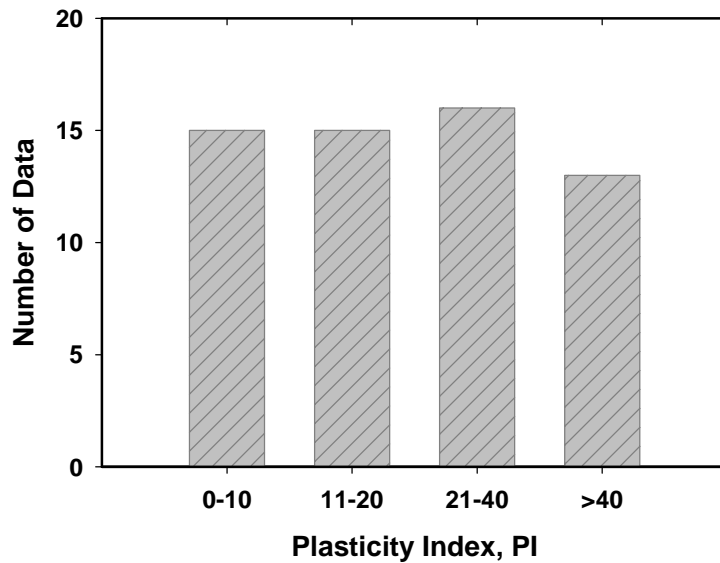
Figure 3.2-3. Histogram of PI values

Specific gravity (G_s) of each sample is also determined in accordance with "ASTM D854 Standard Test Method for Specific Gravity of Soil" (ASTM, 1998). For the tested specimens, G_s values are observed to vary in the range of 2.55 to 2.70. These values are reported along with the corresponding grain size distribution and consolidation test data, later in the chapter.

Grain size distribution of some representative samples were also determined in accordance with "ASTM D422 Standard Test Method for Particle Size Analysis of Soils" (ASTM, 1998) by performing both hydrometer and sieve analysis. Table 3.2-1 summarizes the important descriptive parameters, such as fines content (FC), percent of particles smaller than 5 μm and 2 μm, which are used by liquefaction susceptibility criteria of Wang (1979), Seed and Idriss (1982), Andrews and Martin (2000), etc. Moreover, Figure 3.2-4 presents the available test data to present a range for database; whereas individual test results are presented in Appendix A.
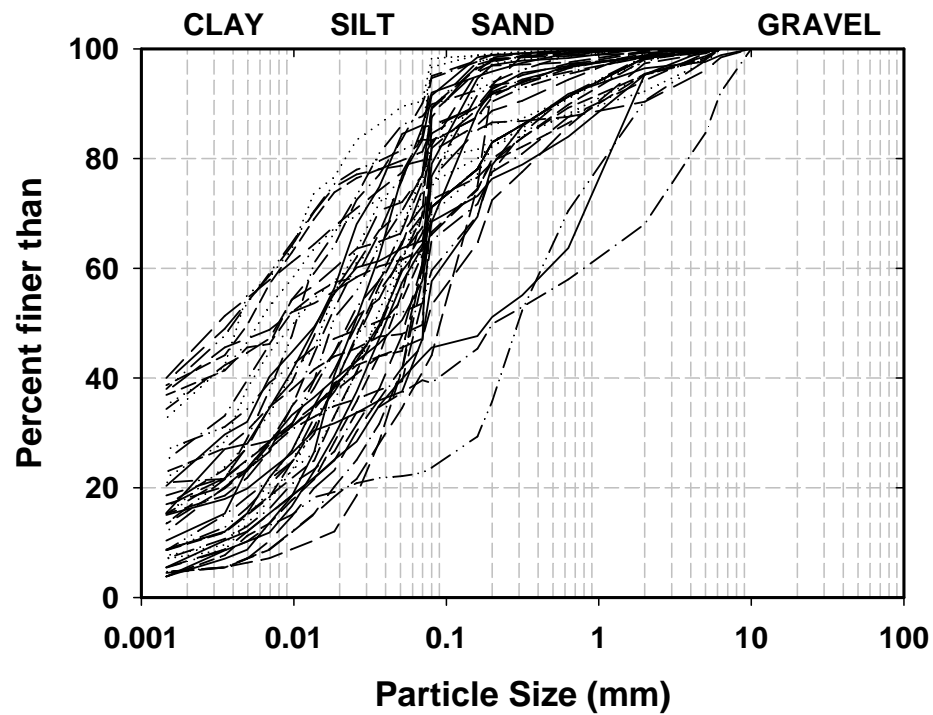
Figure 3.2-4. Summary of grain size distribution of samples tested in this study

Table 3.2-1. Summary of specimens' grain size characteristics

Sample ID	Test ID	FC (%)	<2μm (%)	<5μm (%)
GD1-3M	CTXT11	71.1	9.4	15
GD1-3T	CTXT12	71.1	9.6	16.3
GB1-5M	CTXT15	44.2	4.8	6.9
GB1-5B	CTXT16	44.2	4.8	6.9
V4 TB	CTXT23	72.5	15.1	23.2
V4 M	CTXT24	23.6	6.2	10.1
SK7-UD1-B	CTXT25	39.1	8	12.8
SK7-UD1-M	CTXT26	39.1	8	12.8
TSK2-1B	CTXT27	71.1	23	33.1
GA1-5T	CTXT30	89.1	16.8	25
GA1-5B	CTXT31	89.3	13.9	23.3
BA2-3B	CTXT32	91.5	5	8
BA2-3T	CTXT33	74.6	7.5	13
BA2-3T1	CTXT34	74.6	7.5	13
THAMES 1-2B	CXTT35	71.1	36.8	45
THAMES 2-1	CTXT36	71.1	36.8	45

Table 3.2-2. cont'd. Summary of specimens' grain size characteristics

Sample ID	Test ID	FC (%)	<2μm (%)	<5μm (%)
BH2-3M	CTXT37	59.6	28.1	34.8
BH2-3B	CTXT38	66.2	38.3	45.7
BH5-1M	CTXT40	53.3	18	27.6
BH5-1B	CTXT42	65	23.2	21.1
BH6-3B	CTXT43	75.7	32.2	47.4
BH6-3M	CTXT44	71.1	17.5	31.2
BH6-3T	CTXT45	71.1	10.2	18.2
BH4-3M	CTXT46	83.3	54.6	41
BH4-3B	CTXT47	83.1	40.4	51.1
BH4-3T	CTXT48	85.5	54.9	42.4
BH3-2M	CTXT49	95	44.5	55.1
BH3-2B	CTXT50	94.6	27.2	40.2
BH1-5M	CTXT51	64	15	20
BH1-5T	CTXT52	79.9	23.5	38.6
BH1-5B	CTXT53	45.5	6.6	11.8
BH7-2M	CTXT54	84.6	19.4	25
BH7-2B	CTXT55	81.3	17.8	23.4
BH7-2T	CTXT56	81.7	16.1	21.6
BH3-4M	CTXT58	96.6	17.4	28.2
BH7-4M	CTXT59	68.5	9.5	14.9
BH7-4T	CTXT60	83.5	9.5	14.8
BH7-4T	CTXT61	83.5	9.5	14.8
BH7-4B1	CTXT62	68.5	9.5	14.9
BH7-5T	CTXT63	66.6	9.5	15
BH7-5M	CTXT64	66.6	9.5	15

3.3 TRIAXIAL TESTING

Consolidated – undrained, strain controlled static (monotonic) and stress – controlled cyclic triaxial tests were performed on both isotropically- and anisotropically-consolidated undisturbed fine-grained soil samples. As triaxial testing constitutes an integral part of this research; a detailed description of the testing equipment used and procedures applied will be introduced next.

3.3.1 Triaxial Testing System Components

All triaxial tests were performed by using a modified version of GEONOR type triaxial testing system. Custom made loading and data acquisition systems are the

main improvements over the original triaxial testing apparatus. The system components include:

- GEONOR type triaxial cell.

- A loading frame including a hydraulic press.

- An electro-pneumatic loading system converting the electronic command signal to pneumatic pressure, which in turn applies the cyclic load.

- A custom designed data acquisition system which includes the instrumentation of an external load cell and external LVDT to monitor the axial load and vertical displacement, respectively.

- Three differential pressure transducers to measure cell and pore pressures and volume change.

- Process interface unit providing communication link between the loading sensor system and personal computer.

- Dedicated personal computer to run the software for controlling the equipment and to translate the recorded data to ASCII format.

A general view of the triaxial testing equipment is presented in Figure 3.3-1.
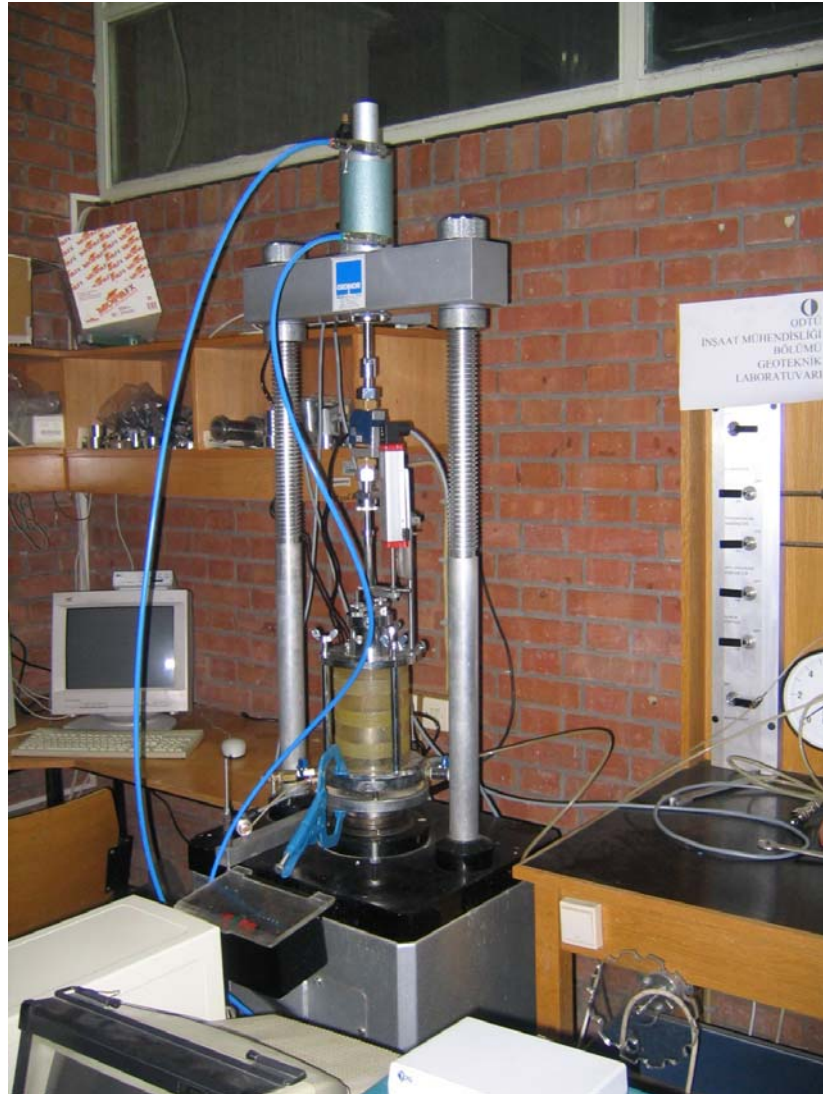
Figure 3.3-1. View of triaxial testing equipment used in this study

3.3.2 Static Triaxial Testing

Static (monotonic) triaxial tests were performed over seven decades to determine mechanical properties of all types of soils. It was reported that the first triaxial test on clays, under both drained and undrained conditions, with pore pressure measurements were carried out in Vienna, Austria, by Rendulic in 1933 (Rendulic, 1937), under the supervision of Karl Terzaghi. On the other hand, similar tests had

not been performed until 1944 and 1950 in USA and England, respectively (Taylor, 1944; Bishop and Eldin, 1950). Significant advancements in the development of testing equipments, measurement systems and standardization of testing have been achieved since these early efforts.

In this study, strain-controlled consolidated-undrained static triaxial compression tests were performed in accordance with the "ASTM D4767-04 Standard Test Method for Consolidated-Undrained Triaxial Test on Cohesive Soils" (ASTM, 1998) which includes specimen preparation, mounting, saturation, consolidation and undrained loading for a typical test.

Samples are retrieved by large diameter thin-walled Shelby tubes diameter of which enabled extraction of two identical specimens from each cross-section by using thin walled cylindrical pipes. While one of these specimens is put into a desiccator to preserve its initial moisture content, and reserved for a cyclic test, the other one is used to determine their static shear strength response.

First, specimen is extracted from the thin-walled pipe using the sample ejector. The specimen is cut from both ends to obtain a 6.9 to 7.1 cm long specimen. After cutting operation, trimmed pieces are reserved for moisture content determination, which is carried out in accordance with the "ASTM D2216 Determining the Moisture Content of Soil Conventional Oven Method" (ASTM, 1998). Then, exact height (h_0) and diameter (d_0) of the specimen are determined by using a caliper. Diameter of the specimen is determined by making three measurements at different heights and then taking the average of them. Later, specimen is weighed. While performing these measurements, specimen should be handled very carefully to minimize any disturbance.

In the following step, specimen is covered with saturated filter paper to speed up pore water pressure dissipation during consolidation, and pore water pressure equalization within the specimen during shearing. It is important to saturate the filter

paper before covering, otherwise it absorbs the moisture from the specimen or prolongs back-pressure saturation process.

Before mounting the specimen to the testing apparatus, the system (including cell, back- and pore-pressure units) should be checked against leakage by applying high pressure and keeping valves closed. A thin coating of silicon grease is also applied on the pedestal for sealing and then, a rubber membrane is placed on the pedestal and it is fixed by using at least two O-rings, which also provides further sealing. A previously boiled porous stone is then placed on pedestals. Next, volume change (transducer) burette is filled with de-aired water and is connected to the cell pedestal from consolidation channel. After the volume change valve is opened, surface of porous stone becomes wet and then a thin film of water occurs on the surface of the porous stone. De-aired water is let to be circulated through the system until the pore pressure channel is completely saturated (i.e. when there is no visible air bubbles flowing along the channel), and then volume change valve is closed. While channel saturation is going on, the upper side of the membrane is rolled onto the membrane stretcher, then by applying some vacuum it is kept tight and stuck to the stretcher. After that, specimen is carefully placed on the cell pedestal and subsequently encased in the rubber membrane. It is very important to hold membrane smooth and untwisted since any disturbance may exert initial shear stress to the specimen which may change the response significantly. Another pre-boiled porous stone is placed on the specimen. Before placing the top cap on top of them, it is also saturated. Back pressure channel is used to achieve this, and then silicon grease is also applied on lateral surfaces of the cap and at least two O-rings are used to provide additional sealing.

After placement of top cap, the GEONOR type triaxial cell is lowered and cell ram is locked to the top cap which is especially necessary for cyclic tests, as it includes both compressive and tensile loads. While doing so, special care is required to prevent ram from compressing specimen, which results in additional disturbance. After assemblage of triaxial cell, water inlet valve and air vent are opened; and then cell is

filled with de-aired water. When water fills the cell completely, bleeding occurs and at that moment both water inlet and air vent are closed. Afterwards, position of cell ram is fixed.

After mounting the specimen, saturation process starts by applying approximately 30 kPa of cell pressure on specimen by using constant pressure unit. By recording the increase in pore water pressure, soils initial degree of saturation, which varies from 0.6 to 0.8 for tested specimens, can be determined. Below ground water table, soil is fully-saturated; however sampling results in a decrease in effective stress on soil which transforms dissolved air back to air bubles. The aim of saturation process is to simulate in-situ conditions by filling all voids in the specimen with water, without undesirable pre-stressing of the specimen or allowing the specimen to swell. In this study, the state of "full saturation" is achieved by back-pressure saturation technique, which involves simultaneous increases in the back (i.e. pore water) and confining pressures so that constant effective stress can be maintained throughout the specimen. Back-pressure is applied incrementally ($\sim$ 10 kPa) from the top cap. It takes a while to observe a pore pressure response at the bottom of the specimen, due to low permeability of tested materials. Luckily filter paper side drains accelerates this process. When back-pressure equalization takes place through the specimen, back pressure valve is closed and cell pressure is increased by 10 kPa to keep effective stress constant throughout the specimen. After each increment, degree of saturation is checked by calculating B value which is defined as follows:

$$B = \frac{\Delta u}{\Delta \sigma_3}$$
(3 - 1)

where Δu and $\Delta \sigma_3$ are the corresponding increases in pore water and cell pressures. Consistent with the related ASTM standard, this process is repeated until a minimum B value of 0.95 is obtained. When back-pressure saturation is completed, the specimen becomes ready for testing.

Specimens were consolidated to a horizontal to vertical effective stress ratios (σ'_h / σ'_v) varied in the range of 0.4 to 1.0; where the upper limit indicated isotropical consolidation. Horizontal stress is equal to the cell pressure in the triaxial compression tests and its value is adjusted by using the constant pressure cell units. For isotropically-consolidated specimens, cell ram is kept locked during consolidation to prevent effect of uplift due to increase in cell pressure. On the other hand, for anisotropically-consolidated specimens, vertical stress is applied via both cell pressure and dead weights which are held on hangers connected to the cell ram. However, before doing so, cell ram should be unlocked and additional dead weights must also be used to balance uplift force due to cell pressure. For both types of consolidation upon application of vertical and horizontal stresses, volume change valve is opened and volume change (ΔV_{cons}) is measured. For anisotropically-consolidated specimens, change in height (δh_{cons}) is also recorded during consolidation by using an external LVDT. The end of consolidation can be determined by closing the consolidation valve and observing pore water pressure readings. In case there is no increase in pore water pressure, it can be concluded that consolidation is completed. Similarly the process can also be observed from volume change burette. In case water level remains constant for a while, consolidation is accepted to be completed.

Following the saturation and consolidation stages, axial strain is applied at a rate of 1%/min until the specimen fails. During monotonic straining of specimens, i) cell pressure, ii) pore water pressure, iii) axial deformation in specimen, and iv) axial load were recorded at every 2 seconds. Each test has been carried on until reaching an axial strain which guarantees for specimen to exhibit a pronounced contractive or dilative response. Presentation of test results along with data processing efforts is available in the following sections of this chapter.

3.3.3 Cyclic Triaxial Testing

Cyclic triaxial test is probably the most widely used testing procedure to investigate dynamic response of soils. The basic philosophy of this test is the application of a deviator load in a cyclic manner. Cyclic triaxial test was first introduced by Seed and Lee (1966). In 1977, Silver published a paper defining the general rules and procedures of cyclic triaxial testing. Li et al. (1988) developed an automated cyclic triaxial apparatus in 1988. Through years, with the development of sophisticated data acquisition and servo systems, the reliability of collected data and control over test conditions have increased significantly. In 1996, "ASTM D5311 Standard Test Method for Load Controlled Cyclic Triaxial Strength of Soil" was published and then it was further updated in 2004. However, based on researchers' different aims, custom designed apparatuses and test procedures are often adopted.

Cyclic triaxial test is conducted by applying an all around pressure and then a deviator load in a cyclic manner in axial direction without allowing drainage. The combinations of stress conditions acting on a specimen were originally presented by Seed and Lee (1966) and are shown in Figure 3.3-2.

Cyclic triaxial testing has various advantages such as: i) stress and drainage conditions can be controlled easily, ii) measurement of axial and volumetric strains is trivial, and iii) there exist a huge database from previous studies. Yet, there also exist some criticism regarding the simulation of seismic loading conditions including; i) triaxial test does not reproduce in-situ K_0 conditions, ii) there exist stress concentrations at the ends of specimen, iii) 90° rotation of direction of the major principal stresses during the two halves of the loading cycle, and iv) in field, soil elements are subjected to multi-directional shaking; whereas cyclic triaxial tests simulates only unidirectional shaking. The second and fourth items are valid for most of the laboratory test procedures followed to study cyclic response of soils. The effects of the other items on cyclic strength of sands have been studied well (e.g. Seed, 1979); however for cohesive soils further attention is required.
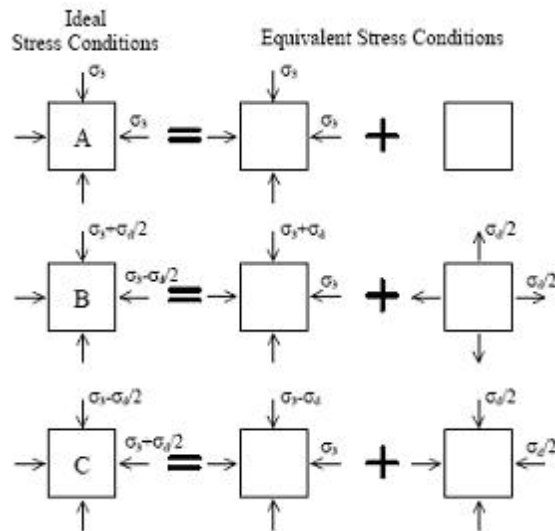
Figure 3.3-2. Equivalent and applied stress conditions during a cyclic triaxial test (Seed and Lee, 1966)

These are the issues often listed while criticizing cyclic triaxial testing, but it is important to notice that in case of an existing structure; different load conditions exist along potential failure surfaces beneath shallow foundations subjected to cyclic loading as presented in Figure 3.3-3. Recently, Sancio (2003) studied the stress conditions under a foundation during a cyclic loading and presented how these stress conditions and also corresponding Mohr Circle's varied for soil elements: i) in free-field, ii) under the center of a structure, and iii) under the corner (or edge) of a structure. Observations after fine-grained ground soil failure case histories of 1999 Adapazari earthquake revealed that the most critical stress combinations occurred under the corner of structures. At the edges of the footing, soil is subjected to i) vertically acting overburden (σ'_{v0}) and structure-induced stresses ($\Delta\sigma_{bldg}$) along with vertically acting cyclic stress due to the racking of structure ($\Delta\sigma_{v,cyc}$), ii) horizontally acting stress ($K_0 \cdot (\sigma'_{v0} + \Delta\sigma_{bldg} + \Delta\sigma_{v,cyc})$ where K_0 is the coefficient of earth pressure at rest), and also iii) shear stresses due to vertically propagating S-waves. These stresses and also the corresponding Mohr circle are presented in Figure

47

3.3-4. This loading pattern is quite complex and difficult to simulate in the laboratory, yet it is best approximated by the cyclic triaxial test.
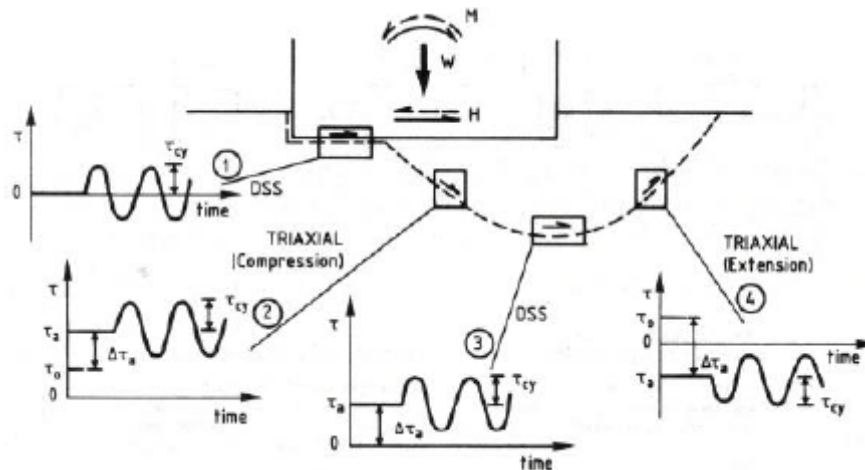
Figure 3.3-3. Simplified load conditions for soils elements along a potential failure surface beneath a shallow foundation (Andersen and Lauritzsen, 1988)

Typical procedure of a cyclic triaxial test is identical to a static test with the exception of undrained loading stage. Therefore, after preparing and mounting the specimen to the testing apparatus, it is saturated and consolidated by following the procedure given in Section 3.3.2.
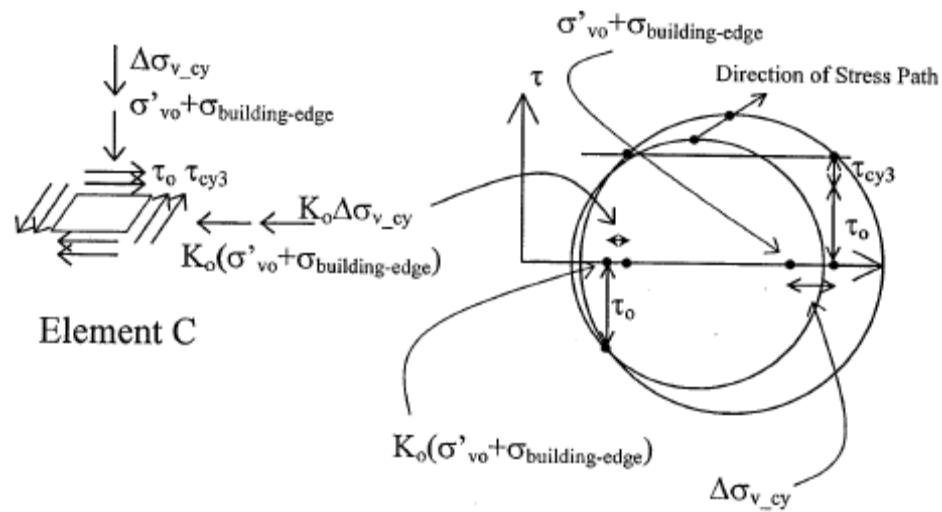
Figure 3.3-4. Idealized stress conditions under the corner of a building due to earthquake assuming inertial interaction between building and soil (Sancio, 2003)

Before adjusting the shape and amplitude of cyclic load, cell ram is locked so specimen is not disturbed while performing the following operations. First, the pressure supply unit and power function generator are opened. Position of vertical displacement LVDT is checked and load cell is assembled. Before connecting the load cell to pneumatic load actuator, actuator's position is stabilized using electro pneumatic transformer unit which also sets the net force on actuator to zero and prevents application of initial shear stresses on the specimen. The pattern and amplitude of cyclic load are adjusted via power function generator. In this testing program, only sine-waves are adopted as loading pattern, consistent with most of the literature. After these adjustments, cell ram is unlocked and cyclic loads are applied to the specimen with a frequency of 1 Hz considering the effects of loading rate on cyclic response of silt and clay mixtures, which was discussed thoroughly in Chapter 2. Specimen is subjected to 20 cycles of loading corresponding to the number of equivalent cycles of a moment magnitude (M_w) 7.5 earthquake, consistent with the findings of Liu et al. (2001).

During cyclic loading, i) cell pressure, ii) pore water pressure, iii) axial deformation and iv) axial load were recorded at every 25 milliseconds. After the 20th cycle, loading is stopped. Even after stopping the cyclic loading, an increase in pore water pressure was observed. As discussed in the previous chapter, this delayed response is mainly due to low permeability of specimens and adopted rapid loading rates. After excess pore water pressure stabilization occurs, the ultimate value of pore water pressure is recorded and then post-cyclic volume change (ΔV_{pc}) is measured per a differential pressure transducer (volume change burette). Similarly, the resulting residual axial deformation is also recorded for specimens consolidated anisotropically and it is used for the calculation of residual shear strain levels.

3.3.4 Processing Triaxial Test Data

Static and cyclic triaxial tests constituted an integral part of this study. Hence, effective presentation is essential for benefiting from the full potential of available data. Starting from the compiled raw test data, details of presentation and processing of static and cyclic test results will be discussed next.

3.3.4.1 Original Test Data

For both static and triaxial testing, direct measurements of four channels along with the time were recorded by TDG data acquisition system. Instrumentation of these channels was summarized in Table 3.3-1 along with the measured quantities.

Table 3.3-1. Instrumentation of triaxial testing system

MEASURED QUANTITY	CHANNEL #	INSTRUMENT	UNIT
Axial Load (F)	1	Load cell	N
Axial Deformation	2	LVDT	mm
Cell Pressure (σ_c)	3	Pressure transducer	atm
Pore Pressure (u)	4	Pressure transducer	atm

Besides these measurements, volume change in specimen is measured visually from the volume change instrument during the initial consolidation (ΔV_{cons}) and post-cyclic (ΔV_{pc}) consolidation stages.

These raw data will be used to obtain the parameters required for the presentation of test results.

3.3.4.2 Presentation of Static Triaxial Tests

Motivation behind performing static triaxial tests is to obtain the undrained shear strength (s_u) of the specimen under selected consolidation stress conditions before performing cyclic test. For strain-softening soils, defining the undrained shear strength is rather trivial due to a well-defined peak deviatoric stress ($\sigma_{d,peak}$). However, due to lack of a well-defined $\sigma_{d,peak}$ for strain-hardening materials, maximum effective stress obliquity (σ'_1 / σ'_3) criterion consistent with the recommendations of ASTM D4767-04 (ASTM, 1998) is adopted. Following is the definition of parameters required for effective presentation of static test results.

Deviatoric stress (σ_d) is defined by Equation (3 – 2).

$$\sigma_d = \frac{F^*}{A_{corrected}} - \Delta\sigma_{rm} - \Delta\sigma_{fpsd} \qquad (3 - 2)$$

where F^* is the total deviatoric load acting on the specimen including the initial anisotropic consolidation load, if it exists. $\Delta\sigma_{rm}$ and $\Delta\sigma_{fpsd}$ are the corresponding rubber membrane and filter paper side drain corrections, respectively, which are determined according to methods proposed by Duncan and Seed (1967) and La Rochelle (1967), respectively. $A_{corrected}$ is the area of the specimen during shear and defined as follows:

$$A_{corrected} = \frac{A_0{}^*}{1 - \varepsilon_a} \qquad (3 - 3)$$

where $A_0{}^*$ is the area of specimen at the start of shear and ε_a is the axial strain which is defined as follows:

$$\varepsilon_a = \frac{\delta h}{h_0{}^*} \qquad (3 - 4)$$

where $h_0{}^*$ is the initial height of specimen at the start of shear and δh^* denotes the change in height during test. For isotropically-consolidated specimens $h_0{}^*$ is adopted as the initial height of specimen before consolidation (h_0); whereas for anisotropically-consolidated specimens change in height during consolidation (δh_{cons}) should also be taken into account when calculating $h_0{}^*$. Similarly, for isotropically-consolidated specimens, $A_0{}^*$ is assumed to be equal to initial area of specimen (A_0); whereas for anisotropically-consolidated specimens $A_0{}^*$ is calculated as follows:

$$A_0{}^* = \left(\frac{\pi \cdot d_0{}^2 \cdot h_0}{4} - \Delta V_{cons} \right) \cdot \frac{1}{h_0{}^*} \qquad (3 - 5)$$

where ΔV_{cons} is change in volume of specimen during consolidation.

Stress obliquity is defined as the ratio of major and minor effective principal stresses, σ'_1 and σ'_3, respectively. For triaxial compression tests, σ'_1 and σ'_3 are equal to vertical and horizontal effective stresses, respectively; and they are defined as follows:

$$\sigma'_1 = \sigma_c + \sigma_d - u \qquad (3 - 6)$$

$$\sigma'_3 = \sigma_c - u \qquad (3 - 7)$$

where σ_c and u are cell and pore water pressures, respectively.

Mean effective stress (p') and half of the deviatoric stress (q) are used for the presentation of stress path plots and they are defined as given in Equations $(3 - 8)$ and $(3 - 9)$, respectively.

$$p' = \frac{\sigma'_1 + \sigma'_3}{2} \qquad\qquad (3 \text{ - } 8)$$

$$q = \frac{\sigma_d}{2} \qquad\qquad (3 \text{ - } 9)$$

An illustrative test result of an ML type (LL=31 and PI=6) specimen retrieved from Adapazari, consolidated isotropically under an effective confinement pressure of 100 kPa is presented in Figure 3.3-5 based on the parameters defined in Equations $(3 - 2)$ to $(3 - 9)$.

As revealed by Figure 3.3-5, $\sigma_{d,peak}$ is observed at around 12 % axial strain and estimated as 277 kPa. The maximum effective stress obliquity, $(\sigma'_1 / \sigma'_3)_{max}$, is recorded at 5.5 % axial strain and corresponding σ_d is determined as 205 kPa from the σ_d vs. ε_a plot. Luckily, both peak deviatoric stress and maximum stress obliquity criteria produce comparable s_u values as 138 and 103 kPa, respectively. In this case, s_u is accepted as 138 kPa since a well-defined $\sigma_{d,peak}$ exists. From the stress path (i.e., q - p' plot), the peak effective angle of friction (ϕ') is estimated as 40º, which may seem to be unexpectedly high but consistent with the findings of other researchers (e.g.: Sancio, 2003) due to extreme dilative nature of Adapazari silts.

Results of all individual static triaxial tests are presented in Appendix B.
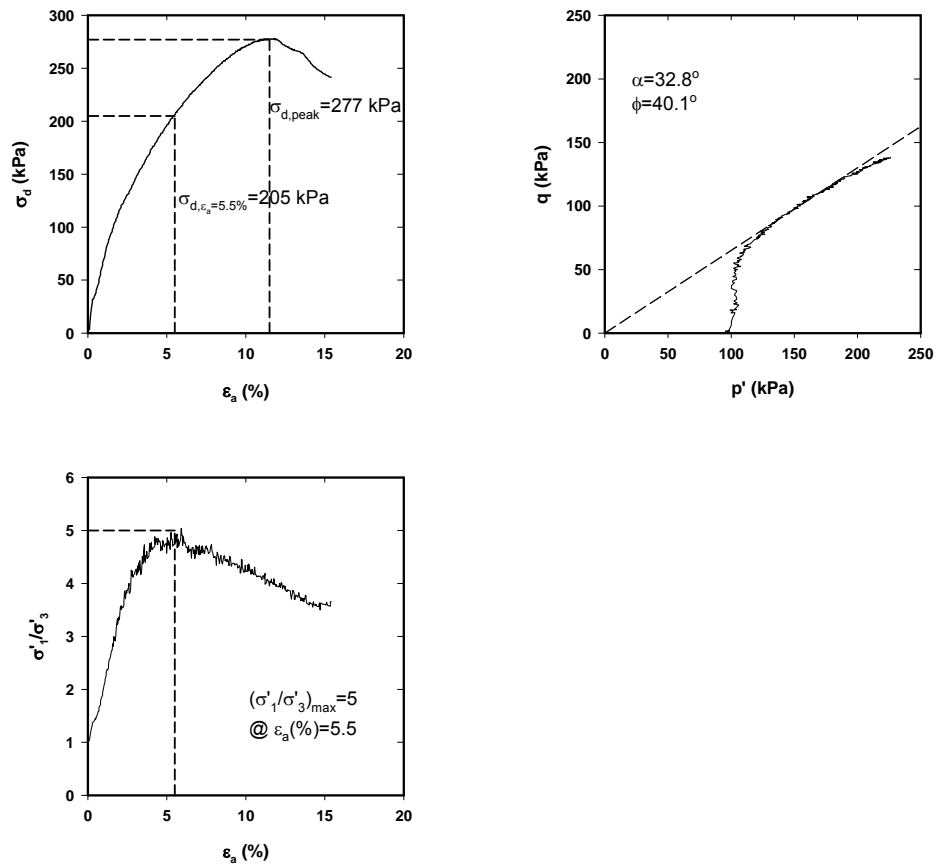
Figure 3.3-5. Presentation of a typical static triaxial test

3.3.4.3 Presentation of Cyclic Triaxial Tests

Results of cyclic triaxial tests are presented in four identically scaled figures of i) normalized vertical effective stress (*NVES*) vs. stress ratio (*SR*), ii) number of cycles (*N*) vs. excess pore water pressure ratio (r_u), iii) shear strain (γ) vs. stress ratio (*SR*), and iv) number of cycles (*N*) vs. shear strain (γ). It is believed that these four plots summarize the cyclic response in a complete manner. Next, parameters required for the construction of these plots are introduced.

NVES is defined as a function of σ_c , u , $\sigma_{c,0}$ and σ_d as follows:

$$NVES = \frac{\sigma_c - u + \sigma_d}{\sigma_{c,0}} \qquad (3-10)$$

It should be noted that throughout the test unless quite large strains are observed, the value of σ_c remains equal to $\sigma_{c,0}$ (σ_c at the start of cyclic loading).

SR is analogous to cyclic stress ratio (CSR) which is generally used to represent the level of cyclic stresses. However, since the pioneer work of Seed and Chan (1966) As given in Equation (3 − 11), SR is conventionally defined as a function of s_u rather than vertical effective stress (σ'_v) as shear strength of cohesive soils does not solely depend on σ'_v.

$$SR = \frac{\tau_{st} + \tau_{cyc}}{s_u} \qquad (3-11)$$

where s_u is the undrained shear strength of tested specimen obtained from corresponding static triaxial test for selected consolidation stress conditions, τ_{st} and τ_{cyc} are static and cyclic shear stresses, respectively and they are defined by Equations (3 − 12) and (3 − 13), respectively.

$$\tau_{st} = \frac{(F_{st,0}/2)}{A_{corrected}} \qquad (3-12)$$

where $F_{st,0}$ is the axial deviatoric load applied in anisotropic consolidation stage, and it is equal to zero for isotropic consolidation. $A_{corrected}$ can be determined by Equation (3 − 3).

$$\tau_{cyc} = \frac{(F_{cyc}/2)}{A_{corrected}} \qquad (3-13)$$

where F_{cyc} is the cyclic deviator stress.

Shear strain (γ) is defined in terms of ε_a as given by Equation (3 – 14) since in conventional triaxial equipments, only axial deformations can be measured.

$$\gamma = 1.5 \cdot \varepsilon_a \qquad (3 - 14)$$

The coefficient relating shear and axial strains are derived based on elasticity theory with undrained loading assumption. The validity of this coefficient was proven by Cetin et al. (2009) per results of a discriminant analysis for saturated clean sands. Same coefficient is also conventionally used for cohesive soils under stress-controlled loading; whereas for strain-controlled loading a value of $\sqrt{3}$ was recommended by Vucetic and Dobry (1988).

Excess pore water pressure ratio (r_u) is defined as follows:

$$r_u = \frac{u}{\sigma'_{c,0}} \qquad (3 - 15)$$

Last but not least, post-cyclic volumetric (reconsolidation) strain ($\varepsilon_{v,pc}$) is defined as:

$$\varepsilon_{v,pc} = \frac{\Delta V_{pc}}{V_0^*} \qquad (3 - 16)$$

where ΔV_{pc} is the volume change after cyclic shearing due to dissipation of excess pore water pressure, and V_0^* is the volume of specimen before cyclic loading.

An illustrative cyclic triaxial test result is presented in Figure 3.3-6 for an ML type soil specimen with PI of 9 and LL of 26. Its w_c / LL value was determined as 0.9 (considering the volume change after consolidation) fulfilling the potentially liquefiable criteria of both Seed et al. (2003) and Bray and Sancio (2006). The specimen was consolidated isotropically under a confinement pressure of 110 kPa and subjected to cyclic deviatoric stress of 65 kPa. In these four-way plots, the upper left plot is the representation of stress path followed during cyclic testing. However, due to rapid loading rate and delayed pore pressure responses due to equalization

problem, stress path plots may seem to be awkward. Thus, this plot may not be informative for especially high plasticity soils, but still the contraction and dilation cycles are traceable. The upper right plot shows the stress-strain relationship and stiffness degradation of the specimen. Moreover, the cyclic mobility and cyclic liquefaction type soil responses can also be observed in the form of "football" and "banana loops", respectively from this plot. The lower right plot presents the accumulation of shear strain with loading cycles, and it gives probably the most important information for this study. For each test, the double amplitude cyclic shear strain value ($\gamma_{max,20}$) is recorded from this plot at the end of 20th loading cycle. On the other hand, the lower left plot shows how excess pore water pressure ratio changes with loading cycles. The problems due to delayed response regarding the construction of stress path are also valid for this plot. As stated in Section 3.3.3, at the end of cyclic loading the ultimate stabilized value of excess pore water pressure was recorded for each test. Then, for each cycle peak values of r_u ($r_{u,N}$) is re-calculated by following a linear correction scheme based on this ultimate value. These re-calculated peak $r_{u,N}$ values are also presented on this lower left figure by a dashed line, and they are further used in the development of cyclic-r_u model, which will be introduced in Chapter 5. If specimen "liquefies" and well-defined contraction-dilation cycles (i.e. banana loops) occur, then stress – strain plot can be used to determine minimum cyclic shear strength ($s_{u_{cyc,min}}$) of specimen. In case of significant remolding and excess pore water pressure generation, only the cohesive bonds between soil minerals contribute to shear strength which could be determined based on breadth of the stress – strain loop corresponding to zero effective stress range.

The complete documentation of cyclic triaxial test results is available in Appendix C; whereas, Table 3.3-2 summarizes the resulting database including the maximum double amplitude cyclic shear strain (γ_{max}), post-cyclic volumetric (reconsolidation) volumetric strain ($\varepsilon_{v,pc}$) and residual shear strain (γ_{res}) at the end of 20th loading

cycle, and post-liquefaction shear strength ($s_{u_{cyc,min}}$) along with specimen's index and state parameters; *LL*, *PI* and w_c / LL, ratio of horizontal to vertical consolidation stresses ($\sigma'_{3,c} / \sigma'_{1,c}$), corresponding undrained shear strength (s_u), applied static and cyclic shear stress ratios, τ_{st} / s_u and τ_{cyc} / s_u, respectively. The corresponding locations of these data are also schematically presented in Figure 3.3-7. If the s_u of the specimen is selected as the capacity term, then the ratio of τ_{cyc} / s_u (x-axis) and τ_{st} / s_u (y-axis) on this figure indicate the ratio of capacity used by cyclic and static loads (i.e. demands), respectively. As also revealed by this figure, for some tests either applied τ_{cyc} or the sum of τ_{st} and τ_{cyc} exceeds s_u of the specimen. For these cases, it is possible to interpret occurrence of failure even at the end of first cycle; however, due to their rate dependent response, cohesive soils can show greater resistance to cyclic loads and do not fail instantaneously after exceedence of statically determined failure loads.

Cyclic double amplitude maximum shear strain and corrected excess pore water pressure ratio pairs are presented in Figure 3.3-8.
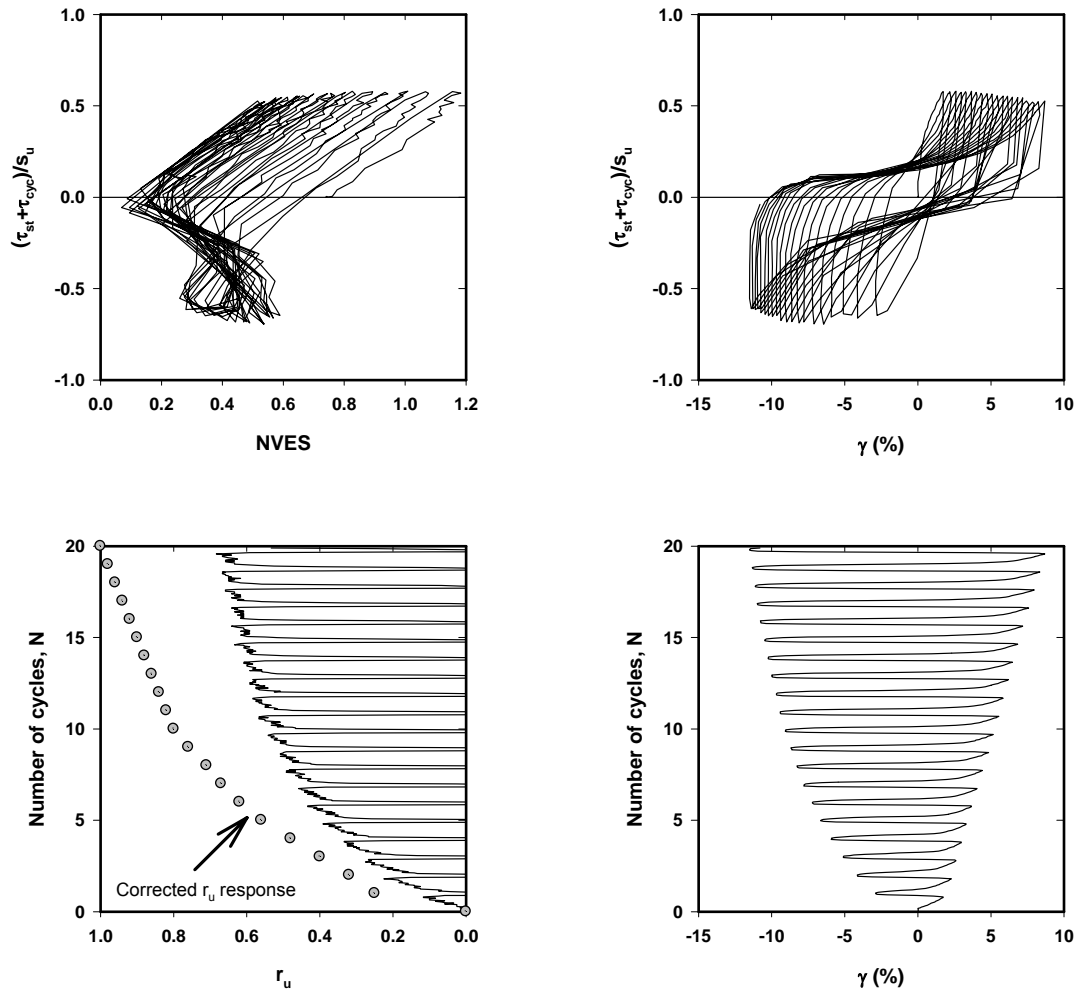
Figure 3.3-6. Presentation of a typical cyclic triaxial test

Table 3.3-2. A summary of triaxial test parameters and results

Test ID	LL	PI	w_c/LL	$\sigma'_{3,c} / \sigma'_{1,c}$	s_u (kPa)	τ_{cyc}/s_u	τ_{st}/s_u	N_{app}	$s_{u,cyc,min} / s_u$	γ_{max} (%)	$\varepsilon_{v,pc}$ (%)	γ_{res} (%)
CTXT1	36	14	1.08	1.0	82	0.60	0.00	20	-	11.2	-	-
CTXT2	39	18	1.00	0.9	72	0.60	0.10	20	-	5.5	-	0.10
CTXT3	37	13	1.06	0.7	110	0.52	0.30	20	0.13	13.1	-	1.20
CTXT4	50	26	0.72	0.7	96	0.34	0.26	20	-	0.5	-	0.06
CTXT5	35	8	0.96	1.0	107	0.62	0.00	20	-	20.1	-	-
CTXT6	44	19	0.83	0.6	94	0.54	0.39	20	-	2.3	0.3	1.00
CTXT7	40	20	0.75	0.6	115	0.28	0.43	20	-	0.4	0.05	0.11

Table 3.3-2. cont'd. A summary of triaxial test parameters and results

Test ID	LL	PI	w_c/LL	$\sigma'_{3,c}/\sigma'_{1,c}$	s_u (kPa)	τ_{cyc}/s_u	τ_{st}/s_u	N_{app}	$s_{u,cyc,min}/s_u$	γ_{max} (%)	$\varepsilon_{v,pc}$ (%)	γ_{res} (%)
CTXT9	41	18	0.74	1.0	96	0.59	0.00	20	-	3.8	-	-
CTXT10	41	18	0.70	0.4	166	0.30	0.59	20	-	0.5	-	0.82
CTXT11	35	9	0.96	0.7	74	0.74	0.45	20	0.17	14.7	-	1.30
CTXT12	35	9	0.89	0.6	101	0.60	0.34	20	0.17	10.7	-	2.08
CTXT13	32	8	1.07	0.5	97	0.53	0.43	20	0.1	11.1	-	7.70
CTXT14	34	10	0.71	0.4	316.6	0.16	0.19	20	-	0.7	-	3.14
CTXT15	28	7	0.82	1.0	23	1.17	0.00	20	-	14.45	2.21	-
CTXT16	31	10	0.84	1.0	40	1.13	0.00	20	-	13.3	1.4	-
CTXT18	42	16	0.58	0.8	85	0.71	0.35	20	-	1.2	0.15	0.22
CTXT19	37	8	0.92	0.6	132	0.35	0.26	20	-	5.4	-	2.04
CTXT20	40	17	0.78	0.6	105	0.43	0.33	20	-	0.5	0.14	0.08
CTXT21	40	14	0.80	0.7	108.5	0.51	0.18	20	-	5.4	1.04	2.04
CTXT22	44	15	0.89	0.7	92	0.47	0.22	20	-	6.9	1.5	1.87
CTXT23	34	16	1.02	0.9	40	0.83	0.13	9	-	26.9	-	-
CTXT24	25	9	0.96	0.8	82.5	0.38	0.12	14	-	21.8	-	-
CTXT25	27	11	0.43	0.7	85	0.45	0.29	20	-	0.7	0.2	0.25
CTXT26	28	10	0.99	0.7	78	0.42	0.17	13	-	26.1	-	-
CTXT27	52	27	0.73	0.7	90	0.44	0.19	20	-	1.8	0.29	0.02
CTXT28	30	8	0.95	1.0	102	0.37	0.00	20	-	6.2	1.8	-
CTXT29	30	5	1.02	1.0	102	0.55	0.00	20	-	23.6	2.7	-
CTXT30	40	16	0.62	0.5	119	0.25	0.50	20	-	0.2	0.15	0.05
CTXT31	38	14	0.71	0.5	119	0.40	0.50	20	-	0.8	0.4	1.10
CTXT32	34	10	0.79	0.8	145	0.26	0.10	20	-	2.6	0.7	0.87
CTXT33	30	5	0.93	0.8	145	0.23	0.11	20	0.14	8.44	2	2.72
CTXT34	30	5	0.70	0.8	145	0.21	0.10	20	-	0.4	0.15	0.20
CXTT35	60	34	0.48	0.4	80	0.45	0.71	20	-	1.3	0.15	-
CTXT36	60	32	0.63	0.6	70	0.43	0.53	20	-	1.2	0.3	0.58
CTXT37	69	42	0.54	1.0	68.5	0.58	0.00	20	-	2.77	0.37	-
CTXT38	67	40	0.50	0.5	108	0.51	0.40	20	-	0.85	0.44	2.69
CTXT40	47	21	0.73	1.0	42.5	0.59	0.00	20	-	3.11	-	-
CTXT42	49	22	0.90	0.9	40	1.38	0.12	20	-	38.8	3.5	-
CTXT43	68.4	36.3	0.25	0.5	117	0.19	0.29	20	-	0.18	0.16	0.06
CTXT44	60	30.6	1.07	0.9	44	0.80	0.17	20	-	10.24	1.62	0.63
CTXT45	66	35	0.89	0.9	44	0.98	0.17	20	-	15.45	0.89	1.76
CTXT46	87	53.4	0.77	0.7	58	0.71	0.43	20	-	4.16	1.48	1.16
CTXT47	82.9	49.3	0.75	0.5	90	0.38	0.63	20	-	1.01	0.31	1.59
CTXT48	78	45.9	0.97	0.4	85	0.32	0.71	20	-	1	1.06	2.77
CTXT49	74	50	0.67	0.3	110	0.32	0.85	20	-	1.1	0.44	-
CTXT50	68.5	42.8	0.69	0.5	82.5	0.79	0.65	20	-	8.22	-	-

Table 3.3-2. cont'd. A summary of triaxial test parameters and results

Test ID	LL	PI	w_c/LL	$\Sigma'_{3,c}$ / $\sigma'_{1,c}$	s_u (kPa)	τ_{cyc}/s_u	τ_{st}/s_u	N_{app}	$s_{u,cyc,min}$ / s_u	γ_{max} (%)	$\varepsilon_{v,pc}$ (%)	γ_{res} (%)
CTXT51	62	37	0.89	1.0	39.2	1.02	0.00	20	-	6.99	0.6	-
CTXT52	93.5	58.9	0.56	0.6	62	0.81	0.63	20	-	3.97	0.37	1.53
CTXT53	58.2	34.3	0.52	0.6	67.4	0.31	0.58	20	-	0.31	0.45	0.40
CTXT54	75	41.5	0.77	1.0	45	1.09	0.00	20	-	11.44	0.83	0.06
CTXT55	73.5	42.3	0.73	0.5	84	0.30	0.58	20	-	0.54	0.6	0.87
CTXT56	71.7	41.1	0.74	0.6	49.3	0.51	0.51	20	-	1.23	0.63	1.21
CTXT58	66.8	40.7	0.71	0.4	92	0.33	0.63	20	-	0.72	0.23	2.40
CTXT59	71	40.7	0.61	0.7	52	0.62	0.38	20	-	1.43	0.62	1.08
CTXT60	82.6	49.3	0.68	1.0	46.5	0.73	0.00	20	-	3.6	0.77	-
CTXT61	66	36.5	0.64	0.6	52	0.55	0.66	20	-	1.16	0.63	2.96
CTXT62	66	36.5	0.68	0.6	52	0.81	0.66	20	-	3.94	1.1	3.79
CTXT63	48	22	0.69	0.5	60	0.57	0.80	20	-	0.37	0.29	0.86
CTXT64	47.8	21.7	0.62	0.7	82.5	0.52	0.30	20	-	1.39	0.74	1.61
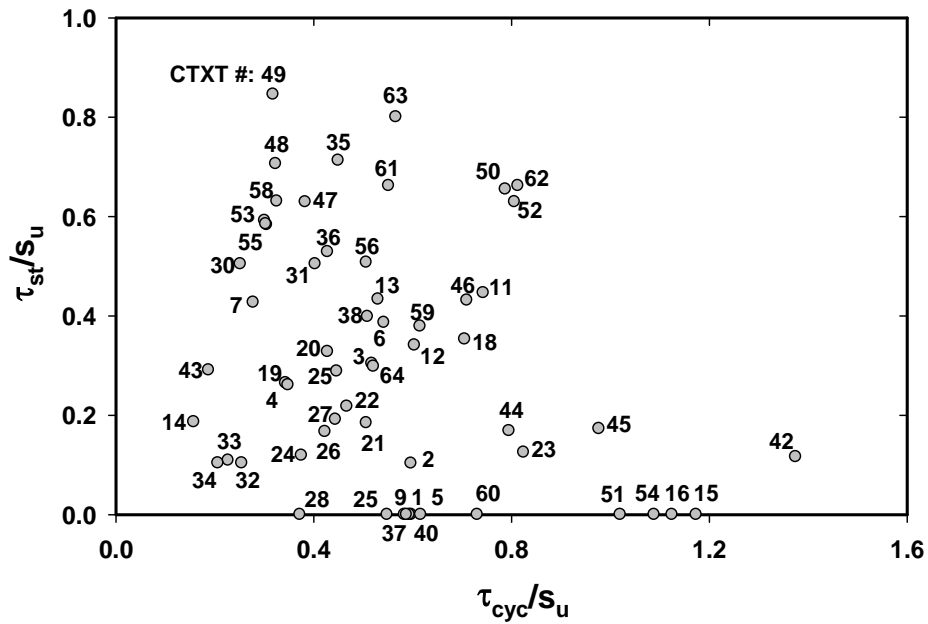
Figure 3.3-7. Summary of test data on normalized static and cyclic shear stress domain
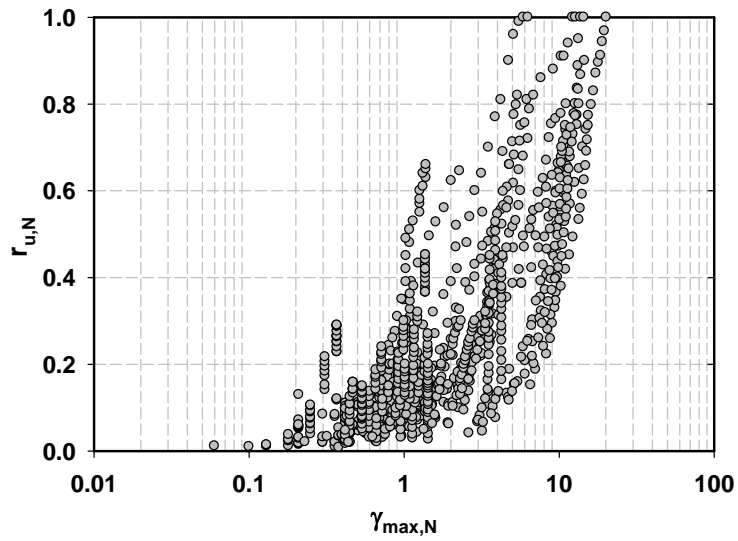
Figure 3.3-8. $r_{u,N}$ vs. $\gamma_{max,N}$ database

3.4 OEDOMETER TESTS

For the purpose of determining the consolidation stress history of specimens, consolidation tests were performed in accordance with "ASTM D 2435-04 Standard Test Method for One-Dimensional Consolidation Properties of Soils Using Incremental Loading" (ASTM, 1998). As pointed out in Chapter 2, the most of previous research studies have benefited from the consolidation theory to establish post-cyclic volumetric straining models. Consequently, the results of oedometer tests become crucial as input parameters. In this study, post-cyclic volumetric straining potential is assessed by not only 1-D consolidation theory, but also also adopting an improved alternative new methodology. The available oedometer test data is presented in Table 3.4.1 in terms of pre-consolidation pressure (p'_0), initial void ratio (e_0), compression and recompression indices, C_c and C_r, respectively.

Table 3.4-1. Summary of consolidation test data

Sample ID	Test ID	e_0	p'_c (kPa)	C_c	C_r
GD2-2B	CTXT6	1.118	150	0.465	0.028
GB1-5M	CTXT15	1.075	110	0.31	0.025
GB1-5B	CTXT16	1.075	110	0.31	0.025
BF1-3T	CTXT18	1.129	125	0.324	0.031
BF1-3M	CTXT20	1.129	125	0.324	0.031
BH4-1B	CTXT21	0.904	250	0.196	0.018
BH4-1M	CTXT22	0.904	250	0.196	0.018
SK7-1B	CTXT25	0.974	130	0.362	0.029
GA1-5B	CTXT31	0.933	110	0.31	0.025
BH6-3B	CTXT43	1.317	130	0.465	0.047
BH6-3M	CTXT44	1.317	130	0.465	0.047
BH6-3T	CTXT45	1.317	130	0.465	0.047
BH4-3M	CTXT46	1.475	90	0.531	0.047
BH4-3B	CTXT47	1.475	90	0.531	0.047
BH4-3T	CTXT48	1.475	90	0.531	0.047
BH1-5M	CTXT51	1.228	82	0.498	0.043
BH1-5T	CTXT52	1.228	82	0.498	0.043
BH1-5B	CTXT53	1.228	82	0.498	0.043
BH7-2M	CTXT54	1.224	80	0.332	0.0255
BH7-2B	CTXT55	1.224	80	0.332	0.0255
BH7-2T	CTXT56	1.224	80	0.332	0.0255
BH3-4M	CTXT58	1.364	105	0.465	0.0396
BH7-4M	CTXT59	1.262	90	0.382	0.0405
BH7-4T	CTXT60	1.262	90	0.382	0.0405
BH7-4B	CTXT61	1.262	90	0.382	0.0405
BH7-4B1	CTXT62	1.262	90	0.382	0.0405

A complete documentation of oedometer test results is presented in Appendix D, in terms of e vs. $\log(p')$ curves. Test results indicated that pre-consolidation pressure (p'_c) vary in the range of 100 to 250 kPa, and 80 to 130 kPa for the samples retrieved from Adapazari and Ordu regions, respectively.

3.5 DATA COMPILATION FROM LITERATURE

For the purpose of increasing the number and variability of test data, literature has been reviewed carefully, and more than 250 individual tests have been extensively

studied from various data sources, including Seed and Chan (1966), Castro and Christian (1976), Idriss et al. (1978), Azzouz et al. (1989), Ansal and Erken (1989), Zergoun and Vaid (1994), Pekcan (2001), Sancio (2003), Chu (2006), Erken et al. (2006), Donahue (2007). As a result, a total of 63 maximum double amplitude shear and 38 post-cyclic volumetric strains, 40 $r_{u,N}$ vs. $\gamma_{max,N}$ histories, 47 post-liquefaction shear strength and 108 index test data along with their corresponding cyclic test results were possible to be used.

Reasons for filtering out some test data vary. For the development of cyclic shear strain assessment model, filtering reasons include: i) missing or inconsistently reported values of one or more of the following data; LL, PI, w_c, consolidation stress state ($\sigma'_{3,c}$ and $\sigma'_{1,c}$) and corresponding shear strength, applied τ_{st} and τ_{cyc}, maximum double amplitude shear strain at 20th loading cycle or complete strain – number of cycles history, and ii) tests adopting a loading frequency other than 1 Hz. On the other hand, for post-cyclic volumetric straining model, filtering criteria can be listed as: i) missing pairs of post-cyclic volumetric and maximum double amplitude shear strains along with related values of LL, PI and w_c, ii) missing values of C_r, e_0 and final r_u, and ii) tests adopting loading frequency other than 1 Hz. For residual shear strain model, following test data is filtered out; i) missing pairs of residual and maximum shear strains along with applied τ_{st} and τ_{cyc}, PI and s_u, and ii) initial τ_{st} is equal to zero. For the development of excess pore water pressure model, $r_{u,N}$ vs. $\gamma_{max,N}$ history is needed and simply if this history along with related values of LL, PI and w_c are not available, then this data is filtered out. For the $s_{u,liq}$ database, data which cannot satisfy the following criteria are filtered out; i) well-defined contraction-dilation cycles should occur, and ii) corresponding LL, PI and w_c data should be available. Grain size distribution data along with corresponding values of LL, PI, w_c and also related cyclic test results are used for establishing new methods

to assess liquefiability of fine-grained soils and to evaluate existing liquefaction susceptibility criteria.

After filtering out some data based on listed screening criteria, Pekcan (2001), Sancio (2003), Chu (2006) and Donahue (2007) remained as the data sources of this study.

Pekcan (2001) database presented results of stress-controlled triaxial tests performed on the undisturbed samples of Adapazarı silt and clay mixtures. As the purpose of that study was to assess the liquefaction potential of Adapazarı soils, only cyclic triaxial tests were performed on specimens without mentioning the undrained shear strength of specimens which is essential part of this study. Fortunately, a detailed site investigation study was performed as part of a PEER project (Bray et al., 2003) at those sites, from which tested samples were retrieved. Hence either a related in-situ vane shear or pocket penetrometer or at least a SPT-blow count value is available for this data set. While in-situ vane shear test directly gives undrained shear strength, pocket penetrometer test gives unconfined compressive strength (q_u) which is twice the value of s_u by definition. When none of these tests are available, SPT-N blow counts were used to estimate shear strength using the following simple relation proposed by Stroud (1974);

$$s_u = f_1 \cdot N_{60} \qquad\qquad (3-17)$$

where N_{60} is the procedure corrected SPT-N value and f_1 is defined as a function PI as presented in Figure 3.5-1. As consolidation stresses are selected in accordance with the field conditions, those s_u estimates are directly used in calculation of static and cyclic shear stress ratios.

Sancio (2003) database is the primary data source of this study. Sancio (2003) presents results of stress controlled cyclic triaxial and simple shear tests performed on undisturbed specimens retrieved from Adapazari city. The aim of that research was to establish liquefaction susceptibility criteria for fine-grained soils, and this

database was utilized by the recent works of Seed et al. (2003) and Bray and Sancio (2006). Most of the samples were tested by using cyclic triaxial equipment; whereas a limited number of specimens (a total 6 specimens) were tested under simple shear conditions. Similar to Pekcan (2001), Sancio (2003) did not report s_u of specimens tested under cyclic loading conditions. Thus, results of available site investigation data (Bray et al., 2003) was used in conjunction with the available consolidation test data of Sancio (2003) for the estimation of s_u. For most of the specimens, there exist results of field vane shear, pocket penetrometer, SPT and CPT tests. While field vane shear and pocket penetrometer provides s_u values directly, existing correlations are used to predict s_u values based on SPT and CPT data. For the SPT data, correlation of Stroud (1974) is used again; whereas for CPT data following formula is utilized.

$$s_u = \frac{q_t - \sigma_v}{N_{kt}} \qquad (3-18)$$

where q_t is CPT cone tip resistance, σ_v is total vertical stress and N_{kt} is the cone factor varies from 10 to 20 and its average value (15) is adopted in this study (Lunne et al., 1997).

In case when more than one field test data is available, field vane shear test is accepted as the main reference; yet the estimates from other test data are also taken into account in s_u estimations. However, if there is a significant difference between those estimates for a data point, this data was discarded directly from the database. Oedometer test data of Sancio (2003) indicated that Adapazarı soils are slightly over-consolidated and pre-consolidation pressure varies from 150 to 250 kPa which was significantly higher than the consolidation stress conditions adopted by testing program of Sancio (2003); therefore these s_u estimates are directly used in the analysis.

This data source is the only one reporting post-cyclic volumetric strain data, and similarly all of the $s_{u,liq} / s_{u,st}$ data is also compiled from this database.
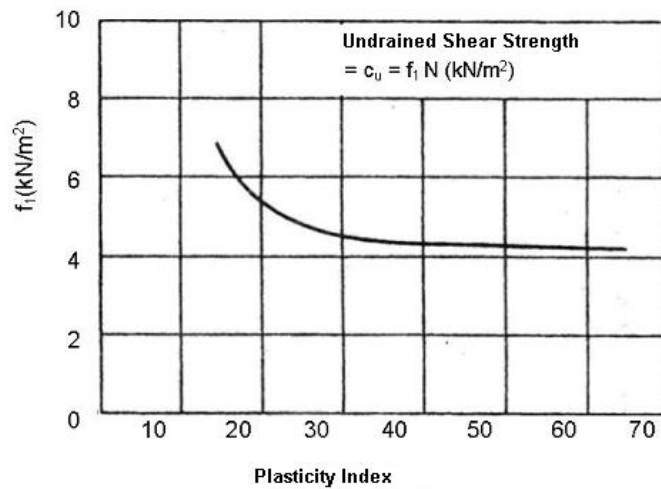
Figure 3.5-1. Relation between f_1 and PI (Stroud, 1974)

Chu (2006) performed stress-controlled cyclic triaxial tests on undisturbed silt and clay mixtures retrieved from sites where liquefaction induced ground deformations were documented after 1999 Taiwan Chi-Chi earthquake. The aim of that study was to assess the cyclic softening potential of those soils. Although limited number of specimens was tested, corresponding s_u values were documented by the author. However, almost perfectly symmetrical nature of shear strain – number of cycle histories, some of the results were judged to be questionable for specimens of quite low plasticity (< 3), which were subjected to initial static shear stresses. .

The final data source is Donahue (2007), where stress-controlled simple shear tests performed on laboratory reconstituted low plasticity silt clay mixtures were presented. This recent study aimed to determine factors affecting cyclic response and liquefaction susceptibility of fine-grained soils. Donahue (2007) tested laboratory reconstituted specimens using slurry deposition and in-place wet pluviation methods. It is well known that reconstituted and undisturbed specimens may exhibit different responses mainly due to significant differences between the time of confinement and consequent cementation, but it is assumed that time of confinement affects also the

monotonic shear strength of the specimens and consequently counterbalance its effects on cyclic response. Donahue (2007) reported related monotonic test data which was used in s_u determination. Only a limited number of data could be compiled from this study as most of tests were performed under a loading frequency of 0.005 Hz. Yet these data are considered to be valuable as it contains simple shear test results on reconstituted specimens, which definitely increase data variability.

A complete summary of the compiled databases is presented in Table 3.5-1, which lists test name (as given by the original data sources), available information regarding soil index properties (LL, PI, w_c / LL, FC, and percent finer than 2 and 5 μm), consolidation stress conditions ($\sigma'_{3,c} / \sigma'_{1,c}$), undrained shear strength (s_u), applied static and cyclic stress ratios (τ_{st} / s_u and τ_{cyc} / s_u, respectively), applied number of loading cycles and resulting maximum shear strain at the end of 20th loading cycle, and end of cyclic shearing (γ_{max} and $\gamma_{max,f}$, respectively), post-cyclic volumetric strain ($\varepsilon_{v,pc}$), oedometer test data in terms of e_0, p'_c and C_r, post-cyclic residual shear strain (γ_{res}) and ratio of post-liquefaction shear strength to initial monotonic shear strength ($s_{u_{cyc,min}} / s_{u,st}$). Moreover Figure 3.5-2 presents $r_{u,N}$ vs. $\gamma_{max,N}$ data pairs obtained from these tests.

As this brief introduction on data sources reveals, all of these studies focused on different aspects of the problem. As a result the needs of these different purposes are slightly diverse, e.g. most of these studies do not need monotonic shear strength for their aims, for this reason some of the reported data had to be discarded due to reasons other than data quality issues. It is also obvious that most of the tests were performed on "undisturbed" Adapazarı soils under isotropic consolidation conditions. However, it is still believed that this additional database compilation efforts increases not only the quantity of data, but also their variability by involving tests performed i) at different laboratories, ii) by using different equipments, and iii) to some extent on specimens of different origin.

Table 3.5-1. Summary of compiled database

Data Source	Test ID	FC	<2 μm	<5 μm	LL	PI	w_c/LL	$\sigma'_{3,c}/\sigma'_{1,c}$	s_u (kPa)	τ_{cyc}/s_u	τ_{st}/s_u	N_{app}	$\gamma_{max,20}$ (%)	e_0	p'_c (kPa)	C_r	$\gamma_{max,f}$ (%)	$\varepsilon_{v,pc}$ (%)	γ_{res} (%)	$s_{u,cyc,min}/s_{u,st}$
Pekcan (2001)	C1-1*	99	36.6	51.8	58	23	0.67	1	50	0.5	0	20	1.95	-	-	-	-	-	-	-
	C1-3*	94	21.5	32.9	34	25	1.06	1	50	0.7	0	20	5.87	-	-	-	-	-	-	-
	D2-1*	73	14.3	20.9	30	23	1.07	1	50	0.6	0	20	9.71	-	-	-	-	-	-	-
	D2-2	78	17.1	25.9	31	8	0.94	-	-	-	-	-	-	-	-	-	-	-	-	-
	E1-2	99	31.1	53.8	61	32	0.64	-	-	-	-	-	-	-	-	-	-	-	-	-
	E1-3*	99	35	52.2	62	35	0.52	1	52.5	0.6	0	20	1.65	-	-	-	-	-	-	-
	G2-1*	93	9.7	17.4	26	8	1	1	74	0.4	0.2	20	5.55	-	-	-	-	-	0.3	-
	G2-3	97	9.5	18.4	58	30	0.84	-	-	-	-	-	-	-	-	-	-	-	-	-
	J3-2*	87	9.7	15.1	30	6	1	-	-	-	-	-	-	-	-	-	-	-	-	-
Sancio (2003)	A5-P2A	51	10	11	27	NP	1.17	0.67	38	0.5	0.3	20	3	-	-	-	-	-	-	0.1
	A5-P5B*	94	25	35	39	13	0.9	-	-	-	-	-	-	0.99	160	0.019	6.2	1.5	2.4	0.2
	A5-P6A	-	20	26	34	9	0.91	1	40	0.5	0	16	15	0.84	120	0.017	15	2.7	-	-
	A5-P6B	84	22	30	36	11	0.86	1	40	0.4	0	20	1	-	-	-	-	-	-	-
	A5-P9A	96	30	23	41	17	0.9	1	46	0.5	0	20	5.55	0.94	200	0.024	14	2.6	-	0.2
	A6-P10A	97	32	45	44	18	0.89	1	70	0.3	0	20	1.9	1.08	220	0.014	11	2.4	-	0.2
	A6-P10B	90	27	35	38	14	1.08	-	-	-	-	-	-	-	-	-	-	-	-	-
	A6-P1A	84	16	21	27	3	1.33	-	-	-	-	-	-	0.88	220	0.019	12	3.4	-	-
	A6-P2B	99	40	61	53	23	0.72	1	40	0.4	0	20	3.2	-	-	-	12	2.5	-	-
	A6-P3A	100	51	68	69	40	0.63	1	79	0.2	0	20	0.6	-	-	-	-	-	-	-
	A6-P5A	81	20	25	31	9	1.06	1	34	0.9	0	19	18	0.84	200	0.021	18	4.1	-	-
	A6-P5B	90	24	32	39	15	0.97	-	-	-	-	-	-	0.96	200	0.021	15	3.1	-	-
	A6-P6A	95	21	30	38	11	0.95	1	23.5	0.8	0	20	12	-	-	-	-	-	-	0.3
	A6-P6B*	-	24	31	36	12	0.97	-	-	-	-	-	-	-	-	-	-	-	-	-

Table 3.5-1. cont'd. Summary of compiled database

Data Source	Test ID	FC	<2 μm	<5 μm	LL	PI	w_c/LL	$\sigma'_{3,c}/\sigma'_{1,c}$	s_u (kPa)	τ_{cyc}/s_u	τ_{st}/s_u	N_{app}	$\gamma_{max,20}$ (%)	e_0	p'_c (kPa)	C_r	$\gamma_{max,f}$ (%)	$\varepsilon_{v,pc}$ (%)	γ_{res} (%)	$s_{u,cyc,min}/s_{u,st}$
Sancio (2003)	A6-P7A*	79	18	20	27	NP	1.15	0.67	41	0.6	0.2	14	9	-	-	-	-	-	-	-
	A6-P8A	99	43	57	55	26	0.75	1	52.3	0.3	0	20	0.5	-	-	-	-	-	-	-
	A6-P8B	93	30	39	42	16	1	1	50	0.4	0	20	7.6	1.02	135	0.02	15	3	-	0.2
	A6-P9A	95	21	27	35	12	1.06	1	37	0.5	0	20	5.72	0.95	110	0.024	13	2.5	-	0.2
	A6-P9B	91	24	32	39	15	1.1	-	-	-	-	-	-	1.03	110	0.024	12	2.7	-	-
	C10-P3A	100	32	47	47	19	0.86	-	-	-	-	-	-	1.16	200	0.023	15	2.7	-	0.4
	C10-P3B	97	24	32	38	14	1.06	-	-	-	-	-	-	1.09	200	0.023	15	3.4	-	0.1
	C10-P4A	100	49	69	60	31	0.74	1	45	0.3	0	20	0.81	-	-	-	-	-	-	-
	C10-P4B	100	61	84	69	38	0.66	1	45	0.4	0	20	1.65	-	-	-	-	-	-	-
	C10-P8A	56	7	8	NP	NP		-	-	-	-	-	-	-	-	-	-	-	-	0.1
	C10-P8B*	83	9	11	27	NP	1.33	-	-	-	-	-	-	-	-	-	-	-	-	-
	C11-P2A	87	20	26	32	11	1.1	1	80	0.1	0	20	2.4	1	120	0.009	10	2.7	-	-
	C11-P2B*	99	29	40	44	18	0.88	0.67	51	0.5	0.2	12	9	1.08	120	0.009	10	1.7	-	-
	C11-P4A	99	33	47	48	22	0.87	-	-	-	-	-	-	-	-	-	-	-	-	-
	C11-P4B	99	19	25	38	14	1.01	1	51	0.3	0	20	4.58	-	-	-	12	2.4	-	0.2
	C12-P2A	79	12	16	24	NP	1.33	-	-	-	-	-	-	-	-	-	-	-	-	0.1
	C12-P2B	74	19	23	30	9	1	-	-	-	-	-	-	-	-	-	-	-	-	-
	C12-P3A	95	27	35	40	16	1.03	1	60	0.2	0	20	1.8	-	-	-	10	2.6	-	0.2
	C12-P3B	89	26	31	37	15	0.99	0.67	52	0.4	0.2	5	8.85	-	-	-	11	2.2	-	-
	C12-P4A	98	31	50	50	25	0.9	-	-	-	-	-	-	-	-	-	-	-	-	-
	C14-P2A	98	26	34	38	14	1.05	1	52	0.3	0	20	6	1.05	130	0.014	9.5	2.2	-	0.2
	C14-P2B	96	25	34	36	13	1.06	-	-	-	-	-	-	1.04	130	0.014	9.6	2.5	-	-
	D4-P2A	75	9	13	27	6	1.27	-	-	-	-	-	-	-	-	-	-	-	-	0.1
	D4-P2B	84	8	12	33	11	1	-	-	-	-	-	-	-	-	-	11	2	-	0.1

Table 3.5-1. cont'd. Summary of compiled database

Data Source	Test ID	FC	<2 μm	<5 μm	LL	PI	w_c/LL	$\sigma'_{3,c}/\sigma'_{1,c}$	s_u (kPa)	τ_{cyc}/s_u	τ_{st}/s_u	N_{app}	$\gamma_{max,20}$ (%)	e_0	p'_c (kPa)	C_r	$\gamma_{max,f}$ (%)	$\varepsilon_{v,pc}$ (%)	γ_{res} (%)	$s_{u,cyc,min}/s_{u,st}$
Sancio (2003)	D4-P3A*	79	13	18	29	9	1.04	0.66	30	0.8	0.4	16	12.45	-	-	-	12	1.3	-	-
	D4-P3B*	89	12	17	33	11	1.08	0.67	30	1	0.4	5	12.6	-	-	-	14	1.9	-	-
	D4-P4A	92	7	14	37	14	1	1	47	0.2	0	20	0.6	-	-	-	12	2.3	-	-
	D5-P2A	68	4	6	25	NP	1.12	-	-	-	-	-	-	-	-	-	-	-	-	0.1
	D5-P2B*	70	5	7	28	8	1.07	-	-	-	-	-	-	-	-	-	14	2.5	-	0.1
	F4-P2A	67	13	17	24	NP	1.33	-	-	-	-	-	-	-	-	-	-	-	-	-
	F4-P2B	61	12	15	22	NP	1.45	-	-	-	-	-	-	-	-	-	-	-	-	-
	F4-P6A	97	25	38	45	18	0.82	1	26	1.1	0	20	9.23	-	-	-	-	-	-	0.4
	F4-P7A	93	14	21	33	7	1.06	1	85	0.2	0	20	5.25	-	-	-	-	-	-	0.1
	F4-P7B	69	16	22	32	8	1.03	-	-	-	-	-	-	-	-	-	-	-	-	0.2
	F5-P2A	80	16	21	33	9	0.99	0.67	125	0.1	0.1	20	0.7	-	-	-	6.3	1.5	0.5	-
	F5-P2B	78	14	17	28	5	1.07	-	-	-	-	-	-	-	-	-	11	2.4	-	-
	F6-P3B	68	8	11	28	2	1.14	-	-	-	-	-	-	-	-	-	11	2.3	-	-
	F6-P4A	92	15	20	31	5	1.03	-	-	-	-	-	-	-	-	-	-	-	-	-
	F6-P4B	99	17	22	35	9	0.97	-	-	-	-	-	-	-	-	-	-	-	-	0.2
	F7-P1A*	88	16	22	34	8	0.91	-	-	-	-	-	-	-	-	-	-	-	-	0.1
	F7-P1B	81	15	20	31	7	1	1	68	0.2	0	20	3.75	-	-	-	-	-	-	0.1
	F7-P3A*	77	12	16	27	NP	1.04	-	-	-	-	-	-	-	-	-	-	-	-	0.1
	F7-P3B	61	8	10	24	NP	1.25	-	-	-	-	-	-	-	-	-	-	-	-	0.1
	F7-P4A	77	13	17	33	9	1	-	-	-	-	-	-	-	-	-	6.6	1.7	-	-
	F7-P4B*	87	16	21	33	9	1.03	0.67	64	0.3	0.2	20	4.73	0.86	280	0.022	15	4	2.1	-
	F8-P3A*	71	10	15	26	4	1.15	-	-	-	-	-	-	-	-	-	-	-	-	-
	F8-P3B	58	6	8	24	NP	1.08	-	-	-	-	-	-	-	-	-	-	-	-	0.1
	F9-P2A*	81	12	17	29	NP	1.03	-	-	-	-	-	-	-	-	-	-	-	-	-

Table 3.5-1. cont'd. Summary of compiled database

Data Source	Test ID	FC	<2 μm	<5 μm	LL	PI	w_c/LL	$\sigma'_{3,c}/\sigma'_{1,c}$	s_u (kPa)	τ_{cyc}/s_u	τ_{st}/s_u	N_{app}	$\gamma_{max,20}$ (%)	e_0	p'_c (kPa)	C_r	$\gamma_{max,f}$ (%)	$\varepsilon_{v,pc}$ (%)	γ_{res} (%)	$s_{u,cyc,min}/s_{u,st}$
Sancio (2003)	F9-P2B	-	-	-	NP	NP		-	-	-	-	-	-	-	-	-	-	-	-	-
	G4-P2B	91	7	12	36	13	0.99	-	-	-	-	-	-	-	-	-	-	-	-	-
	G4-P4A	47	6	9	NP	NP		-	-	-	-	-	-	-	-	-	-	-	-	0.1
	G4-P4B	64	8	10	NP	NP		-	-	-	-	-	-	-	-	-	-	-	-	-
	G4-P5A	89	24	32	37	14	0.97	1	94	0.3	0	20	7.4	-	-	-	-	-	-	0.1
	G4-P5B	56	8	10	NP	NP		-	-	-	-	-	-	-	-	-	-	-	-	-
	G5-P1A	67	10	13	26	5	1.16	1	114	0.1	0	20	3.15	-	-	-	-	-	-	0.1
	G5-P2B	75	8	10	27	NP	1.24	-	-	-	-	-	-	-	-	-	13	2.5	-	0.1
	I2-P7B	82	12	17	32	NP	1.06	-	-	-	-	-	-	-	-	-	-	-	-	-
	I4-P5B	87	15	23	37	12	1	1	31	0.7	0	20	12.9	-	-	-	-	-	-	-
	I6-P4	90	18	27	31	9	1.13	1	61	0.3	0	20	6.6	-	-	-	-	-	-	0.2
	I6-P5	92	17	25	35	11	0.89	1	95	0.1	0	20	0.75	-	-	-	-	-	-	0.2
	I6-P6	80	15	22	34	7	0.91	-	-	-	-	-	-	1.05	140	0.015	9	1.8	-	-
	I6-P7*	90	18	25	41	14	0.9	-	-	-	-	-	-	-	-	-	-	-	-	-
	I7-P1	100	57	82	71	36	0.51	-	-	-	-	-	-	-	-	-	-	-	-	-
	I8-P1A	83	22	28	35	13	0.92	1	24	0.7	0	20	9.9	-	-	-	14	2.9	-	0.2
	I8-P1B	47	4	7	23	NP	1.57	-	-	-	-	-	-	-	-	-	-	-	-	0.1
	I8-P2A	75	18	25	35	13	1.07	1	73	0.4	0	18	15	-	-	-	13	2.9	-	0.2
	I8-P2B	89	25	35	42	18	0.9	1	73	0.3	0	20	1.4	-	-	-	15	3.8	-	0.2
	I8-P3A	68	3	4	28	NP	1.35	-	-	-	-	-	-	-	-	-	-	-	-	-
	I8-P5A	98	23	29	41	15	0.88	1	95	0.3	0	20	4.4	-	-	-	-	-	-	0.1
	I8-P5B	78	10	14	29	NP	1.07	1	135	0.3	0	20	7.95	-	-	-	-	-	-	-
	J5-P2A	56	6	9	24	NP	1.58	-	-	-	-	-	-	-	-	-	-	-	-	0.1
	J5-P2B	84	15	20	34	12	0.88	-	-	-	-	-	-	-	-	-	15	3	-	0.2

Table 3.5-1. cont'd. Summary of compiled database

Data Source	Test ID	FC	<2 μm	<5 μm	LL	PI	w_c/LL	$\sigma'_{3,c}/\sigma'_{1,c}$	s_u (kPa)	τ_{cyc}/s_u	τ_{st}/s_u	N_{app}	$\gamma_{max,20}$ (%)	e_0	p'_c (kPa)	C_r	$\gamma_{max,f}$ (%)	$\varepsilon_{v,pc}$ (%)	γ_{res} (%)	$s_{u,cyc,min}/s_{u,st}$
Sancio (2003)	J5-P3A	70	10	16	27	7	1.15	1	60	0.3	0	20	10	-	-	-	15	2.8	-	0.1
	J5-P3B	57	5	8	23	NP	1.7	-	-	-	-	-	-	-	-	-	-	-	-	0.1
	J5-P4A*	87	13	20	32	9	0.99	-	-	-	-	-	-	-	-	-	-	-	-	0.2
	J5-P6A	100	37	55	52	25	0.84	1	65	0.3	0	20	1.95	-	-	-	14	3	-	0.2
	A5-P9B-3*+	-	-	-	38	11	0.76	0.57	46	0.8	0	19	16	-	-	-	-	-	-	-
	G4-P3-3*+	-	-	-	36	11	1	0.6	140	0.2	0	20	1.7	-	-	-	-	-	-	-
	G4-P3-5*+	-	-	-	36	11	0.97	0.59	140	0.2	0.2	20	1.2	-	-	-	-	-	-	-
	G4-P3-6*+	-	-	-	40	14	0.93	0.6	140	0.3	0.2	5	7.5	-	-	-	-	-	-	-
	G4-P3-7*+	-	-	-	40	14	0.9	0.6	140	0.2	0.2	5	2.5	-	-	-	-	-	-	-
	A5-P9B-2*+	-	-	-	38	11	0.92	0.6	46	0.8	0.2	10	9	-	-	-	-	-	-	-
Chu (2006)	WAS3-5*	93	11	38	19	3	1.13	-	-	-	-	-	-	-	-	-	-	-	-	-
	WAS3-6*	93	11	38	19	3	1.13	0.78	159	0.6	0.1	3	6.3	-	-	-	-	-	-	-
	WAS4-1*	98	NA	37	31	16	0.63	0.78	123	0.5	0.2	20	2.3	-	-	-	-	-	0.2	-
	WAS4-2*	98	NA	37	30	15	0.65	0.78	123	0.4	0.2	20	0.49	-	-	-	-	-	-	-
	WAS4-3*	98	NA	37	30	11	0.67	0.78	123	0.5	0.2	4	3.35	-	-	-	-	-	-	-
	WAS4-4*	98	NA	30	22	3	1.02	0.78	159	0.4	0.1	12	4.9	-	-	-	-	-	-	-
	WAS4-7	-	-	-	29	10	0.66	1	119	0.4	0	20	1.85	-	-	-	-	-	-	-
	WAS4-8	-	-	-	30	11	1	1	119	0.5	0	10	4.2	-	-	-	-	-	-	-
Donahue (2007)	PluvA20+	76	5	13	31	3	1.13	0.73	43	0.5	0	13	21	-	-	-	-	-	-	-
	PluvG16+	80	14	20	31	10	1	0.73	29.5	0.9	0	4	17	-	-	-	-	-	-	-
	SDM-A10+	76	5	13	31	3	0.84	0.74	75	0.4	0	11	18	-	-	-	-	-	-	-
	SDM-G8+	80	14	20	31	10	0.82	0.74	50	0.6	0	5	38	-	-	-	-	-	-	-

"-" : either this value is not available or this data is filtered out based on listed criteria,"*": used in excess pore water pressure generation model,"+": simple shear test
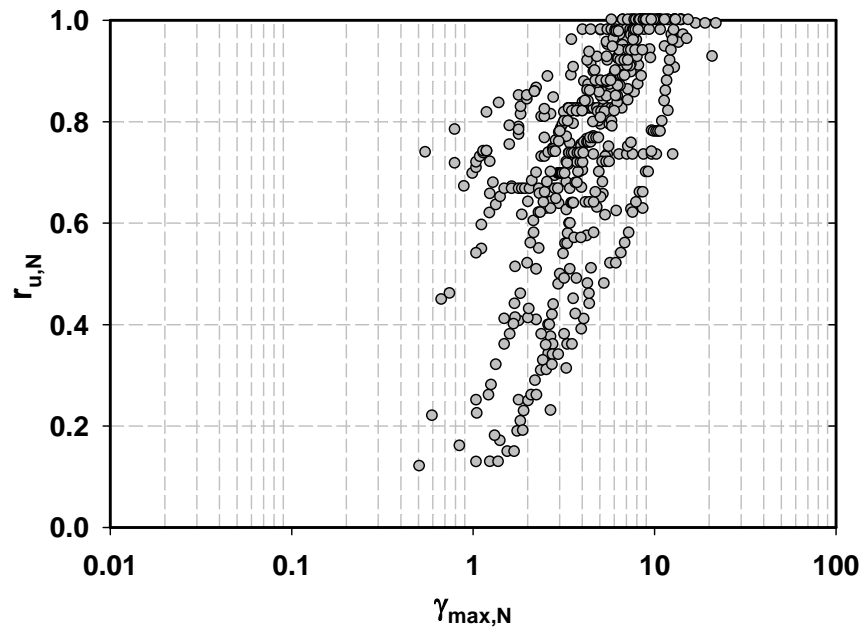
Figure 3.5-2. $r_{u,N}$ vs. $\gamma_{max,N}$ database compiled from literature

CHAPTER 4

LIQUEFACTION SUSCEPTIBILITY OF FINE-GRAINED SOILS

4.1 INTRODUCTION

Assessment of soil's liquefaction susceptibility is listed as the primary step of seismic soil liquefaction engineering by Seed et al. (2003) in their state-of-the-art work. Today liquefaction susceptibility is considered as one of the hottest topics of geotechnical earthquake engineering. As pointed out in Chapter 2, there has been an increasing research interest on this issue to produce improved tools for screening potentially liquefiable soils. It is believed that all of these studies are major improvements over Chinese Criteria-like methodologies; yet they also suffer from certain issues, such as their dependency on adopted liquefaction definitions (either strain- or r_u -based) and selected test conditions (CSR vs. number of cycles relation), which are thoroughly discussed earlier in Section 2.2.5.

Considering the importance of this issue and being inspired by the limitations of previous efforts, it is intended to develop improved criteria for evaluating liquefaction susceptibility of fine-grained soils. In the following sections, first proposed liquefaction definition is introduced, and then details of the proposed

criteria are presented. This chapter is concluded by comparing the performance of proposed and existing criteria by using compiled database.

4.2 NEW CRITERIA FOR EVALUATING LIQUEFACTION SUSCEPTIBILITY OF FINE-GRAINED SOILS

4.2.1 Laboratory-based Liquefaction Definitions

First requirement for the development of new liquefaction susceptibility criteria involves clearly stating the definition of soil liquefaction. In the literature, there exist various γ_{max} and r_u-based liquefaction definitions, where onset of liquefaction is defined as number of cycles to first occurrence of threshold levels of either γ_{max} and r_u. For γ_{max}-based definitions, these threshold varies from 3 to 20 % (3% by Boulanger et al., 1991; 5 % by Lee and Roth, 1977; 7.5 % Ishihara, 1993; 10 % by Lee et al., 1975; 15 % by Andersen et al., 1988; 20 % by Lee and Seed, 1967); whereas, r_u-based definitions vary from 0.8 (Wu et al., 2004) to 1.0 (Lee and Albaisa, 1974; Ishihara, 1993). Although a single variable-based liquefaction definition may be quite satisfactory for liquefaction triggering analysis, where assessments are performed for a unique combination of cyclic stress ratio (CSR) and number of equivalent loading cycle (i.e., moment magnitude of the earthquake), adopting such definitions produces mostly unconservatively-biased classifications, since any susceptibility criteria must cover not a unique but all combinations of CSR and number of cycles relations. It is believed that even high plasticity clays can satisfy widely used r_u=1.0 or γ_{max}=7.5% criterion in case they are subjected to selected loading levels long enough. For this reason, instead of using a threshold level of either γ_{max} and r_u, occurrence of contraction and dilation cycles, i.e. banana loops, is selected as the manifestation of liquefaction triggering since this stress-strain response is commonly associated with liquefaction mechanisms. However, various r_u - γ_{max} couples are also adopted to define the onset of liquefaction triggering, and their predictive reliabilities are also checked as

76

alternative methodologies. Inspired from available test data and also current state of literature, plasticity and liquidity indices, PI and LI, respectively, are selected as the main parameters of the proposed criteria. Yet the influence of fines content is also investigated. Liquidity index, which is defined in Equation $(4-1)$, is the most informative index parameter, and its use along with PI is believed to provide satisfactory information to classify soil.

$$LI = \frac{w_c - PL}{PI} \qquad (4-1)$$

Among previous efforts, only Seed et al. (2003) followed a similar approach by using PI, LL and w_c/LL as screening parameters. However, Seed et al. (2003) neither clearly emphasize how they developed their criteria nor stated their liquefaction definition; therefore model development stage of these criteria remained to be mysterious. Boulanger and Idriss (2004 and 2006) also mentioned LI as a better screening tool compared to w_c/LL; yet at the end, they preferred a completely different path and used neither w_c/LL nor LI in their criteria, which is based solely on PI of fine-grained soils.

Figure 4.2-1 presents the liquefiable and non-liquefiable soil data, which have been summarized by Tables 3.2-1 and 3.5-1, on PI vs. LI domain based on the assumption that occurrence of contraction and dilation cycles are manifestation of liquefaction triggering. Even visual inspection on this figure reveals a separation between liquefiable and non-liquefiable data classes. This, by itself confirms the validity of the adopted liquefaction definition. Besides this definition, some r_u-γ_{max} couples are also tested as possible liquefaction definitions for comparison purposes. According to these kinds of definitions, soil specimens are accepted to be liquefiable if excess pore water pressure ratio induced at the selected γ_{max} level exceeds the selected r_u threshold. Figures 4.2-2 to 4.2-4 presents data classified based on r_u-

γ_{max} couples of 0.70 – 3.5 %, 0.80 – 5.0 %, and 0.90 – 7.5%, respectively, on *PI* vs. *LI* domain.
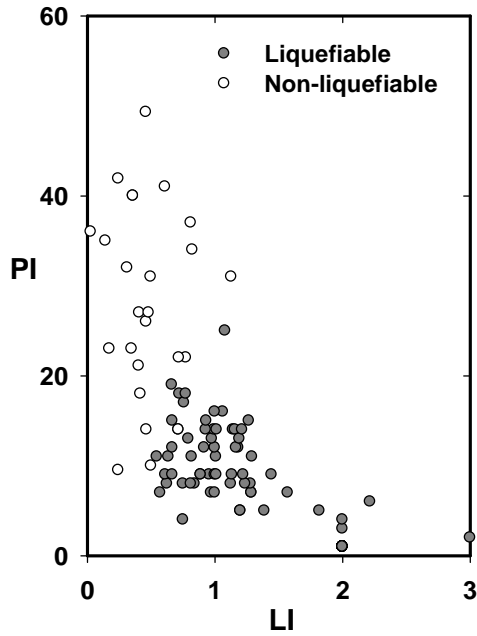
Figure 4.2-1. Classification of data on PI vs. LI domain according to occurrence of contraction and dilation cycles
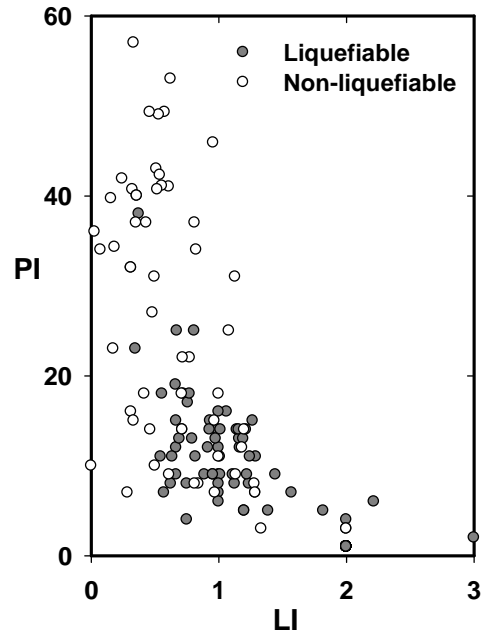
Figure 4.2-2. Classification of data on PI vs. LI domain according to $r_{u,\gamma_{max}=3.5\%}$ =0.7 criterion
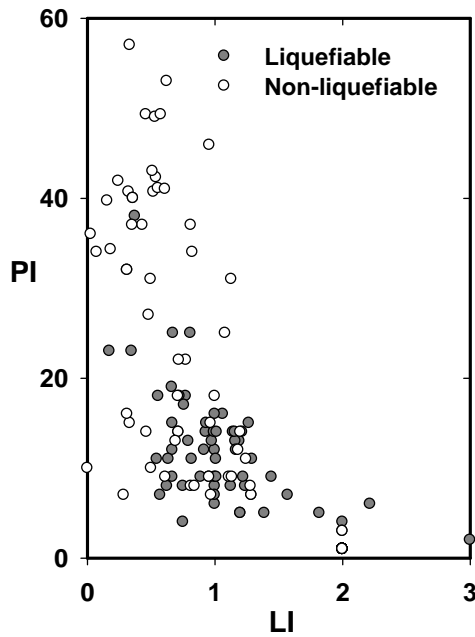
Figure 4.2-3. Classification of test on PI vs. LI domain according to $r_{u,\gamma_{max}=5\%}$=0.8 criterion
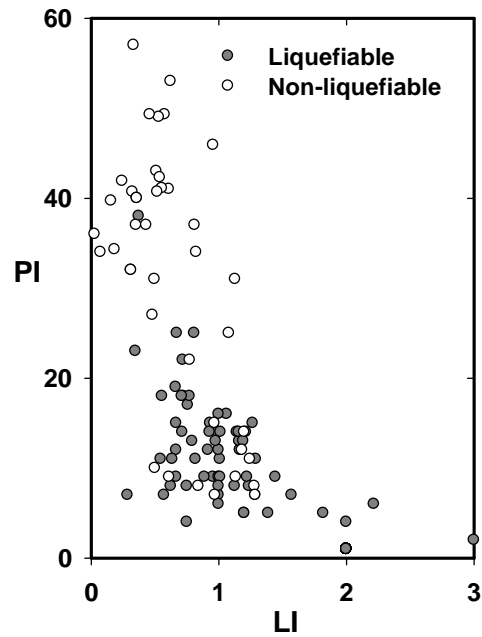
Figure 4.2-4. Classification of test on PI vs. LI domain according to $r_{u,\gamma_{max}=7.5\%}$=0.9 criterion

4.2.2 Development of Probabilistically-based Liquefaction Susceptibility Criteria

Selection of a limit state expression capturing the essential parameters of the problem is the first step in developing a probabilistic model. The model for the limit state function has the general form g = g (**x, Θ**) where x is a set of descriptive parameters and Θ is the set of unknown model parameters. Consistent with the usual definition in structural reliability theory, the soil specimen is assumed to be liquefiable when g (**x, Θ**) takes a negative value and the limit state surface g (**x, Θ**) = 0 also denotes liquefaction susceptibility. Inspired by the existing trends in the compiled database, various functional forms have been tested, some of which are listed in Table 4.2-1. Among these models, the following functional form produced

the best fit to the observed behavioral trends and is adopted as the proposed limit state function:

$$g(PI, LI, \Theta) = \theta_1 \cdot \ln(PI) - LI + \theta_2 \pm \varepsilon \qquad (4-2)$$

where ε is the random model correction term used to account for the facts that i) possible missing descriptive parameters which can affect liquefaction susceptibility of fine-grained soils, and ii) the adopted mathematical expression may not have the ideal functional form. It is reasonable and also convenient to assume that ε has normal distribution with zero mean for the aim of producing an unbiased model (i.e., one that in the average makes correct predictions). The standard deviation of ε, denoted as σ_ε, however is unknown and must be estimated.

Table 4.2-1. Limit state models for liquefaction susceptibility problem

Trial #	Model Mathematical Form
1	$g(PI, LI, \Theta) = \theta_1 \cdot \ln(PI) - LI + \theta_2 \pm \varepsilon$
2	$g(PI, LI, \Theta) = \theta_1 \cdot ln(PI) + \theta_2 - LI \cdot (1 + \theta_3 \cdot FC) - \theta_4 \cdot FC \pm \varepsilon$
3	$g(PI, LI, \Theta) = \theta_1 \cdot ln(PI) - w_c / LL + \theta_2 \pm \varepsilon$
4	$g(PI, LI, \Theta) = \theta_1 \cdot ln(PI) + \theta_2 - w_c / LL \cdot (1 + \theta_3 \cdot FC) - \theta_4 \cdot FC \pm \varepsilon$

Let PI_i and LI_i be the values of PI and LI of the ith soil specimen, respectively, and let ε_i be the corresponding model correction term. If the ith soil specimen is potentially liquefiable, then $g(PI_i, LI_i, \varepsilon_i, \theta_i) \leq 0$; whereas, if the ith soil specimen is not potentially liquefiable, then $g(PI_i, LI_i, \varepsilon_i, \theta_i) > 0$. Assuming each specimen's liquefaction susceptibility potential to be statistically independent, likelihood function can be written as the product of the probabilities of the observations as follows;

$$g(PI, LI, \varepsilon, \Theta) = \prod_{liquefiable} P[g(PI_i, LI_i, \varepsilon_i, \theta) \leq 0] \cdot \prod_{nonliquefiable} P[g(PI_i, LI_i, \varepsilon_i, \theta) > 0] \quad (4-3)$$

Suppose the values of PI_i and LI_i for each specimen are exact, i.e. no measurement error exists, noting that $g(...) = \hat{g}(...) + \varepsilon_i$ has the normal distribution with mean $\hat{g}(...)$ and standard deviation σ_ε, the likelihood function can be written as in Equation $(4-4)$.

$$L(\theta, \sigma_\varepsilon) = \prod_{liquefiable} \Phi\left[-\frac{\hat{g}(PI_i, LI_i, \theta)}{\sigma_\varepsilon}\right] \times \prod_{nonliquefiable} \Phi\left[-\frac{\hat{g}(PI_i, LI_i, \theta)}{\sigma_\varepsilon}\right] \qquad (4-4)$$

where $\Phi[.]$ is the standard normal cumulative probability function.

Next, consistent with the maximum likelihood methodology, model coefficients maximizing the value of this likelihood function are estimated and then presented in Table 4-2.2. Same table also summarizes material coefficients and corresponding values of maximum likelihood functions for other limit state functions which have been summarized in Table 4-2.1. Noting that smaller σ_ε and higher likelihood value ($\sum lh$) are the indications of a superior model, selected limit state function (Trial #1) produces the best predictions while screening liquefiable soils.

Based on these findings, it is concluded that fine-grained soils with PI>30 are not vulnerable to cyclic liquefaction but only to cyclic mobility. For fine-grained soils with PI< 30, they are concluded to be susceptible to cyclic liquefaction if the following condition is satisfied:

- $LI \geq 0.578 \cdot \ln(PI) - 0.940$

Proposed liquefaction susceptibility boundary along with ± 1 standard deviation curves are presented schematically in Figure 4.2-5 along with the compiled data pairs. On this figure, soils having PI values in excess of 30 are presented on PI =30 boundary.

Table 4.2-2. Summary of model coefficients and performances of limit state
functions tested for liquefaction susceptibility problem

Trial #	Model Coefficients					$\sum lh$
	θ_1	θ_2	θ_3	θ_4	σ_ε	
1	0.578	-0.940	-	-	0.101	-10.49
2	0.792	-0.822	0.008	0.107	0.105	-10.63
3	0.181	0.376	-	-	0.102	-12.73
4	0.440	0.371	0.002	0.009	0.142	-22.94
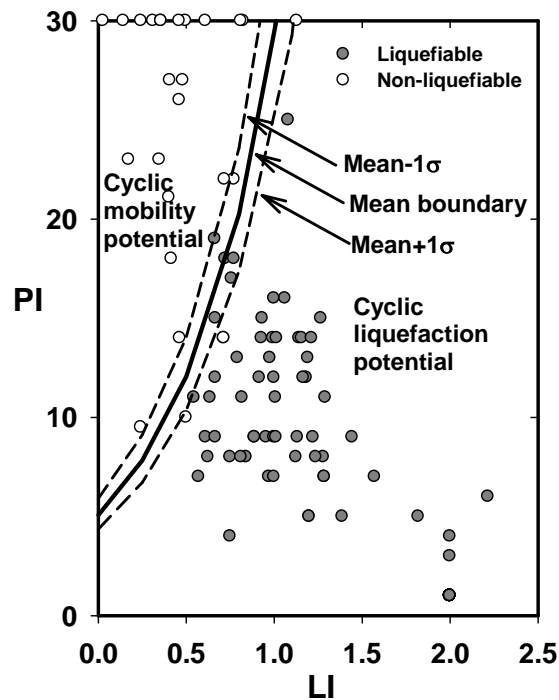
Figure 4.2-5. Proposed liquefaction susceptibility criteria

Following the same procedure, liquefaction susceptibility boundaries are also prepared for other liquefaction definitions; i) γ_{max}=3.5% - r_u=0.7, ii) γ_{max}=5.0% - r_u=0.8, iii) γ_{max}=7.5% - r_u=0.9. These boundaries and their corresponding equations are presented along with the test data in by Figures 4.2-6 through 4.2-8,

respectively. As revealed by these figures, the development of dilation-contraction cycles is a better indication of soil liquefaction triggering as opposed to predefined threshold r_u and γ_{max} pairs.
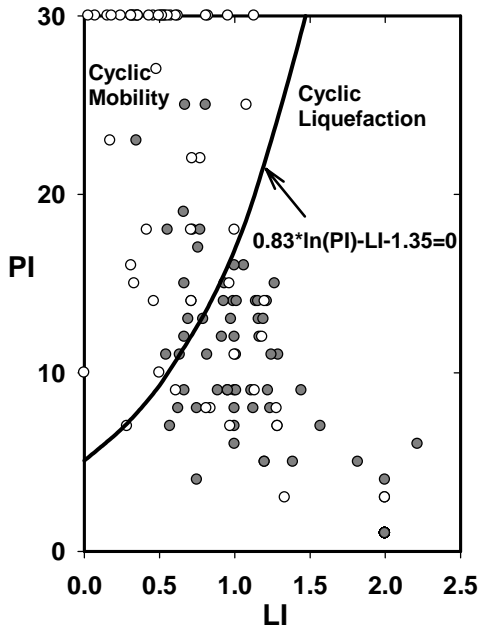
Figure 4.2-6. Liquefaction susceptibility criteria for $r_{u,\gamma_{max}=3.5\%}=0.7$
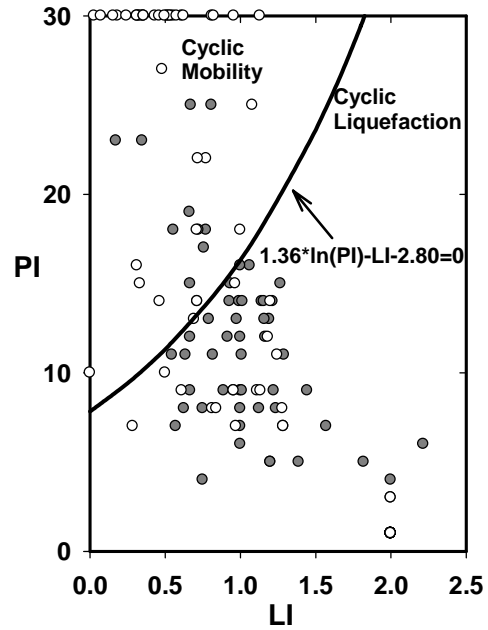
Figure 4.2-7. Liquefaction susceptibility criteria for $r_{u,\gamma_{max}=5\%}=0.8$

LI was correlated with mechanical properties of soils such as, undrained shear strength (e.g. Bjerrum and Simons, 1960, etc.) and remolded shear strength (e.g. Houston and Mitchell, 1969, etc.). For the purpose of providing an insight on variation of *LI* with shear strength of fine-grained soils the correlation of Bjerrum and Simons (1960) is used. Figures 4.2-9 and 4.2-10 present the study of Bjerrum and Simons (1960) and its application on the proposed liquefaction susceptibility criteria, respectively.
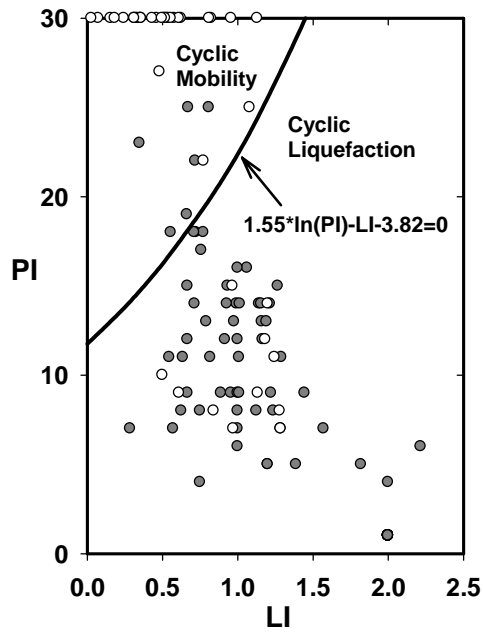
Figure 4.2-8. Liquefaction susceptibility criteria for $r_{u,\gamma_{max}=7.5\%}=0.9$
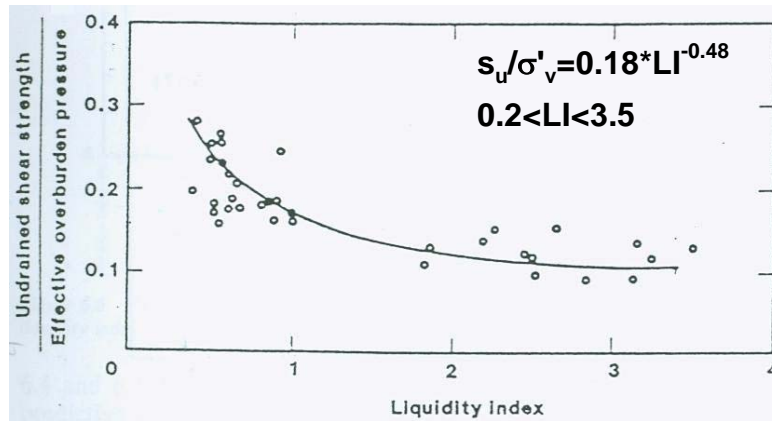
Figure 4.2-9. Relationship between s_u/σ'_v and LI (Bjerrum and Simons, 1960)
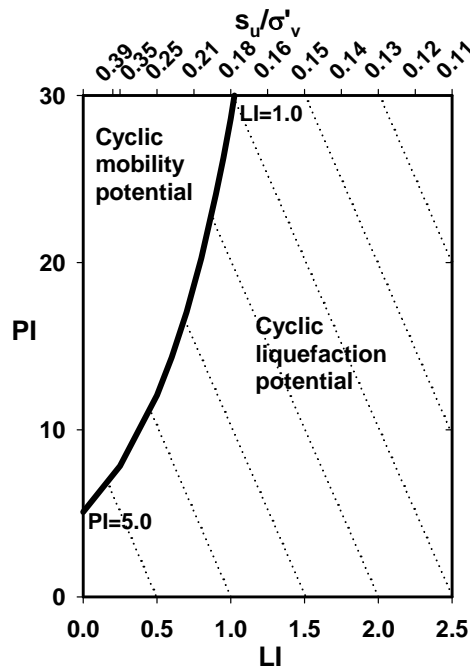
Figure 4.2-10. Liquefaction susceptibility criteria on LI-PI-s_u/σ'_v domain

4.3 PERFORMANCE EVALUATION OF PROPOSED AND EXISTING LIQUEFACTION SUSCEPTIBILITY CRITERIA

As referred to earlier, various researchers have focused on liquefaction susceptibility assessment of fine-grained soils to better understand the governing mechanisms. Consequently some criteria were developed to screen out soils susceptible to liquefaction. A detailed discussion on these previous efforts was presented in Chapter 2, and new criteria were introduced in the previous section considering the limitations of existing studies.

Within the confines of this section, it is aimed to compare predictive performances of proposed criteria and recently published criteria of Bray and Sancio (2006) and Boulanger and Idriss (2006). It is definitely more desirable to assess performance of all existing criteria in this comparison study. However, except the selected ones, none of the other studies clearly stated how they defined occurrence of liquefaction triggering. It is believed that presumably adopting assuming a liquefaction definition

and evaluating predictive performances based on this assumption will not produce fair and defendable results. Yet, fortunately two of the most recent and widely used criteria can be included in this comparison scheme.

Comparisons are performed by using the compiled database, which is presented in Tables 3.2-1 and 3.5-1 of Chapter 3. Each data is evaluated separately according to the liquefaction definition adopted by the individual liquefaction susceptibility criteria. For instance, according to Bray and Sancio (2006), the onset of liquefaction triggers at 3 % axial strain in extension or 5 % double amplitude axial strain; whereas, Boulanger and Idriss (2006) stated that only "sand-like" soils liquefy and for these soils state of r_u =1.0 typically corresponds to γ_{max} value of 3 % according to the early work of Boulanger et al. (1991). On the other hand, occurrence of contraction – dilation cycles are accepted to be the manifestation of liquefaction triggering according to this study as stated in the previous section. Table 4.3-1 summarizes how each specimen is classified based on both each reference's corresponding liquefaction definition and criteria. As revealed by this table, some of specimens can not be classified based on adopted liquefaction definitions, since these specimens were not subjected to cyclic shearing long enough to have a solid idea about its liquefaction susceptibility. This case is valid especially for our test data where only 20 loading cycles are applied.

Table 4.3-1. Evaluation of test data by selected liquefaction susceptibility criteria

Test ID	Bray and Sancio (2006)		Boulanger and Idriss (2006)		This Study	
	Liquefied?	Prediction	Liquefied?	Prediction	Liquefied?	Prediction
CTXT1	N	TEST	N	N	-	Y
CTXT2	N	TEST	N	N	-	Y
CTXT3	Y	Y	N	N	Y	Y
CTXT4	N	N	N	N	N	N
CTXT5	Y	Y	N	TEST	Y	Y
CTXT6	N	TEST	N	N	-	N
CTXT7	N	N	N	N	-	N
CTXT9	N	N	N	N	N	N

Table 4.3-1. cont'd. Evaluation of test data by selected liquefaction susceptibility criteria

Test ID	Bray and Sancio (2006)		Boulanger and Idriss (2006)		This Study	
	Liquefied?	Prediction	Liquefied?	Prediction	Liquefied?	Prediction
CTXT10	N	N	N	N	-	N
CTXT11	Y	Y	N	N	Y	Y
CTXT12	Y	Y	N	N	Y	Y
CTXT13	Y	Y	N	N	Y	Y
CTXT14	N	N	N	N	-	N
CTXT15	N	N	N	TEST	-	Y
CTXT16	N	N	N	N	N	Y
CTXT18	N	N	N	N	N	N
CTXT19	N	Y	N	N	-	Y
CTXT20	N	N	N	N	-	N
CTXT21	N	TEST	N	N	N	N
CTXT22	N	TEST	N	N	N	Y
CTXT23	N	TEST	N	N	-	Y
CTXT24	Y	Y	N	N	Y	Y
CTXT25	N	N	N	N	-	N
CTXT26	Y	Y	N	N	-	Y
CTXT27	N	N	N	N	N	N
CTXT28	N	Y	N	N	Y	Y
CTXT29	Y	Y	N	TEST	Y	Y
CTXT30	N	N	N	N	-	N
CTXT31	N	N	N	N	-	N
CTXT32	N	N	N	N	N	N
CTXT33	N	Y	N	TEST	Y	Y
CTXT34	N	N	N	TEST	N	N
CTXT35	N	N	N	N	-	N
CTXT36	N	N	N	N	-	N
CTXT37	N	N	N	N	N	N
CTXT38	N	N	N	N	-	N
CTXT40	N	N	N	N	N	N
CTXT42	N	N	N	N	N	N
CTXT43	N	N	N	N	-	N
CTXT44	N	N	N	N	N	N
CTXT45	N	N	N	N	N	N
CTXT46	N	N	N	N	-	N
CTXT47	N	N	N	N	-	N
CTXT48	N	N	N	N	-	N
CTXT49	N	N	N	N	-	N
CTXT50	N	N	N	N	-	N
CTXT51	N	N	N	N	N	N
CTXT52	N	N	N	N	-	N

Table 4.3-1. cont'd. Evaluation of test data by selected liquefaction susceptibility criteria

Test ID	Bray and Sancio (2006)		Boulanger and Idriss (2006)		This Study	
	Liquefied?	Prediction	Liquefied?	Prediction	Liquefied?	Prediction
CTXT53	N	N	N	N	-	N
CTXT54	N	N	N	N	N	N
CTXT55	N	N	N	N	-	N
CTXT56	N	N	N	N	-	N
CTXT58	N	N	N	N	-	N
CTXT59	N	N	N	N	-	N
CTXT60	N	N	N	N	N	N
CTXT61	N	N	N	N	-	N
CTXT62	N	N	N	N	-	N
CTXT63	N	N	N	N	-	N
CTXT64	N	N	N	N	-	N
F5-P2B	Y	Y	Y	TEST	Y	Y
F7-P1B	Y	Y	Y	TEST	Y	Y
J5-P4A	Y	Y	Y	N	Y	Y
C11-P2A	Y	Y	Y	N	Y	Y
I2-P7B	Y	N	Y	Y	Y	Y
F6-P3B	Y	Y	Y	Y	Y	Y
F7-P4A	Y	Y	Y	N	Y	Y
F7-P3B	Y	N	Y	Y	Y	Y
F6-P4A	Y	Y	Y	TEST	Y	Y
F8-P3A	Y	Y	N	TEST	Y	Y
G5-P1A	Y	Y	Y	TEST	Y	Y
G5-P2B	Y	N	Y	Y	Y	Y
C12-P2A	Y	N	Y	Y	Y	Y
C12-P2B	Y	Y	Y	N	Y	Y
A5-P2A	Y	N	Y	Y	Y	Y
D5-P2A	Y	N	Y	Y	Y	Y
D5-P2B	Y	Y	Y	N	Y	Y
D4-P2A	Y	Y	Y	TEST	Y	Y
D4-P2B	Y	Y	Y	N	Y	Y
J5-P3A	Y	Y	Y	TEST	Y	Y
J5-P3B	Y	N	Y	Y	Y	Y
J5-P2A	Y	N	N	Y	Y	Y
J5-P2B	Y	Y	Y	N	Y	Y
I6-P4	Y	Y	Y	N	Y	Y
I6-P6	Y	Y	Y	TEST	Y	Y
I6-P5	Y	Y	Y	N	Y	Y
I8-P1B	Y	N	Y	Y	Y	Y
I4-P5B	Y	Y	N	N	Y	Y
A5-P6A	Y	Y	Y	N	Y	Y

Table 4.3-1. cont'd. Evaluation of test data by selected liquefaction susceptibility criteria

Test ID	Bray and Sancio (2006)		Boulanger and Idriss (2006)		This Study	
	Liquefied?	Prediction	Liquefied?	Prediction	Liquefied?	Prediction
A5-P6B	Y	Y	Y	N	Y	Y
A6-P6A	Y	Y	Y	N	Y	Y
A6-P9A	Y	Y	Y	N	Y	Y
F4-P7A	Y	Y	Y	TEST	Y	Y
I8-P3A	Y	N	Y	Y	Y	Y
F4-P2A	Y	N	Y	Y	Y	Y
A6-P5A	Y	Y	Y	N	Y	Y
A6-P1A	Y	Y	Y	Y	Y	Y
F9-P2A	Y	N	Y	Y	Y	Y
F4-P2B	Y	N	Y	Y	Y	Y
F9-P2B	Y	N	N	Y	Y	Y
F7-P1A	Y	Y	Y	N	Y	Y
F7-P3A	Y	N	Y	Y	Y	Y
F6-P4B	Y	Y	Y	N	Y	Y
F8-P3B	Y	N	Y	Y	Y	Y
F4-P7B	Y	Y	N	N	Y	Y
A6-P6B	Y	Y	Y	N	Y	Y
I6-P7	Y	TEST	N	N	Y	Y
C14-P2B	Y	TEST	Y	N	-	Y
D4-P4A	Y	TEST	Y	N	Y	Y
C14-P2A	Y	TEST	Y	N	Y	Y
C12-P3A	Y	TEST	Y	N	Y	Y
C10-P3B	Y	TEST	Y	N	Y	Y
C10-P3A	Y	TEST	Y	N	Y	N
C11-P4B	Y	TEST	Y	N	Y	Y
G4-P2B	Y	TEST	Y	N	Y	Y
A6-P5B	Y	TEST	Y	N	Y	Y
A6-P8B	Y	TEST	Y	N	Y	Y
A6-P10A	Y	TEST	Y	N	Y	N
A5-P9A	Y	TEST	Y	N	Y	Y
F4-P6A	Y	TEST	Y	N	-	N
A6-P9B	Y	TEST	Y	N	Y	Y
I8-P1A	Y	TEST	Y	N	Y	Y
I8-P2A	Y	TEST	Y	N	Y	Y
I8-P2B	Y	TEST	Y	N	Y	Y
A6-P10B	Y	TEST	Y	N	Y	Y
I7-P1	N	N	N	N	N	N
A6-P2B	Y	N	Y	N	N	N
A6-P3A	N	N	N	N	N	N
C10-P4A	N	N	N	N	N	N

Table 4.3-1. cont'd. Evaluation of test data by selected liquefaction susceptibility criteria

Test ID	Bray and Sancio (2006)		Boulanger and Idriss (2006)		This Study	
	Liquefied?	Prediction	Liquefied?	Prediction	Liquefied?	Prediction
C11-P4A	N	N	N	N	N	N
C12-P4A	Y	N	Y	N	-	N
C10-P4B	Y	N	Y	N	-	N
J5-P6A	Y	N	Y	N	-	N
A6-P8A	N	N	N	N	N	N
A6-P3A	N	N	N	N	N	N
F5-P2A	N	Y	N	N	-	Y
F7-P4B	Y	Y	N	N	-	Y
D4-P3A	Y	Y	N	N	Y	Y
D4-P3B	Y	Y	N	N	-	Y
A5-P5B	Y	TEST	N	N	-	Y
A6-P7A	Y	N	N	Y	-	Y
C12-P3B	Y	TEST	N	N	-	Y
C11-P2B	N	TEST	N	N	-	N
C10-P8A	Y	N	Y	Y	Y	Y
C10-P8B	Y	N	Y	Y	Y	Y
I8-P5A	Y	TEST	Y	N	Y	Y
I8-P5B	Y	N	Y	Y	Y	Y
G4-P4A	Y	N	Y	Y	Y	Y
G4-P4B	Y	N	Y	Y	Y	Y
G4-P5B	Y	N	Y	Y	Y	Y
G4-P5A	Y	TEST	Y	N	Y	Y
WAS4-1	N	N	N	N	-	N
WAS4-2	N	N	N	N	-	N
WAS4-3	N	N	N	N	-	N
WAS4-4	N	Y	N	Y	-	Y
WAS3-5	N	Y	N	Y	Y	Y
WAS3-6	N	Y	N	Y	-	Y
WAS4-7	N	N	N	N	-	N
WAS4-8	N	Y	N	N	-	Y
C1-1	N	N	N	N	N	N
C1-3	Y	N	N	N	Y	Y
D2-1	Y	Y	N	TEST	Y	Y
D2-2	Y	Y	N	N	Y	Y
E1-2	N	N	N	N	N	N
E1-3	N	N	N	N	N	N
G2-1	Y	Y	N	N	-	Y
J3-2	Y	Y	N	TEST	-	Y

Y: Susceptible to Liquefaction , N: Not Susceptible to Liquefaction, TEST: further assessment is proposed, -: Not classified

For quantitative comparisons of predictive performances, following statistical metric definitions are decided to be used: overall accuracy (Acc), precision (P), recall (R) and F-score (F_β). These classifiers are determined from the elements of comparison matrix, which is a matrix of the observed versus predicted classes as presented in Table 4.3-2. Diagonal elements of this matrix present correctly classified cases; whereas the remaining elements present misclassifications.

Table 4.3-2. Elements of comparison matrix

		Observed	
		Yes	No
Predicted	Yes	TL	FL
	No	FNL	TNL

In this table, TL denotes for "true liquefiable" which presents the sum of the instances where potentially liquefiable soils are classified correctly, and TNL denotes for "true non-liquefiable" presenting the sum of the instances where potentially non-liquefiable soils are classified correctly. On the other hand, FL denotes for "false liquefiable" which is the sum of instances non-liquefied soils are classified as potentially liquefiable and FNL denotes for "false non-liquefiable" presenting the sum of instances where potentially liquefiable soils are classified as non-liquefiable. Selected statistical metrics are defined based on these classifiers as follows:

$$Acc = \frac{TL + TNL}{TL + TNL + FL + FNL} \qquad (4-4)$$

$$P = \frac{TL}{TL + FL} \qquad (4-5)$$

$$R = \frac{TL}{TL + FNL} \qquad (4-6)$$

$$F_\beta = \frac{(1+\beta^2)\cdot(P\cdot R)}{(\beta^2\cdot P + R)} \qquad\qquad (4-7)$$

where β is a measure of the importance of recall to precision and its value is defined by the user. For this specific problem, its value is selected as 1.0, i.e. precision and recall are accepted to have same importance.

Overall accuracy is a common validation metric and an accuracy of 0.90 means that 90 % of the data have been classified correctly. However, it does not mean that 90 % of the each class has been correctly classified, especially when there is a class imbalance in database. This argument is valid for this database since the numbers of liquefaction susceptible not susceptible cases are not equal; therefore, overall accuracy can be misleading when it is used alone. Consequently, precision and recall become more valuable measures. The former classifier presents the ratio of cases correctly classified as "liquefiable" to the sum of all cases classified as "liquefiable"; whereas, the latter one presents the ratio of cases correctly classified as "liquefiable" to the sum of truly "liquefiable" cases. On the other hand, F-score is the weighted harmonic mean of precision and recall and it is important since it combines two classifiers to a single metric.

Both Bray and Sancio (2006) and Boulanger and Idriss (2006) defined "test" and "transition" zones, respectively to highlight the difficulty in predicting the cyclic response of some fine-grained soils and the necessity for further assessment. While determining the values of classifiers, in favor of those studies, it is accepted that those criteria correctly classifies the soil whenever soil is located in "test" or "transition" zones of Bray and Sancio (2006) or Boulanger and Idriss (2006), respectively. On the other hand, there is no such need for the proposed methodology. Table 4.3-3 summarizes the calculated values of Acc, P, R and F_β.

Table 4.3-3. Summary of statistical metrics for each criterion

Statistical Metric	Bray & Sancio (2006)	Boulanger & Idriss (2006)	This Study
Acc	0.780	0.716	0.964
P	0.896	0.811	0.976
R	0.704	0.423	0.976
F_β	0.789	0.556	0.976

Clearly revealed by Table 4.3-3, predictions by the proposed criteria are significantly superior compared to widely referred works of Bray and Sancio (2006) and Boulanger and Idriss (2006). Using *LI* -which is the most informative parameter regarding index properties of soils- along with *PI* as screening parameters and also adopting a liquefaction definition -which represents soil response much better compared to strain or r_u based definitions- are believed to be the possible reasons of this superior performance. Among these other two criteria, Bray and Sancio produces better results which is due to using w_c / LL as a screening tool; while criteria of Boulanger and Idriss use only *PI* for this purpose. Author of this dissertation believes that Seed et al. (2003) can be better option compared to works of Bray and Sancio (2006) and Boulanger and Idriss (2006), since it is developed based on *PI* , w_c / LL and also *LL* ; yet since Seed et al. neither clearly stated how they developed their criteria nor defined which soil response was called as "liquefaction", it is not possible to test performance of that study fairly.

Although the proposed methodology is shown to be a better alternative to existing liquefaction susceptibility criteria, it is just the introductory assessment stage of liquefaction engineering, and for a complete assessment of seismic soil response and performance, more needs to be done. Thus, cyclically-induced straining potential and post-cyclic shear strength assessment methodologies also need to be developed. For this reason, following chapters of this thesis are devoted to establish frameworks for the engineering assessment of these two problems.

CHAPTER 5

ASSESSMENT OF CYCLIC STRAINING POTENTIAL OF FINE-GRAINED SOILS

5.1 INTRODUCTION

This chapter is devoted to the development of probabilistically-based semi empirical models for the engineering assessment of the cyclically-induced maximum shear and post-cyclic volumetric (reconsolidation) and residual shear straining potentials of silt and clay mixtures.

Efforts aiming to develop a semi-empirical or empirical model naturally require the compilation of a high quality database, which was introduced in Chapter 3. Results of testing program and compiled data from literature reveal the following:

i)   Consistent with previous findings from available literature (e.g. Ishihara et al., 1980; Vucetic and Dobry, 1991; Boulanger and Idriss, 2004), *PI* is concluded to be an important controlling parameter for cyclic straining response of cohesive fine-grained soils. Various researchers have studied the effects of *PI* on different aspects of problem varying from cyclic strength and stiffness degradation to liquefaction susceptibility. Based on experimental results, different threshold *PI* values were adopted depending on the purpose. However, based on test results, it is observed

that beyond *PI* of 15, cyclic straining potential is concluded to be limited (i.e. < 7.5%) for a cyclic shear stress ratio (τ_{cyc} / s_u) of 0.50.

ii)   Amplitude of cyclic shear stress ratio (τ_{cyc} / s_u) is important as it is the cyclic demand term. Although Boulanger and Idriss (2004 and 2006) reported CRR ($= \tau_{cyc} / s_u$) values in the order of 0.75 to 1.01, existing experimental data from this study and also other data sources indicate that τ_{cyc} / s_u values of even 0.40 may result in shear strains in the order of 6% at moderate number of loading cycles depending on *PI* and w_c / LL. This minimum stress ratio level, which produces significant strains, is not considerably different than the threshold stress ratio (called as "critical level of repeated stress") which was used by various researchers (e.g. Sangrey et al., 1978; Ansal and Erkmen, 1989; Vaid and Zergoun, 1994) Although this threshold shear strain depends on frequency of loading, the reported values varied in the range of 0.50 to 0.60.

iii)   The ratio of applied static stress to cyclic shear stress (i.e. τ_{st} / τ_{cyc}) is also important as it determines the occurrence of stress reversal. τ_{st} / s_u represents the shear strength capacity used under static loading conditions, on top of which cyclic loads are applied. Recent ground failure case histories after 1999 Adapazari and Chi-Chi earthquakes clearly revealed that the presence of initial static shear stresses may change cyclic response of soils. Previous studies of Konrad and Wagg (1993) and Sancio (2003) highlighted that existence of initial static shear stresses decrease the number of cycles to a threshold shear strain level. They have also reported that lower excess pore water pressures are generated due to reduced shear stress reversal. These studies mostly focused on residual shear strains, without taking into account the cyclic

shear straining, which decreases significantly when degree of stress reversal decrease. Available test data also supports this argument, and it is observed that in case τ_{st} / τ_{cyc} ratio exceeds 0.6, the amplitude of cyclic shear strain is limited.

iv)   The findings from liquefaction susceptibility studies of Wang (1979), Seed et al. (2003) and Bray and Sancio (2006) revealed that w_c / LL ratio is an important parameter indicating proximity of the specimen to viscous liquid state. Hence, as w_c / LL decreases, shear straining potential of specimens also decreases, and below a value of 0.7, no significant shear stains are observed under moderate to high levels of shaking.

v) PI and w_c / LL are accepted to be primary factors affecting straining potential of silt and clay mixtures, as they capture the effects of soil mineralogy. It is also believed that the amount of fines (FC) also influences the straining response of silt and clay mixtures. This influence is not as significant as the effects of PI and w_c / LL , but it is still considered in model development stage.

vi)   A detailed review of previous efforts focusing on the close relationship between residual excess pore water pressure and post-cyclic volumetric strain based on the theory of 1-D consolidation was given in Chapter 2. It has been recognized since the early studies of Silver and Seed (1977) for dry sands and the later the works of Sasaki et al. (1982), Nagase and Ishihara (1988), Ishihara and Yoshimine (1992), Shamoto et al. (1998), Tsukamoto et al. (2004), Duku et al. (2008), Cetin et al. (2009) for saturated clean sands that there exist a strong correlation between cyclic shear and post-cyclic volumetric strains. For fine-grained soils the relationship between residual excess pore water pressure and $\varepsilon_{v,pc}$ was

utilized by various researchers (e.g. Ohara and Matsuda, 1988; Yasuhara et al., 1992). There exist a strong correlation between cyclically-induced pore water pressure and shear straining, as will be shown later in this chapter. Considering the problems associated with pore water pressure measurements under rapid loading conditions (i.e.: delayed pore pressure response), it is concluded that estimating $\varepsilon_{v,pc}$ as a function of γ_{max} would be more practical, as presented in Figure 5.1-1. As revealed by this figure there exist a unique relationship between γ_{max} and $\varepsilon_{v,pc}$.

vii)   Owing to its nature, residual shear straining problem is more difficult to assess compared to the former post-cyclic strain component. Yet, detailed inspection on available test data indicated that residual shear strain (γ_{res}) potential of silt and clay mixtures tends to increase with increasing cyclic maximum shear strain potential (γ_{max}), τ_{st}/s_u, SSR and also PI.

The individual model components of cyclic-induced straining problem for fine grained soils are assessed through a probabilistically-based framework. Starting from cyclic shear strain potential, which is believed to be the key component since its amplitude affects both $\varepsilon_{v,pc}$ and γ_{res} potentials; this chapter proceeds with the assessment of post-cyclic volumetric straining problem. It is concluded with the assessment of residual shear strains for soils subjected to initial static shear strains.
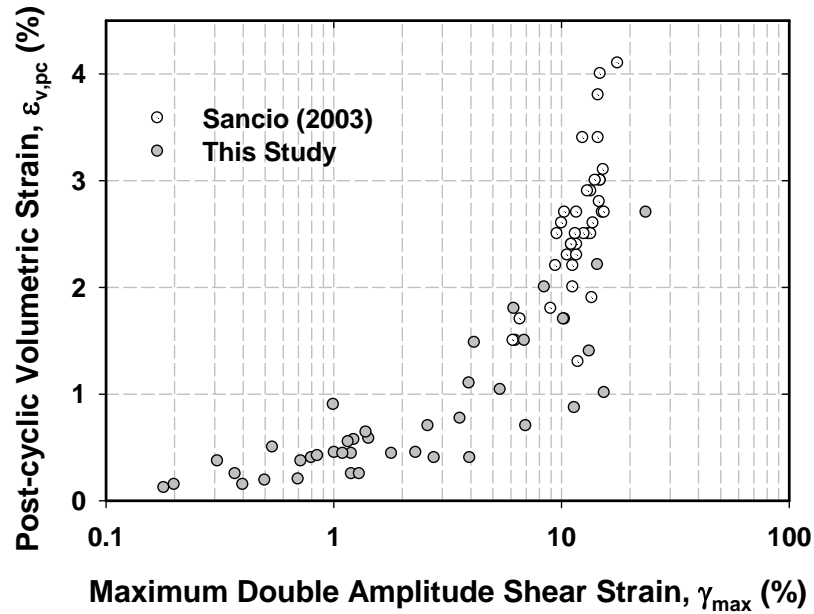
Figure 5.1-1. Relationship between maximum cyclic shear and post-cyclic volumetric strains

5.2   ASSESSMENT OF CYCLIC SHEAR STRAIN POTENTIAL

The first step in developing a probabilistic model is to develop a limit state expression that captures the essential parameters of the problem. The model for the limit state function has the general form $g = g\,(\mathbf{x}, \mathbf{\Theta})$ where x is a set of descriptive parameters and Θ is the set of unknown model parameters. Inspired by data trends as presented in Tables 3.3-2 and 3.5-1, various functional forms were tested, some of which are listed in Table 5.2-1. Among these, the following functional form produced the best fit to the observed behavioral trends and is adopted as the limit state function for maximum cyclic shear strain estimation at the end of 20th loading cycle (γ_{max}), where θ_i represent the set of unknown model coefficients:

$$g_{\gamma_{max}}(\frac{w_c}{LL}, PI, \frac{\tau_{cyc}}{s_u}, \frac{\tau_{st}}{s_u}, \gamma_{max}, \Theta) = \ln(\gamma_{max})$$

$$-\ln\left(\theta_1 \cdot \frac{\theta_2^{\left(\theta_3 \cdot \frac{w_c}{LL}\right)}}{\ln(PI)} \cdot \frac{\theta_4 - \sqrt{\left(\frac{\tau_{st}}{s_u} - \theta_5\right)^2 + \left(\frac{\tau_{cyc}}{s_u} - \theta_6\right)^2}}{\theta_4 - \theta_7} \cdot \left(1 - \theta_8 \ln\left(\frac{\theta_9}{PI}\right)\right)\right) \pm \varepsilon_{\gamma_{max}} \qquad (5-1)$$

The proposed model includes a random model correction term (ε) to account for the facts that i) possible missing descriptive parameters with influence on cyclic straining may exist; and ii) the adopted mathematical expression may not have the ideal functional form. It is reasonable and also convenient to assume that ε has normal distribution with zero mean for the aim of producing an unbiased model (i.e., one that in the average makes correct predictions). The standard deviation of ε, denoted as σ_ε, however is unknown and must be estimated. The set of unknown parameters of the model, therefore, is $\Theta = (\theta, \sigma_\varepsilon)$.

Formulation of likelihood function is the next step. When formulating the likelihood functions, it is important to take into account the following issues: i) for the compiled data, shear strength values were predicted based on existing in-situ test data rather than performing monotonic loading tests on identically consolidated soil specimens, and ii) for some tests, cyclic loading was stopped sooner than the 20th loading cycle.

Assuming the maximum shear strain values of each test to be statistically independent, the likelihood function can be written as the product of the probabilities of the observations for "k" and "l" tests from this study and literature, respectively where exact strain values are available (i.e. values at the end of the 20th loading cycle are available), and for "m" and "n" tests from this study and literature, respectively, where strain values are available at the end of cyclic loading less than 20.

$$L_{\gamma_{max}}(\mathbf{\theta},\sigma_{\varepsilon}) = \prod_{i=1}^{k} P\left[g_{\gamma_{max}}(.) = 0\right] \cdot \prod_{i=1}^{l} P\left[g_{\gamma_{max}}(.) = 0\right] \cdot$$
$$\prod_{i=1}^{m} P\left[g_{\gamma_{max}}(.) \leq 0\right] \cdot \prod_{i=1}^{n} P\left[g_{\gamma_{max}}(.) \leq 0\right]$$

$$(5-2)$$

Table 5.2-1. Alternative limit state models for cyclic shear straining problem

Trial #	Model Mathematical Form
1	$\gamma_{max} = \theta_1 \cdot \dfrac{\exp(w_c / LL)}{\ln(PI)} \cdot \left(\dfrac{\tau_{st}}{s_u} + \theta_2 \dfrac{\tau_{cyc}}{s_u}\right)^{\theta_3}$
2	$\gamma_{max} = \theta_1 \cdot \dfrac{\theta_2^{\left(\frac{w_c}{LL}\cdot\theta_3\right)}}{\ln(LL+PI)} \cdot \dfrac{\theta_4 - \sqrt{\left(\dfrac{\tau_{st}}{s_u}-\theta_5\right)^2 + \left(\dfrac{\tau_{cyc}}{s_u}-\theta_6\right)^2}}{\theta_4 - \theta_7}$
3	$\gamma_{max} = \theta_1 \cdot \dfrac{\theta_2^{\left(\frac{w_c}{LL}\cdot\theta_3\right)}}{ln(PI)} \cdot \dfrac{\theta_4 - \sqrt{\left(\dfrac{\tau_{st}}{s_u}-\theta_5\right)^2 + \left(\dfrac{\tau_{cyc}}{s_u}-\theta_6\right)^2}}{\theta_4 - \theta_7} \cdot \left(1 - \theta_8 \cdot \dfrac{\tau_{st}}{\tau_{cyc}}\right)$
4	$\gamma_{max} = \dfrac{\theta_1 \cdot \theta_2^{\left(\frac{w_c}{LL}\cdot\theta_3\right)} \cdot \left(1 - \theta_8 \cdot \ln\left(\dfrac{\theta_9}{PI}\right)\right)}{\ln(PI)} \cdot \dfrac{\theta_4 - \sqrt{\left(\dfrac{\tau_{st}}{s_u}-\theta_5\right)^2 + \left(\dfrac{\tau_{cyc}}{s_u}-\theta_6\right)^2}}{\theta_4 - \theta_7}$
5	$\gamma_{max} = \dfrac{\theta_1 \cdot \theta_2^{(LI\cdot\theta_3)} \cdot \left(1 - \theta_8 \cdot ln\left(\dfrac{\theta_9}{PI}\right)\right)}{ln(PI)} \cdot \dfrac{\theta_4 - \sqrt{\left(\dfrac{\tau_{st}}{s_u}-\theta_5\right)^2 + \left(\dfrac{\tau_{cyc}}{s_u}-\theta_6\right)^2}}{\theta_4 - \theta_7}$

As referred to earlier in Chapter 3, monotonic triaxial tests were performed to determine undrained shear strength (s_u) of "undisturbed" specimens as a part of a strain controlled static testing program. However for the test data compiled from available literature, results of in-situ tests were used for this purpose. Therefore, these s_u values are neither exact nor free from errors and to model this fact, ach estimation or measurement of s_u is written in terms of a mean value (μ_{s_u}) and an error term (ε_{s_u}) as follows:

$$s_{u,i} = \widehat{s}_{u,i} + \varepsilon_{s_{u,i}} \tag{5-3}$$

where the error term for each estimation or measurement, s_u can be assured to have zero mean and a standard deviation (σ_{s_u}) having normal distribution.

For data compiled from literature, total variance in likelihood approximation could be written as the sum of the model error and error due to inexact s_u measurements as follows:

$$\sigma^2{}_{tot} = \sigma^2{}_\varepsilon + \sigma^2{}_{s_u} \cdot \left\{ \frac{d}{ds_u}(\gamma_{max}) \right\}^2 \tag{5-4}$$

where $\dfrac{d}{ds_u}(\gamma_{max})$ is derived based on Equation (5 – 1) as follows:

$$\frac{d}{ds_u}(\gamma_{max}) = \frac{\left[\frac{\tau_{st}}{s_u{}^2}\left(\frac{\tau_{st}}{s_u} - \theta_5 \right) + \frac{\tau_{cyc}}{s_u{}^2}\left(\frac{\tau_{cyc}}{s_u} - \theta_6 \right) \right]}{\left[\theta_4 - \sqrt{\left(\frac{\tau_{st}}{s_u} - \theta_5 \right)^2 + \left(\frac{\tau_{cyc}}{s_u} - \theta_6 \right)^2} \right] \cdot \sqrt{\left(\frac{\tau_{st}}{s_u} - \theta_5 \right)^2 + \left(\frac{\tau_{cyc}}{s_u} - \theta_6 \right)^2}} \tag{5-5}$$

Suppose the values of $(w_c / LL)_i$ and PI_i at the each data point are exact for whole database; whereas values of $(\tau_{st} / s_u)_i$ and $(\tau_{cyc} / s_u)_i$ are not exact for the data compiled from the available literature, then the likelihood function can be written as a function of unknown coefficients as in Equation (5 – 6). In this equation, $\varphi[\cdot]$ and $\Phi[\cdot]$ are the standard normal probability density and cumulative distribution functions, respectively.

$$L_{\gamma_{max}}(\boldsymbol{\theta}, \sigma_\varepsilon) = \prod_{i=1}^{k} \left\{ \varphi\left[\frac{\widehat{g}(\cdot)}{\sigma_\varepsilon} \right] \right\} \cdot \prod_{i=k+1}^{k+l} \left\{ \varphi\left[\frac{\widehat{g}(\cdot)}{\sigma_{tot}} \right] \right\} \cdot$$
$$\prod_{i=k+l+1}^{k+l+m} \left\{ \Phi\left[\frac{\widehat{g}(\cdot)}{\sigma_\varepsilon} \right] \right\} \cdot \prod_{i=k+l+m+1}^{k+l+m+n} \left\{ \Phi\left[\frac{\widehat{g}(\cdot)}{\sigma_{tot}} \right] \right\} \tag{5-6}$$

Consistent with the maximum likelihood methodology, model coefficients are estimated by maximizing the likelihood function given in Equation $(5-6)$ and these coefficients are presented in Table 5.2-2.

Table 5.2-2. Coefficients of γ_{max} model

θ_1	9.939
θ_2	26.163
θ_3	0.995
θ_4	25.807
θ_5	5.870
θ_6	-25.085
θ_7	31.740
θ_8	0.076
θ_9	21.080
σ_ε	0.537

The final form of the proposed model is presented in Equation $(5-7)$ along with $\pm$ one standard deviation range.

$$ln(\gamma_{max}) = ln\left[\frac{9.939 \cdot \dfrac{26.163^{\left(0.995 \cdot \frac{w_c}{LL}\right)}}{ln(PI)} \cdot \left(1 - 0.076 \cdot ln\left(\dfrac{21.08}{PI}\right)\right) \cdot}{25.807 - \sqrt{\left(\dfrac{\tau_{st}}{s_u} - 5.870\right)^2 + \left(\dfrac{\tau_{cyc}}{s_u} - (-25.085)\right)^2}}{25.807 - 31.740}\right] \pm 0.537 \quad (5-7)$$

Same procedure is applied for all of the limit state functions presented in Table 5.2-1. Estimated model coefficients along with corresponding maximum likelihood values are presented in Table 5.2-3. Noting that proposed limit state function (i.e. Trial #4) produces the most accurate and unbiased strain predictions since higher likelihood value ($\sum lh$) and smaller σ_ε are indications of a superior model.

Table 5.2-3. Summary of model coefficients and performances of limit state functions tested for maximum cyclic shear strain potential

Trial #	Model Coefficients										$\sum lh$
	θ_1	θ_2	θ_3	θ_4	θ_5	θ_6	θ_7	θ_8	θ_9	σ_ε	
1	0.0005	1393	1.38	-	-	-	-	-	-	0.715	-45.6
2	9.287	26.15	1.17	25.81	5.85	-25.09	31.65	-	-	0.479	-31.3
3	10.755	26.16	0.99	25.81	5.88	-25.09	31.72	0.076	-	0.460	-29.7
4	9.939	26.16	0.99	25.81	5.87	-25.09	31.74	0.076	21.08	0.461	-29.6
5	65.08	25.01	0.40	25.81	5.87	-25.09	31.77	-0.15	21.02	0.464	-30.3

Although the proposed closed-form equation is recommended to be directly used for the assessment of cyclic double amplitude shear straining potential of fine grained soils, for the sake of enabling some visual comparisons strain boundaries are also derived and presented in τ_{st}/s_u vs. τ_{cyc}/s_u domain for three representative scenarios corresponding to w_c/LL and PI pairs of i) 1.0 and 5, ii) 0.9 and 10, and iii) 0.8 and 20, as given in Figures 5.2-1, 5.2-2 and 5.2-3 respectively along with the compiled test data.
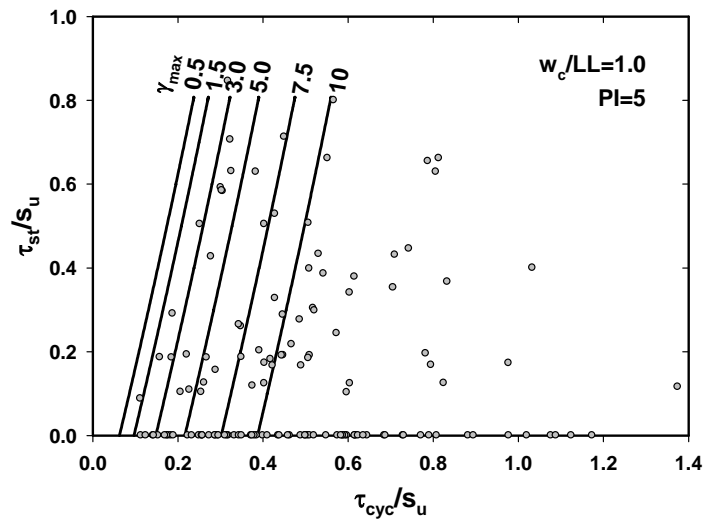
Figure 5.2-1. Maximum shear strain boundaries for w$_c$/LL=1.0 and PI=5
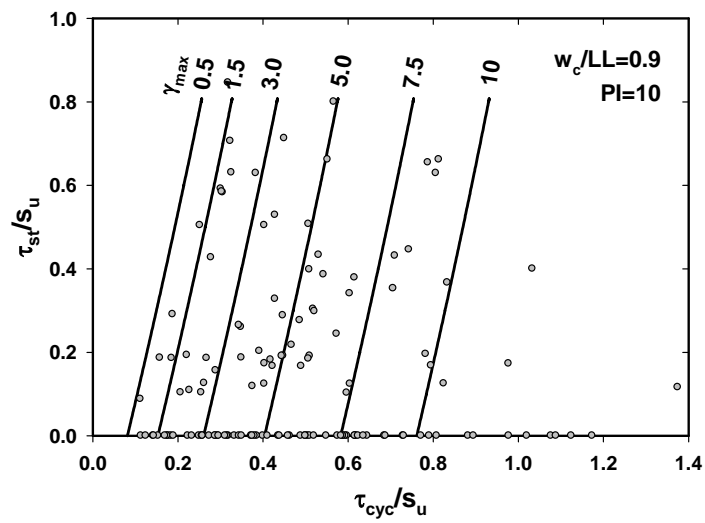
Figure 5.2-2. Maximum shear strain boundaries for w$_c$/LL=0.9 and PI=10
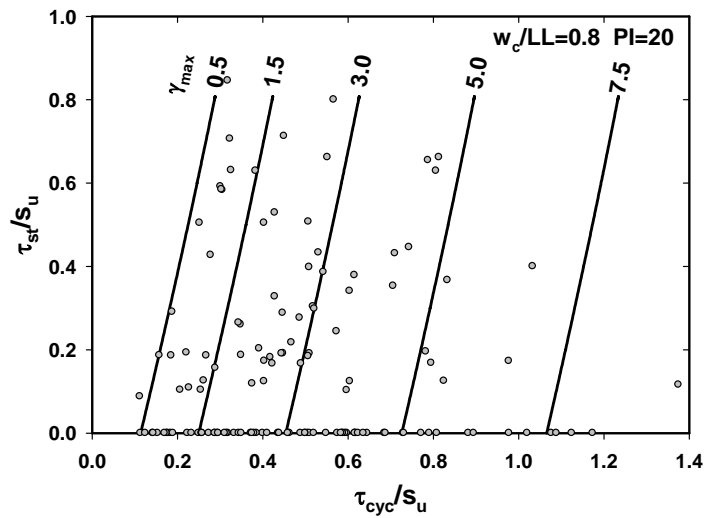
Figure 5.2-3. Maximum shear strain boundaries for w_c/LL=0.8 and PI=20

For the purpose of performance evaluation of the proposed model, measured and predicted cyclic double amplitude shear strains are paired and shown on Figure 5.2-4 along with the 1:2 and 1:0.5 boundary lines. 87.8 % of the predictions lie within these ranges, suggesting that the cyclic shear strain levels can be estimated within a factor 2 by using the proposed framework. Thus, the proposed model is judged to produce reasonable and unbiased predictions.

Besides this visual observation, the performance of the model predictions are also expressed by Pearson product moment correlation coefficient, R^2, and reported on Figure 5.2-4 as 0.83 (or 83 %) which is another indication of model's success considering how challenging the assessment of cyclic straining task is.
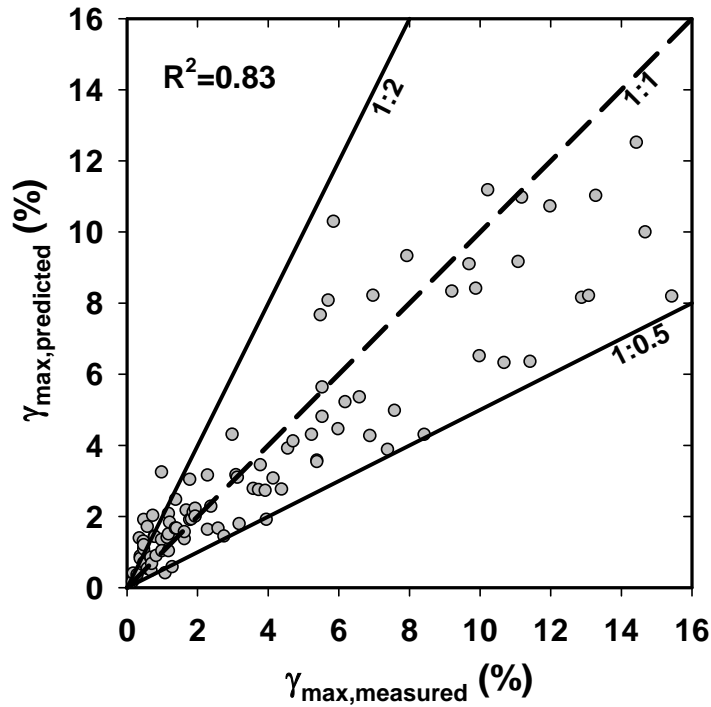
Figure 5.2-4. Comparison between measured and predicted cyclic shear strains at 20th loading cycle

The power of the proposed mathematical form (i.e. limit state function) is also assessed by simple statistics (i.e. mean and standard deviation) of residual which is defined as follows:

$$Residual = ln(\gamma_{max,predicted} / \gamma_{max,measured})$$ (5 − 8)

A smaller absolute mean residual, $\left|\mu_{residual}\right|$, and $\sigma_{residual}$ can be simply interpreted as a relatively more accurate and precise model. For the proposed model, $\mu_{residual}$ and $\sigma_{residual}$ are calculated as 0.005 and 0.484, respectively. A positive $\mu_{residual}$ means that the model predictions are greater than actual test values (i.e.: conservatively biased) and for this case, $\mu_{residual}$ of 0.005 indicates that model predictions are just 0.46 % greater than the measured test values in the average.

106

Plots of residual vs. PI, w_c / LL, τ_{cyc} / s_u and τ_{st} / s_u are also prepared and shown in Figures 5.2-5 through 5.2-8, respectively; to check if any trend as a function of model input variables (descriptors) is left in residuals. No clear trend as a function of any of these input variables is observed confirming the validity of selected functional form.
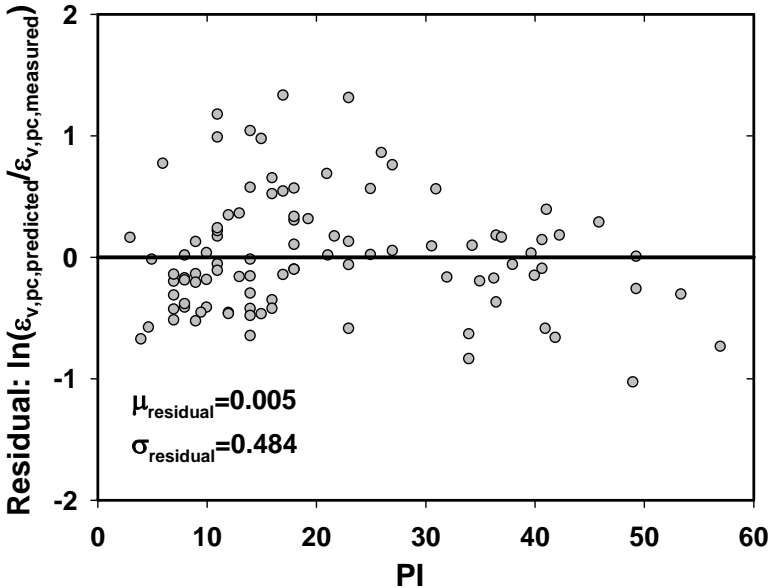
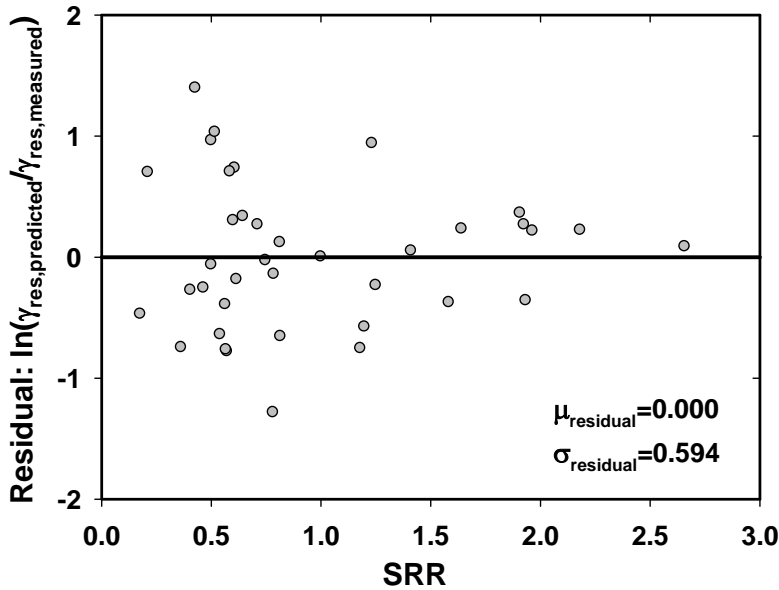**Figure 5.2-5. Scatter of residuals with PI**
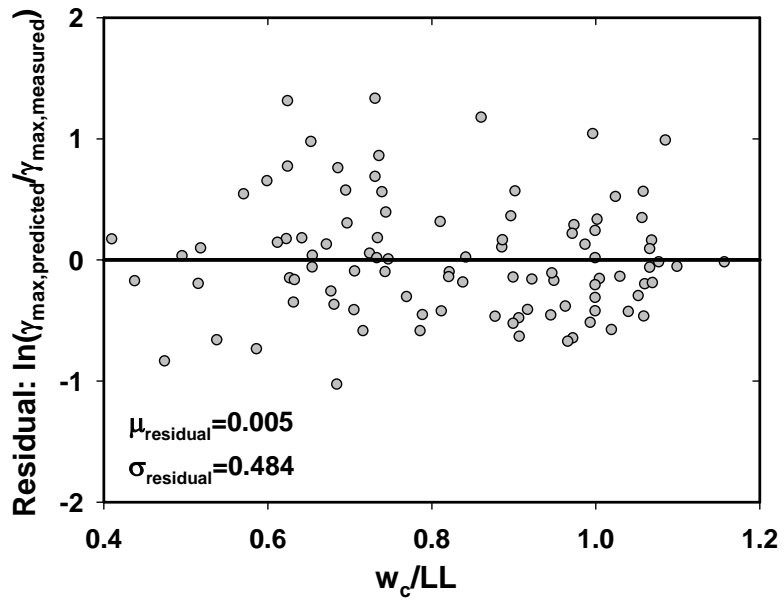
Figure 5.2-6. Scatter of residuals with w_c/LL
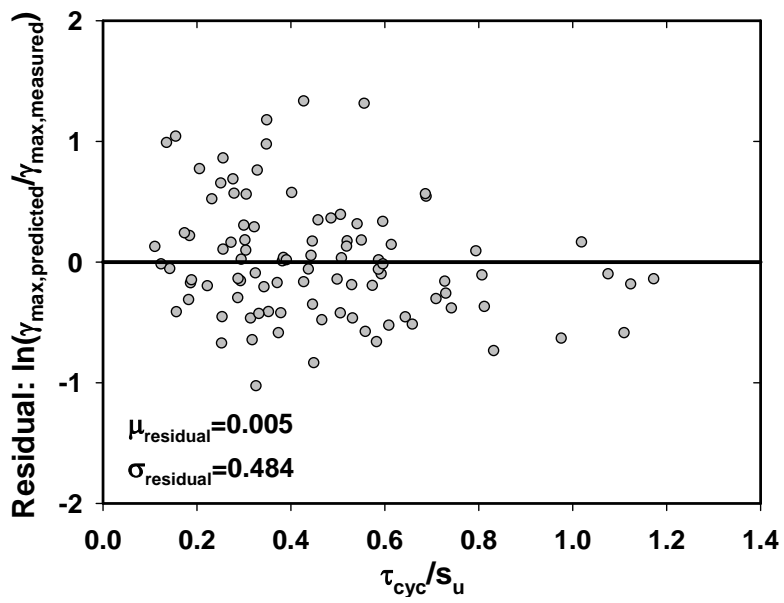
Figure 5.2-7. Scatter of residuals with τ_{cyc}/s_u
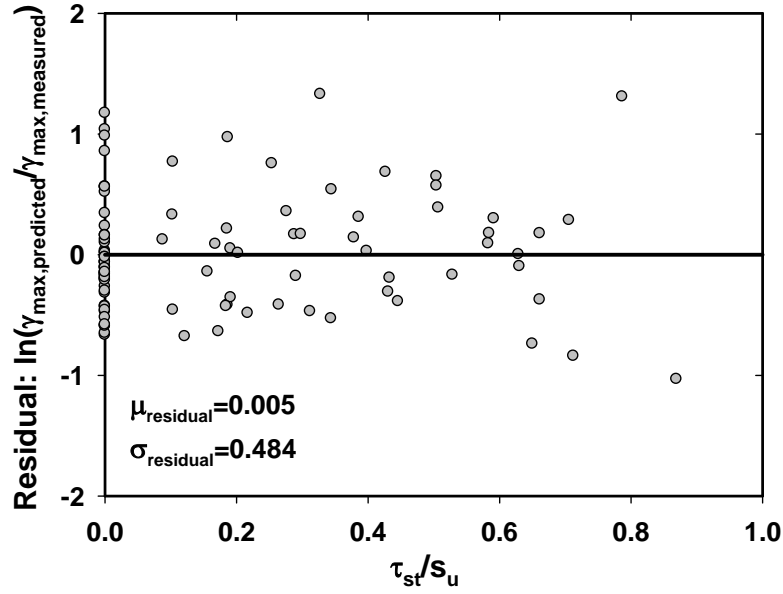
Figure 5.2-8. Scatter of residuals with τ_{st}/s_u

Last but not least, the possible influence of fines content (FC) is also considered by adopting the following limit state model as presented in Equation $(5-9)$.

$$g_{\gamma_{\max}}(\frac{w_c}{LL}, PI, FC, \frac{\tau_{cyc}}{s_u}, \frac{\tau_{st}}{s_u}, \gamma_{\max}, \Theta) = \ln(\gamma_{\max}) -$$

$$\ln\left(\theta_1 \cdot \frac{\theta_2^{\theta_3 \cdot \frac{w_c}{LL} \cdot \ln\left(\frac{FC}{\theta_{10}}\right)}}{\ln\left(\frac{PI \cdot FC}{\theta_{11}}\right)} \cdot \left(1 - \theta_8 \ln\left(\frac{\theta_9}{PI \cdot FC}\right)\right) \cdot \frac{\theta_4 - \sqrt{\left(\frac{\tau_{st}}{s_u} - \theta_5\right)^2 + \left(\frac{\tau_{cyc}}{s_u} - \theta_6\right)^2}}{\theta_4 - \theta_7}\right) \pm \varepsilon_{\gamma_{\max}} \qquad (5-9)$$

Following a similar procedure, likelihood function is formed and then consistent with the maximum likelihood methodology, model coefficients are estimated by maximizing this new likelihood function. These set of coefficient are summarized in Table 5.2.4.

109

Table 5.2-4. Coefficients of γ_{max} model for Equation $(5-9)$

θ_1	21.509
θ_2	21.788
θ_3	0.092
θ_4	3.473
θ_5	1.007
θ_6	-3.262
θ_7	17.805
θ_8	0.061
θ_9	29.878
θ_{10}	0.00067
θ_{11}	61.843
σ_ε	0.468

Performance of this new model is evaluated by comparing measured and predicted cyclic double amplitude shear strains as shown in Figure 5.2-9 along with the 1:2 and 1:0.5 boundary lines. It is observed that 88.2 % of the predictions lie within these ranges and Pearson product moment correlation coefficient, R^2, is calculated as 0.83 (or 83 %) as reported on Figure 5.2-9 which is equal to R^2 value of previous model. Yet, the mean and standard deviation of residuals, which are calculated as -0.0038 and 0.470, respectively, indicated that including *FC* as a model parameter results in more refined predictions. However, models given by Equations $(5-1)$ and $(5-8)$ do not produce very different predictions, and the task of balancing the cost of an additional parameter for the price of a slightly improved prediction is left to users.

Figure 5.2-9. Comparison between measured and predicted cyclic shear strains at 20th loading cycle for Equation (5 – 9)

5.3 ASSESSMENT OF POST-CYCLIC VOLUMETRIC STRAIN POTENTIAL

Assessment of post-cyclic volumetric (reconsolidation) straining potential of fine-grained soils attracted more research interest relative to shear straining potential. As reviewed in Chapter 2, earlier efforts (e.g. Ohara and Matsuda, 1988; Yasuhara et al. (1992), are mostly based on1-D consolidation theory. Within the confines of this section, besides the development of a new semi-empirical procedure for engineering assessment of $\varepsilon_{v,pc}$, 1-D consolidation theory based approaches are also evaluated comparatively. Finally an alternative formulation is proposed after introducing a new excess pore water pressure generation model for silt and clay mixtures.

111

Figure 5.2-9. Comparison between measured and predicted cyclic shear strains at 20th loading cycle for Equation (5 – 9)

5.3 ASSESSMENT OF POST-CYCLIC VOLUMETRIC STRAIN POTENTIAL

Assessment of post-cyclic volumetric (reconsolidation) straining potential of fine-grained soils attracted more research interest relative to shear straining potential. As reviewed in Chapter 2, earlier efforts (e.g. Ohara and Matsuda, 1988; Yasuhara et al. (1992), are mostly based on1-D consolidation theory. Within the confines of this section, besides the development of a new semi-empirical procedure for engineering assessment of $\varepsilon_{v,pc}$, 1-D consolidation theory based approaches are also evaluated comparatively. Finally an alternative formulation is proposed after introducing a new excess pore water pressure generation model for silt and clay mixtures.

111

5.3.1 Proposed New Semi-Empirical Model

Model development efforts begin with the selection of a limit state expression capturing the essential parameters of the problem. Inspired by prior research studies (Silver and Seed, 1971; Sasaki et al., 1982; Castro, 1987; Ishihara and Yoshimine, 1992) and strong correlation between $\gamma_{\max}$ and $\varepsilon_{v,pc}$ as presented in Figure 5.1-1 and Table 3.3-2, various functional forms were tested, some of which are listed in Table 5.3-1. Among these, the following functional form produced the best fit to the observed behavioral trends and is adopted as the limit state function, where θ_i represents the set of unknown model coefficients:

$$g_{\varepsilon_{v,pc}}\left(\frac{w_c}{LL}, PI, \gamma_{\max}, \varepsilon_{v,pc}, \Theta\right) = \ln(\varepsilon_{v,pc}) - \ln\left(\frac{\theta_1 \cdot \gamma_{\max}^{\theta_2}}{\theta_3 + \theta_4 \cdot \ln(PI) - \dfrac{w_c}{LL}}\right) \pm \varepsilon_{\varepsilon_{v,pc}} \qquad (5-10)$$

Similar to the $\gamma_{\max}$ model, this one also includes a random model correction term (ε) to account for the facts that i) possible missing descriptive parameters with influence on cyclic straining may exist; and ii) the adopted mathematical expression may not have the ideal functional form. Based on similar arguments, it is assumed that ε follows normal distribution with zero mean for the aim of producing an unbiased model. The standard deviation of ε, denoted as σ_ε, however is unknown and must be estimated. The set of unknown parameters of the model, therefore, is Θ = (θ, σ_ε).

112

Table 5.3-1. Alternative limit state models for post-cyclic volumetric straining problem

Trial #	Model Mathematical Form
1	$\varepsilon_{v,pc} = \theta_1 \cdot \gamma_{max}^2 + \theta_2 \cdot \gamma_{max}$ (adopted by Bilge and Cetin, 2007)
2	$\varepsilon_{v,pc} = \theta_1 \cdot \gamma_{max}^{\theta_2}$ (adopted by Bilge and Cetin, 2008)
3	$\varepsilon_{v,pc} = \dfrac{\theta_1 \cdot \gamma_{max}^{\theta_2}}{\theta_3 + \theta_4 \cdot \ln(PI) - w_c / LL}$

$\varepsilon_{v,pc}$ is expressed as a function of γ_{max}, PI and w_c / LL, which are directly available as part of laboratory test results. It is assumed that there exist no uncertainties associated to laboratory testing. It is also important to note that $\varepsilon_{v,pc}$ is linked to the cyclic shear strain, corresponding to the loading cycle at the end of which consolidation valve is opened for volume change measurements. Therefore, any kind of upper or lower boundaries (for loading cycles greater or smaller than 20, respectively) is not required for the formulation. If γ_{max} value corresponds to 20th loading cycle then resulting $\varepsilon_{v,pc}$ will be also correspond to the same loading cycle by definition.

Assuming the post-cyclic volumetric strain values of each test to be statistically independent, the likelihood function for "n" tests can be written as the product of the probabilities of the observations.

$$L_{\varepsilon_{v,pc}}(\boldsymbol{\theta}, \sigma_\varepsilon) = \prod_{i=1}^{n} P \left[g_{\varepsilon_{v,pc}} \left(\frac{w_c}{LL_i}, PI_i, \gamma_{max,i}, \theta \right) = 0 \right] \qquad (5-11)$$

Suppose the values of $(w_c / LL)_i$, PI_i, and $(\gamma_{max})_i$ at the each data point are exact, i.e. no measurement error is present, noting that $g(...) = \widehat{g}(...) + \varepsilon_i$ has the normal distribution with mean $\widehat{g}$ and standard deviation σ_ε, then the likelihood function can

be written as a function of unknown coefficients as in Equation $(5 - 12)$. In this equation, $\varphi[\cdot]$ is the standard normal probability density function.

$$L_{\varepsilon_{v,pc}}(\mathbf{\theta},\sigma_\varepsilon) = \prod_{i=1}^{n} \varphi \left[\frac{\hat{g}_{\varepsilon_{v,pc}}\left(\frac{w_c}{LL_i}, PI_i, \gamma_{\max,i}, \theta\right)}{\sigma_{\varepsilon_{v,pc}}} \right] \qquad (5-12)$$

Consistent with the maximum likelihood methodology, model coefficients are estimated by maximizing the likelihood function given in Equation $(5 - 12)$ and they are presented in Table 5.3-2.

Table 5.3-2. Coefficients of $\varepsilon_{v,pc}$ model

θ_1	0.400
θ_2	0.562
θ_3	1.805
θ_4	-0.036
σ_ε	0.297

The final form of the proposed model is presented in Equation $(5 - 13)$ along with $\pm$ one standard deviation range.

$$ln(\varepsilon_{v,pc}) = ln\left[\frac{0.400 \cdot \gamma_{max}^{0.562}}{1.805 + (-0.036) \cdot PI - w_c / LL} \right] \pm 0.297 \qquad (5-13)$$

Same procedure is applied for all of the limit state functions presented in Table 5.3-1. Estimated model coefficients along with corresponding maximum likelihood value are presented by Table 5.3-3. Note that the proposed limit state function (i.e. Trial #3) produces the most accurate and unbiased strain predictions, since higher likelihood value $(\sum lh)$ and smaller σ_ε are indications of a superior model.

Table 5.3-3. Summary of model coefficients and performances of limit state functions tested for post-cyclic volumetric strain potential

Trial #	Model Coefficients					$\sum lh$
	θ_1	θ_2	θ_3	θ_4	σ_ε	
1	-0.007	0.282	-	-	0.45	-21.0
2	0.397	0.692	-	-	0.336	-11.1
3	0.400	0.562	1.805	-0.036	0.297	-6.9

For the purpose of performance assessment, measured and predicted post-cyclic volumetric strains are paired and shown in Figure 5.3-1 along with the 1:2 and 1:0.5 boundary lines. 96 % of the predictions lie within these ranges, hence the proposed model is judged to produce reasonable and unbiased predictions.

Besides this visual observation, the performance of the model predictions are also expressed by Pearson product moment correlation coefficient, R^2, and reported in Figure 5.3-1 as 0.80 (or 80 %), which is considered as a quite satisfactory value considering challenging nature of the problem.
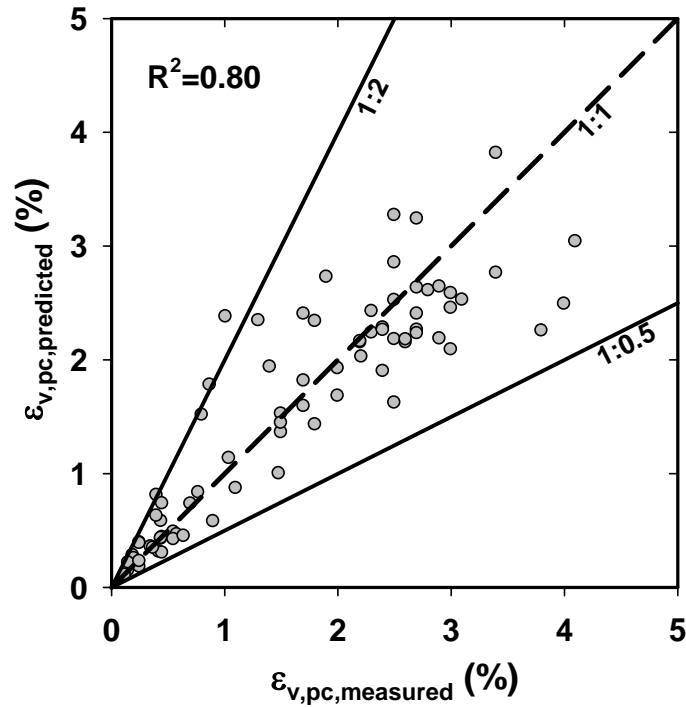
Figure 5.3-1. Comparison between measured and predicted post-cyclic volumetric strains

A similar procedure is also followed for the strain component, and the validity of the proposed mathematical form (i.e. limit state function) is also assessed by simple statistics (i.e. mean and standard deviation) of residuals, which are defined as follows:

$$Residual = ln(\,\varepsilon_{v,pc,predicted}\,/\,\varepsilon_{v,pc,measured}\,) \qquad\qquad (5-14)$$

For the proposed model, $\mu_{residual}$ and $\sigma_{residual}$ are calculated as 0.000 and 0.299, respectively. A zero $\mu_{residual}$ means that the model completely unbiased estimates in the average. Plots of residual vs. PI, $w_c\,/\,LL$, and γ_{max} are also prepared and shown in Figures 5.3-2 through 5.3-4, respectively; to check if any trend as a function of model input variables (descriptors) is left in residuals. However no clear

116

trend as a function of any of these input variables is observed confirming the validity of selected functional form.

As revealed by Equations (5 − 10) and (5 − 14), the proposed methodology requires a priori the knowledge of maximum cyclic shear strain (γ_{max}) potential, which is useful to incorporate indirectly the effects of applied cyclic and consolidation stress histories. For this purpose, Equation (5 − 13) is recommended to be used in conjunction with the proposed cyclic shear strain assessment model which is given by Equation (5 − 7).
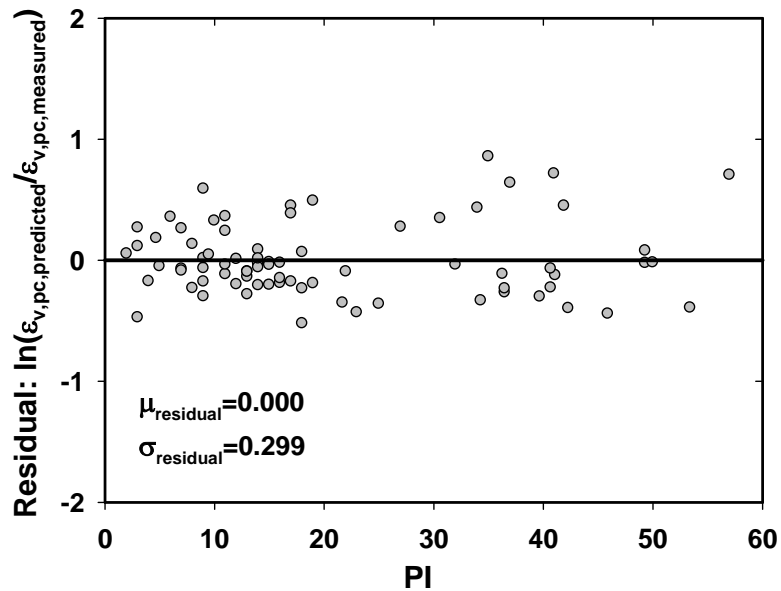
Figure 5.3-2. Scatter of residuals with PI
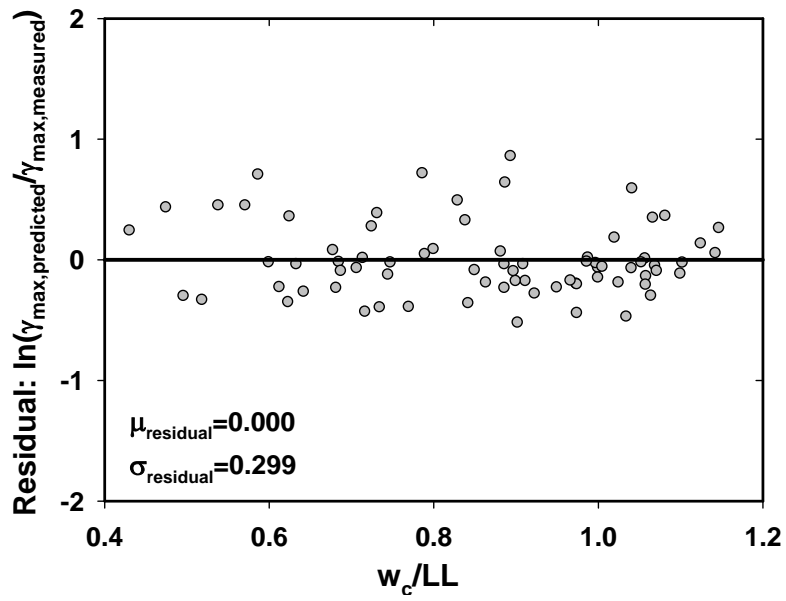
Figure 5.3-3. Scatter of residuals with w_c/LL
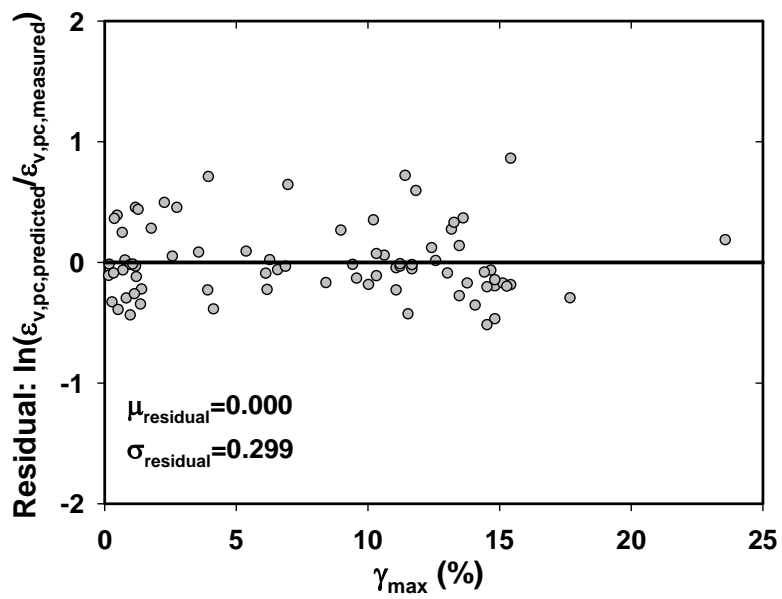
Figure 5.3-4. Scatter of residuals with τ_{cyc}/s_u

118

5.3.2 1-D Consolidation Theory-Based Approaches

As reviewed in Chapter 2, various researchers have assessed post-cyclic volumetric (reconsolidation) strains based on 1-D consolidation theory. Within the confines of this section, models of Ohara and Matsuda (1988), Yasuhara et al. (1992) and Hyde et al. (2007) are comparatively assessed. Both for comparison and calibration purposes, for each model, two alternatives were followed: model implemented with i) the original, and ii) the updated model coefficients. Moreover, an alternative model is also proposed by addressing the limitations of those previous efforts. Data presented in Tables 3.3-2, 3.4-1 and 3.5-1 are used in model calibration, comparison and development purposes.

Both for comparison and calibration purposes, for each model, two alternatives were followed: model implemented with i) the original, and ii) the updated model coefficients. First alternative presents an opportunity to make a judgment regarding which model, in its original form, is the least biased, and naturally, what should be average calibration (correction) factors. As a result of the second assessment (i.e.: by comparing the "updated" models) it is possible to decide which model has the best limit state model or functional form. In simpler terms, a framework may have a better functional form (limit state) but poorly estimated model coefficients in its original form may reduce its accuracy.

For the "updated" models (models which have the same functional form as with the original models but with updated model coefficients), maximum likelihood approach, as discussed earlier, was used for the estimation of model coefficients. A summary of the functional forms as well as model coefficients and also maximum value of likelihood functions are presented in Table 5.3-3. It should be noted that a higher likelihood value and lower σ_d of the model error term indicate superior model predictions. The model performances are also assessed by simple statistics (i.e.: mean and standard deviation) of residuals. A smaller absolute mean residual, $\left| \mu_{residual, \ln(\varepsilon_{v,pc})} \right|$, and $\sigma_{residual, \ln(\varepsilon_{v,pc})}$ can be simply interpreted as a relatively more

accurate and precise model. Predictions by "original" Ohara and Matsuda (1988) and Hyde et al. (2007) models are 84.6 and 17.2 % higher than the actual values of $\varepsilon_{v,pc}$; however, predictions by "original" Yasuhara et al. (1992) model are 14.4 % smaller than the actual $\varepsilon_{v,pc}$ values. Residuals of updated models are zero by definition as maximum likelihood methodology, aims to produce unbiased predictions; yet standard deviation of residuals is an indication of model performance, and a relatively higher model error standard deviation means a less precise model prediction. For example, based on only $\mu_{residual,\ln(\varepsilon_{v,pc})}$, "original" Hyde et al.'s model may be judged as a more successful compared to Ohara and Matsuda (1988) model; yet other descriptors clearly address that Hyde et al. (2007) exhibit the least successful predictions.

Table 5.3-4. A summary of 1-D consolidation theory-based limit state functions, coefficients and model performances

Model	Limit State Function		Model Parameters						
			θ_1	θ_2	θ_3	σ_ε	$\sum ml$	μ_{res}	σ_{res}
Ohara & Matsuda (1988)	$\varepsilon_{v,pc} = \dfrac{C_{dyn}}{1+e_0} \cdot log\left(\dfrac{1}{1-r_u}\right)$ where; $C_{dyn} = \theta_1 \cdot OCR^2 + \theta_2 \cdot OCR + \theta_3$	[1]	0.0016	-0.016	0.106	0.788	-22.56	0.613	0.501
		[2]	0.0052	-0.038	0.092	0.406	-9.91	0.000	0.411
Yasuhara et al. (1992)	$\varepsilon_{v,pc} = \dfrac{\theta_1 \cdot C_r}{1+e_0} \cdot log\left(\dfrac{1}{1-r_u}\right)$	[1]	1.5	-	-	0.454	-12.04	-0.156	0.432
		[2]	1.753	-	-	0.427	-10.84	0.000	0.432
Hyde et al. (2007)	$\varepsilon_{v,pc} = \dfrac{\theta_1}{e^{\theta_2 \cdot q_s / p'_c}} \cdot \varepsilon_{a,pc}{}^{\theta_3}$	[1]	1.74	1.71	0.461	1.001	-27.14	0.159	1.000
		[2]	1.368	10.28	0.165	0.869	-24.42	0.000	0.879

[1] original model coefficients, [2] updated model coefficients

Although consolidation theory-based approaches produce easy-to-use and theoretically robust solutions to post-cyclic volumetric straining problem, one should note that relatively successful efforts of Ohara and Matsuda (1988) and Yasuhara et al. (1992) used C_r value which is obtained for an "undisturbed" soil;

whereas, during course of cyclic loading soils exhibit significant strains and their response is believed to vary significantly. Hence it is decided to re-define dynamic recompression index as a function of amplitude of cyclic shear strain along with PI, OCR and C_r. For $OCR \leq 3$, C_{dyn} is defined as follows:

$$C_{dyn} = \left(1 + \frac{\theta_1 \cdot OCR^2 + \theta_2 \cdot OCR + \theta_3}{1 - \theta_4 \cdot \gamma_{max}^{\theta_5} + \theta_6 \, ln \, PI} \right) \cdot C_r \qquad (5-15)$$

For $OCR > 3$, it is recommended to use value of C_{dyn} corresponding to $OCR = 3$.

The model coefficients were estimated by maximum likelihood methodology, and are presented in Table 5.3-4 along with a summary of simple statistics of residuals.

Table 5.3-5. A summary of proposed 1-D consolidation theory-based model

θ_1	0.530
θ_2	-3.233
θ_3	5.927
θ_4	-1.118
θ_5	-0.404
θ_6	0.829
σ_ε	0.396
$\sum ml$	-9.421
μ_{res}	0.014
σ_{res}	0.400

In terms of σ_ε, $\sum ml$ and σ_{res} proposed model produces the most successful estimations; whereas $\mu_{residual, \ln(\varepsilon_{v,pc})}$ indicates that predictions by proposed approach are 1.41 % higher than the actual measurements (i.e.: conservatively biased).

For a soil with C_r =0.02 and PI =10, variation of C_{dyn} for different cyclic shear strain levels of γ_{max} =2.5 and 25 % are presented in Figure 5.3-5. As revealed by

this figure increasing γ_{max} (i.e. increasing cyclic-induced remolding) results in increasing C_{dyn}.
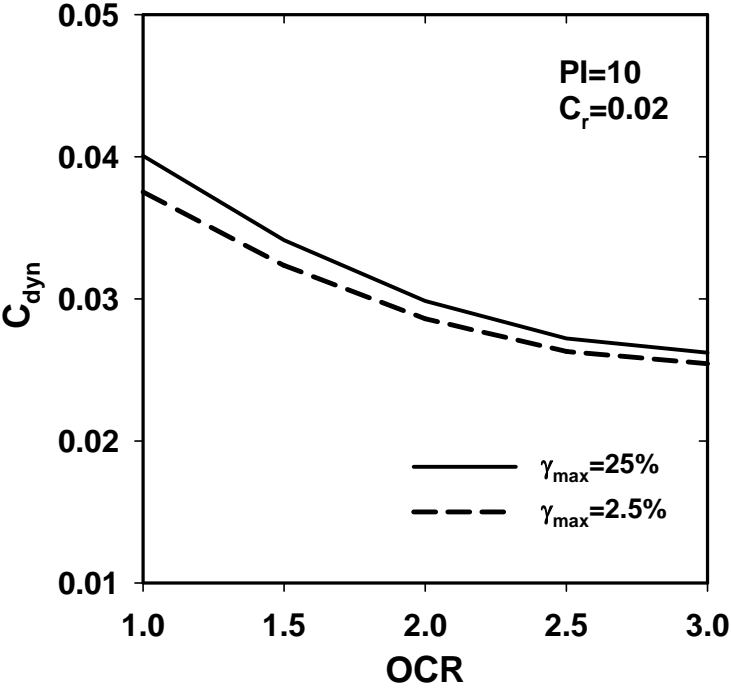
Figure 5.3-5. Variation of C_{dyn} with OCR as a function of γ_{max}

1-D consolidation theory-based approaches provide a robust methodology for the assessment of post-cyclic volumetric straining potential of silt and clay mixtures owing to its robust theoretical basis. However, their potential use is limited unless r_u values throughout cyclic loading can be reliably assessed. As briefly mentioned previously, existing models have only limited use as they were defined in terms of some material constants requiring further cyclic testing. For the purpose of eliminating such kind of limitation for the proposed model, it is also intended to develop a new excess pore water pressure generation model based on existing

experimental data. After briefly reviewing existing studies, details of model development will be introduced next.

5.3.3 New Cyclic Pore Water Pressure Generation Models for Fine-Grained Soils

Silt and clay mixtures were considered to be less vulnerable to cyclic shearing and probably based on this reasoning; this problem attracted less research interest compared to sandy soils. Yet, a number of researchers have studied this issue. Inspired from the early work of Seed et al. (1975), El Hosri et al. (1984) proposed r_u curves presented in Figure 5.3-6 based on available test data. However, as mentioned previously due to ambiguity in liquefaction definitions (i.e.: estimation of number of cycles to liquefaction triggering, N_L), this method has very limited use.

Ohara et al. (1984) developed an empirical pore water pressure model for normally-consolidated clays based on strain-controlled cyclic test data, and expressed r_u as a function of cyclic shear strain (γ_{cyc}), number of loading cycles and a number of material constants estimated for laboratory-reconstituted kaolinite clay powder with liquid limit (LL), plasticity index (PI) and moisture content (w_c) of 53.5, 28.5 and 80 %, respectively. Later, Ohara and Matsuda (1987 and 1988) extended the use of this model to over-consolidated clays, and proposed the following expression to predict occurrence of negative pore water pressures at the initial loading cycles;

$$r_u = \frac{n}{A(\gamma_{cyc})^m + \{\gamma_{cyc} /(B + C \cdot \gamma_{cyc})\} \cdot n} - D - E \cdot \log(\gamma_{cyc}) \qquad (5 - 16)$$

where n, A, B, C, D and E are material coefficients. Determination of these coefficients requires strain-controlled cyclic direct shear testing and it is considered to be the major limitation of both this pore pressure model and also the corresponding post-cyclic volumetric straining model.

123
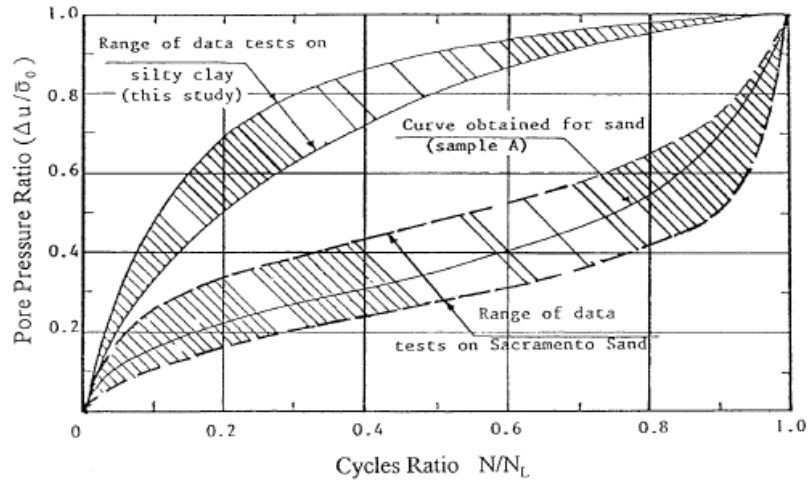
Figure 5.3-6. Pore water pressure build-up in saturated cohesive and cohesionless soils (El Hosri et al., 1984)

Hyde and Ward (1985) performed a study on Keuper Marl with liquid limit (LL), plasticity index (PI) and moisture content (w_c) of 36, 15 and 62 %, respectively; and modeled excess pore water pressure as follows:

$$\frac{u_e}{p_e} = \frac{\alpha}{\beta+1} \cdot (n^{\beta+1} - 1) + \alpha \qquad (5 - 17)$$

where p_e is the equivalent pressure, β is the pore pressure decay constant defined as -1.124 and -0.986 for OCR of 1 and 4, respectively; whereas α is defined as follows:

$$\log(\alpha) = A + B \cdot \frac{q'_r}{p_e} \qquad (5 - 18)$$

where q'_r is the cyclic deviator stress and coefficients A and B are defined for OCR = 1 as -1.892 and 2.728, and OCR = 4 as -2.288 and 1.659, respectively. For different soils, cyclic testing is required to derive the actual values of these coefficients.

Matasovic and Vucetic (1992 and 1995) developed an alternative methodology which was applicable to both normally- and over-consolidated clays. In this study, r_u is modeled as a function of γ_{cyc}, OCR and number of loading cycles (N) based on strain-controlled cyclic tests in VNP clay with liquid limit (LL), plasticity index (PI) and moisture content (w_c) of 71 - 93, 45 ± 6, 41 - 49 %, respectively. Proposed model is given in Equation (5 – 19).

$$r_u = A \cdot N^{-3 \cdot s(\gamma_c - \gamma_{tv})^r} + B \cdot N^{-2 \cdot s(\gamma_c - \gamma_{tv})^r} + C \cdot N^{-s(\gamma_c - \gamma_{tv})^r} + D \qquad (5 - 19)$$

where A, B, C, D, s and r are curve fitting parameters; whereas γ_{tv} is the threshold shear strain for positive pore water pressure generation, and it is material related constants. Authors presented the values of these curve fitting parameters for VNP clay as a function of OCR (from 1.0 to 4.0). Further testing is required to determine these curve fitting parameters for different soils which limit practical value of this model.

All those models are based on valuable efforts, however they suffer from one big drawback; as they require further cyclic testing, the results of which can be used to obtain pore water pressure build-up response directly. This drawback of previous studies and also the need for a re-visit on this critical problem with increasing number of high quality cyclic test data constitute the major inspiration of this effort.

Model development study begins with selection of a limit state expression capturing the essential parameters of the problem. The model for the limit state function has the general form g = g (**x, Θ**) where x is a set of descriptive parameters and Θ is the set of unknown model parameters. Inspired by data trends as presented by Figures 3.3-3 and 3.5-1, various functional forms were tested. The following functional form produced the best fit to observed behavioral trends and is adopted as the limit state function for modeling cyclically-induced r_u:

$$g_{r_{u,N}}(\gamma_{max,N}, PI, LI, FC, \Theta) = ln(r_{u,N}) -$$

$$ln\left(1 - exp\left(\frac{\gamma_{max,N}}{\theta_1 \cdot exp(\theta_2 \cdot PI - \theta_3 \cdot LI) \cdot \left[ln\left(\frac{FC}{\theta_4}\right)\right]^{\theta_5}}\right)\right) \pm \varepsilon_{r_{u,N}} \qquad (5-20)$$

where θ_i represent the set of unknown model coefficients, *PI* is plasticity index and *LI* is liquidity index.

The proposed model include a random model correction term (ε) to account for the facts that i) possible missing descriptive parameters with influence on cyclic pore pressure generation response may exist; and ii) the adopted mathematical expression may not have the ideal functional form. It is reasonable and also convenient to assume that ε has normal distribution with zero mean for the aim of producing an unbiased model (i.e., one that in the average makes correct predictions). The standard deviation of ε, denoted as σ_ε, however is unknown and must be estimated. As will be illustrated later, data scatter is observed to be reduced by increasing maximum shear strain levels, thus, model uncertainty is preferred to be a function of $\gamma_{max,N}$, itself. This suggests a heteroscedastic σ_ε model as expressed in Equation (5 – 21). The set of unknown parameters of the model, therefore, is $\Theta = (\mathbf{\theta}, \sigma_\varepsilon)$.

$$\sigma_{\varepsilon_{\ln(r_{u,N})}} = \frac{1}{\left(\gamma_{max,N}\right)^{\theta_6} + \theta_7} \qquad (5-21)$$

Assuming that each excess pore water pressure data is statistically independent, the likelihood function for "n" tests can be written as the product of the probabilities of the observations.

$$L_{r_{u,N}}(\mathbf{\theta}, \sigma_\varepsilon) = \prod_{i=1}^{n} P\left[g_{r_{u,N}}\left(PI_i, LI_i, FC_i, \gamma_{max,N,i}, \theta\right) = 0\right] \qquad (5-22)$$

126

Suppose the values of PI_i, LI_i, FC_i and $(\gamma_{\max,N})_i$ at the each data point are exact, i.e. no measurement error is present, noting that $g(...) = \widehat{g}(...) + \varepsilon_i$ has the normal distribution with mean $\widehat{g}$ and standard deviation σ_ε, then the likelihood function can be written as a function of unknown coefficients as in Equation (5 – 23). In this equation, $\varphi[\cdot]$ is the standard normal probability density function.

$$L_{r_{u,N}}(\boldsymbol{\theta}, \sigma_\varepsilon) = \prod_{i=1}^{n} \varphi\left[\frac{\widehat{g}_{r_{u,N}}\left(PI_i, LI_i, FC_i, \gamma_{\max,N,i}, \theta\right)}{\sigma_{r_{u,N}}} \right] \qquad (5-23)$$

Consistent with the maximum likelihood methodology, model coefficients are estimated by maximizing the likelihood function given in Equation (5 – 23) and they are presented in Table 5.3-6.

Table 5.3-6. Coefficients of $r_{u,N}$ model

θ_1	-1.991
θ_2	0.020
θ_3	0.050
θ_4	0.010
θ_5	0.328
θ_6	0.378
θ_7	0.506

The final form of the proposed model is presented in Equation (5 – 24) along with $\pm$ one standard deviation range.

$$\ln(r_{u,N}) = \ln\left[1 - \exp\left(\frac{\gamma_{\max,N}}{-1.991 \cdot \exp(0.02 \cdot PI - 0.05 \cdot LI) \cdot \left[\ln\left(\frac{FC}{0.01}\right) \right]^{0.328}} \right) \right] \qquad (5-24)$$
$$\pm \left(\frac{1}{\gamma_{\max,N}^{0.378} + 0.506} \right)$$

To develop an understanding of the range of model predictions, Figure 5-3.7 presents r_u vs. γ_{max} curves for mean values of database, PI =20, LI =0.63 and FC =80 along with ± one standard deviation (σ_ε) curves and compiled data. On the same figure, r_u vs. γ_{max} response of specimens with PI, LI and FC values close to the means of database are presented separately at upper left portion with a smaller scale.
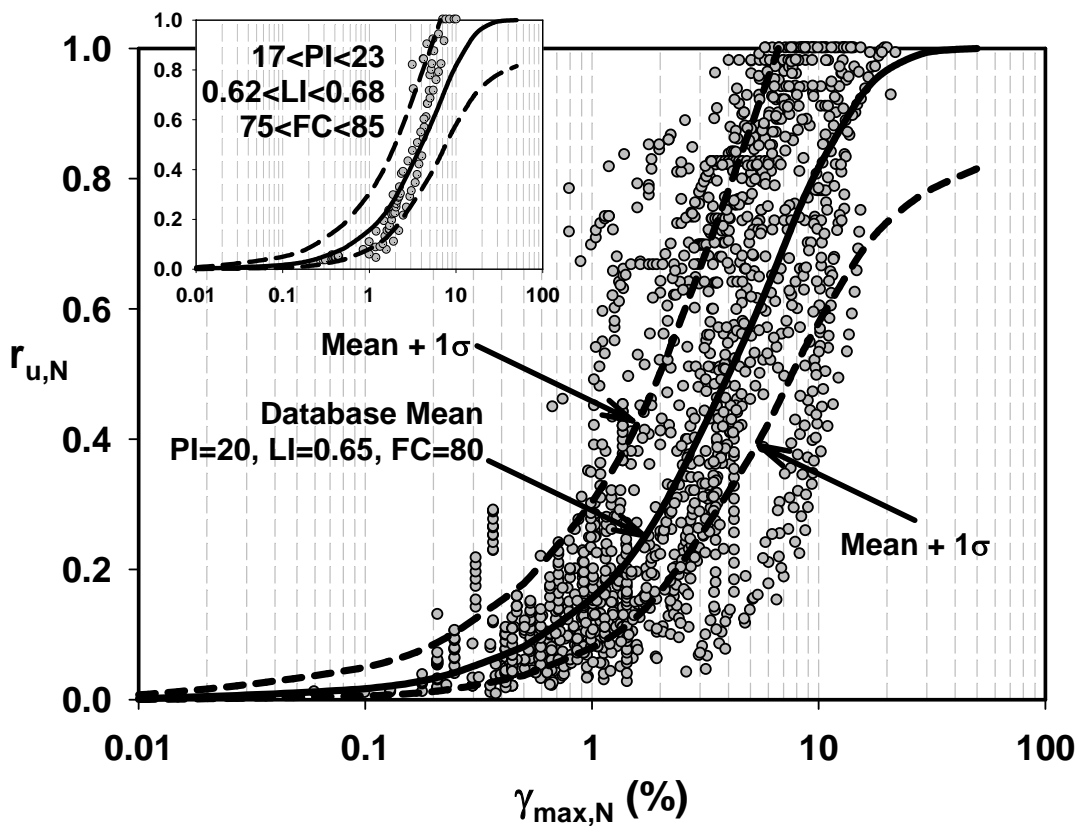
Figure 5.3-7. Proposed r_u vs. γ_{max} model along with compiled data

Last but not least, to check the power of the proposed mathematical form (i.e.: limit state functions) and to see if any trend as a function of model input variables (descriptors) is left in residuals, which is defined by Equation (5 – 25), residuals vs.

$\gamma_{max,N}$, *PI*, *LI* and *FC* plots are prepared and presented in Figures 5.3-8, 5.3-9, 5.3-10 and 5.3-11, respectively. No clear trend as a function of any of these input variables is observed confirming the validity of selected functional forms.

$$Residual = ln(r_{u,predicted} / r_{u,measured}) \qquad\qquad (5-25)$$
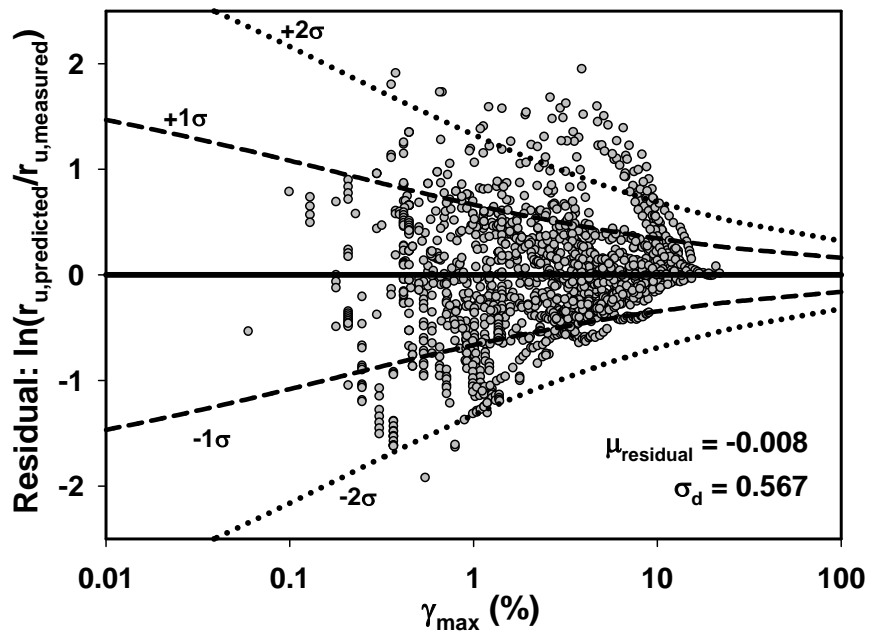
Figure 5.3-8. Residuals of the proposed r_u model
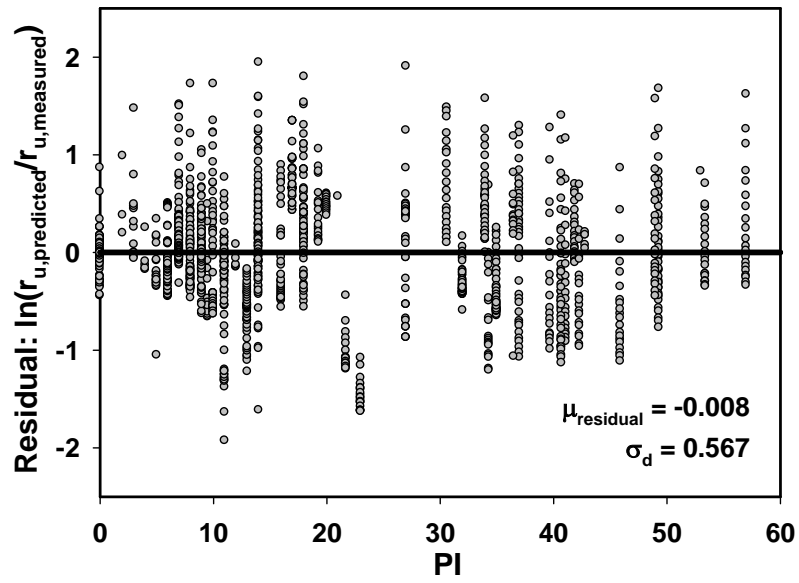
Figure 5.3-9. Scatter of residuals with PI
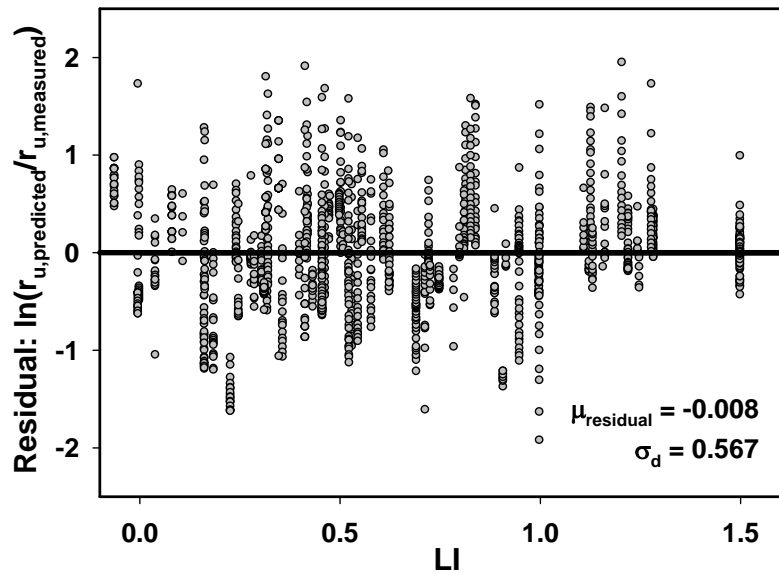
Figure 5.3-10. Scatter of residuals with LI
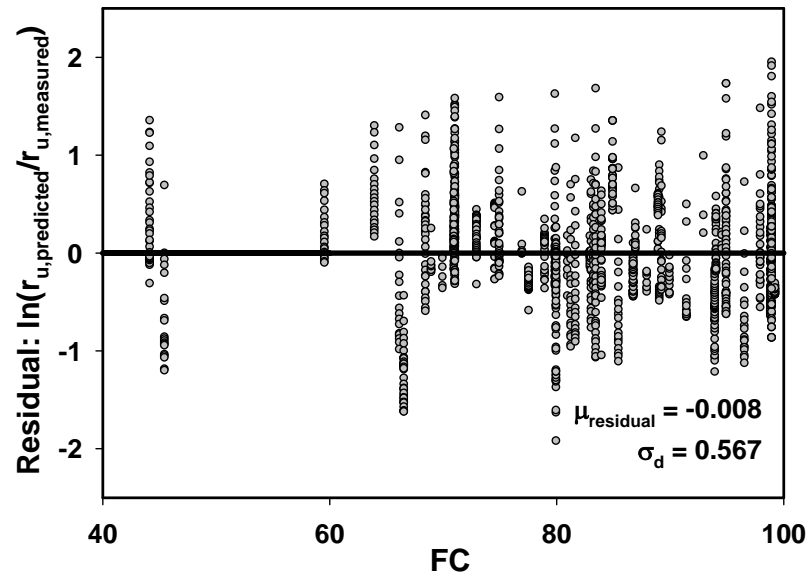
Figure 5.3-11. Scatter of residuals with FC

A smaller absolute mean residual, $\left|\mu_{residual}\right|$, and $\sigma_{residual}$ can be simply interpreted as a relatively more accurate and precise model. For the proposed model, $\mu_{residual}$ and $\sigma_{residual}$ are calculated as -0.008 and 0.567, respectively. A negative $\mu_{residual}$ means that the model predictions are lower than actual test values (i.e.: unconservatively biased) and for this case, $\mu_{residual}$ of -0.008 indicates that model predictions are 0.8 % lower than the measured test values in the average.

Proposed pore water pressure generation model by Equation $(5 - 24)$ can be adopted for the prediction of r_u as it produces reliable, robust and unbiased predictions of r_u based on simple index values (*PI* and *LI*) and cyclic shear strain potential, which can be determined using the proposed model defined by Equation $(5 - 7)$. It is believed that this r_u model increases the potential use of these 1-D consolidation theory-based models considerably.

5.4   ASSESSMENT OF RESIDUAL SHEAR STRAIN POTENTIAL

The last component of cyclic-induced straining problem is post-cyclic residual shear straining, which is quite critical considering its importance in deviatoric soil deformations. However it is, arguably, the least trivial component to assess. Yet it is intended to propose a semi-empirical model for the assessment of residual shear straining potential of silt and clay mixtures based on the available test data and existing trends.

As explained thoroughly in previous sections, the first step of model development is selecting a limit state expression capturing the essential parameters of the problem. Inspired by existing trends in database as summarized in Section 5.1, various functional forms were tested, some of which are listed in Table 5.4-1. Among these, the following function form produced the best fit to the observed behavioral trends and is adopted as the limit state function, where θ_i represents the set of unknown model coefficients:

$$g_{\gamma_{res}}\left(PI, \gamma_{max}, \frac{\tau_{st}}{s_u}, SRR, \gamma_{res}, \Theta\right) = \ln(\gamma_{res}) -$$
$$\ln\left(\gamma_{max}\left(\theta_1 \cdot \gamma_{max}{}^{\theta_2} + \theta_3 \cdot SRR^{\theta_4} + \theta_5 \cdot \left(\ln PI\right)^{\theta_6} + \theta_7 \cdot \left(\frac{\tau_{st}}{s_u}\right)^{\theta_8} + \theta_9\right)^{\theta_{10}}\right) \pm \varepsilon_{\gamma_{res}}$$

$$(5-26)$$

Similar to other proposed models, this one also include a random model correction term (ε) to account for the facts that i) possible missing descriptive parameters with influence on cyclic straining may exist; and ii) the adopted mathematical expression may not have the ideal functional form. Based on similar reasoning it is assumed that ε has normal distribution with zero mean for the aim of producing an unbiased model. The standard deviation of ε, denoted as σ_ε, however is unknown and must be estimated. The set of unknown parameters of the model, therefore, is $\Theta = (\theta, \sigma_\varepsilon)$.

Table 5.4-1. Alternative limit state models for post-cyclic residual shear straining problem

Trial #	Model Mathematical Form
1	$\gamma_{res} = exp(\theta_1 \cdot SRR^{\theta_2} + ln(\gamma_{max}))$
2	$\gamma_{res} = \theta_1 \cdot \gamma_{max}{}^{\theta_2} \cdot SRR^{\theta_3} \cdot (ln\,PI\,)^{\theta_4} \cdot \left(\dfrac{\tau_{st}}{s_u}\right)^{\theta_5}$
3	$\gamma_{res} = \gamma_{max} \cdot \left(\theta_1 \cdot \gamma_{max}{}^{\theta_2} + \theta_3 \cdot SRR^{\theta_4} + \theta_5 \cdot (ln\,PI\,)^{\theta_6} + \theta_7 \cdot \left(\dfrac{\tau_{st}}{s_u}\right)^{\theta_8} + \theta_9\right)^{\theta_{10}}$

Assuming the post-cyclic residual shear strain values of each test to be statistically independent, the likelihood function for "n" tests can be written as the product of the probabilities of the observations.

$$L_{\gamma_{res}}(\boldsymbol{\theta},\sigma_\varepsilon) = \prod_{i=1}^{n} P\left[g_{\gamma_{res}}\left(\frac{\tau_{st}}{s_u}\Big|_i, PI_i, SRR_i, \gamma_{max,i}, \boldsymbol{\theta}\right) = 0\right] \qquad (5-27)$$

Suppose the values of $(\tau_{st}/s_u)_i$, PI_i, SRR_i and $(\gamma_{max})_i$ at the each data point are exact, i.e. no measurement error is present, noting that $g(...) = \hat{g}(...) + \varepsilon_i$ has the normal distribution with mean $\hat{g}$ and standard deviation σ_ε, then the likelihood function can be written as a function of unknown coefficients as in Equation $(5-28)$. In this equation, $\varphi[\cdot]$ is the standard normal probability density function.

$$L_{\gamma_{res}}(\boldsymbol{\theta},\sigma_\varepsilon) = \prod_{i=1}^{n} \varphi\left[\frac{\hat{g}_{\gamma_{res}}\left(\frac{\tau_{st}}{s_u}\Big|_i, PI_i, SRR_i, \gamma_{max,i}, \boldsymbol{\theta}\right)}{\sigma_{\gamma_{res}}}\right] \qquad (5-28)$$

Consistent with the maximum likelihood methodology, model coefficients are estimated by maximizing the likelihood function given in Equation $(5-28)$ and they are presented in Table 5.4-2.

Table 5.4-2. Coefficients of γ_{res} model

θ_1	0.845
θ_2	-0.332
θ_3	0.404
θ_4	1.678
θ_5	0.375
θ_6	8.649
θ_7	7.564
θ_8	9.249
θ_9	-0.959
θ_{10}	1.438
σ_ε	0.586

The final form of the proposed model is presented in Equation $(5-29)$ along with $\pm$ one standard deviation range.

$$
ln(\gamma_{res}) = ln\left[\gamma_{max} \cdot \left(\begin{array}{c} 0.845 \cdot \gamma_{max}^{-0.332} + 0.404 \cdot SRR^{1.678} \\ + 0.375 \cdot (ln\,PI)^{0.446} + \\ (7.564) \cdot \left(\dfrac{\tau_{st}}{s_u} \right)^{9.249} - 0.959 \end{array} \right)^{1.438} \right] \pm 0.586 \quad (5-29)
$$

Same procedure is applied for all of the limit state functions presented in Table 5.4-1. Estimated model coefficients along with corresponding maximum likelihood value are presented by Table 5.3-3. Note that selected limit state function (i.e. Trial #3) produces the most accurate and unbiased strain predictions, since higher likelihood value ($\sum lh$) and smaller σ_ε are indications of a superior model.

134

Table 5.4-3. Summary of model coefficients and performances of limit state functions tested for post-cyclic residual shear strain potential

Trial #	Model Coefficients											$\sum lh$
	θ_1	θ_2	θ_3	θ_4	θ_5	θ_6	θ_7	θ_8	θ_9	θ_{10}	σ_ε	
1	-0.374	-1.24	-	-	-	-	-	-	-	-	0.95	-52.0
2	0.235	1.371	0.761	1.07	-0.3	-	-	-	-	-	0.64	-36.8
3	0.845	-0.33	0.40	1.68	0.38	8.65	7.56	9.25	-0.96	1.49	0.59	-33.6

For the purpose of performance assessment, measured and predicted post-cyclic residual strains are paired and shown on Figure 5.4-1 along with the 1:2 and 1:0.5 boundary lines. 71 % of the predictions lie within these ranges and the proposed model produces reasonable and unbiased predictions.

Besides this visual observation, the performance of the model predictions are also expressed by Pearson product moment correlation coefficient, R^2, and reported on Figure 5.4-1 as 0.71 (or 71 %) which is considered to be a quite satisfactory value considering challenging nature of this problem.
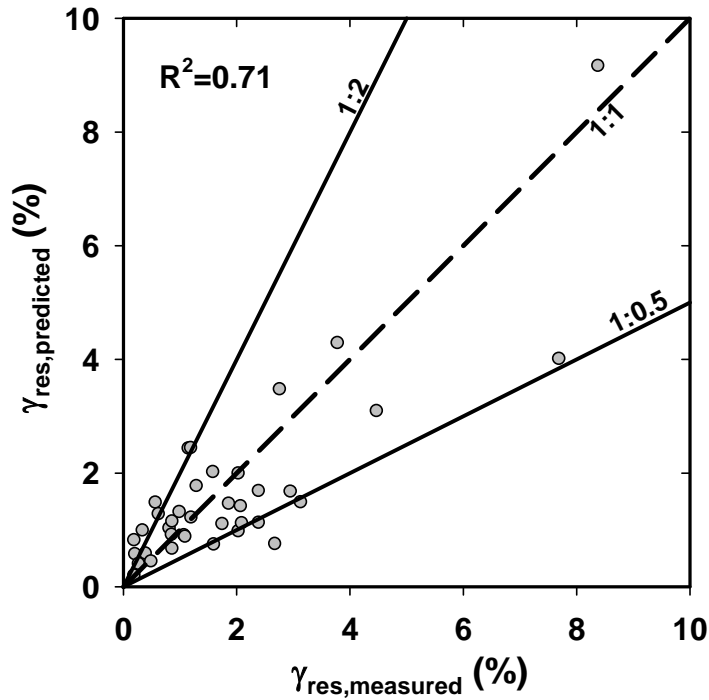
Figure 5.4-1. Comparison between measured and predicted post-cyclic volumetric strains

The validity of the proposed mathematical form (i.e. limit state function) is also assessed by simple statistics (i.e. mean and standard deviation) of residual which is defined as follows:

$$Residual = ln(\gamma_{res,predicted} / \gamma_{res,measured}) \qquad (5-30)$$

For this proposed model, $\mu_{residual}$ and $\sigma_{residual}$ are calculated as 0.002 and 0.619, respectively. A zero $\mu_{residual}$ means that the model completely unbiased estimates in the average and the calculated value of $\mu_{residual}$ indicates that predictions by the proposed model are 0.2% higher than the measured values of γ_{res} in the average. Plots of residual vs., SSR, γ_{max}, τ_{st}/s_u and PI are prepared and presented by

Figures 5.4-2 through 5.4-5, respectively; to check if any trend as a function of model input variables (descriptors) is left in residuals; however no clear trend as a function of any of these input variables is observed confirming the validity of selected functional form.

Figure 5.4-2. Scatter of residuals with SRR
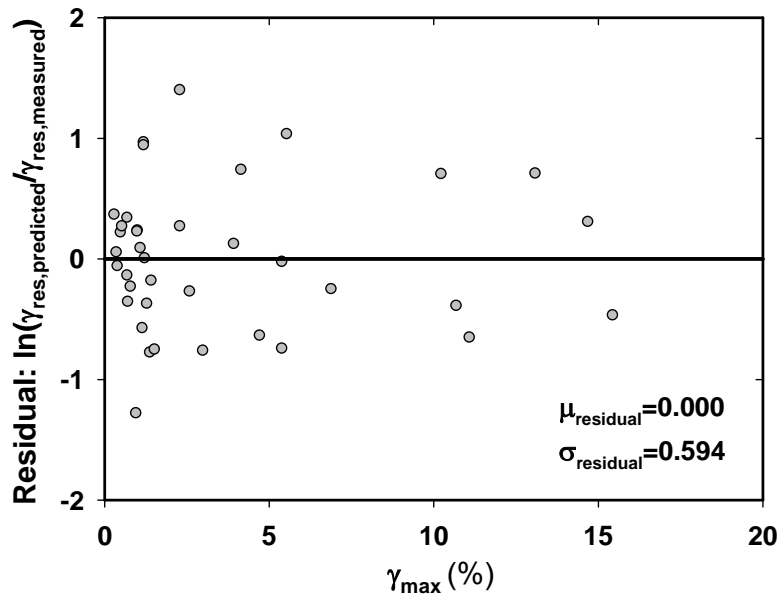
Figure 5.4-3. Scatter of residuals with γ_{max}
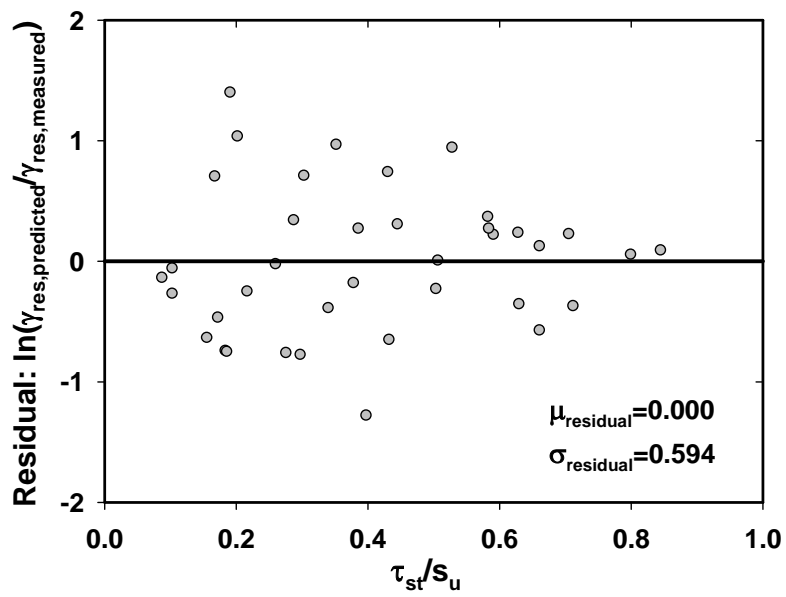
Figure 5.4-4. Scatter of residuals with τ_{st}/s_u

138
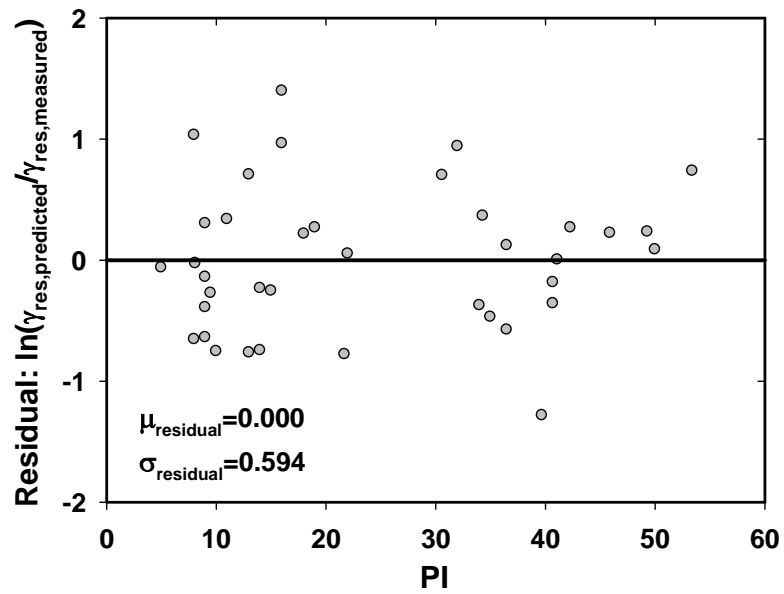
Figure 5.4-5. Scatter of residuals with PI

Limit state function presented in Equation (5 – 26) clearly indicates that maximum cyclic shear strain (γ_{max}) is an input parameter for the proposed model. For this purpose, Equation (5 – 29) is recommended to be used in conjunction with the proposed cyclic shear strain assessment model, which is given in Equation (5 – 7).

CHAPTER 6

ASSESSMENT OF MINIMUM- CYCLIC SHEAR STRENGTH OF FINE-GRAINED SOILS

6.1   INTRODUCTION

Cyclic strain-induced remolding and excess pore water pressure generation reduces shear strength of soils, and quantification of this reduced strength is vital for post-earthquake stability analyses. Although post-cyclic strength loss is accepted to be more critical for saturated cohesionless soils, depending on sensitivity of fine-grained soils and intensity and duration of shaking, it could also produce serious problems for cohesive soils.

As reviewed in Chapter 2, various researchers have studied this issue and they proposed models for predicting post-cyclic shear strength ($s_{u,pc}$). However, it is realized that these early efforts did not focus on the most critical condition in which soil specimen experiences significant straining along with a r_u value reaching to the value of 1.0, i.e. liquefaction is triggered. In simpler terms, during dilation and contraction cycles, the minimum shear strength is expected when effective stresses temporarily fall down to zero. In this worst case, specimen may experience

significant temporary shear strength loss. It is aimed to predict this minimum shear strength level during cyclic loading. For the purpose of avoiding confusion, minimum shear strength will be denoted by $s_{u_{cyc,min}}$ instead of $s_{u,pc}$ to underline the fact that minimum level of shear strength will take place during crossings from origin of stress-strain plots.

The conventional approaches in determining post-cyclic shear strength of soil specimens involve an undrained cyclic loading which is followed by an undrained static loading test on the same specimen. Post-cyclic strength performance of a typical soil varies depending on the degree of remolding along with its dilational characteristics since negative excess pore water pressures may occur resulting in regaining some shear strength during application of monotonic loading. However, in completely remolded state such dilative response is not expected to occur and cohesive forces between clay minerals remain the only component contributing post-cyclic shear strength of soil. Luckily, it is not necessary to perform further monotonic testing on the same specimen for this case since stress − strain plot of the related cyclic test provides this information. Stress − strain loop's breadth at zero effective stress range is accepted to be equal to $s_{u_{cyc,min}}$ as mentioned in Chapter 3.

Following section is devoted to the details of model development and also evaluation of model performance. This chapter will be concluded by a discussion on cases requiring use of $s_{u_{cyc,min}}$ for further stability analysis.

6.2 DEVELOPMENT OF MODELS FOR MINIMUM-CYCLIC SHEAR STRENGTH PREDICTIONS

As explained thoroughly in previous chapters, first step in development of a probabilistic model is selection of a limit state expression capturing the essential parameters of the problem. Inspired by the trends in the presented $s_{u_{cyc,min}}$ database (Tables 3.3-2 and 3.5-1), various functional forms have been tested some which are listed in Table 6.2-1. Among them, following one produced the best fit to the

observed behavioral trends and consequently adopted as the limit state function for predicting the ratio of $s_{u_{cyc,min}}$ to the initial undrained static shear strength ($s_{u,st}$) of the specimen.

$$g\left(LI, PI, \frac{s_{u_{cyc,min}}}{s_{u,st}}, \Theta \right) = ln\left(\frac{s_{u_{cyc,min}}}{s_{u,st}} \right) - ln\left(\theta_1 \cdot PI^{\theta_2} \cdot LI^{\theta_3} \right) \pm \varepsilon \qquad (6-1)$$

Similar to all of the previous models, a random model correction term (ε) is used to account for possible missing descriptive parameters influencing post-liquefaction strength loss and the imperfect mathematical model. ε is assumed to have normal distribution with zero mean for the aim of producing an unbiased model; yet standard deviation of ε (σ_ε) is unknown and must be estimated. The set of unknown parameters of the model, therefore, is $\Theta = (\mathbf{\theta}, \sigma_\varepsilon)$.

Table 6.2-1. Alternative limit state models for minimum-cyclic shear strength

Trial #	Model Mathematical Form
1	$\dfrac{s_{u_{cyc,min}}}{s_{u,st}} = \theta_1 \cdot PI^{\theta_2} \cdot LI^{\theta_3}$
2	$\dfrac{s_{u_{cyc,min}}}{s_{u,st}} = \theta_1 \cdot LI^{\theta_2}$
3	$\dfrac{s_{u_{cyc,min}}}{s_{u,st}} = \theta_1 \cdot (PI^{\theta_2} + \theta_3 \cdot LI^{\theta_4})$
4	$\dfrac{s_{u_{cyc,min}}}{s_{u,st}} = \theta_1 \cdot exp\left(-\dfrac{\theta_2 \cdot ln(LI)}{ln(PI)} \right)$

Following the same methodology, likelihood function is formulated as follows by assuming that $s_{u_{cyc,min}} / s_{u,st}$ of each test to be statistically independent.

$$L(\mathbf{\theta}, \sigma_\varepsilon) = \prod_{i=1}^{m} P\left[g\left(PI_i, LI_i, \frac{s_{u_{cyc,min}}}{s_{u,st}}_i, \theta \right) = 0 \right] \qquad (6-2)$$

Suppose the values of LI_i, PI_i, and $(s_{u_{cyc,min}} / s_{u,st})_i$ at the each data point are exact, i.e. no measurement error is present, noting that $g(...) = \hat{g}(...) + \varepsilon_i$ has the normal distribution with mean $\hat{g}$ and standard deviation σ_ε, then the likelihood function can be written as a function of unknown coefficients as in Equation (6 − 3). In this equation, $\varphi[\cdot]$ is the standard normal probability density function.

$$L(\boldsymbol{\theta}, \sigma_\varepsilon) = \prod_{i=1}^{n} \varphi\left[\frac{\hat{g}\left(LI_i, PI_i, \dfrac{s_{u_{cyc,min}}}{s_{u,st}}_i, \theta \right)}{\sigma_\varepsilon} \right] \tag{6 − 3}$$

Consistent with the maximum likelihood methodology, model coefficients are estimated by maximizing the likelihood function given in Equation (6 − 3) and they are presented in Table 6.2-2.

Table 6.2-2. Model coefficients

θ_1	0.089
θ_2	0.226
θ_3	-0.455
σ_ε	0.213

The final form of the proposed model is presented in Equation (6 − 4) along with ± 1 standard deviation range.

$$ln\left(\frac{s_{u_{cyc,min}}}{s_{u,st}} \right) = ln\left(0.089 \cdot PI^{0.226} \cdot LI^{-0.455} \right) \pm 0.213 \tag{6 − 4}$$

Figure 6.2-1 presents the proposed model on $s_{u_{cyc,min}} / s_{u,st}$ vs. LI domain for a set of PI values along with available test data. As revealed by this figure, increasing LI

and decreasing *PI* results in a more significant decrease in post-cyclic shear strength of silt and clay mixtures.
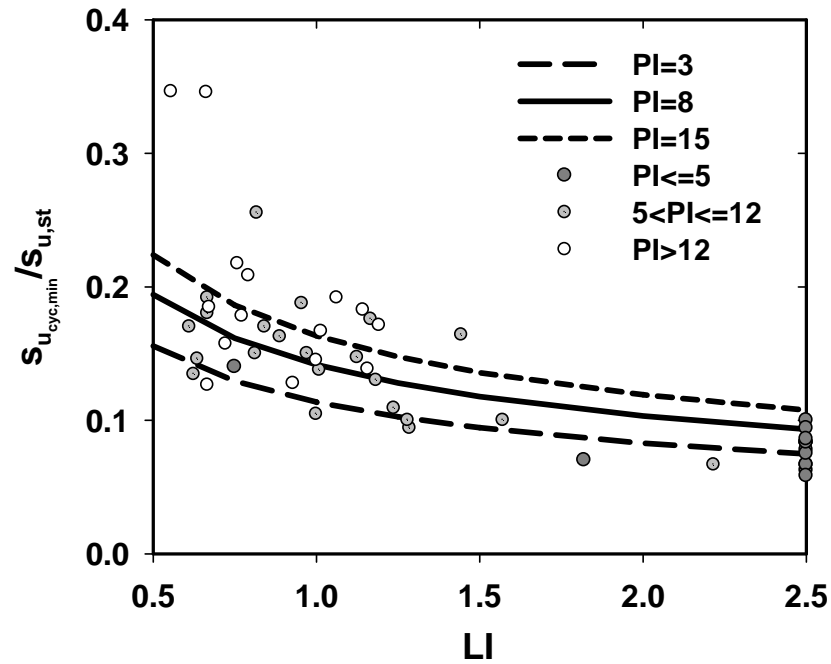
Figure 6.2-1. Variation of $s_{u_{cyc,min}}/s_{u,st}$ **as a function of LI and PI**

For the purpose of performance assessment, measured and predicted post-cyclic volumetric strains are paired and shown on Figure 6.2-2 along with the 1:2 and 1:0.5 boundary lines. As revealed by this figure all of the predictions lie within these ranges and the proposed model produces reasonable and unbiased predictions. Besides this visual observation, the performance of the model predictions are also expressed by Pearson product moment correlation coefficient, R^2, and reported on Figure 6.2-2 as 0.65 (or 65 %) which is considered to be satisfactory value considering challenging nature of this problem.
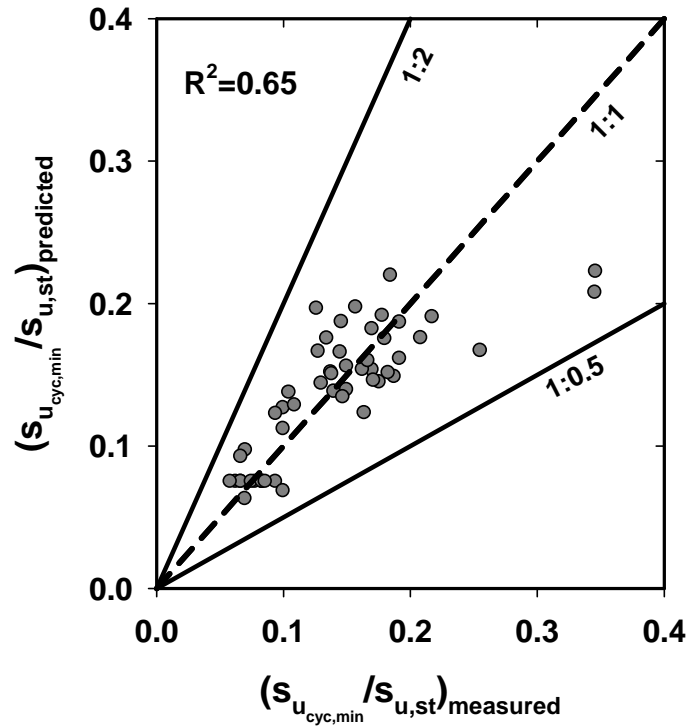
Figure 6.2-2. Comparison between measured and predicted $s_{u_{cyc,min}}/s_{u,st}$

The validity of the proposed mathematical form (i.e. limit state function) is also assessed by simple statistics (i.e. mean and standard deviation) of residual which is defined as follows:

$$Residual = ln((s_{u_{cyc,min}}/s_{u,st})_{predicted}/(s_{u_{cyc,min}}/s_{u,st})_{measured}) \qquad (6-5)$$

For this proposed model, $\mu_{residual}$ and $\sigma_{residual}$ are calculated as 0.000 and 0.215, respectively. A zero $\mu_{residual}$ means that model produces completely unbiased estimates in the average. Plots of residual vs. *LI* and *PI* are also prepared and shown in Figures 6.2-3 and 6.2-4, respectively; to check if any trend as a function of model input variables (descriptors) is left in residuals; however no clear trend as a function of any of these input variables is observed confirming the validity of selected functional form.
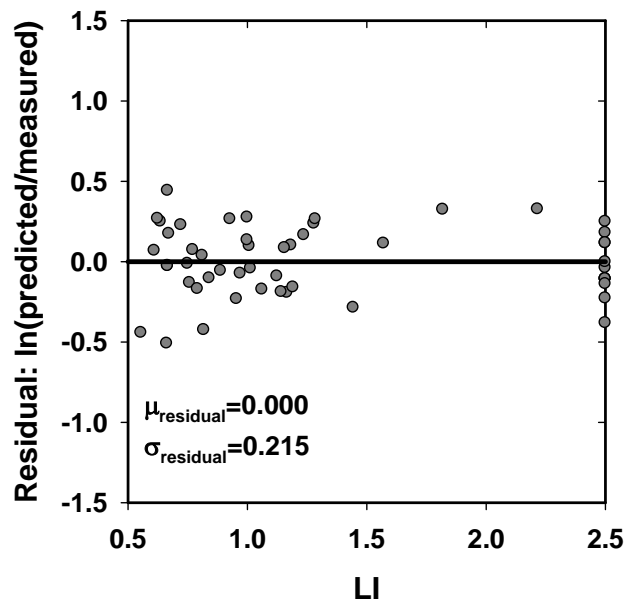
Figure 6.2-3. Scatter of residuals with LI
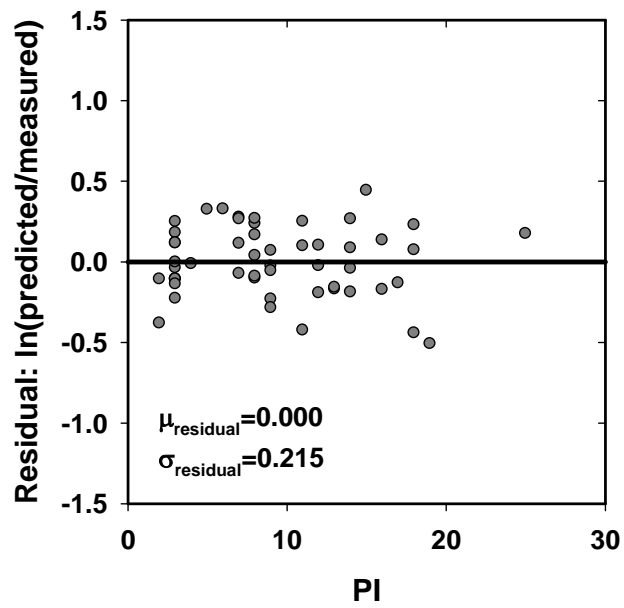
Figure 6.2-4. Scatter of residuals with PI

6.3 DISCUSSION ON WHEN TO USE PROPOSED MINIMUM-CYCLIC SHEAR STRENGTH

Most clayey soils lose some portion of their shear strength upon application of cyclic shear stresses as a result of broken cementation bonds and particle reorientation. Amount of remolding determines the degree of strength loss. In their pioneer study, Thiers and Seed (1969) stated that when cyclic shear strains exceeds half of the strain required to fully mobilize monotonic shear strength of a clayey soil, soil may lose 90 % of its original monotonic shear strength. Although it is a valid approach, its practical value is quite limited due to of difficulties associated with prediction of those strain levels. On the other hand, this study presents a similar approach with tools for cyclic strain predictions. By following the proposed methodology, it is possible to assess shear strength performance of silt and clay mixtures.

First step is evaluation of liquefaction potential of silt and clay mixture of interest. Based on its index properties and natural moisture content, it is possible to determine whether this soil is liquefiable or not according to the criteria given in Section 4.2. If the specimen is not classified as liquefiable, no significant strength loss is expected and any available method (such as Yasuhara, 1994) can be used to determine post-cyclic shear strength of the specimen. On the other hand, if the specimen is classified as liquefiable then next step will be estimation of maximum cyclic shear strain according to applied static and cyclic shear stress conditions using the model given by Equation $(5-7)$ or $(5-9)$. These cyclic shear strain levels will give an intuition regarding level of remolding; yet for complete assessment it is recommended to estimate cyclic-induced excess pore water pressure ratio using Equation (5 - 24). If predicted r_u value exceeds 0.80, then significant strength loss is expected as a result of significant remolding and high excess pore water pressure built-up. It is proposed to use Equation $(6-4)$ to estimate the amount of strength loss and perform further stability analysis based on this value to avoid non-conservative solutions.

Author would like to conclude this discussion by mentioning the similarities between strength loss due liquefaction induced remolding and sensitivity concept which refers to the loss in undrained shear strength that develop upon disturbance of the structure of an undisturbed specimen. Sensitivity ratio (S), which is defined as the ratio of peak and remolded shear strengths, is used as a measure of sensitivity, and this definition is the reciprocal of degree of shear strength loss term ($s_{u_{cyc,min}} / s_{u,st}$) adopted in this study. Besides, some important research studies on this topic (e.g. Bjerrum, 1954; Eden and Kubota, 1962) used LI vs. S domain to present their findings. For the purpose of comparing liquefaction induced strength loss with sensitivity, relations given by these two references are presented along with the findings of this study in Figure 6.3-1. Although both approaches indicates significant strength loss, it is significantly higher (almost 10 times) for sensitive clays especially at higher LI values. This observation is not surprising since strength loss due to structural deterioration under monotonic loads, i.e. sensitivity, creates some of the most critical problems in geotechnical engineering.
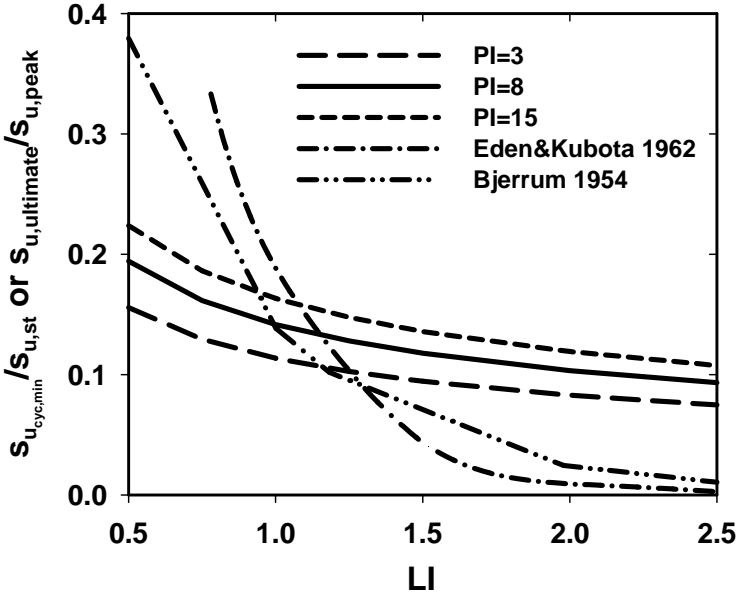
Figure 6.3-1. Comparison of proposed model with sensitivity-LI relations

CHAPTER 7

SUMMARY AND CONCLUSION

7.1 SUMMARY

The purpose of this thesis was to develop robust and defensible probabilistically-based frameworks to assess i) liquefaction susceptibility, ii) cyclic-induced straining potential, and iii) post-liquefaction shear strength of silt and clay mixtures. Parallel to these efforts, it was also intended to resolve cyclic excess pore water pressure generation response of these soils.

Current practice in evaluation of liquefaction susceptibility of fine-grained soils has been largely dominated by recent works of Seed et al. (2003), Bray and Sancio (2006) and Boulanger and Idriss (2006), which are judged to be major developments over the Chinese Criteria-like methodologies. However, these efforts also suffer from one or more of the following issues: i) combining ideally separate assessments of liquefaction susceptibility and liquefaction triggering, ii) unclear or non-existing definitions of liquefaction, and iii) adopting either γ - or r_u -based liquefaction triggering criterion which is believed to be achievable by any high plasticity soil as long as cyclic stresses are applied long enough.

Assessment of cyclic-induced straining potential is a significant problem from performance point of view, yet this topic has not drawn as much research interest as the former issue. Although some inspiring research studies were performed on this issue (e.g. Ohara and Matsuda, 1988; Yasuhara et al., 1992; Hyodo et al., 1994), they suffer from one or the more of the followings: i) except the work of Hyodo et al. (1994), only post-cyclic volumetric straining potential has been taken into account, ii) methodologies based on 1-D consolidation theory need estimations of cyclically-induced-r_u values as input, which requires either further cyclic testing, or 2- or 3-D dynamic numerical analyses, which definitely decrease the practical value of these methods. Probably due to these reasons, cyclic testing on undisturbed specimens is recommended to assess cyclic straining problem of fine grained soils; while there exist easy-to-use semi-empirical models (e.g. Tokimatsu and Seed, 1984; Ishihara and Yoshimine, 1992, Cetin et al., 2009) for saturated sandy soils.

Estimating post-cyclic shear strengths is another obstacle against performance assessment of post-seismic stability analyses. Considering its importance, numerous researchers have focused on this issue since late-60's (e.g. Thiers and Seed, 1969; Castro and Christian, 1976; Yasuhara, 1994); yet it is realized that the worst case scenario, i.e. complete remolding due to liquefaction triggering, has not been considered in detail; and moreover, proposed models were unconservatively developed depending on dilative response of clayey soils.

Considering limitations of these early efforts and significance of these problems, a comprehensive experimental study was performed. Besides the results of laboratory tests performed within the scope of these research efforts, available literature was studied in detail to compile further high quality test data. Consequently, databases were compiled to assess liquefaction susceptibility, cyclic-induced straining and r_u potentials, and post-liquefaction residual shear strength of silt and clay mixtures. Important descriptive (input) parameters affecting each problem are determined by taking into account the existing behavioral trends observed in databases. Various limit state functions were tested to develop models producing more accurate and

150

unbiased answers to these problems. Using maximum likelihood methodology, model coefficients of selected limit state functions were predicted. In addition to model development efforts, performance of each model was assessed via results of linear regression analysis and simple statistics of residuals. Moreover, performances of proposed and existing post-cyclic volumetric strain prediction models were further assessed comparatively per maximum likelihood methodology. As assessment of liquefaction susceptibility results in "yes" or "no" type answers, a different performance evaluation scheme was adopted based on statistical metrics, such as recall, precision, F-score and overall accuracy.

It is observed and presented clearly that all of the proposed models produce satisfactorily accurate and unbiased answers to the problems investigated. Similarly, the comparative performance evaluation studies on liquefaction susceptibility and post-cyclic volumetric straining potential also prove the superiority of the proposed methodologies over the existing ones. Some major findings of these research studies will be presented next.

7.2 CONCLUSIONS

Due to fact that cyclic response of silt and clay mixtures is a very broad and complex phenomenon; these research studies focused on only three aspects of it including a) liquefaction susceptibility, b) cyclic-induced straining potential and c) post-liquefaction residual shear strength. Alternative frameworks allowing detailed inspection of fine grained soils' cyclic responses are constituted and the steps of the proposed procedures are listed as follows:

1. Liquefaction susceptibility of saturated fine-grained soils can be assessed as a function of PI and LI. If PI is greater than 30, then fine grained soils are judged to be not susceptible to cyclic liquefaction. However, if PI is less than 30, then fine grained soils are concluded to be susceptible to cyclic liquefaction if $LI \geq 0.578 \cdot \ln(PI) - 0.940$ condition is satisfied. The

proposed new criteria is schematically shown again in Figure 7.2-1, along with the database used for this purpose.
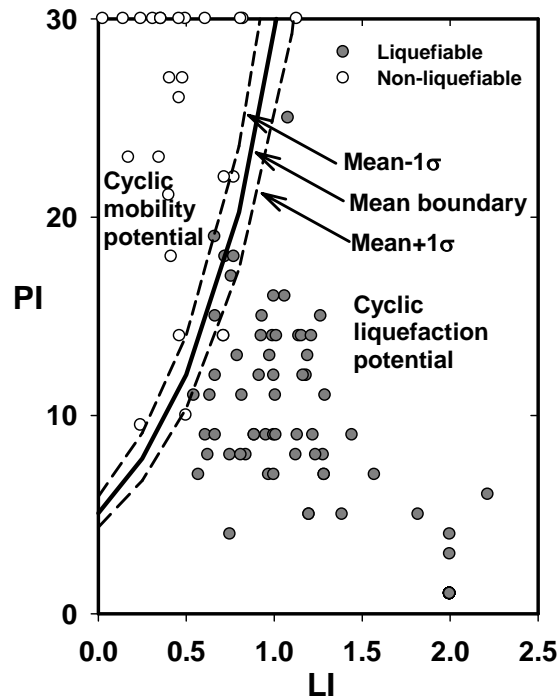
Figure 7.2-1. Proposed liquefaction susceptibility criteria

2. Next step involves the determination of maximum double amplitude cyclic shear strain (γ_{max}) level. As presented again in Equation (7 – 1), γ_{max} can be reliably estimated as functions of natural water content (w_c) liquid limit (LL), plasticity index (PI), fines content (FC) and static and cyclic shear stresses normalized by the undrained shear strength (i.e.: $\dfrac{\tau_{cyc}}{s_u}, \dfrac{\tau_{st}}{s_u}$).

$$\ln(\gamma_{max}) = \ln\left(\frac{21.509 \cdot \frac{21.788^{0.092 \cdot \frac{w_c}{LL} \cdot \ln\left(\frac{FC}{0.00067}\right)}}{\ln\left(\frac{PI \cdot FC}{61.843}\right)} \cdot \left(1 - 0.061 \cdot \ln\left(\frac{29.878}{PI \cdot FC}\right)\right) \cdot}{\frac{3.473 - \sqrt{\left(\frac{\tau_{st}}{s_u} - 1.007\right)^2 + \left(\frac{\tau_{cyc}}{s_u} - (3.262)\right)^2}}{3.473 - 17.805}}\right) \pm 0.468 \quad (7-1)$$

3. Post-cyclic volumetric strain potential ($\varepsilon_{v,pc}$) can be predicted using either semi-empirical model given in Equation (7 – 2) in terms of γ_{max}, *PI* and w_c / LL or updated 1-D consolidation theory-based model using Equation (7 – 3) which is defined as a function of void ratio (e_0), γ_{max}, *PI* and cyclic-induced excess pore water pressure ratio (r_u). The latter component, r_u can be estimated reliably by using γ_{max}, *PI*, liquidity index (*LI*) and *FC* as given in Equation (7 – 4).

$$\ln(\varepsilon_{v,pc}) = \ln\left[\frac{0.400 \cdot \gamma_{max}^{0.562}}{1.805 + (-0.036) \cdot PI - w_c / LL}\right] \pm 0.297 \quad (7-2)$$

$$\varepsilon_{v,pc} = \frac{\left[1 + \frac{0.53 \cdot OCR^2 - 3.233 \cdot OCR + 5.927}{1 - (-1.118) \cdot \gamma_{max}^{-0.408} + 0.829 \cdot \ln PI}\right]}{1 + e_0} \cdot \log\left[\frac{1}{1 - r_u}\right] \quad (7-3)$$

$$\ln(r_{u,N}) = \ln\left[1 - \exp\left(\frac{\gamma_{max,N}}{-1.991 \cdot \exp(0.02 \cdot PI - 0.05 \cdot LI) \cdot \left[\ln\left(\frac{FC}{0.01}\right)\right]^{0.328}}\right)\right] \\ \pm \left(\frac{1}{\gamma_{max,N}^{0.378} + 0.506}\right) \quad (7-4)$$

4. Then, post-cyclic residual shear strain potential (γ_{res}) of fine-grained soils subjected to initial static shear stresses can be predicted using the proposed

semi-empirical model given in Equation (7 – 5), which is defined as a function of γ_{max}, PI, τ_{st} / s_u and stress reversal ratio ($SRR = \tau_{st} / \tau_{cyc}$).

$$ln(\gamma_{res}) = ln\left[\gamma_{max} \cdot \left(\begin{array}{l} 0.845 \cdot \gamma_{max}{}^{-0.332} + 0.404 \cdot SRR^{1.678} \\ + 0.375 \cdot (ln\,PI)^{0.446} + \\ (7.564) \cdot \left(\dfrac{\tau_{st}}{s_u}\right)^{9.249} - 0.959 \end{array}\right)^{1.438}\right] \pm 0.586 \quad (7-5)$$

5. If soil is screened to be potentially liquefiable in Step 1, and cyclic-induced r_u exceeds 0.80, then it is recommended to consider minimum-cyclic shear strength in stability analysis by using Equation (7 – 6), which is defined as a function of soil's PI and LI.

$$ln\left(\frac{s_{u_{cyc,min}}}{s_{u,st}}\right) = ln\left(0.089 \cdot PI^{0.226} \cdot LI^{-0.455}\right) \pm 0.213 \qquad (7-6)$$

The proposed procedure allows i) estimation of cyclically-induced volumetric and deviatoric strain potentials of silt and clay mixtures, which could be further used to estimate seismic-induced ground deformations, ii) reduction in shear strength due to liquefaction-induced remolding and excess pore water pressure generation is also modeled for further post-seismic stability analysis.

7.3 RECOMMENDATIONS FOR FUTURE RESEARCH

Findings of this study have identified various important aspects of cyclic response of silt and clay mixtures, which warrant additional research including:

1. Laboratory test data was used in the development of proposed procedures. It is intended to use as many high quality test data as possible, and consequently one of the most comprehensive databases of this research area

154

has been compiled. However, with the increase in the number of high quality data, proposed models can be further refined and more accurate predictions can be possibly obtained.

2. Considering the possible effects of aging, using "undisturbed" specimens over laboratory-reconstituted ones seems to be advantageous; however, due to inevitable variability in controlling parameters of natural soil samples, interpretation of results becomes more difficult. Thus, performing tests on laboratory-reconstituted specimens may be considered as an alternative approach since it allows performing better controlled tests.

3. The major motivation to propose these strain estimation models is to develop a framework for the determination of seismically-induced ground deformations. Hence, proposed models can be applied and calibrated via ground deformation case histories to predict seismically-induced settlement and lateral spreading problems occurred in soil layers composed of saturated silt and clay mixtures.

4. The proposed γ_{max} estimation model is developed for 20 equivalent loading cycles, simulating duration of an earthquake of moment magnitude (M_w) 7.5 according to findings of Liu et al. (2001). Therefore, to extend model's use to different magnitude events requires a magnitude scaling scheme. Although, this concept has been studied in detail for saturated sandy soils (Cetin and Bilge, 2010b), its application on cohesive soils has not drawn significant research interest yet. Boulanger and Idriss (2004) proposed magnitude scaling factors as a part of their methodology to evaluate cyclic straining potential of silt and clay mixtures, which seems to be the only available option. However, it is believed that this issue deserves further research interest, and findings of a possible effort will be quite valuable for - especially- assessment of seismically-induced ground deformations.

REFERENCES

ASTM Standard D4318, 1998, "Standard Test Methods for Liquid Limit, Plastic Limit, and Plasticity Index of Soils", ASTM International, West Conshohocken, PA.

ASTM Standard D854, 1998, "Standard Test Methods for Specific Gravity of Soil Solids by Water Pycnometer", ASTM International, West Conshohocken, PA.

ASTM Standard D422, 1998, "Standard Test Method for Particle – Size Analysis of Soils", ASTM International, West Conshohocken, PA.

ASTM Standard D2435-04, 1998, "Standard Test Methods for One-Dimensional Consolidation Properties of Soils Using Incremental Loading", ASTM International, West Conshohocken, PA.

ASTM Standard D4767-04, 1998, "Standard Test Methods for Consolidated Undrained Triaxial Compression Test for Cohesive Soils", ASTM International, West Conshohocken, PA.

ASTM Standard D2216, 1998, "Standard Test Method for Laboratory Determination of Water (Moisture) Content of Soil and Rock by Mass", ASTM International, West Conshohocken, PA.

ASTM Standard D5311, 2004, "Standard Test Method for Load Controlled Cyclic Triaxial Strength of Soil", ASTM International, West Conshohocken, PA.

Andersen, K. H., and Lauritzsen, R. (1988). "Bearing capacity for foundations with cyclic loads", J. Geotechnical Eng., ASCE, 114(5), 540-555.

Andersen, K. H., Kleven, A., and Heien, D. (1988). "Cyclic soil data for design of gravity structures" J. Geotechnical Engineering, 114(5), 517-539.

Andrews D.C., and Martin G.R. (2000), "Criteria for liquefaction of silty sands", Proceedings of the 12th World Conference on Earthquake Engineering, Auckland, New Zealand.

Ansal, A., and Erken, A. (1989). "Undrained behavior of clay under cyclic shear stresses", J. Geotechnical Engineering, ASCE, 115(7), 968-983.

Azzouz, A. S., Malek, A. M., and Baligh, M. M. (1989). "Cyclic behavior of clays in undrained simple shear." J. Geotecnical Engineering, ASCE, 115(5), 637-657.

Bilge, H. T., and Cetin, K. O. (2007). "Probabilistic models for the assessment of cyclic soil straining in fine-grained soils", 4th Int. Conf. on Earthquake Geotechnical Eng., Thessaloniki, Greece.

Bilge, H. T., and Cetin, K. O. (2008). "Probabilistic models for the assessment of cyclic soil straining in fine-grained soils", Geotechnical Earthquake Eng. and Soil Dynamics IV, Sacramento, California, USA.

Bishop, A. W., and Eldin, G. (1950). "Undrained triaxial tests on saturated sands and their significance in the general theory of shear strength", Géotechnique, 2, 1-13.

Bjerrum, L. (1954). "Geotechnical properties of Norwegian marine clays", Géotechnique, 4, 49-69.

Bjerrum, L., and Simons, N. E. (1960). "Comparison of shear strength characteristics of normally consolidated clays", Proc. ASCE Research Conf. on Shear Strength of Cohesive Soils, Boulder: 711-726.

Boulanger, R. W., and Idriss, I. M. (2004). "Evaluating the liquefaction or cyclic failure of silts and clays." Report No. UCD/CGM/-04/01, Center of Geotechnical Modeling, Dept. of Civil and Environmental Eng., University of California, Davis.

Boulanger, R.W., and Idriss, I.M. (2006). "Liquefaction susceptibility criteria for silts and clays", J. Geotechnical and Geoenvironmental Engineering, ASCE, 132(11), 1413-1426.

Boulanger, R., Meyers, M. W., Mejia, L. H., and Idriss, I. M. (1998). "Behavior of a fine-grained soil during Loma Prieta earthquake", Canadian Geotechnical Journal, 35, 146-158.

Boulanger, R., Seed, R. B., Chan, C. K., Seed, H. B., and Sousa, J. (1991). "Liquefaction behavior of saturated sands under uni-directional and bi-directional monotonic and cyclic simple shear loading", Report No. UCB/GT/91-08, University of California, Berkeley.

Bray, J. D., and Sancio, R. B. (2006). "Assessment of liquefaction susceptibility of fine-grained soils", J. Geotechnical and Geoenvironmental Eng., 132(9), 1165-1177.

Bray, J. D., Sancio, R. B., Durgunoglu, H. T., Onalp, A., Seed, R. B., Stewart, J. P., Youd, T. L., Baturay, M. L., Cetin, K. O., Christensen, C., Karadayilar, T., and Emrem, C., (2001), "Ground failure in Adapazari, Turkey.", Proceedings of Earthquake Geotechnical Engineering Satellite Conference of the XVth International Conference on Soil Mechanics & Geotechnical Engineering, Istanbul, Turkey, August 24-25.

Bray, J. D., Sancio, R. B., Durgunoglu, T., Onalp, A., Youd, T. L., Stewart, J. P., Seed, R. B., Cetin, K. O., Bol, E., Baturay, M. B., Christensen, C., and Karadayilar, T. (2004). "Subsurface characterization at ground failure sites in Adapazari, Turkey." J. Geotechnical and Geoenvironmental Eng., ASCE, 130(7), 673-685.

Bray, J. D., Sancio, R. B., Youd, T. L., Durgunoglu, H. T., Onalp, A., Cetin, K. O., Seed, R. B., Stewart, J. P., Christensen. C., Baturay, M. B., Karadayilar, T., and Emrem, C. (2003). "Documenting incidents of ground failure resulting from the August 17, 1999 Kocaeli, Turkey earthquake: Data report characterizing subsurface conditions", Geoengineering Research Report No. UCB/GE-03/02, University of California, Berkeley.

Castro, G. (1987). "On the behavior of soils during earthquakes – liquefaction" Soil Dynamics and Liquefaction, A. S. Cakmak, ed., Elsevier, pp. 169-204.

Castro, G., and Christian, J. T. (1976). "Shear strength of soils and cyclic loading", J. Geotechnical Eng., 102(9), 887-894.

Cetin, K. O., and Bilge, H. T. (2010a). "Cyclic large strain and induced pore pressure response of saturated clean sands" J. Geotechnical and Geoenvironmental Eng., ASCE, manuscript in review.

Cetin, K. O., and Bilge, H. T. (2010b). "Performance-based assessment of magnitude (duration) scaling factors" J. Geotechnical and Geoenvironmental Eng., ASCE, manuscript in review.

Cetin K.O., Bilge H.T., Wu J., Kammerer A. and Seed R.B., (2009). "Probabilistic models for cyclic straining of saturated clean sands" J. Geotechnical and Geoenvironmental Eng., ASCE, 135(3), 371-386.

Chu, D. B. (2006). "Case studies of soil liquefaction of sands and cyclic softening of clays induced by the 1999 Taiwan Chi-Chi earthquake" Ph. D. Dissertation, University of California, Los Angeles.

Chu, D. B., Stewart, J. P., Boulanger, R. W., and Lin, P. S. (2008). "Cyclic softening of low-plasticity clay and its effect on seismic foundation performance", J. Geotechnical and Geoenvironmental Eng., ASCE, 134(11), 1595-1608.

Chu, D. B., Stewart, J. P., Lee, S., Tsai, J. S., Lin, P. S., Chu, B. L., Moss, R. E. S., Seed, R. B., Hsu, S. C., Yu, M. S., and Wang, M. C. H. (2003). "Validation of liquefaction-related ground failure models using case histories from Chi-Chi, Taiwan earthquake.", U. S. – Taiwan Workshop on Soil Liquefaction, Hsinchu, Taiwan, November 2-5.

Chu, D. B., Stewart, J. P., Lee, S., Tsai, J. S., Lin, P. S., Chu, B. L., Seed, R. B., Hsu, S. C., Yu, M. S., and Wang, C. M. H. (2004). "Documentation of soil conditions at liquefaction and non-liquefaction sites from 1999 Chi-Chi (Taiwan) earthquake", Soil Dynamics and Earthquake Engineering, 24(9-10), 647-657.

Donahue, J., L. (2007). "The liquefaction susceptibility, resistance, and response of silty and clayey soils" Ph.D. Dissertation, University of California, Berkeley.

Duku, P. M., Stewart, J. P., Whang, D. W., and Yee, E. (2008). "Volumetric strains of clean sands subject to cyclic loads", J. Geotechnical and Geoenvironmental Eng., ASCE, 134(8), 1073-1085.

Duncan, J. M., and Seed, H. B. (1967). "Corrections for strength test data", J. Soil Mechanics and Foundation Div., ASCE, 93(5), 121-137.

Eden, W. J., and Kubota, J. K. (1962). "Some observations on the measurement of sensitivity of clays", Proc. of the American Society for Testing and Materials, Vol. 61, Report No. DBR-RP-157, 1239-1249.

El Hosri, M. S., Biarez, J., Hicher, P. Y. (1984). "Liquefaction characteristics of silty clay", Proc. 8th World Conf. on Earthquake Eng., San Francisco, California, Vol.3, 277-284.

Erken, A., Ulker, B. M. C., Kaya, Z, and Elibol, B. (2006) "The reason of bearing capacity failure at fine-grained soils" Proc. 8th US National Conference on Earthquake Eng., San Francisco, California.

Finn, L. W., Ledbetter, R. H., and Guoxi, W. U. (1994). "Liquefaction in silty soils: design and analysis" Ground Failures under Seismic Conditions, ASCE Geotechnical Special Publication, No. 44, pp. 51-79.

Graham, G., Crooks, J. H. A., and Bell, A. L. (1983). "Time effects on the stress-strain behaviour of soft natural clays", Géotechnique, 33(3), 327-340.

Guidelines for Analyzing and Mitigating Liquefaction Hazards in California (1999). Recommended Procedures for Implementation of DMG Special Publication 117, editors G. R. Martin and M. Lew, Southern California Earthquake Center, Univ. Southern California.

Holzer, T. L., Bennett, M. J., Ponti, D. J., and Tinsley, J. C. (1999). "Liquefaction and soil failure during 1994 Northridge earthquake", J. Geotechnical and Geoenvironmental Eng., ASCE, 125(6), 438-452.

Houston, W. N., and Mitchell, J. K. (1969). "Property interrelationships in sensitive clays", J. Soil Mechanics and Foundation Div., ASCE, 95(4), 1037-1062.

Hyde, A. F. L., and Brown, S. F. (1976). "The plastic deformation of a silty clay under creep and repeated loading", Géotechnique, 26(1), 173-184.

Hyde, A. F. L., and Ward, S. J. (1985). "A pore pressure and stability model for a silty clay under repeated loading", Géotechnique, 35(2), 113-125.

Hyde, A. F. L., Higuchi, T., and Yasuhara, K. (2007). "Postcyclic recompression, stiffness, and consolidated cyclic strength of silt", J. Geotechnical and Geoenvironmental Eng., ASCE, 133(4), 416-423.

Hyodo, M., Yamamoto, Y., and Sugiyama, M. (1994). "Undrained cyclic shear behavior of normally consolidated clay subjected to initial static shear stress" Soils and Foundations, 34(4), 1-11.

Idriss, I. M. (1985). "Evaluating seismic risk in engineering practice" Proc., 11th International Conference on Soil Mechanics and Foundation Eng., San Francisco, Balkema, Rotterdam, 265-320.

Idriss, I. M., Singh, R. D., and Dobry, R. (1978). "Nonlinear behavior of soft clays during cyclic loading" J. Geotechnical Engineering, 104(12), 1427-1447.

Ishihara, K., and Yoshimine, M. (1992). "Evaluation of settlements in sand deposits following liquefaction during earthquakes", Soils and Foundations, 32(1), 173 – 188.

Ishihara, K., Troncoso, J., Kawase, Y., and Takahashi, Y. (1980). "Cyclic strength characteristics of tailings materials", Soils and Foundations, 20(4), 127-142.

Ishihara, K. (1993), "Liquefaction and flow failure during earthquakes" Géotechnique, 43(3), 351-415.

Koester, J. P. (1992). "The influence of test procedure on correlation of Atterberg limits with liquefaction in fine-grained soils" Geotechnical Testing J., ASTM, 15(4): 352-360.

Konrad, J. M., and Wagg, B. T. (1993). "Undrained cyclic loading of anisotropically consolidated clayey silts", J. Geotechnical Eng., ASCE, 119(5), 929-947.

Koutsoftas, D. C. (1978). "Effect of cyclic loads on undrained shear strength of two marine clays", J. Geotechnical Eng., ASCE, 104(5), 609-620.

La Rochelle, P. (1967). "Membrane, drains and area correction in triaxial test on soil samples failing along a single shear plane", 3rd Pan American Conf. Soil Mech., 1, 273-291.

Lee, K. L., and Albaisa, A. (1974). "Earthquake induced settlements in saturated sands.", J. Geotechnical Eng. Div., 100(4), 387-406.

Lee, K. L., and Focht, J. A. (1976). "Strength of clay subjected to cyclic loading", Marine Geotechnology, 1(3), 165-185.

Lee, K. L., and Roth, W. (1977). "Seismic stability analysis of Hawkins hydraulic fill dam.", J. Geotechnical Eng. Div., 103(6), 627-644.

Lee, K. L, and Seed, H. B., (1967). "Cyclic stress conditions causing liquefaction of sand", J. Soil Mechanics and Foundation Div., 93(1), 47-70.

Lee, K. L., Seed, H. B., Idriss, I. M., and Makdisi, F. I. (1975). "Properties of soil in the San Fernando hydraulic fill dams", J. Soil Mechanics and Foundation Division, 101(8), 801-821.

Lefebvre, G., and LeBouef, D. (1987). "Rate effects and cyclic loading on sensitive clays" J. Geotechnical Eng., ASCE, 113(5), 476-489.

Lefebvre, G., and Pfendler, P. (1996). "Strain rate and pre-shear effects in cyclic resistance of soft clay." J. Geotechnical and Geoenvironmental Eng., ASCE, 122(1), 21-26.

Li, D., and Selig, E. T. (1996). "Cumulative plastic deformation for fine-grained subgrade soils", J. Geotechnical Eng., ASCE, 122(12), 1006-1013.

Li, X. S., Chan, C. K., and Shen, C. K. (1988). "An automated triaxial testing system", Advanced Triaxial Testing of Soils and Rocks, ASTM STP977, R.T. Donaghe, R. C. Chaney, M. L. Silver, ASTM, pp.95-106.

Liu A.H., Stewart J.P., Abrahamson N.A and Moriwaki Y. (2001). "Equivalent number of uniform stress cycles for soil liquefaction analysis", Journal of Geotechnical and Geoenvironmental Engineering, ASCE, 127(12), 1017–1026.

Lunne, T., Robertson, P. K., and Powell, J. J. (1997). Cone Penetration Testing in Geotechnical Practice. Blackie Academic & Professional.

Majidzadeh, K., Khedr, S., and Guirguis, H. (1976). "Laboratory verification of a mechanistic subgrade rutting model", Transp. Res. Rec. No. 616, Transportation Research Board, Washington, D. C., 34-37.

Majidzadeh, K., Bayomy, F., and Khedr, S. (1978). "Rutting evaluation of subgrade soils in Ohio", Transp. Res. Rec. No. 671, Transportation Research Board, Washington, D. C., 75-91.

Matasovic, N., and Vucetic, M. (1992). "A pore pressure model for cyclic straining of clay." Soils and Foundations 32(3), 156-173.

Matasovic, N., and Vucetic, M. (1995). "Generalized cyclic degradation – pore pressure generation model for clays." J. Geotechnical Eng., 121(1), 33 – 42.

Matsui, T., Ohara, H., and Itou, N. (1980). "Cyclic stress – strain history and shear characteristics of clay", J. Geotechnical Eng., 106(10), 1101-1120.

Mendoza, M. J., and Auvinet, G. (1988). "The Mexico Earthquake of September 19, 1985 – Behavior of building foundations in Mexico City", Earthquake Spectra, 4(4), 835-852.

Mitchell, J. K. (1976). Fundamentals of Soil Behavior, 1st Edition, John Wiley and Sons, Inc.

Mogami, H., and Kubo, T. (1953). "The behavior of soil during vibration", Proc. 3rd Int. Conf. Soil Mechanics and Foundation Eng., Vol. 1. 152-153.

Nagase, H., and Ishihara, K. (1988). "Liquefaction-induced compaction and settlement of sand during earthquakes", Soils and Foundations, 28(1), 66-76.

National Center for Earthquake Engineering Reseach (NCEER) (1997), "Proceedings of the NCEER Workshop on Evaluation of Liquefaction Resistance of Soils", Edited by Youd, T. L., Idriss, I. M., Technical Report No. NCEER-97-0022, December 31, 1997.

Ohara, S., Matsuda, H., and Kondo, Y. (1984). "Cyclic simple shear tests on saturated clay with drainage", Proc. of the Japan Society of Civil Engineers, Vol. 352, 149-158.

Ohara, S., and Matsuda, H. (1987). "Settlement of saturated clay layer induced by cyclic shear", Proc. 9th Southeast Asian Geotechnical Conf., Bangkok, Thailand, pp. 7/13-22.

Ohara, S, and Matsuda, H. (1988). "Study on the settlement of saturated clay layer induced by cyclic shear", Soils and Foundations, 28(3), 103-113.

Okamura, T. (1971). "The variation of mechanical properties of clay samples depending on its degree of disturbance: specialty session; quality in soil sampling", Proc. 4th Asian Reg. Conf. SMFE, Vol. 1, 73-81.

Pehlivan, M. (2009). "Assessment of liquefaction susceptibility of fine grained soils", M. Sc. Thesis, Middle East Technical University, Ankara, Turkey.

Pekcan, O. (2001). "Cyclic behavior of Adapazari clayey silts", M. Sc. Thesis, Middle East Technical University, Ankara, Turkey.

Perlea, V. G., Guo, T., and Kumar, S. (1999). "How liquefiable are cohesive soils?", Proc. 2nd Int. Conf. on Earthquake Geotechnical Eng., Lisbon, Portugal, Vol. 2, 611-618.

Rendulic, L. (1937). "Ein Grundgesetz der Tonmechanik und sein experimenteller Beweis", Bauingenieur, 18, 459-467.

Robertson, P.K., and Wride, C.E., (1997). "Cyclic Liquefaction Potential and Its Evaluation Based on the SPT and CPT," Proceedings, Workshop on Evaluation of Liquefaction Resistance, NCEER-97-0022, Buffalo, NY, 41-87.

Sancio, R. B. (2003). "Ground failure and building performance in Adapazari, Turkey" Ph.D. Dissertation, University of California, Berkeley, USA.

Sangrey, D. A., Henkel, D. J., and Esrig, M. I. (1978). "The effective stress response of a saturated clay to repeated loading", Canadian Geotechnical Journal, 6(3), 241-252.

Sangrey, D. A., and France, J. W. (1980). "Peak strength of clay soils after a repeated loading history." Proc. Int. Sym. Soils under Cyclic and Transient Loading, Vol. 1, 421-430.

Sasaki, T., Taniguchi, E., Matsuo, O., and Tateyama, S. (1980). "Damage of soil structures by earthquakes", Technical Note of PWRI, No. 1576, Public Works Research Institute.

Sasaki, T., Tatsuoka, F., and Yamada, S. (1982). "Method of predicting settlements of sandy ground following liquefaction", Proc. 17th Annual Convention of Japan Society of Soil Mechanics and Foundation Eng., 1661-1664.

Seed, H. B. (1976). "Liquefaction problems in geotechnical engineering", Proc. Symp. Soil Liquefaction, ASCE National Convention, Philadelphia.

Seed, H. B. (1979). "Soil liquefaction and cyclic mobility evaluation for level ground during earthquakes", J. Geotechnical Eng., ASCE, 105(2), 201-255.

Seed, H. B., and Chan, C. K. (1966). "Clay strength under earthquake loading conditions", J. Soil Mechanics and Foundation Engineering, ASCE, 92(2), 53-78.

Seed, H. B., and Lee, K. L. (1966). "Liquefaction of saturated sands during cyclic loading" J. Soil Mechanics and Foundations Div., ASCE, 97(8), 1099-1119.

Seed, H. B., and Idriss, I. M., (1982). "Ground motions and soil liquefaction during earthquakes" , Earthquake Engineering Research Institute, Berkeley, CA, 134 pp.

Seed, H. B., Martin, P. P., and Lysmer, J. (1975). "The generation and dissipation of pore water pressures during soil liquefaction", Geotechnical Report No. EERC 75-26, University of California, Berkeley.

Seed, H. B., Romo, M. P., Sun, J. J., Jaime, A., and Lysmer, J. (1987). "Relationships between soil conditions and earthquake ground motions in Mexico City in the earthquake of September 19, 1985", Report No. UCB/EERC-87/15, University of California, Berkeley.

Seed, R.B., Cetin, K. O., Moss, R. E. S., Kammerer, A. M., Wu, J., Pestana, J. M., Riemer, M. F., Sancio, R. B., Bray, R. B., Kayen, R. E., and Faris, A. (2003).

"Recent advances in soil liquefaction engineering: a unified and consistent framework", Report No. EERC 2003-06, Earthquake Engineering Research Center, University of California, Berkeley.

Shamoto, Y., Zhang, J., and Tokimatsu, K. (1998). "New charts for predicting large residual post-liquefaction ground deformations." Soil Dynamics and Earthquake Engineering, 17(7-8), Elsevier, New York, 427–438.

Sheahan, T. C., Ladd, C. C., and Germaine, J. T. (1996). "Rate dependent undrained shear behavior of saturated clay", J. Geotechnical Eng., ASCE, 122(2), 99-108.

Sherif, M. A., Ishibashi, I., and Tsuchiya, C. (1977). "Saturation effects on initial soil liquefaction" J. Geotechnical Eng. Div., ASCE, 103(8), 914-917.

Silver, M. L. (1977). "Laboratory triaxial testing procedures to determine the cyclic strength of soils", NUREG-0031, National Technical Information Service, Springfield, VA.

Silver, M. L., and Seed, H. B. (1971). "Volumetric changes in sands during cyclic loading", J. Soil Mechanics and Foundation Div., ASCE, 97(9), 1171-1182.

Stroud, M. A. (1974). "The standard penetration test in insensitive clays and soft rock", Proc. 1st International Symp. on Penetration Testing, Stockholm, Sweden, Vol.2(2), 367-375.

Suzuki, T. (1984). "Settlement of soft cohesive ground due to earthquake", Proc. 38th Annual Meeting on JSCE, Vol. III, 87-88.

Tatsuoka, F, Sasaki, T., and Yamada, S. (1984). "Settlement in saturated sand induced by cyclic undrained simple shear", 8th World Conference on Earthquake Eng., San Francisco, California, USA, Vol. 3, pp. 95-102.

Taylor, D. W. (1944). 10th progress report on shear strength to US engineers, Massachusetts Institute of Technology, USA.

Terzaghi, K., and Peck, R. B. (1948). Soil Mechanics in Engineering Practice, John Wiley and Sons Inc., 1st Edition, 566 pgs.

Thiers, G. R., and Seed, H. B. (1969). "Strength and stress-strain characteristics of clays subjected to seismic loads", ASTM STP 450, Symposium on Vibration Effects of Earthquakes on Soils and Foundations, ASTM, 3-56.

Tokimatsu, K., and Seed, H. B. (1984). "Simplified procedures for the evaluation of settlements in sands due to earthquake shaking", Report No. UCB/EERC-84/16, Earthquake Engineering Research Center, University of California, Berkeley, CA.

Tokimatsu, K., and Seed, H. B. (1987). "Evaluation of settlements in sands due to earthquake shaking", J. Geotechnical Eng., 113(8), 861-878.

Toufigh, M. M., and Ouria, A. (2009). "Consolidation of inelastic clays under rectangular cyclic loading", Soil Dynamics and Earthquake Engineering, 29(2), 356-363.

Tsukamato, Y., Ishihara, K., and Sawada, S. (2004). "Settlement of silty sand deposits following liquefaction during earthquakes", Soils and Foundations, 44(5), 135-148.

Ue, S., Yasuhara, K., and Fujiwara, H. (1991). "Influence of consolidation period on undrained strength of clays", Ground and Construction, 9(1), 51-62.

Vaid, Y. P., Robertson, P. K., and Campanella, R. G. (1979). "Strain rate behaviour of the St. Jean Vianney clay", Canadian Geotechnical Journal, 16(1), 34-42.

Van Eekelen, H. A. M., and Potts, D. M. (1978). "The behaviour of Drammen clay under cyclic loading", Géotechnique, 28, 173-196.

Vucetic, M., and Dobry, R. (1988). "Degradation of marine clays under cyclic loading" J. Geotechnical Eng., ASCE, 114(2), 133-149.

Vucetic, M., and Dobry, R. (1991). "Effect of soil plasticity on cyclic response", J. Geotechnical Eng., 117(1), 89-107.

Wang, W. (1979). Some Findings in Soil Liquefaction. Report Water Conservancy and Hydro-electric Power Scientific Research Institute (pp. 1-17). Beijing, China.

Wilson, N. E., and Greenwood, J. R. (1974). "Pore pressure and strains after repeated loading in saturated clay", Canadian Geotechnical Journal, 11, 269-277.

Wu, J., Kammerer, A. M., Riemer, M. F., Seed, R. B., and Pestana, J. M. (2004). "Laboratory study of liquefaction triggering criteria", 13th World Conf. on Earthquake Eng., Vancouver, B.C., Canada, Paper No. 2580.

Yasuhara, K. (1994). "Post-cyclic undrained strength for cohesive soils" J. Geotechnical Eng., ASCE, 120(11), 1961-1979.

Yasuhara, K., and Andersen, K. H. (1991). "Post-cyclic recompression settlement of clay", Soils and Foundations, 31(1), 83-94.

Yasuhara, K., and Hyde, A. F. L. (1997). "Method for estimating post-cyclic undrained secant modulus of clays", J. Geotechnical and Geoenvironmental Eng., 123(3), 204-211.

Yasuhara, K., Fujiwara, H., Hirao, K., and Ue, S. (1983). "Undrained shear behavior of quasi-overconsolidated clay induced by cyclic loading", Proc. IUTAM Symp., Seabed Mechanics, 17-24.

Yasuhara, K., Hirao, K., and Hyde, A. F. L. (1992). "Effects of cyclic loading on undrained strength and compressibility of clay", Soils and Foundations, 32(1), 100-116.

Yasuhara, K., Hyde, A. F. L., Toyota, N., and Murukami, S. (1997). "Cyclic stiffness of plastic silt with an initial drained shear stress", Géotechnique, Special Issue, Pre-Failure Deformation Behavior of Geomaterials, 371-382.

Yasuhara, K., Murakami, S., Toyota, N., and Hyde, A. F. L. (2001). "Settlements in fine-grained soils under cyclic loading", Soils and Foundations, 41(6), 25-36.

Yasuhara, K, Satoh, K., and Hyde, A. F. L. (1994). "Post-cyclic undrained stiffness for clays", Proc. Int. Symp. Prefailure Deformation of Geomaterials, Vol. 1, 483-489.

Youd, T. L., Idriss, I. M., Andrus, R. D., Arango, I., Castro, G., Christian, J. T., Dobry, E., Finn, W. D. L., Harder Jr., L. F., Hynes, M. E., Ishihara, K., Koester, J.

P., Liao, S. S. C., Marcusson III, W. F., Martin, G. R., Mtchell, J. K., Moriwaki, Y., Power, M. S., Robertson, P. K., Seed, R. B., and Stokoe II, K. H. (2001). "Liquefaction resistance of soils: Summary report from the 1966 NCEER and 1998 NCEER/NSF workshops on evaluation of liquefaction resistance of soils" J. Geotechnical and Geoenvironmental Eng., 124(10), 817-833.

Zavoral, D. C., and Campanella, R. G. (1994). "Frequency effects on damping/modulus of cohesive soils", Dynamic Geotechnical Testing II, ASTM Special Technical Publication No. 1213, R. J. Ebelhar, V. P. Drnevich and B. L. Kutter, ed., 191-201

Zergoun, M., and Vaid, Y. P. (1994). "Effective stress response of clay to undrained cyclic loading", Canadian Geotechnical Journal, 31, 714-727.

Zhang, G., Robertson, P. K., and Brachman, R. W., (2002). "Estimating liquefaction-induced ground settlements from CPT for level ground", Canadian Geotechnical Journal, 35(5), 1168-1180.

APPENDIX A

GRAIN SIZE DISTRIBUTION TEST RESULTS
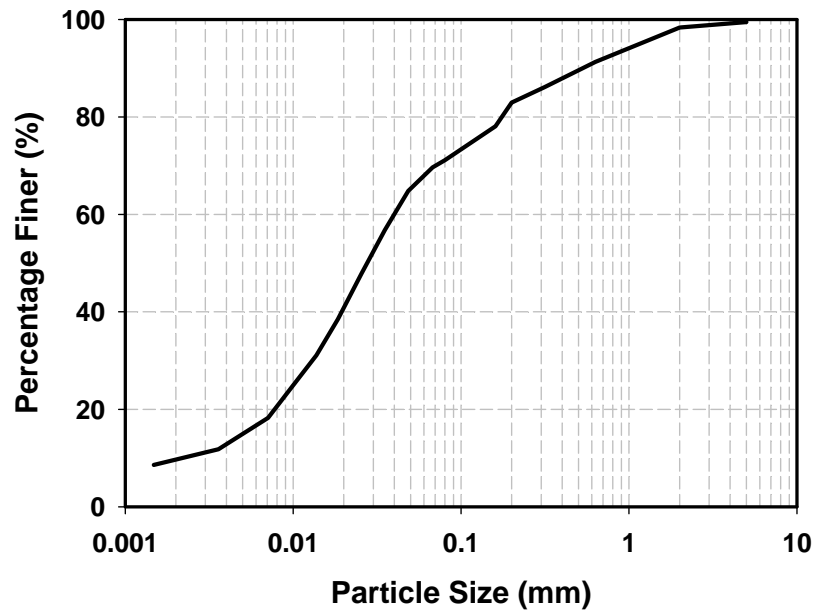
Figure A. 1. Grain size distribution curve for Sample GD1-3M
Related cyclic test: CTXT11, G_S = 2.650
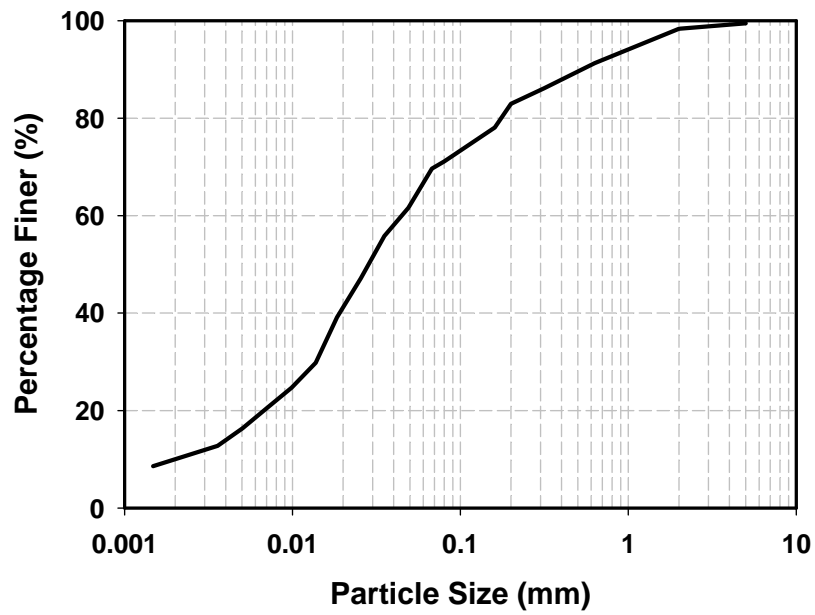
Figure A. 2. Grain size distribution curve for Sample GD1-3T
Related cyclic test: CTXT12, G_S = 2.650
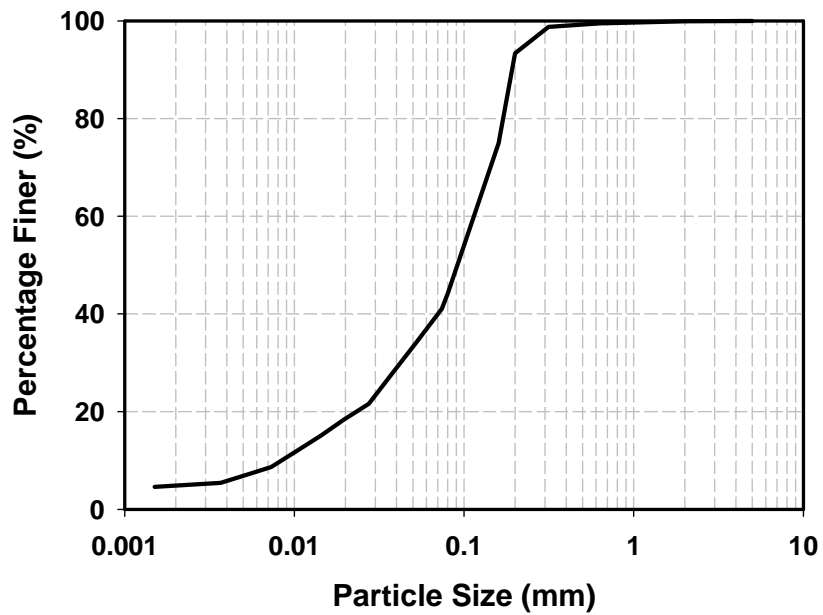
Figure A. 3. Grain size distribution curve for Sample GB1-5M
Related cyclic test: CTXT15, G_S = 2.620
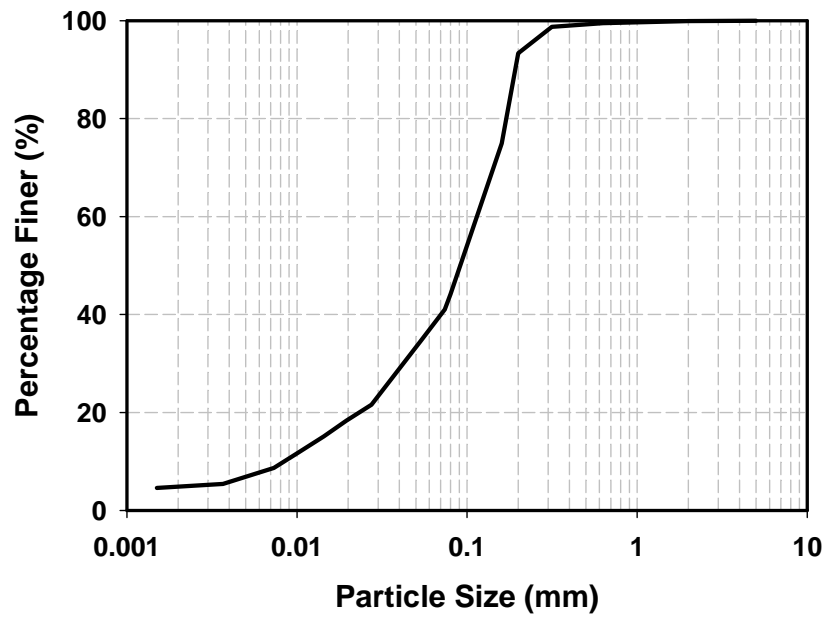
Figure A. 4. Grain size distribution curve for Sample GB1-5M

Related cyclic test: CTXT15, G_S = 2.620
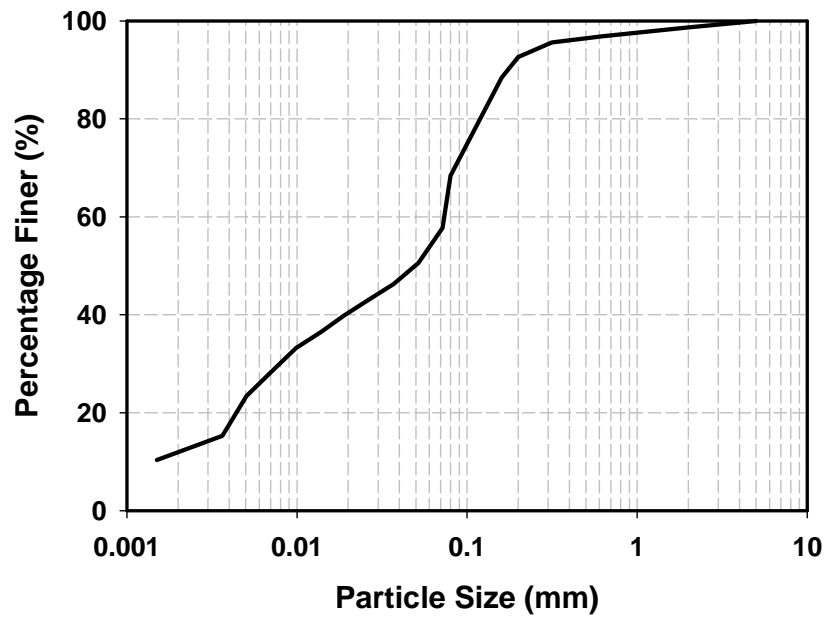
Figure A. 5. Grain size distribution curve for Sample GB1-5B

Related cyclic test: CTXT16, G_S = 2.580
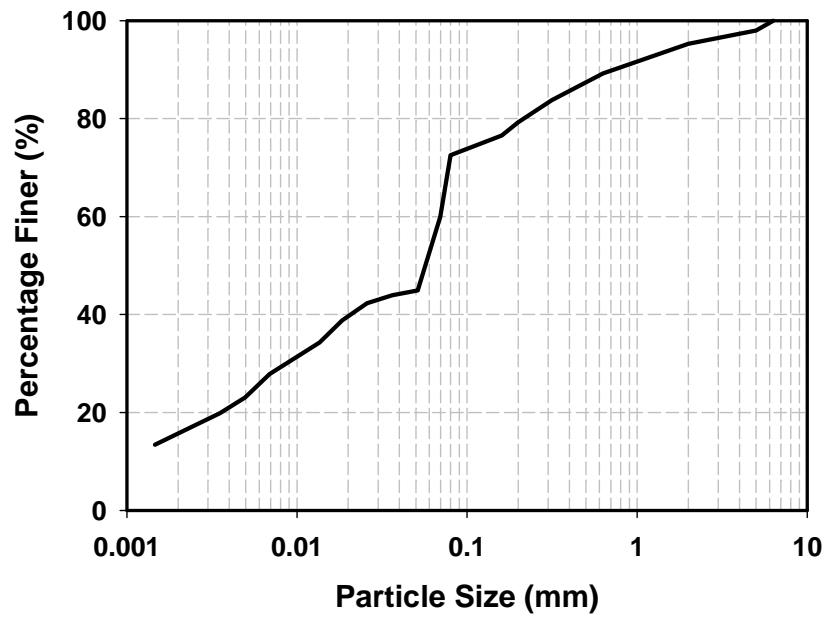
Figure A. 6. Grain size distribution curve for Sample V4-TB
Related cyclic test: CTXT23, G_S = 2.650
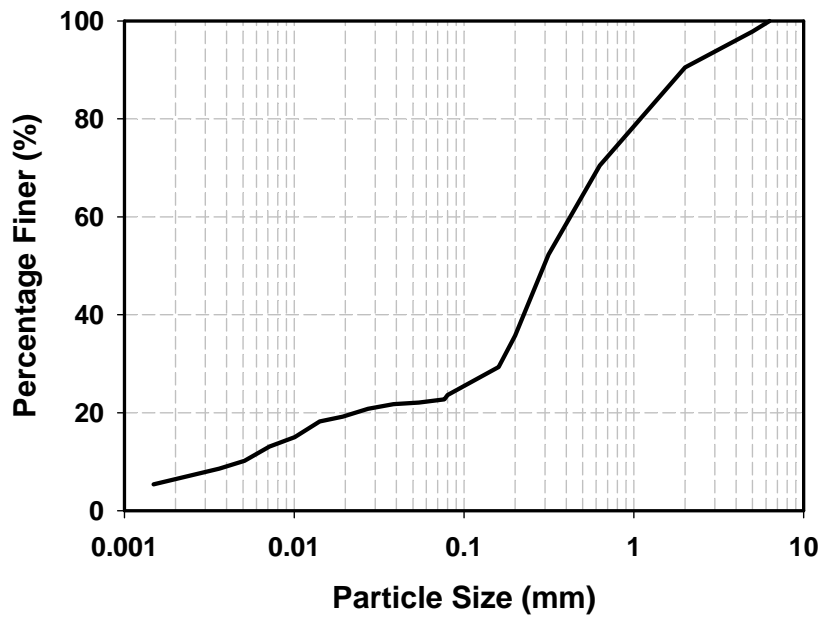
Figure A. 7. Grain size distribution curve for Sample V4-M
Related cyclic test: CTXT24, G_S = 2.650
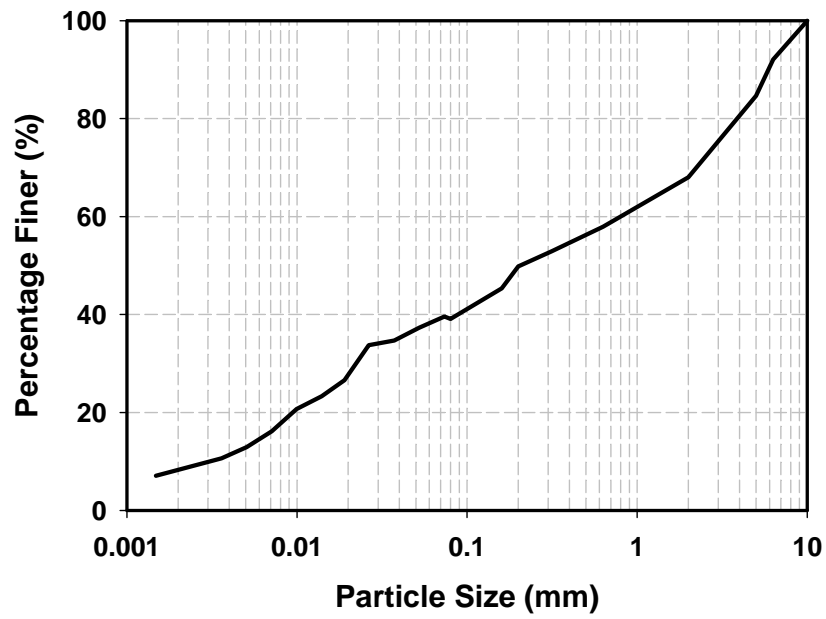
Figure A. 8. Grain size distribution curve for Sample SK7-1B and SK7-1M
Related cyclic test: CTXT25 and CTXT26 , G_S = 2.650
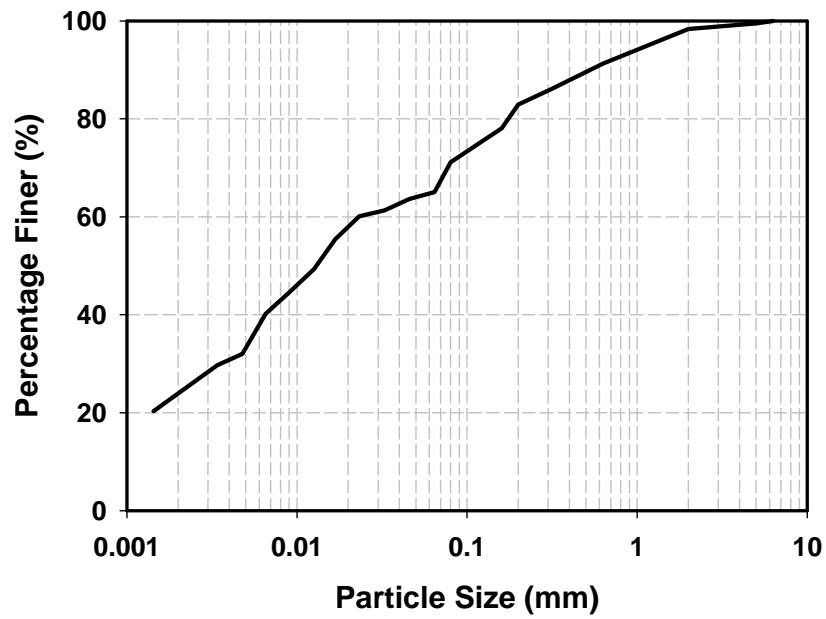
Figure A. 9. Grain size distribution curve for Sample TSK2-1B
Related cyclic test: CTXT27, G_S = 2.600

174
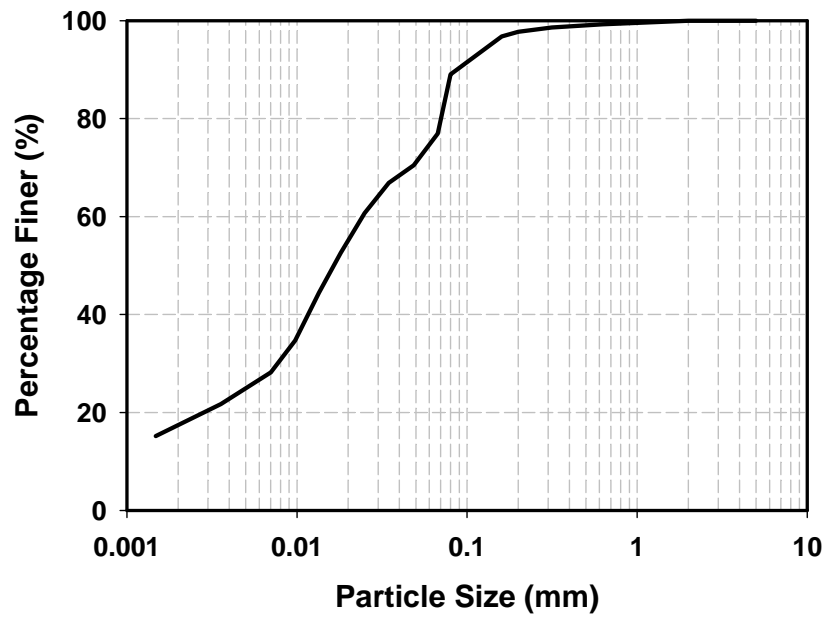
Figure A. 10. Grain size distribution curve for Sample GA1-5T
Related cyclic test: CTXT30, G_S = 2.600
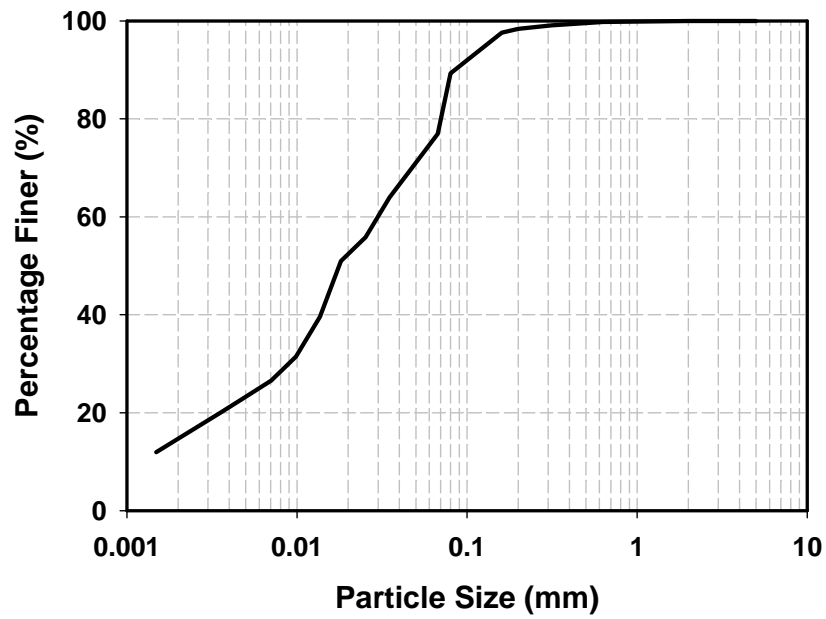
Figure A. 11. Grain size distribution curve for Sample GA1-5B
Related cyclic test: CTXT31, G_S = 2.600
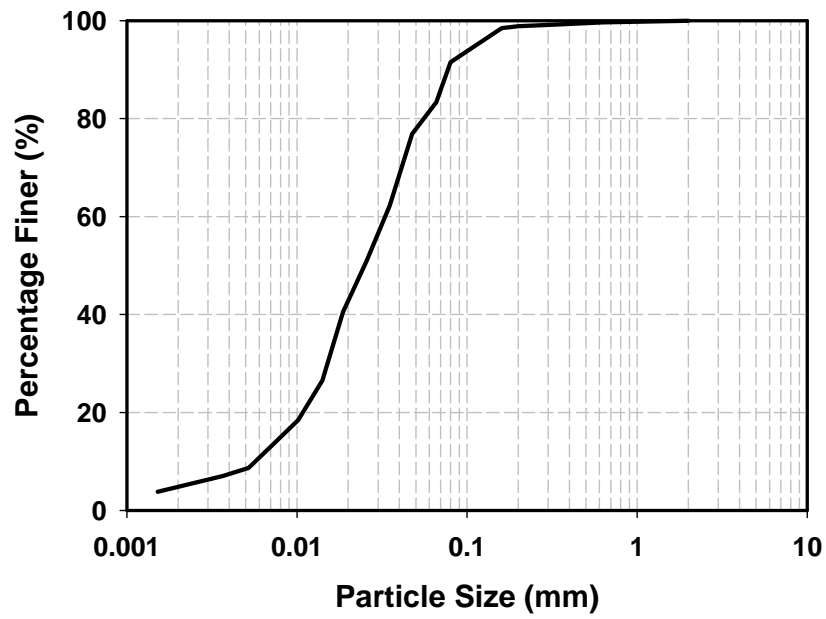
Figure A. 12. Grain size distribution curve for Sample BA2-3B

Related cyclic test: CTXT32, G$_S$ = 2.600
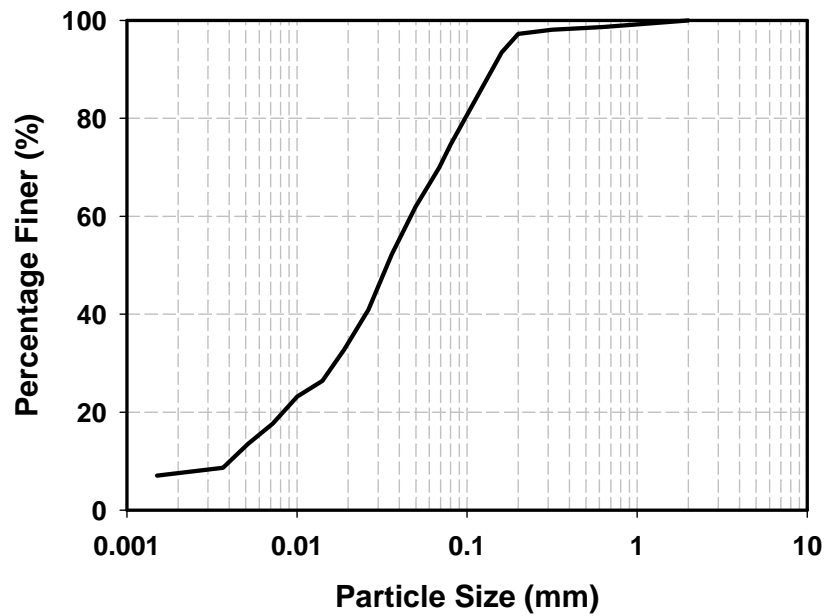
Figure A. 13. Grain size distribution curve for Sample BA2-3T and BA2-3T1

Related cyclic test: CTXT33 and CTXT34, G$_S$ = 2.600

176
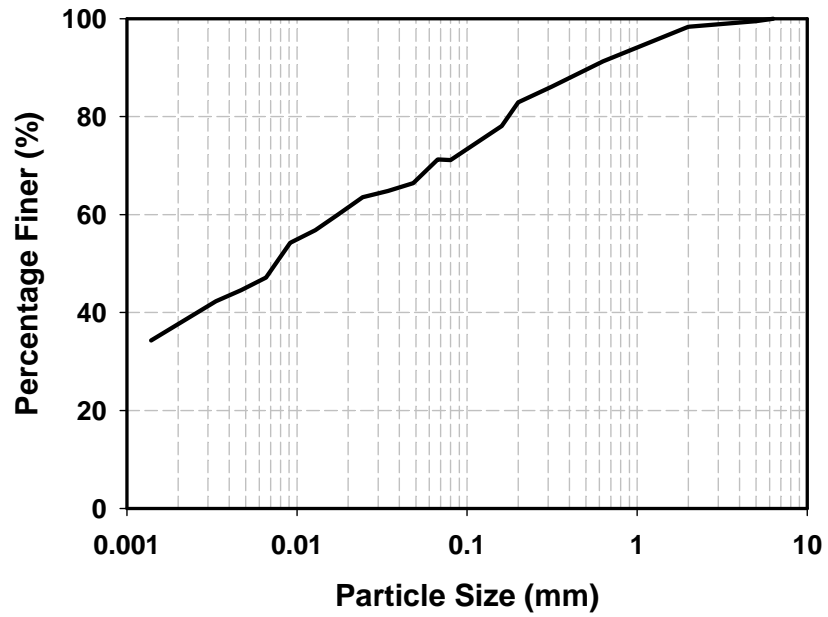
Figure A. 14. Grain size distribution curve for Sample THAMES2-1 & 1-2B
Related cyclic test: CTXT35 and CTXT36, G_S = 2.640
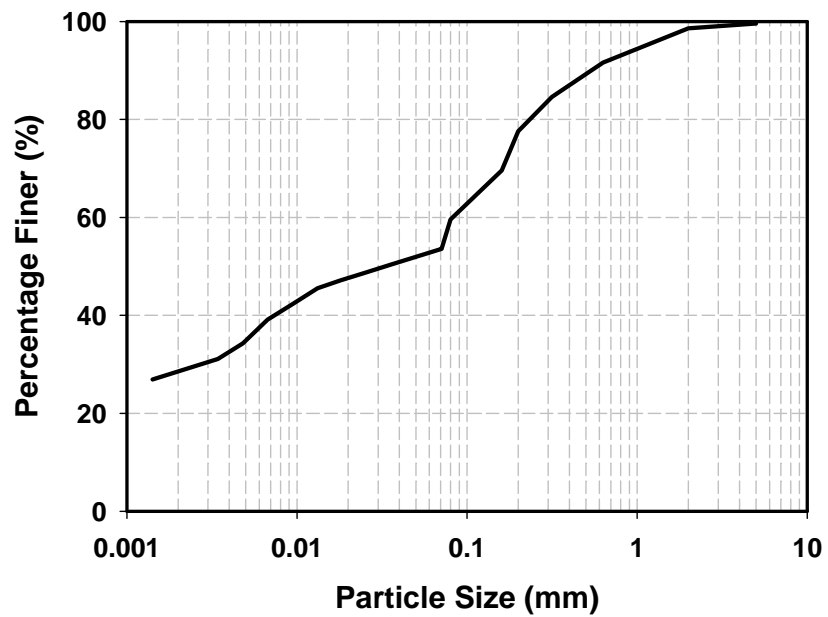
Figure A. 15. Grain size distribution curve for Sample BH2-3M
Related cyclic test: CTXT37, G_S = 2.635
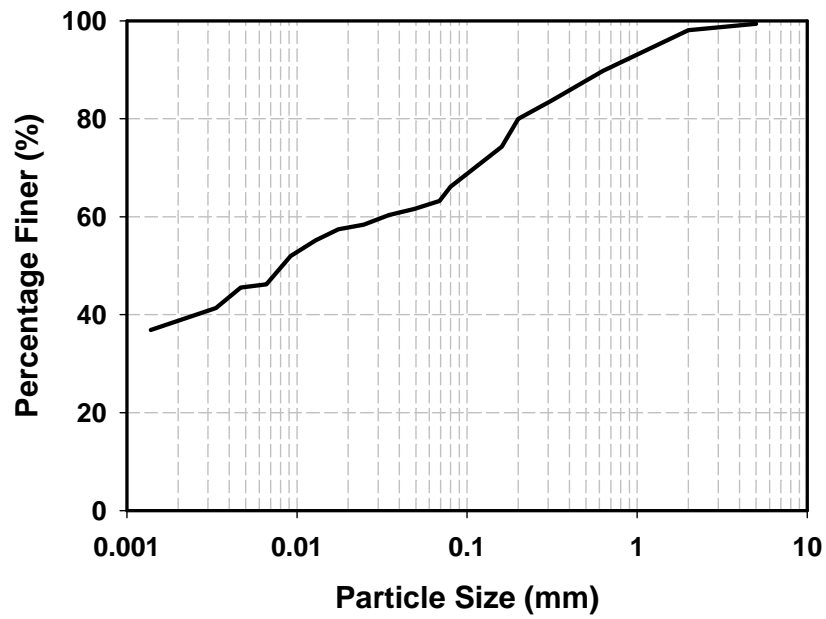
Figure A. 16. Grain size distribution curve for Sample BH2-3B

Related cyclic test: CTXT38, G_S = 2.635
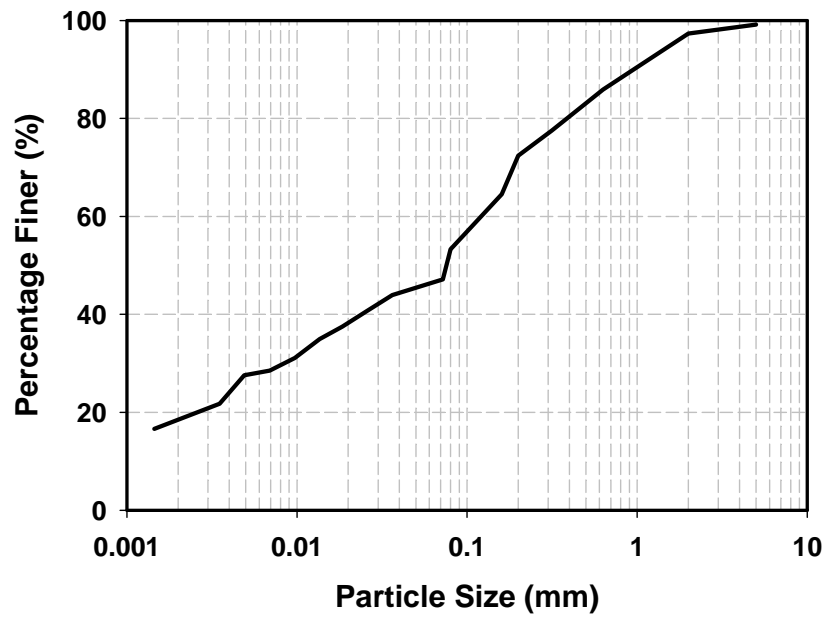
Figure A. 17. Grain size distribution curve for Sample BH5-1M

Related cyclic test: CTXT40, G_S = 2.650
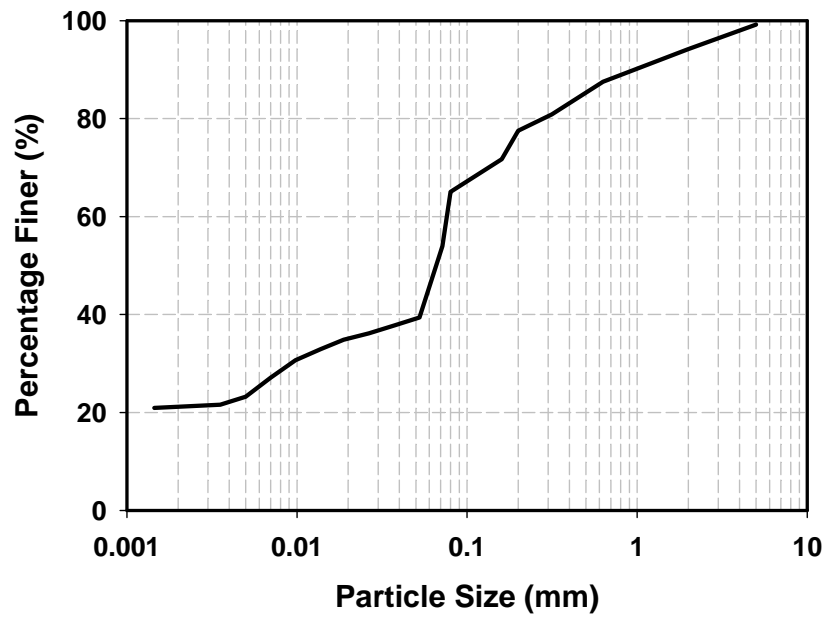
Figure A. 18. Grain size distribution curve for Sample BH5-1B
Related cyclic test: CTXT42, G_S = 2.620
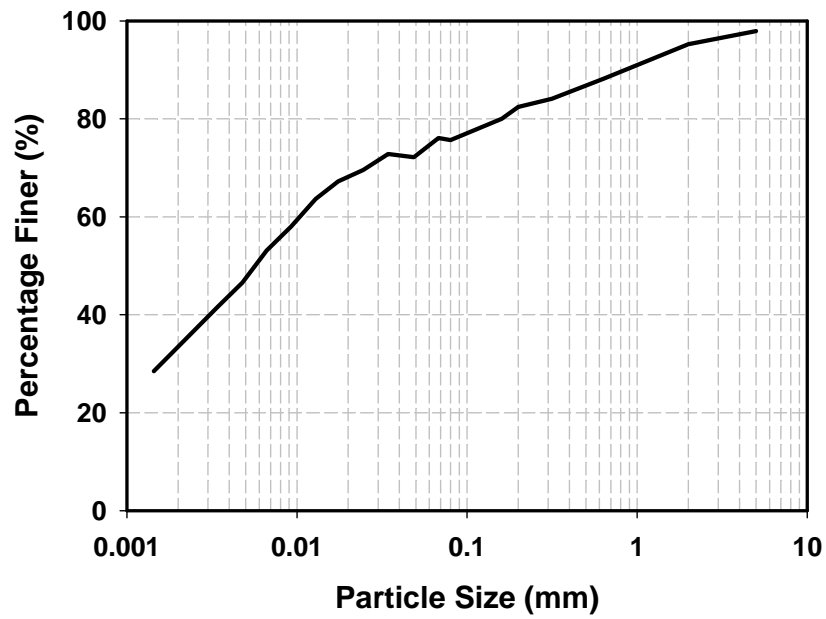
Figure A. 19. Grain size distribution curve for Sample BH6-3B
Related cyclic test: CTXT43, G_S = 2.580
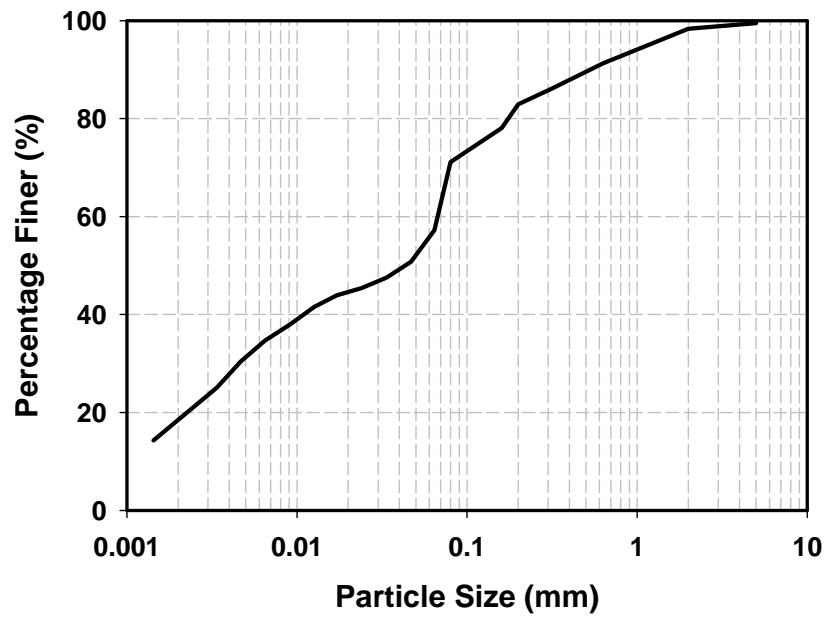
Figure A. 20. Grain size distribution curve for Sample BH6-3B
Related cyclic test: CTXT44, G_S = 2.620
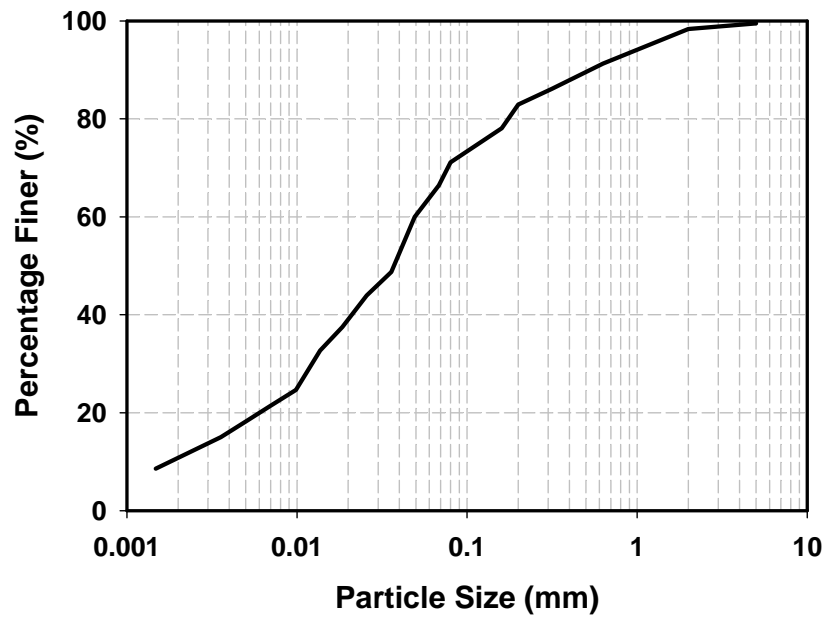
Figure A. 21. Grain size distribution curve for Sample BH6-3T
Related cyclic test: CTXT45, G_S = 2.620
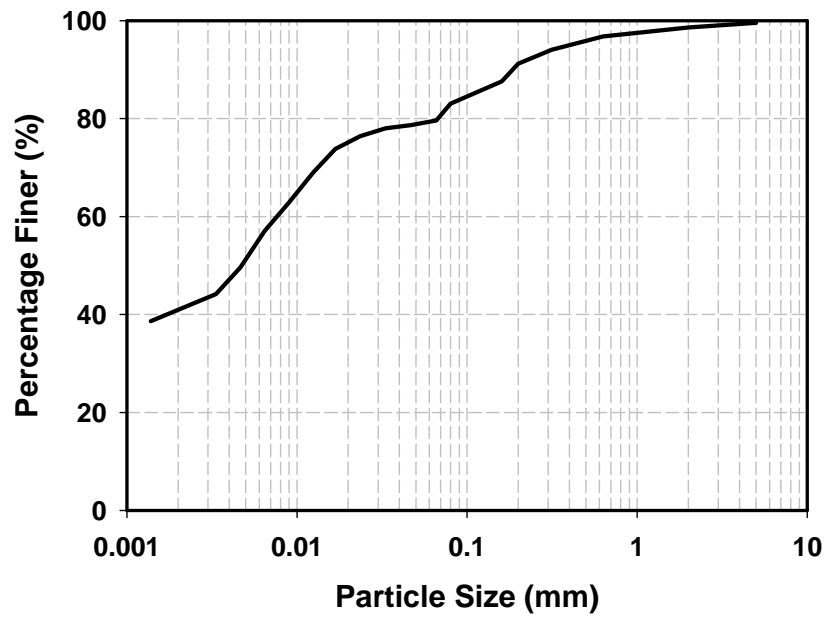
Figure A. 22. Grain size distribution curve for Sample BH4-3M
Related cyclic test: CTXT46, G_S = 2.600
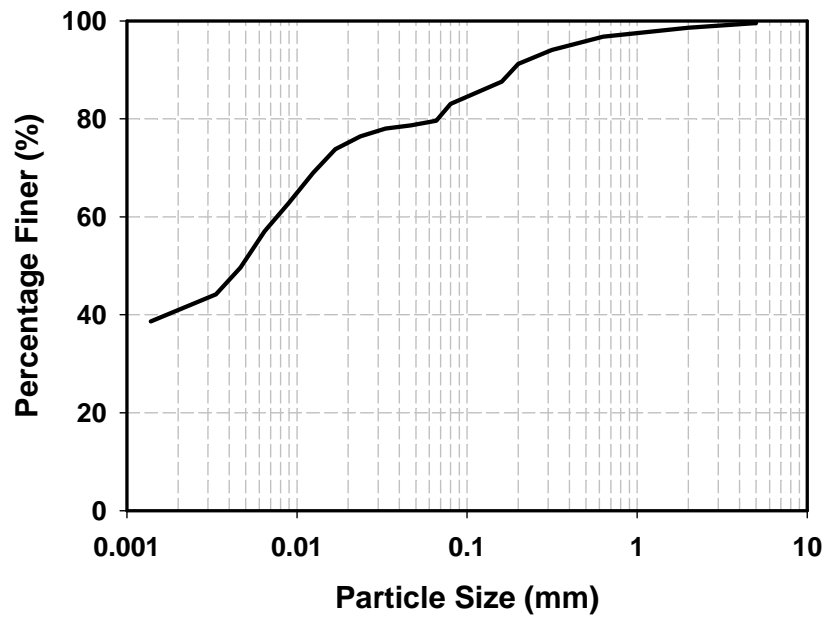
Figure A. 23. Grain size distribution curve for Sample BH4-3B
Related cyclic test: CTXT47, G_S = 2.630
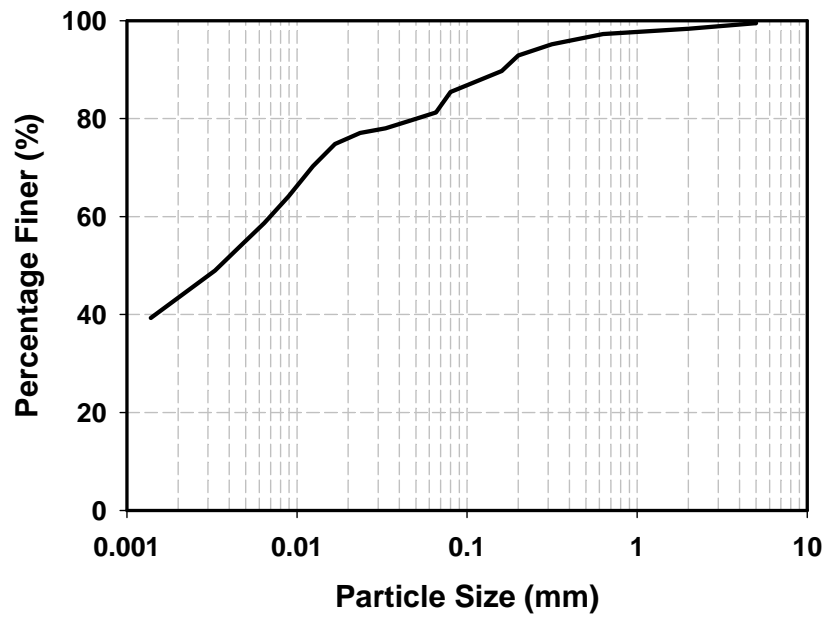
Figure A. 24. Grain size distribution curve for Sample BH4-3T
Related cyclic test: CTXT48, G_S = 2.630
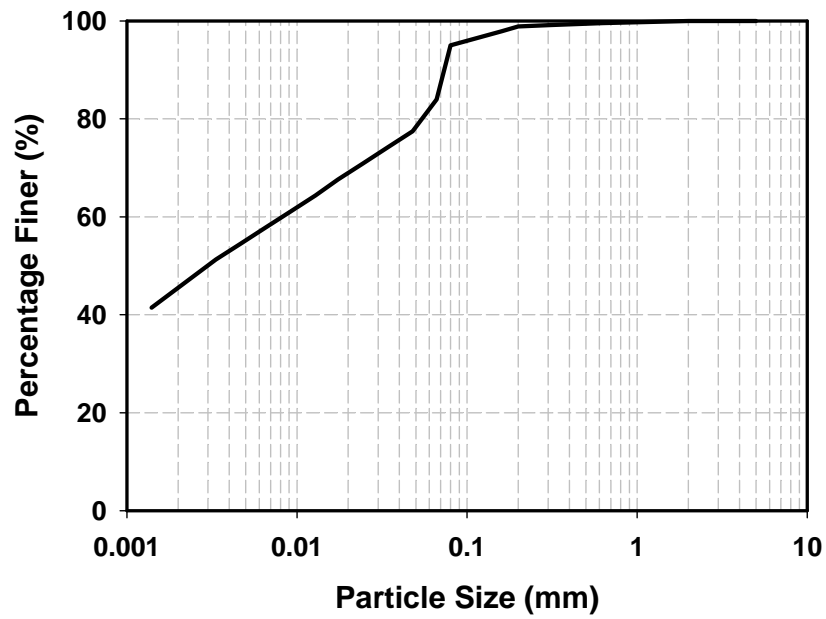
Figure A. 25. Grain size distribution curve for Sample BH3-2M
Related cyclic test: CTXT49, G_S = 2.580
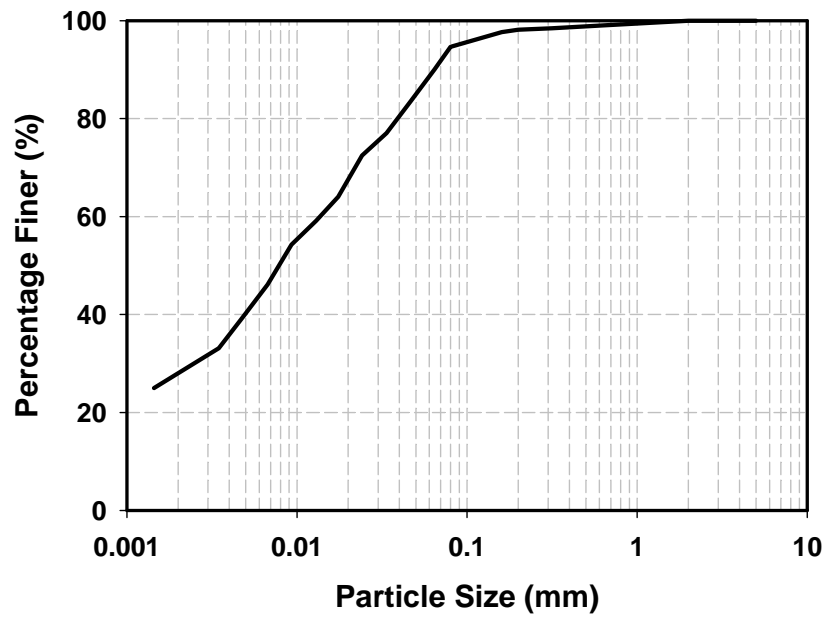
Figure A. 26. Grain size distribution curve for Sample BH3-2B
Related cyclic test: CTXT50, G_S = 2.580
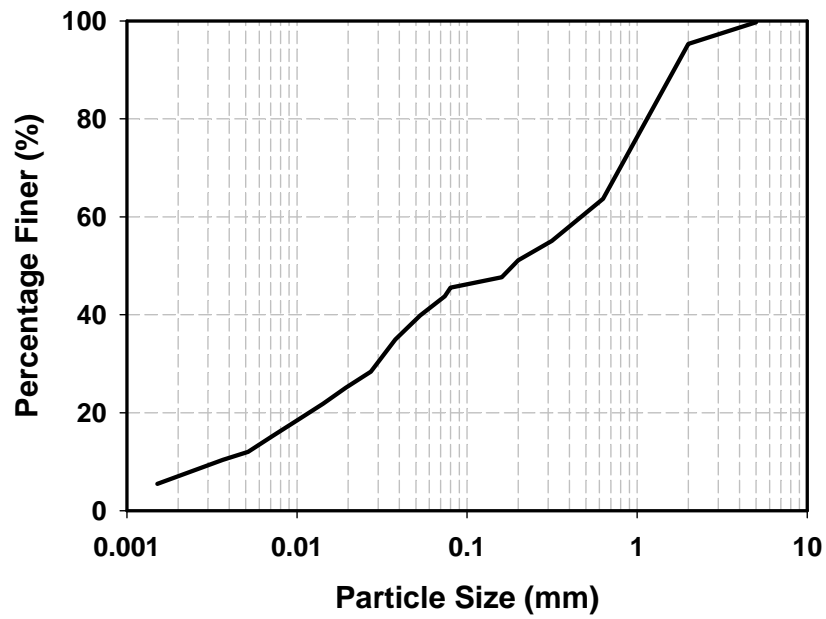
Figure A. 27. Grain size distribution curve for Sample BH1-5M & 1-5B
Related cyclic test: CTXT51 and CTXT53, G_S = 2.600
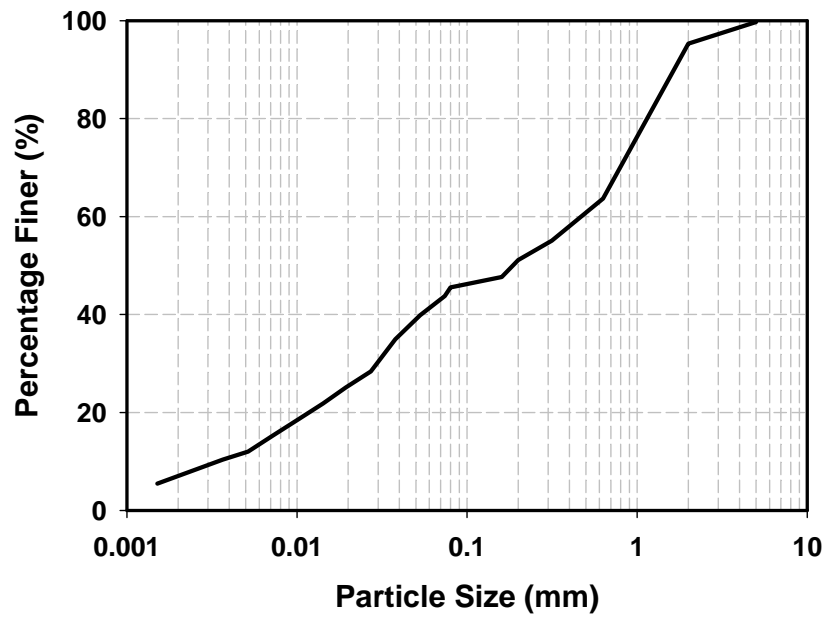
Figure A. 28. Grain size distribution curve for Sample BH1-5T

Related cyclic test: CTXT52, G_S = 2.580
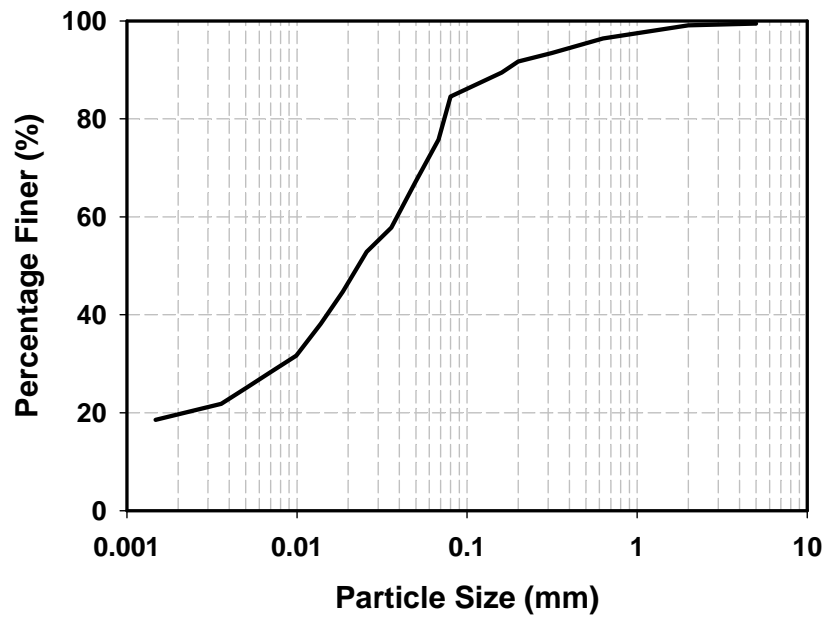
Figure A. 29. Grain size distribution curve for Sample BH7-2M

Related cyclic test: CTXT54, G_S = 2.580
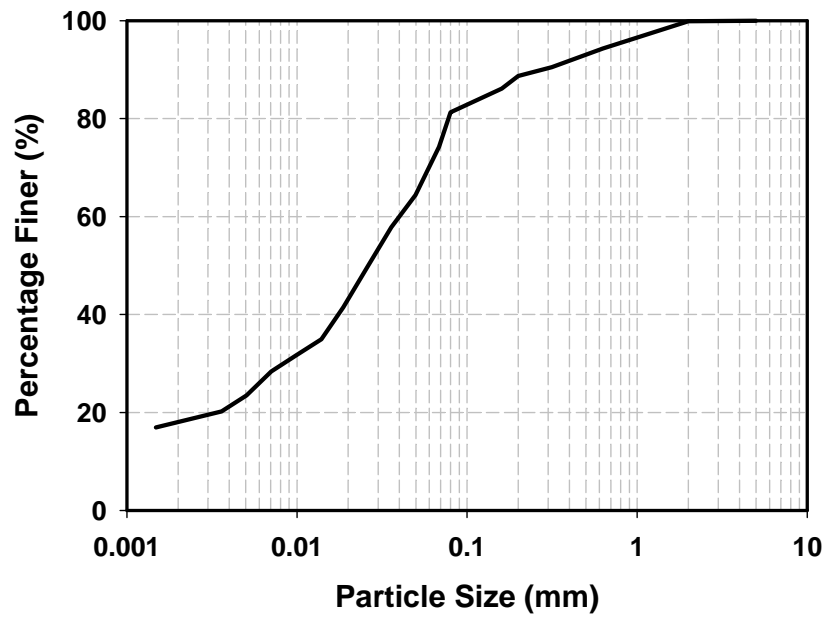
Figure A. 30. Grain size distribution curve for Sample BH7-2B
Related cyclic test: CTXT55, G_S = 2.580
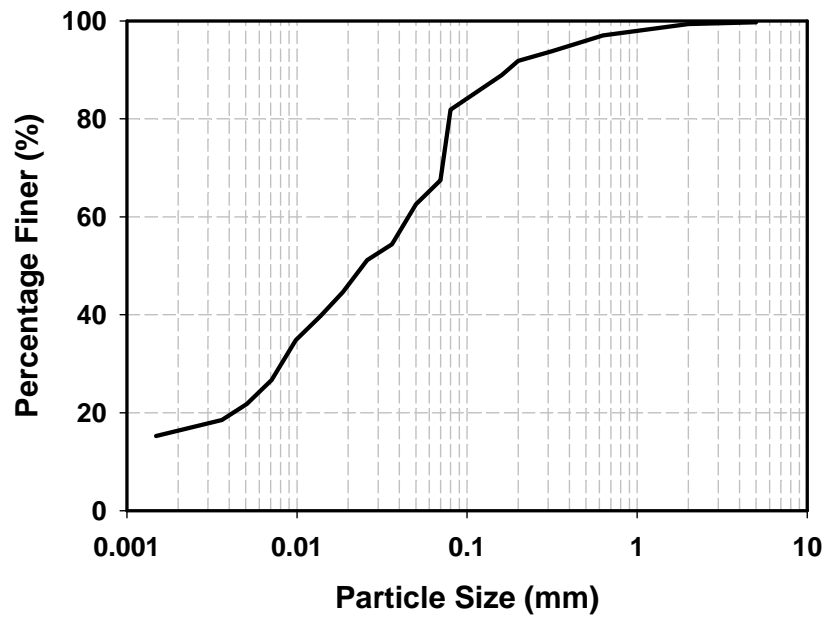
Figure A. 31. Grain size distribution curve for Sample BH7-2T
Related cyclic test: CTXT56, G_S = 2.580

185
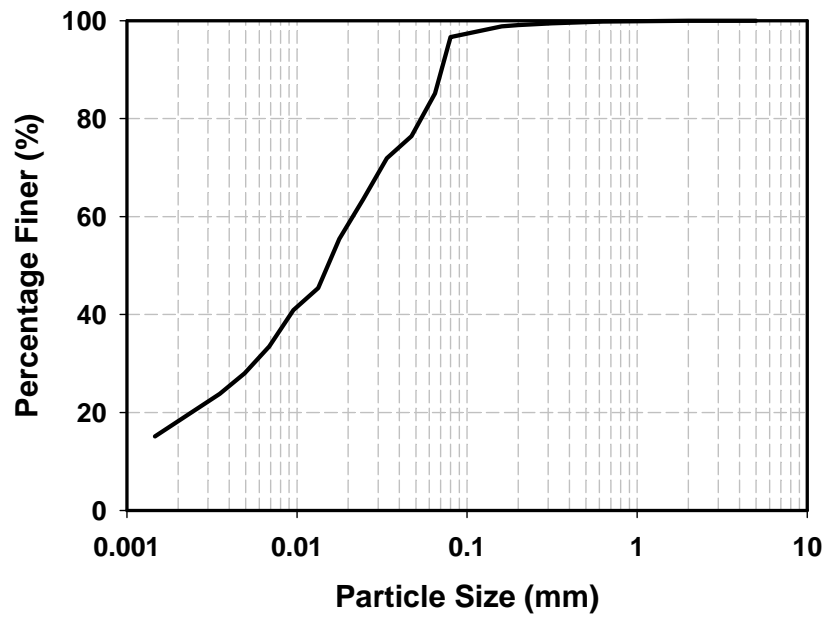
Figure A. 32. Grain size distribution curve for Sample BH3-4M
Related cyclic test: CTXT58, G_S = 2.630
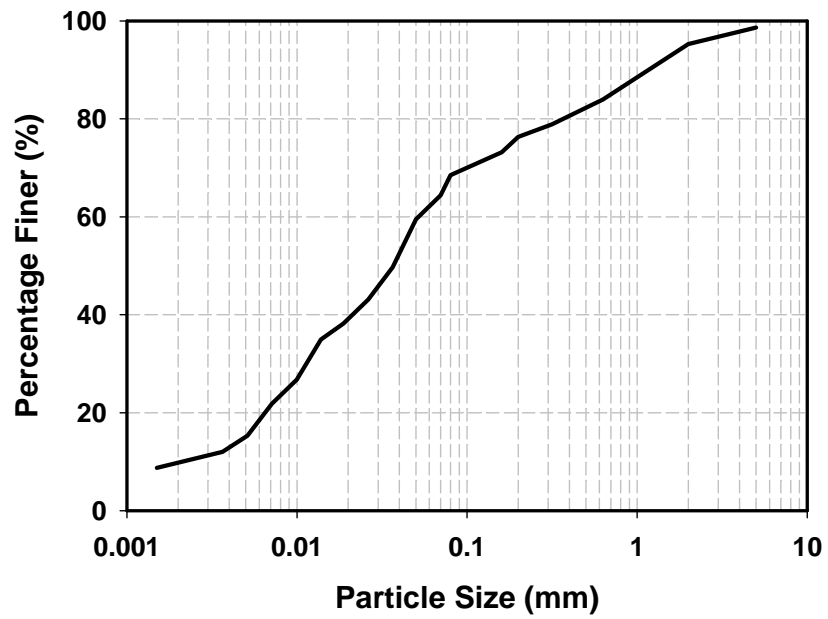
Figure A. 33. Grain size distribution curve for Sample BH7-4M & 7-4B
Related cyclic test: CTXT59 and CTXT62, G_S = 2.600
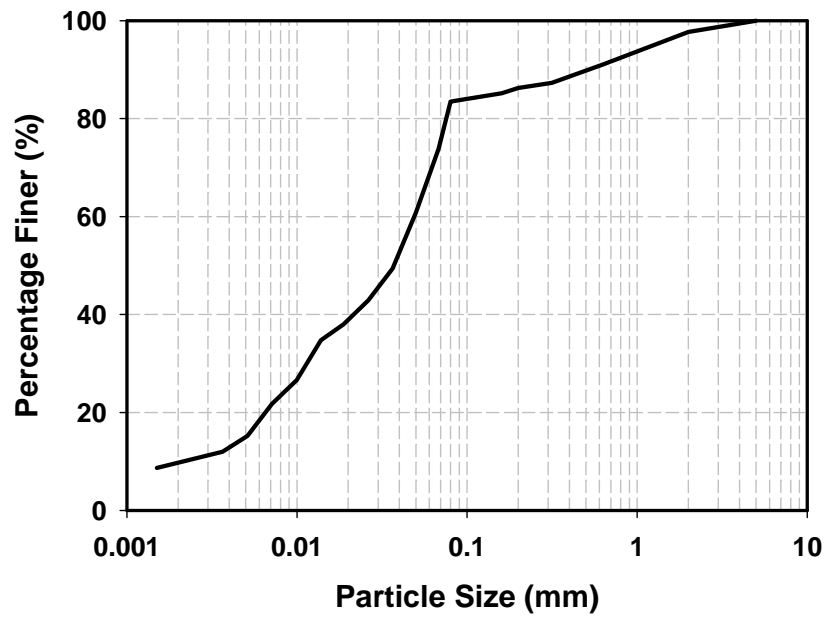
Figure A. 34. Grain size distribution curve for Sample BH7-4T & 7-4T1
Related cyclic test: CTXT60 and CTXT61, G_S = 2.600
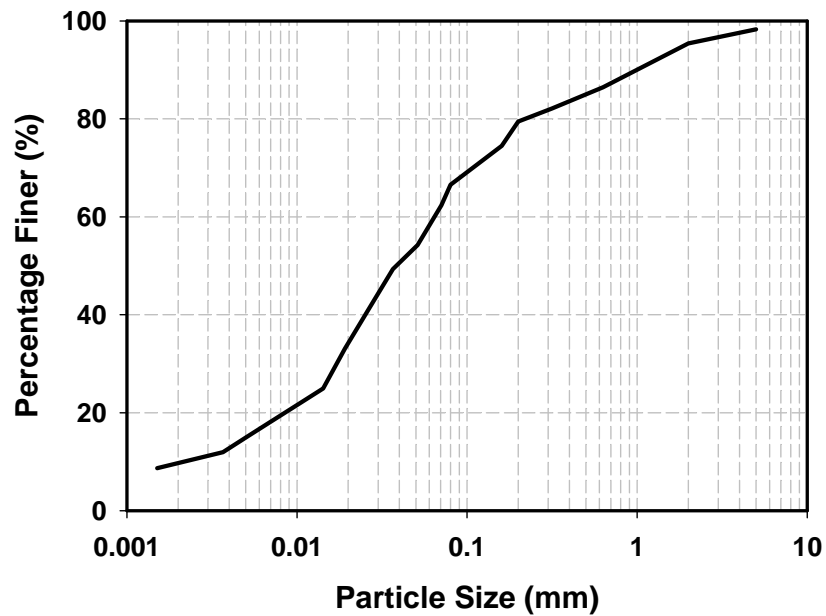
Figure A. 35. Grain size distribution curve for Sample BH7-5T & 7-5M
Related cyclic test: CTXT63 and CTXT64, G_S = 2.580

APPENDIX B

RESULTS OF STATIC TRIAXIAL TESTS
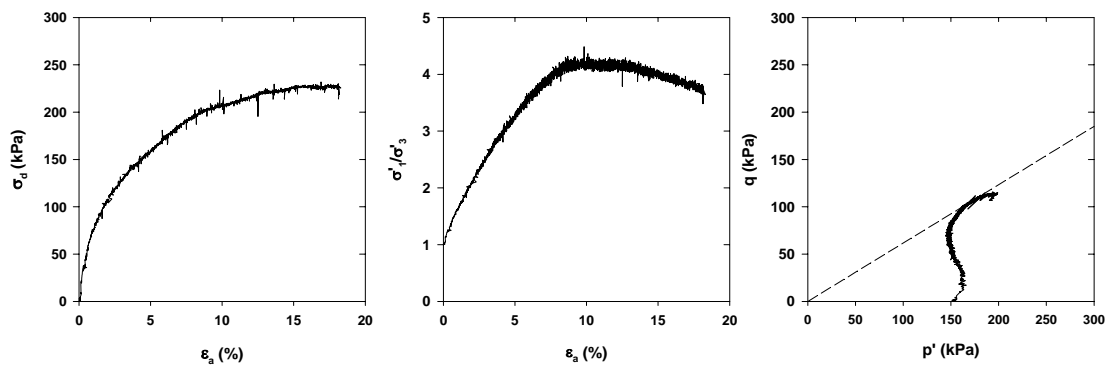
Figure B. 1. Presentation of STXT1
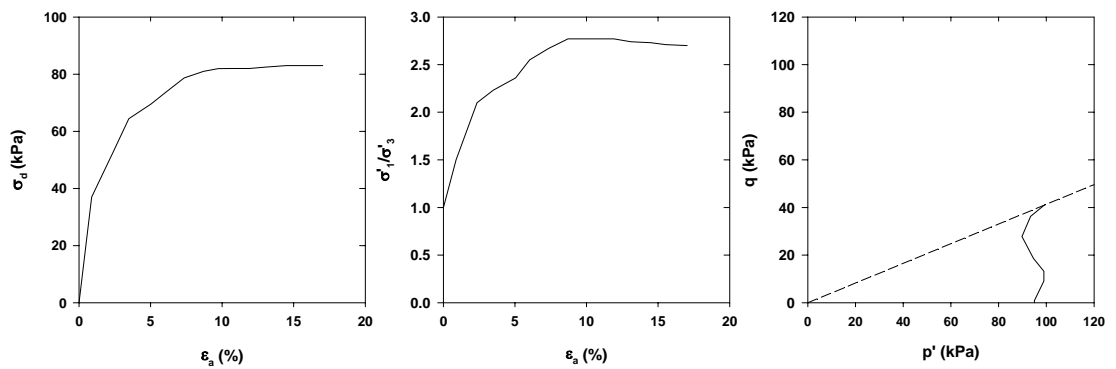
Figure B. 2. Presentation of STXT2
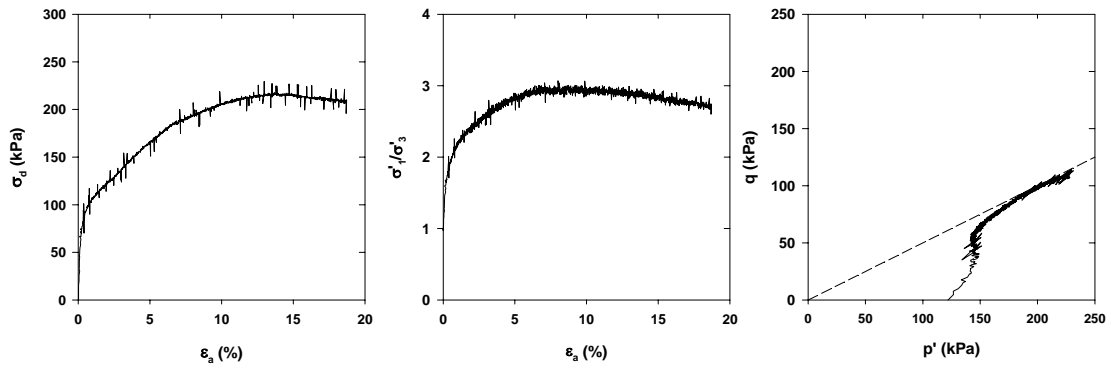
Figure B. 3. Presentation of STXT3
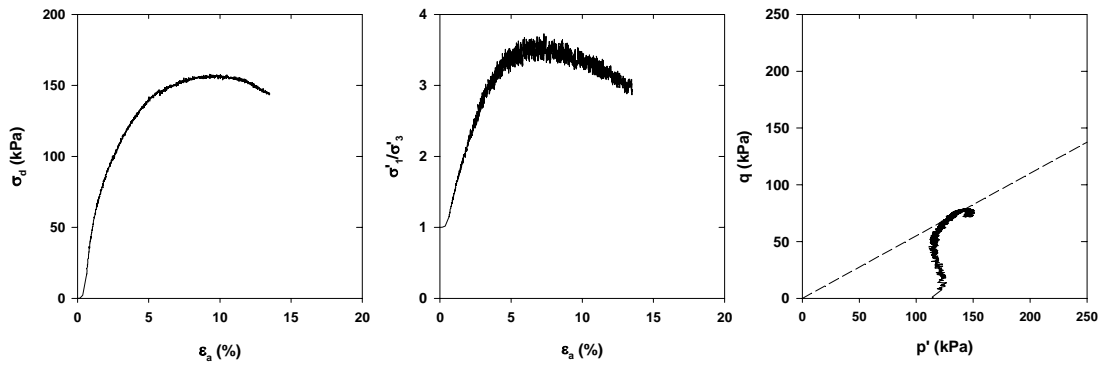
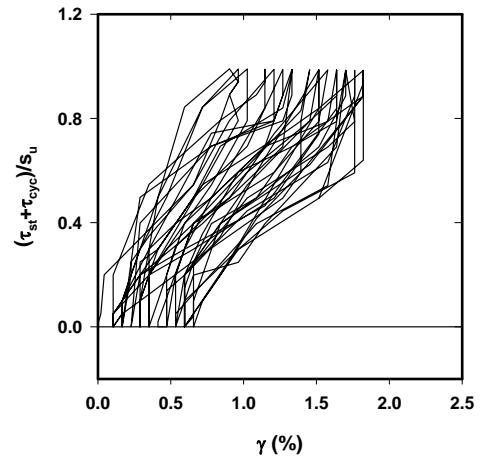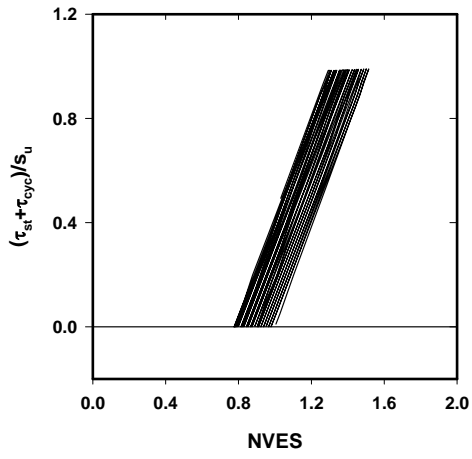**Figure B. 4. Presentation of STXT4**
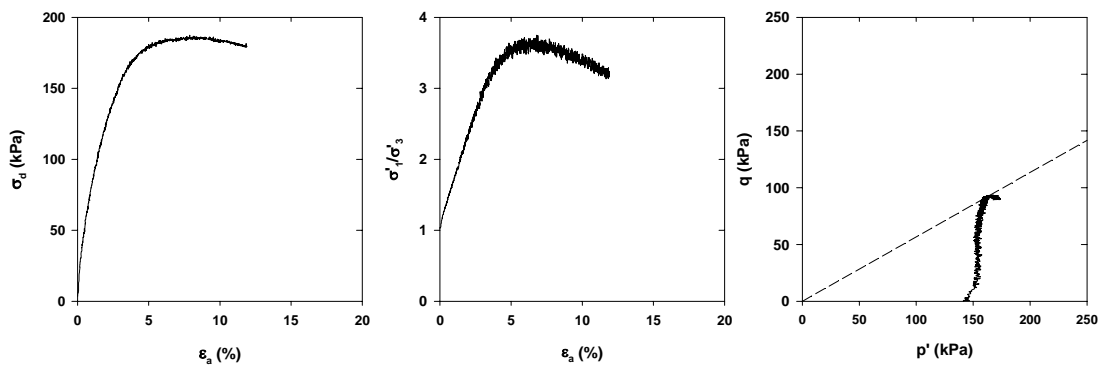
Figure B. 5. Presentation of STXT5
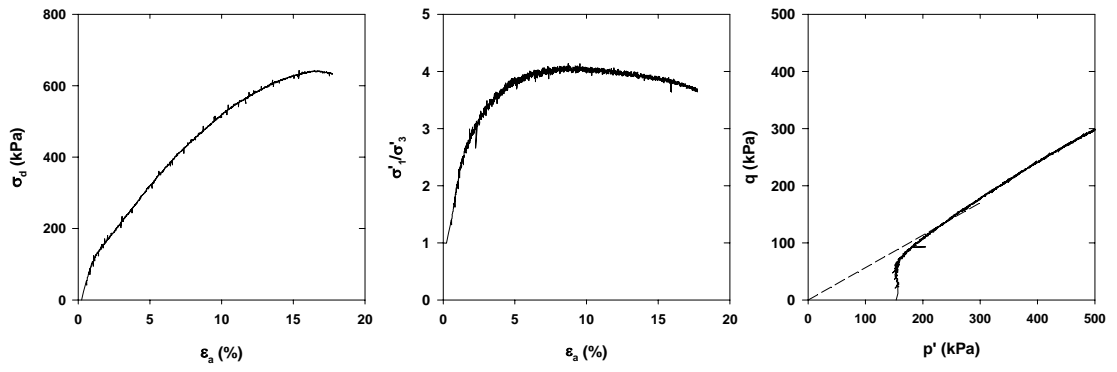
Figure B. 6. Presentation of STXT6
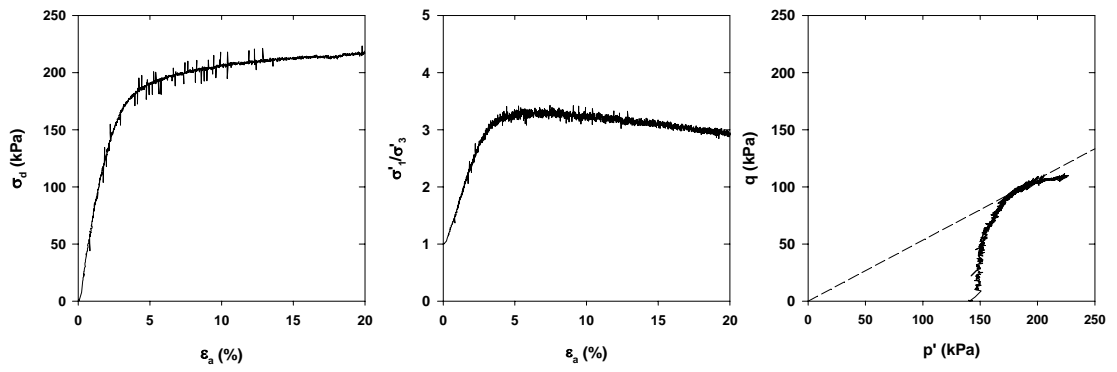
Figure B. 7. Presentation of STXT7
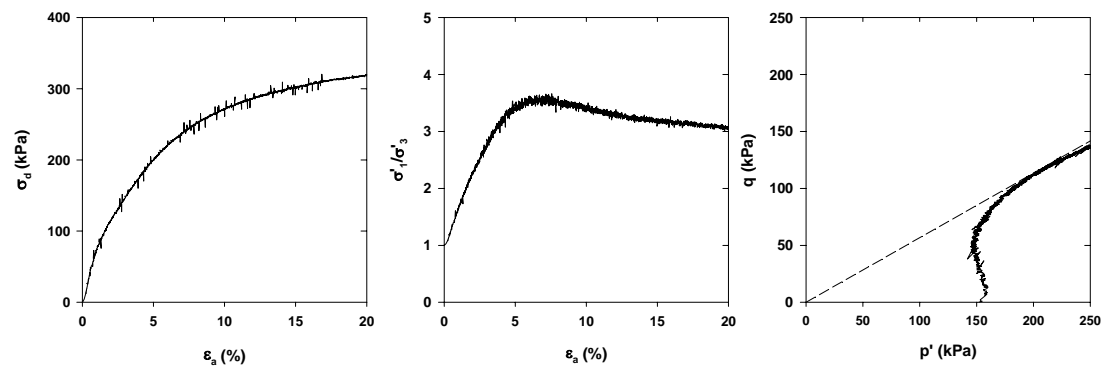
Figure B. 8. Presentation of STXT8
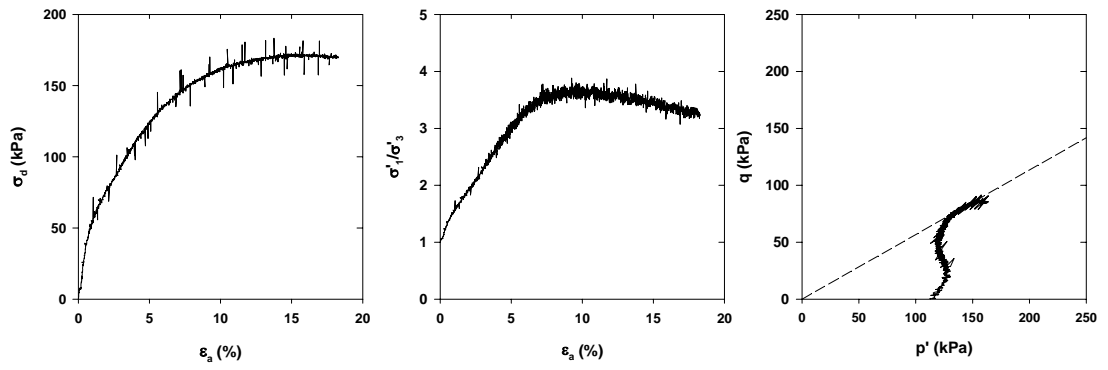
Figure B. 9. Presentation of STXT9
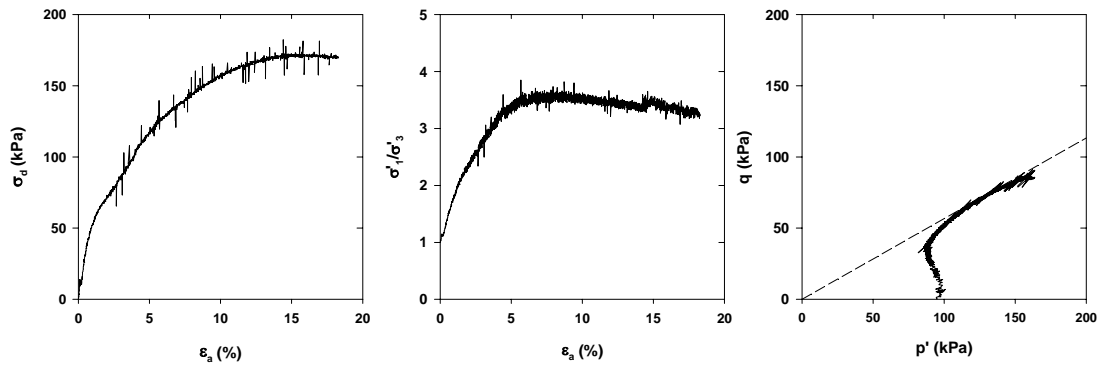
Figure B. 10. Presentation of STXT10
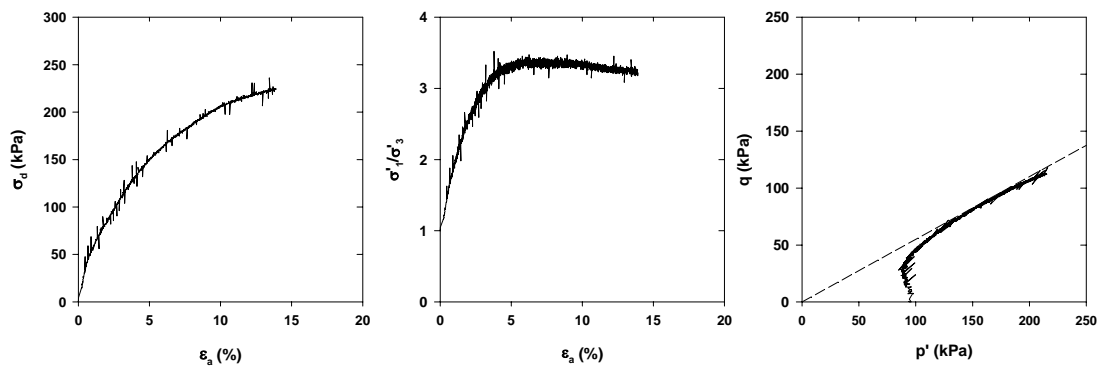
Figure B. 11. Presentation of STXT11
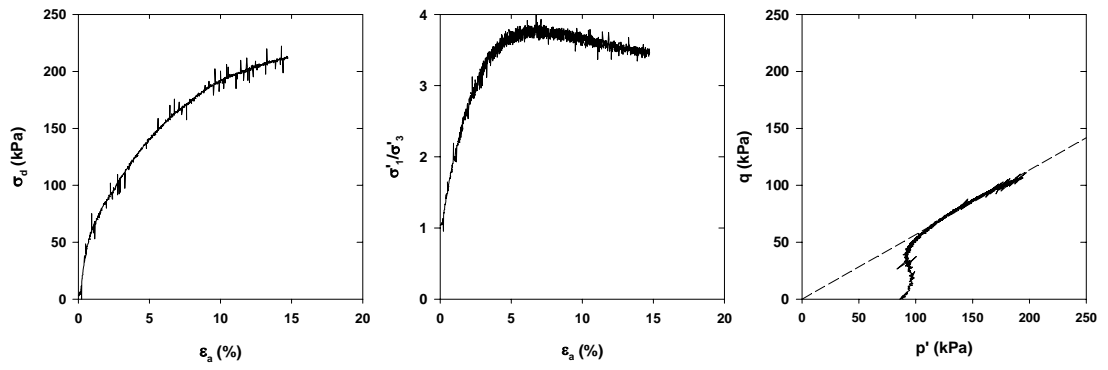
Figure B. 12. Presentation of STXT12
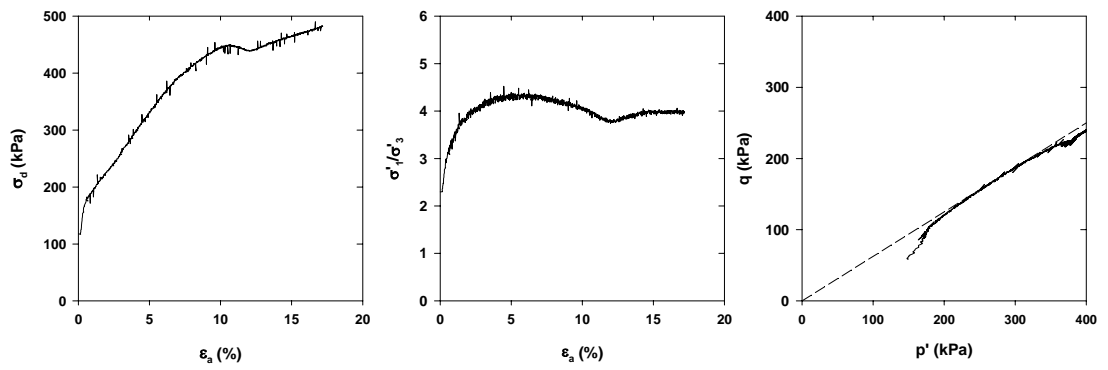
Figure B. 13. Presentation of STXT13
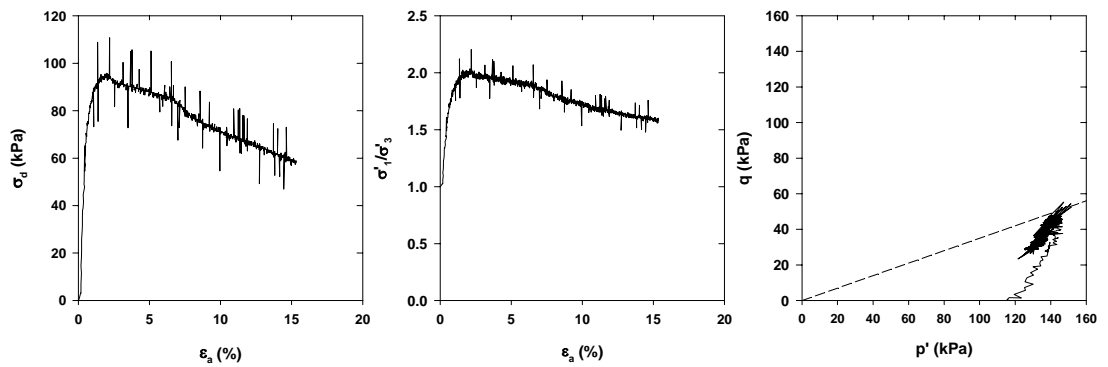
Figure B. 14. Presentation of STXT14

192
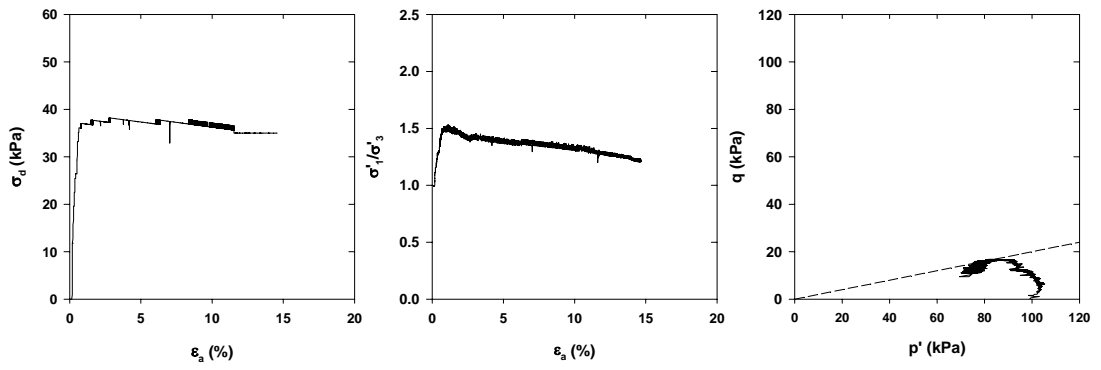
Figure B. 15. Presentation of STXT15
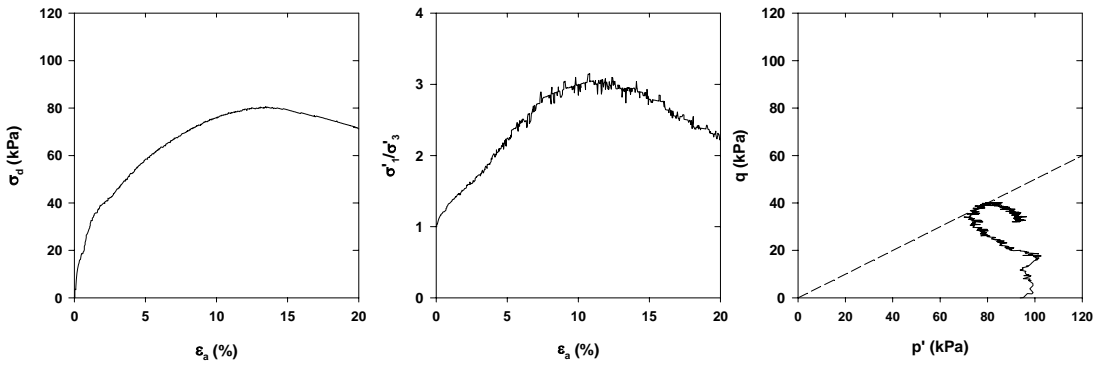
Figure B. 16. Presentation of STXT16
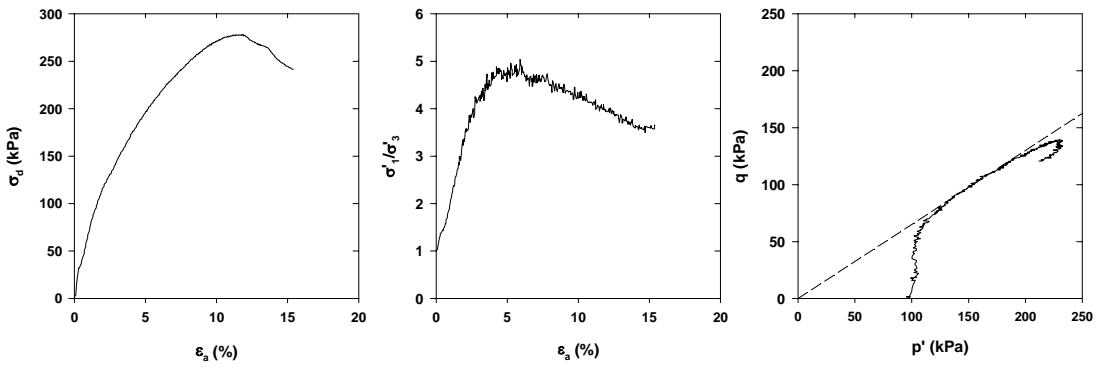

Figure B. 17. Presentation of STXT17

193
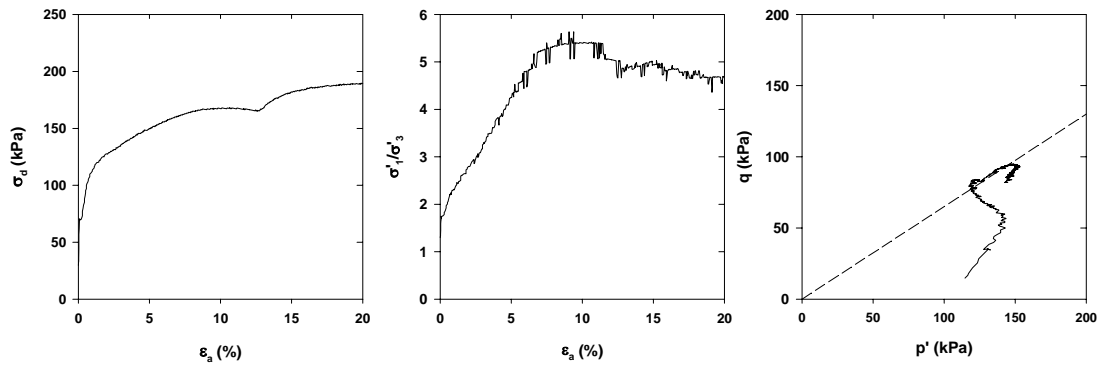
Figure B. 18. Presentation of STXT18
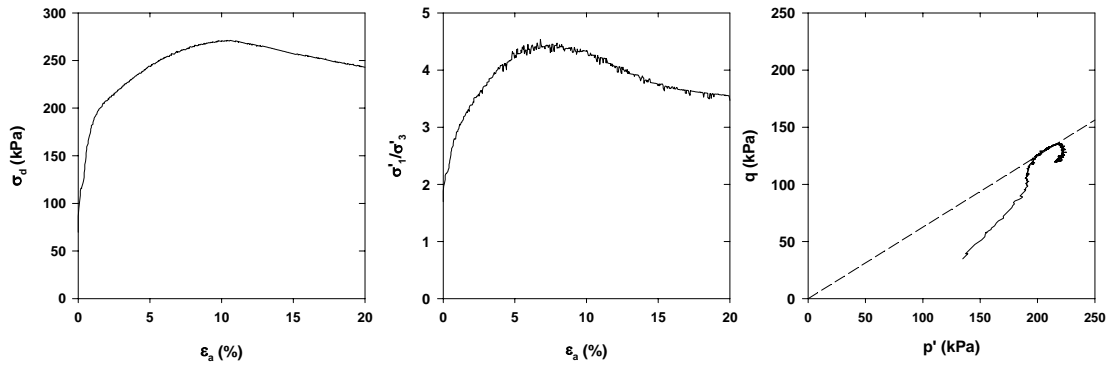
Figure B. 19. Presentation of STXT19
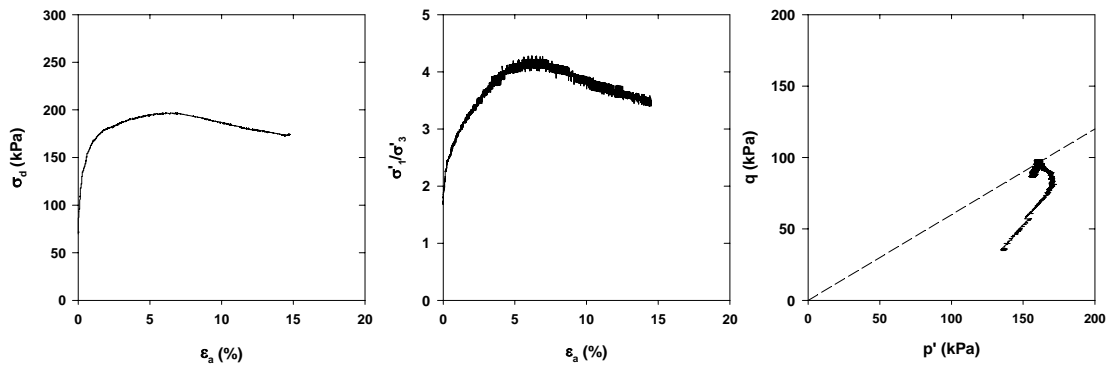
Figure B. 20. Presentation of STXT20
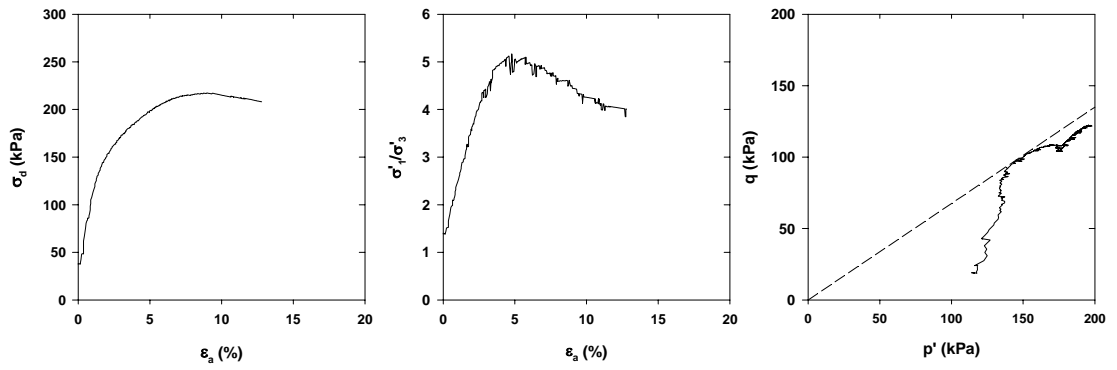
Figure B. 21. Presentation of STXT21
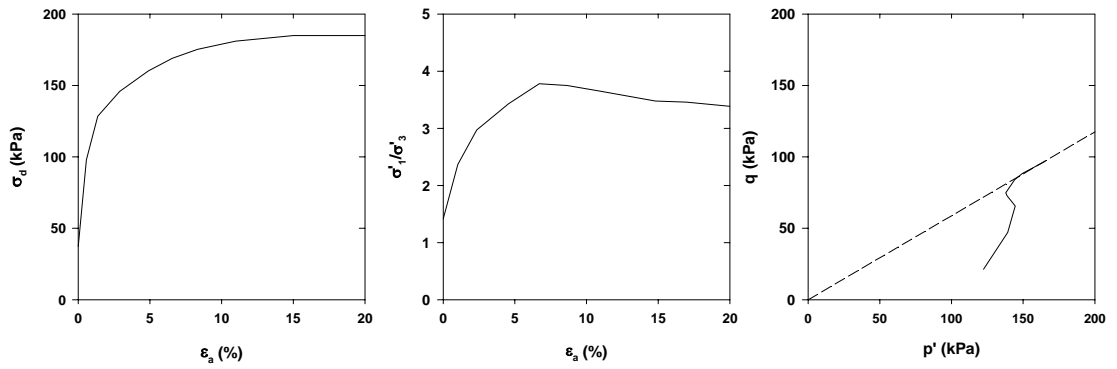
Figure B. 22. Presentation of STXT22
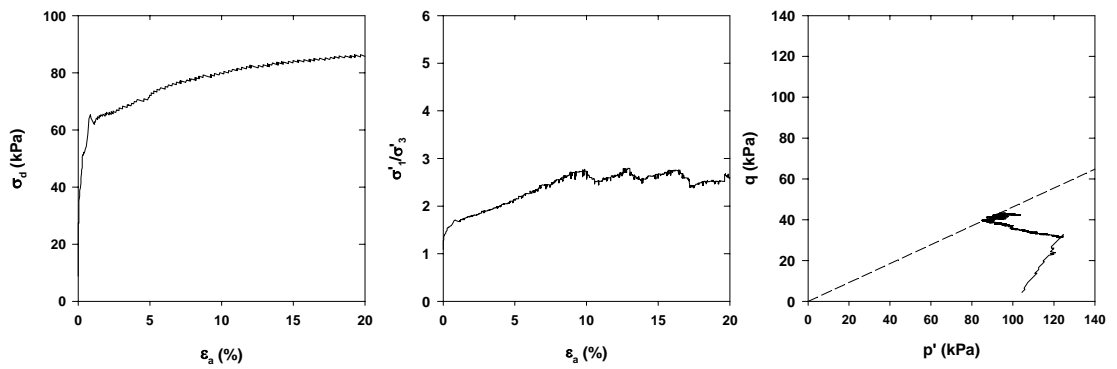
Figure B. 23. Presentation of STXT23
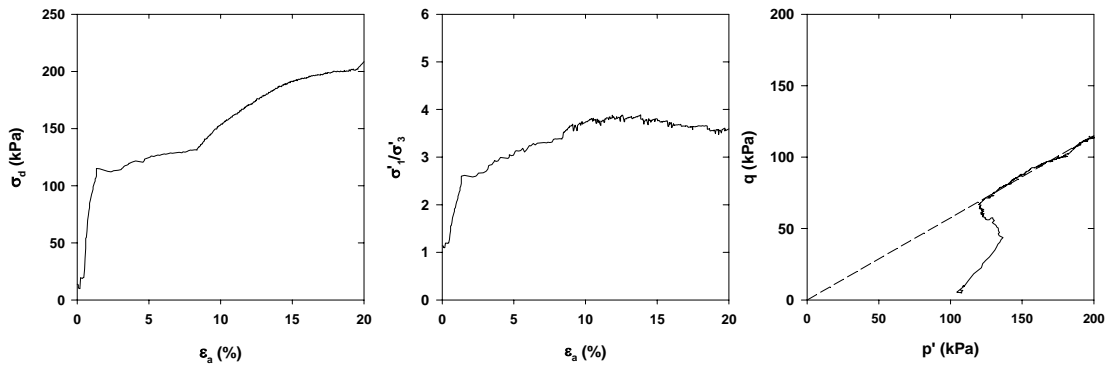
Figure B. 24. Presentation of STXT24
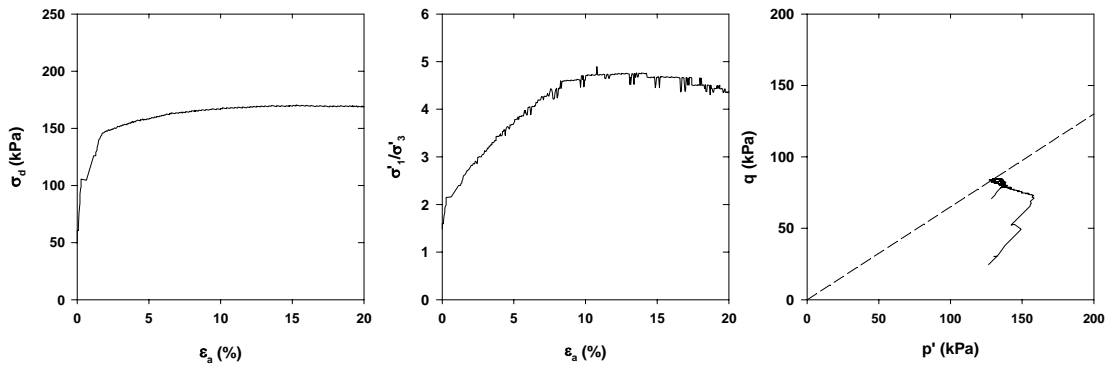
Figure B. 25. Presentation of STXT25
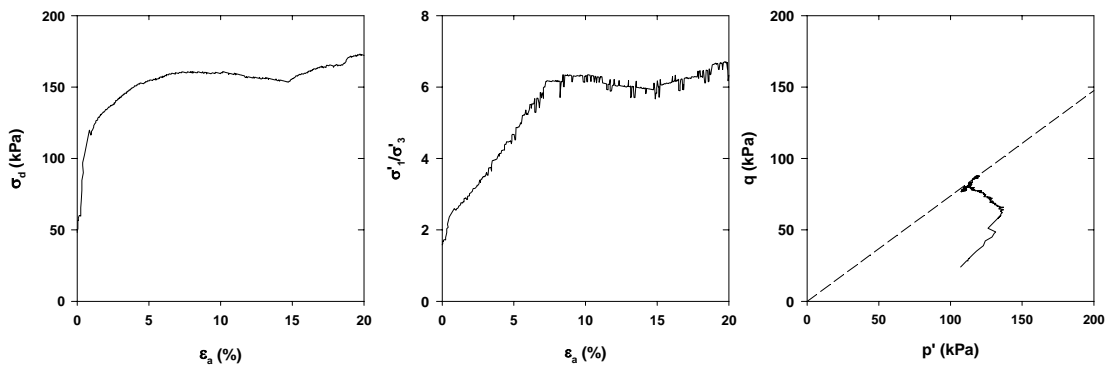
Figure B. 26. Presentation of STXT26
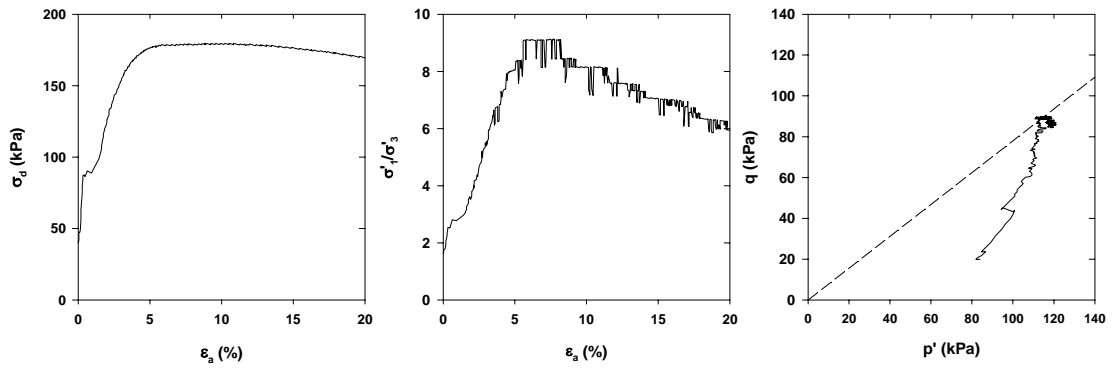
Figure B. 27. Presentation of STXT27
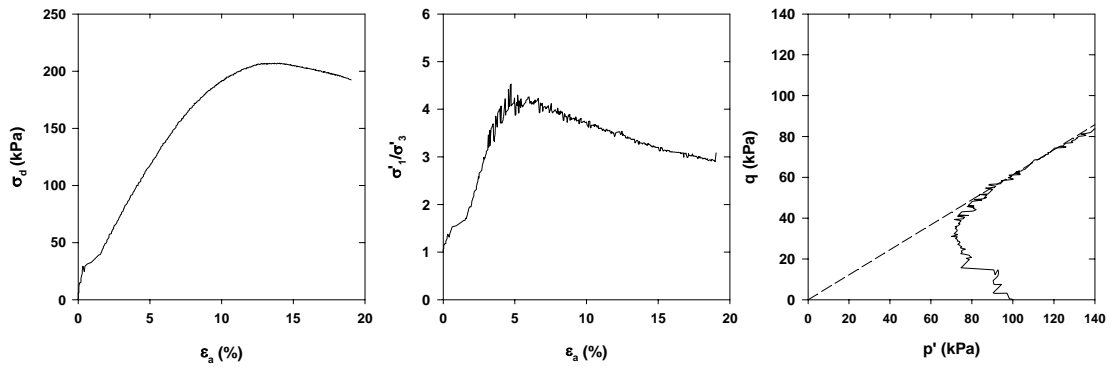
Figure B. 28. Presentation of STXT28
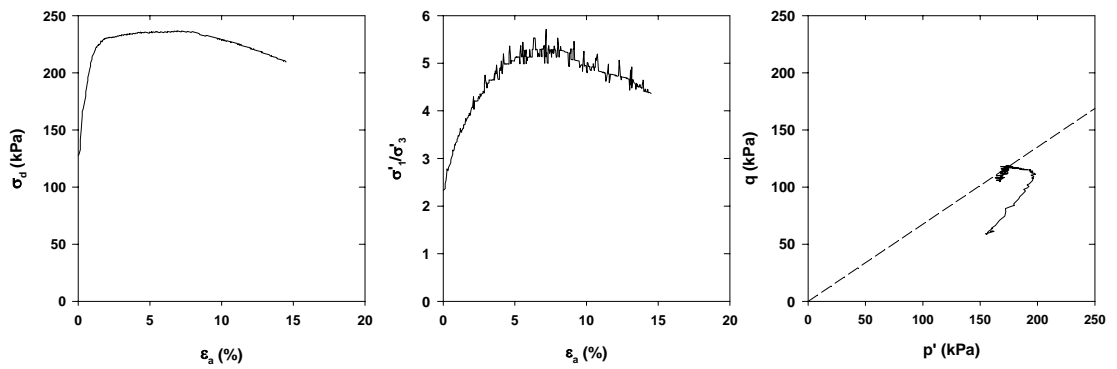
Figure B. 29. Presentation of STXT29
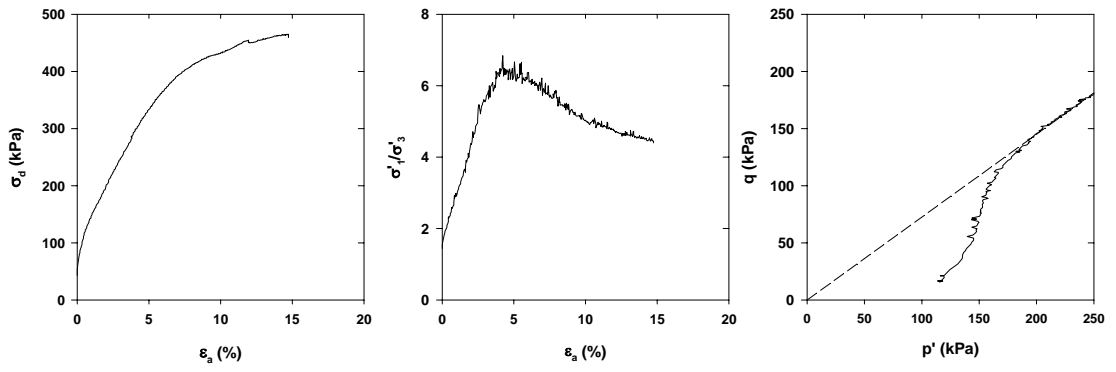
Figure B. 30. Presentation of STXT30
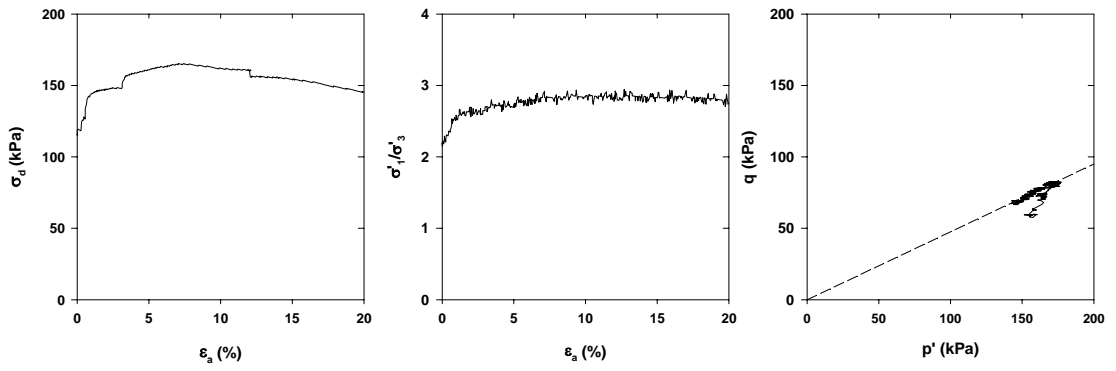
Figure B. 31. Presentation of STXT31
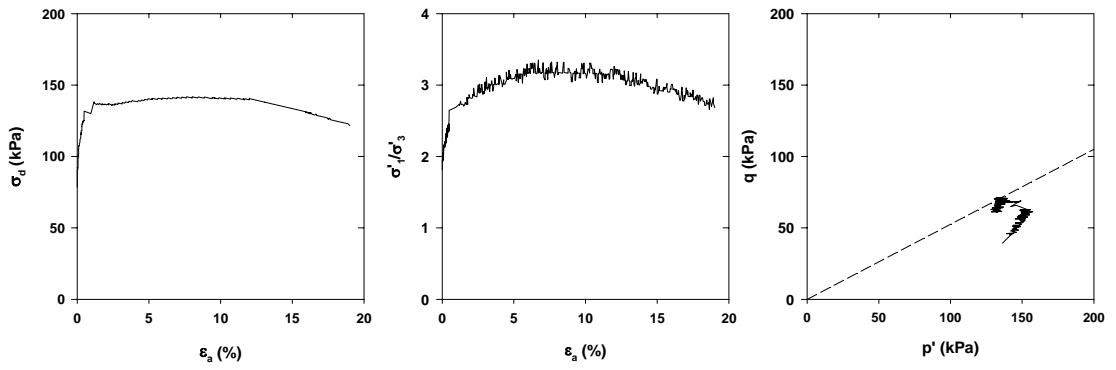
Figure B. 32. Presentation of STXT32

198
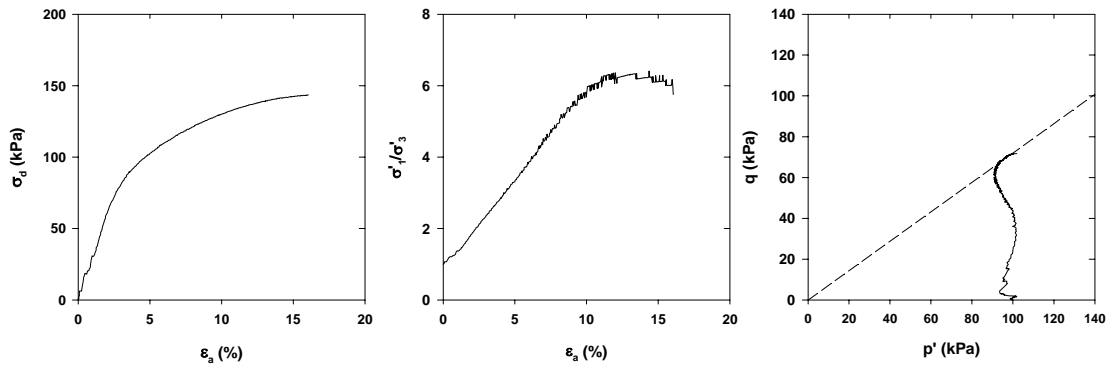
**Figure B. 33. Presentation of STXT33**
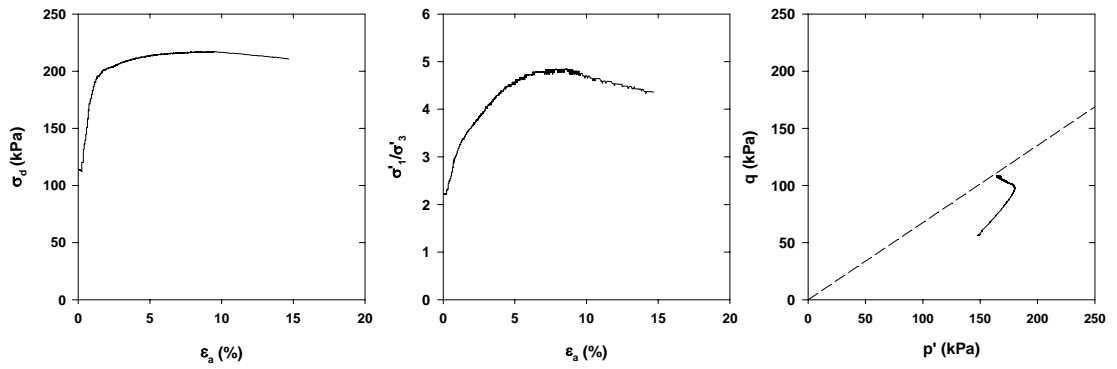
Figure B. 34. Presentation of STXT34
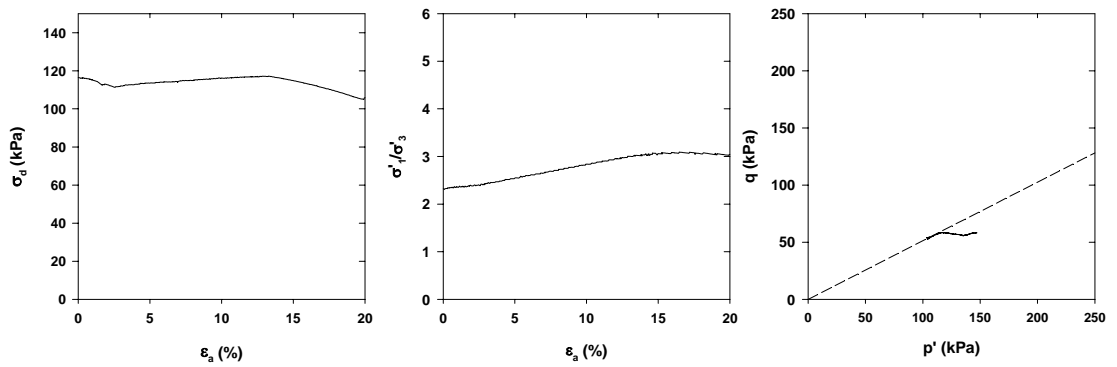
Figure B. 35. Presentation of STXT35

199
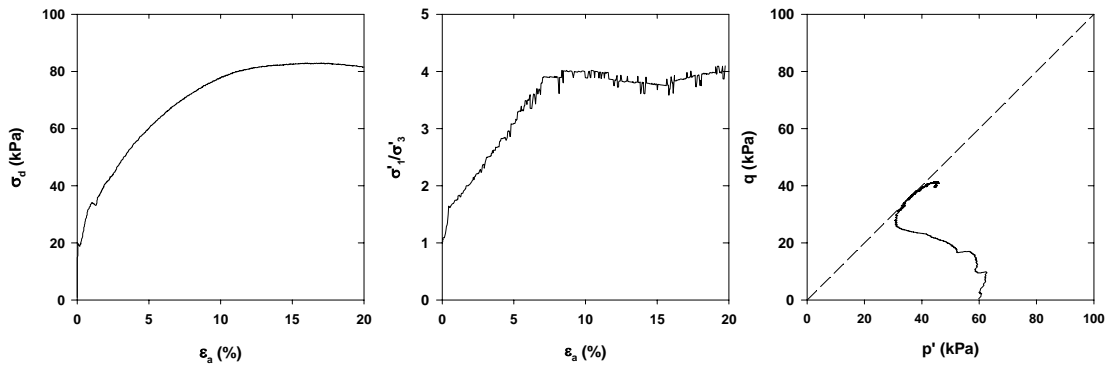
Figure B. 36. Presentation of STXT36
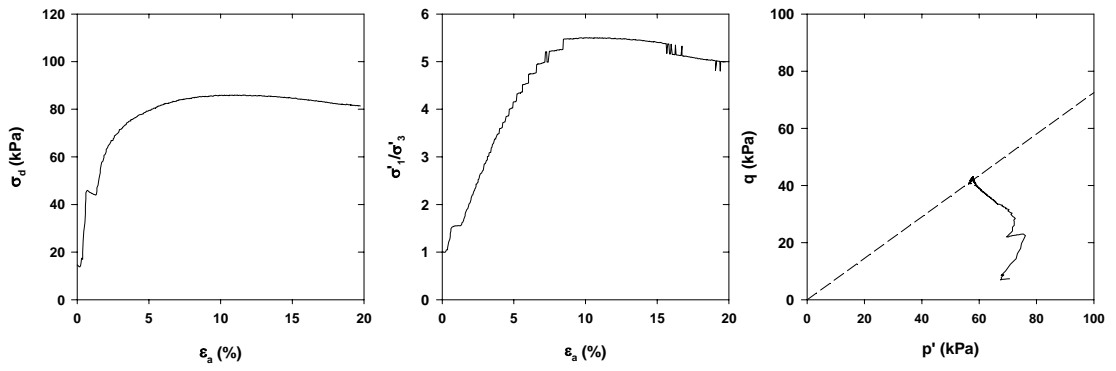
Figure B. 37. Presentation of STXT37
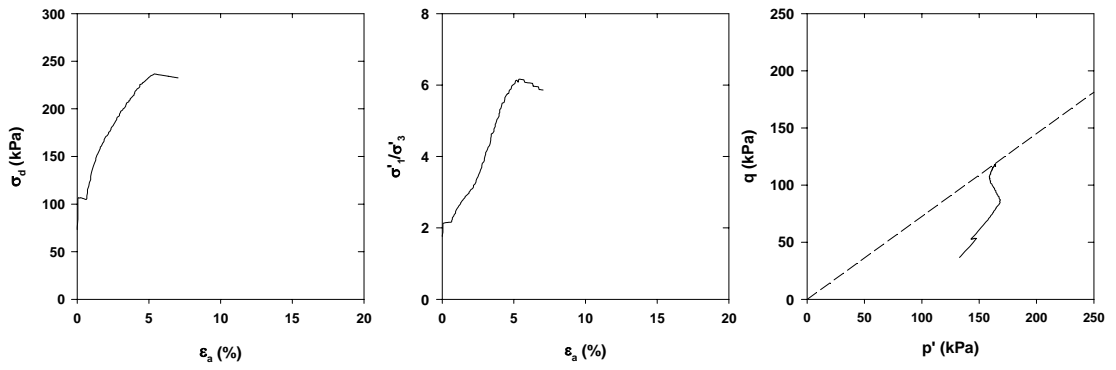

Figure B. 38. Presentation of STXT38
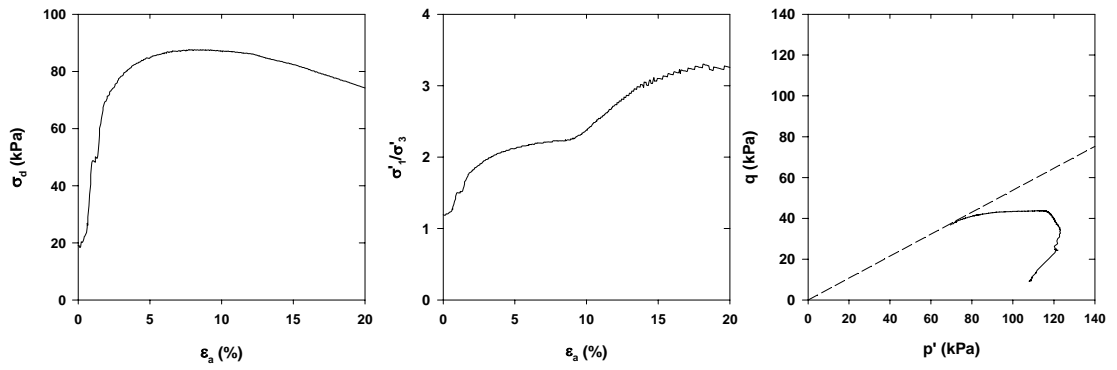
Figure B. 39. Presentation of STXT39
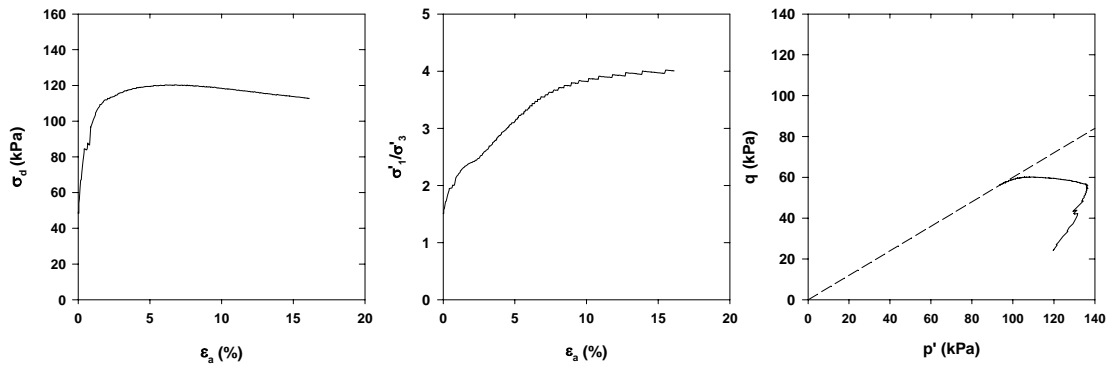
Figure B. 40. Presentation of STXT40
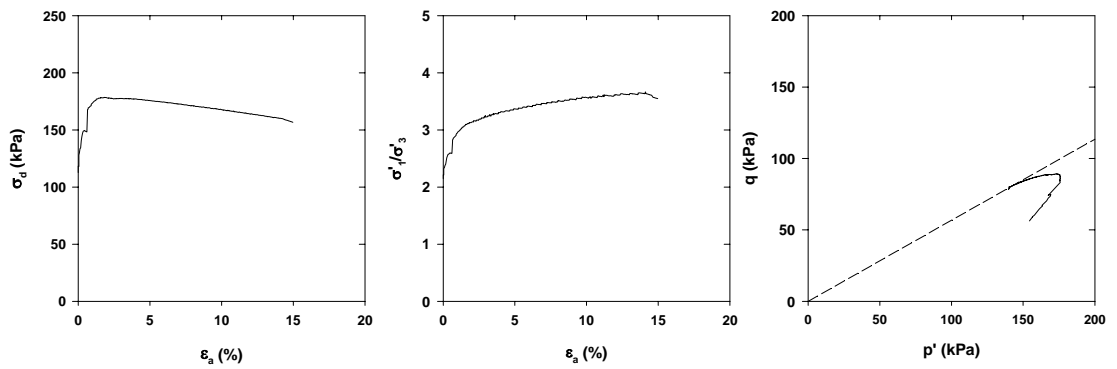
Figure B. 41. Presentation of STXT41

201
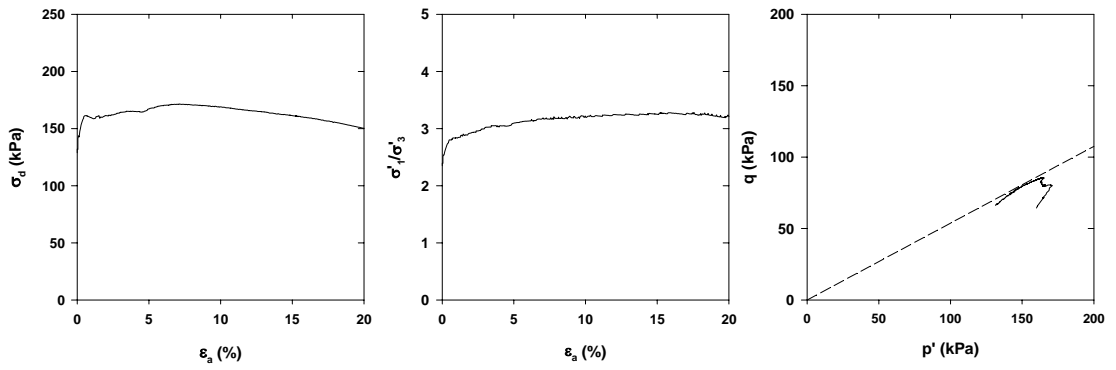
Figure B. 42. Presentation of STXT42
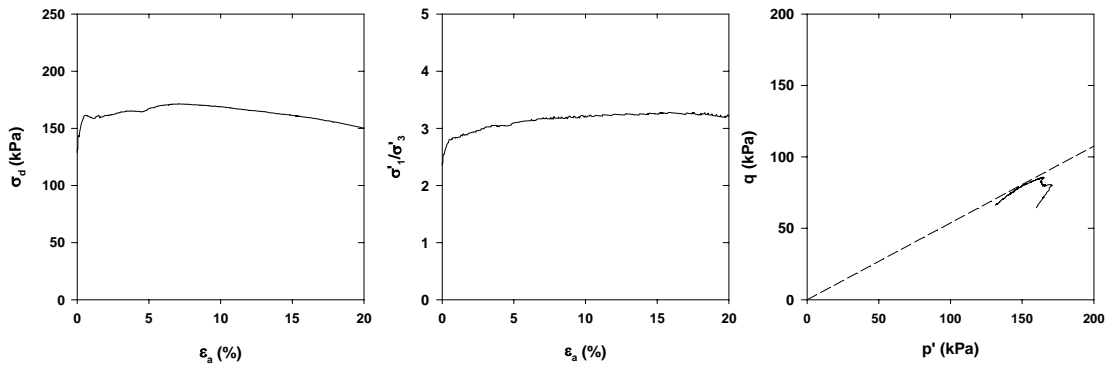

Figure B. 43. Presentation of STXT43
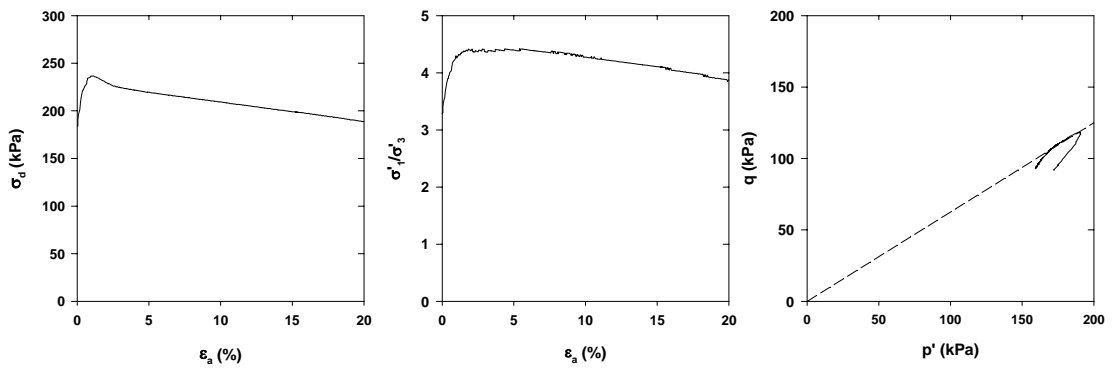
Figure B. 44. Presentation of STXT44
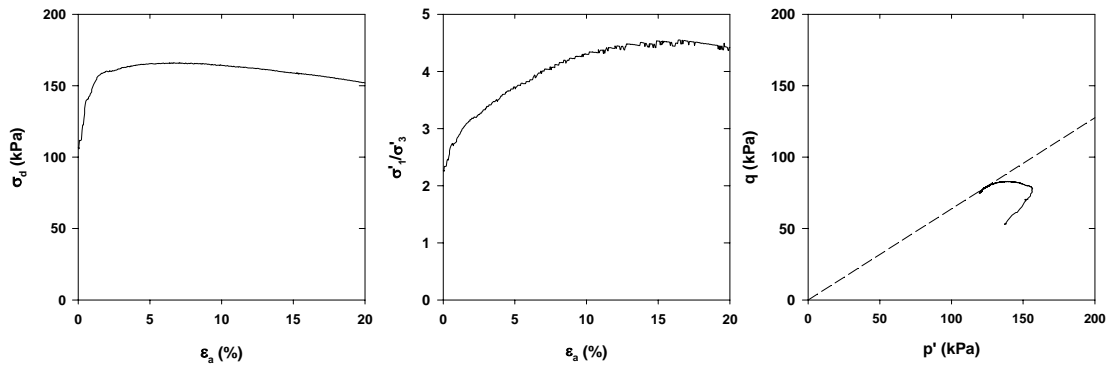
Figure B. 45. Presentation of STXT45
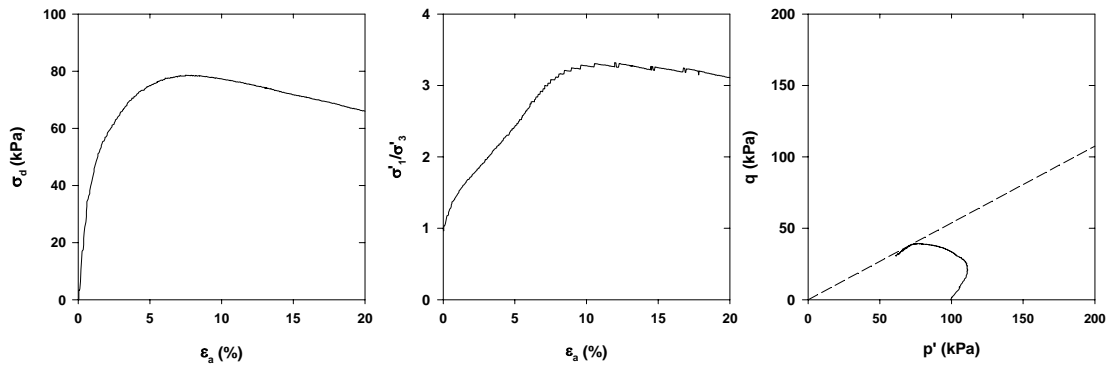
Figure B. 46. Presentation of STXT46
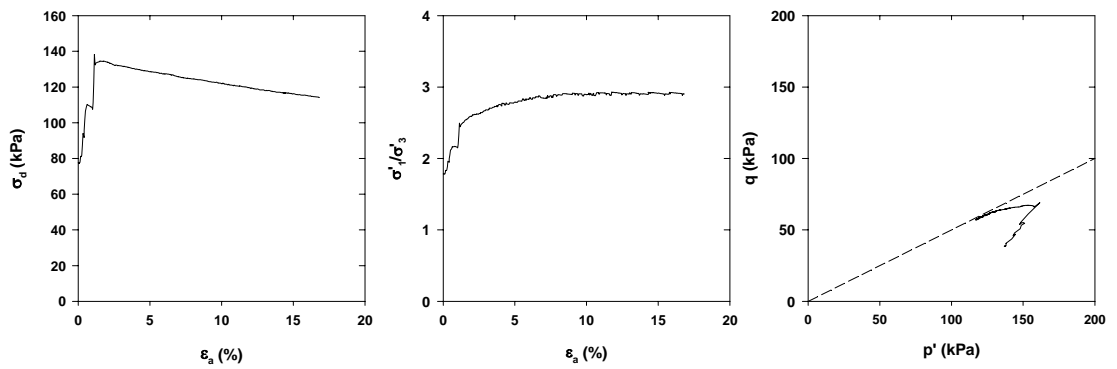
Figure B. 47. Presentation of STXT47
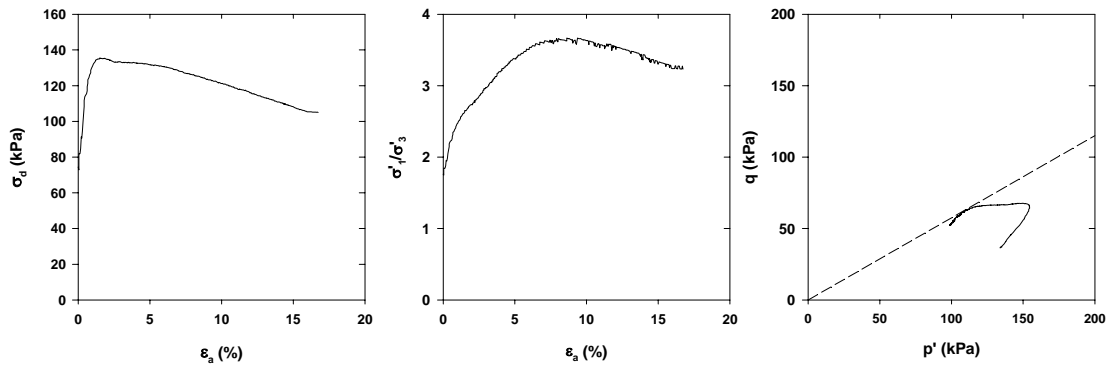
Figure B. 48. Presentation of STXT48
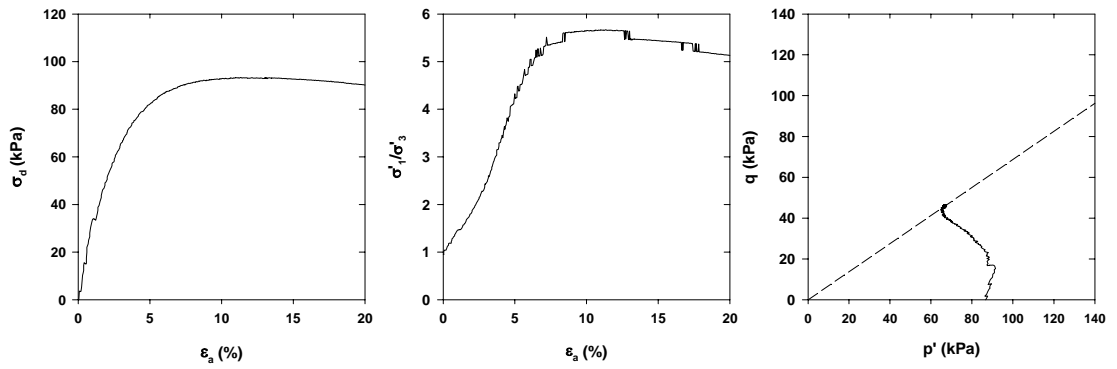
Figure B. 49. Presentation of STXT49
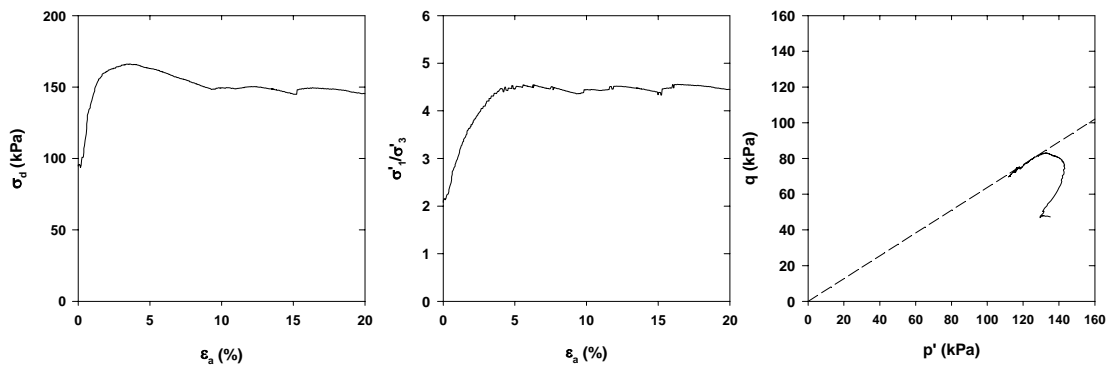
Figure B. 50. Presentation of STXT50
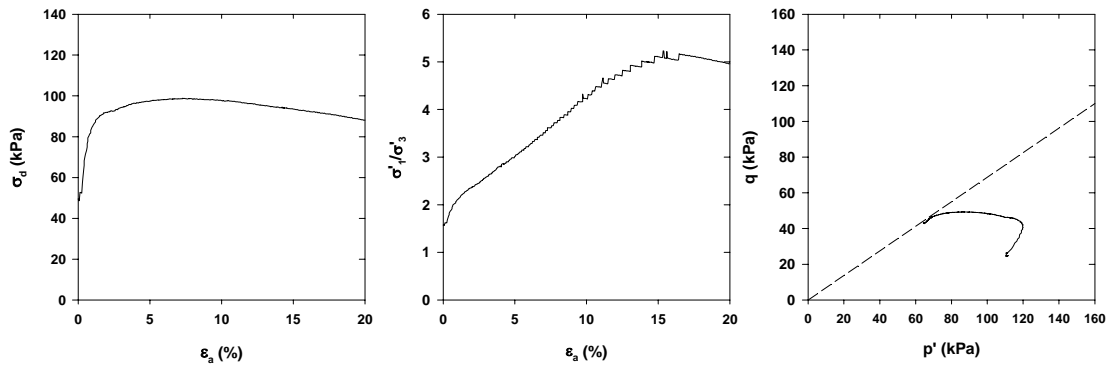
Figure B. 51. Presentation of STXT51
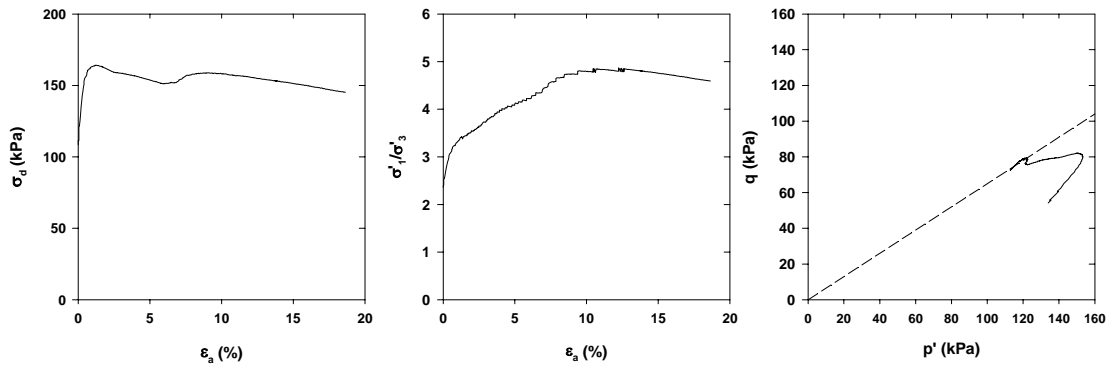

**Figure B. 52. Presentation of STXT52**
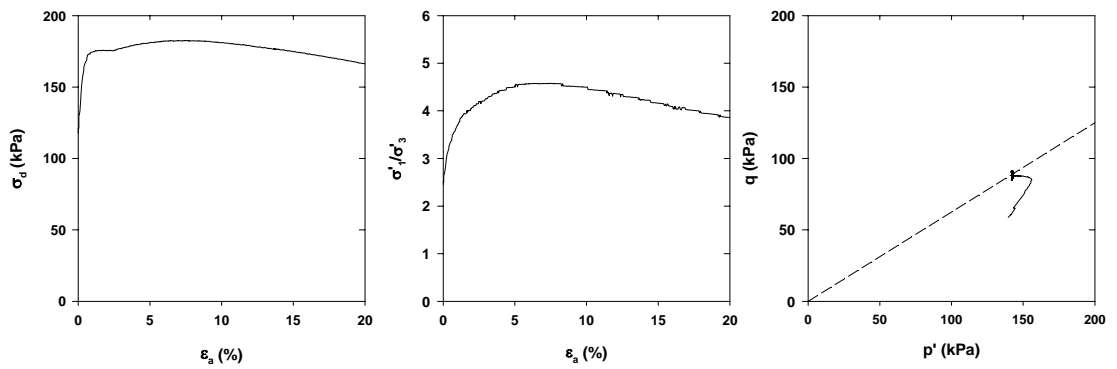
Figure B. 53. Presentation of STXT53
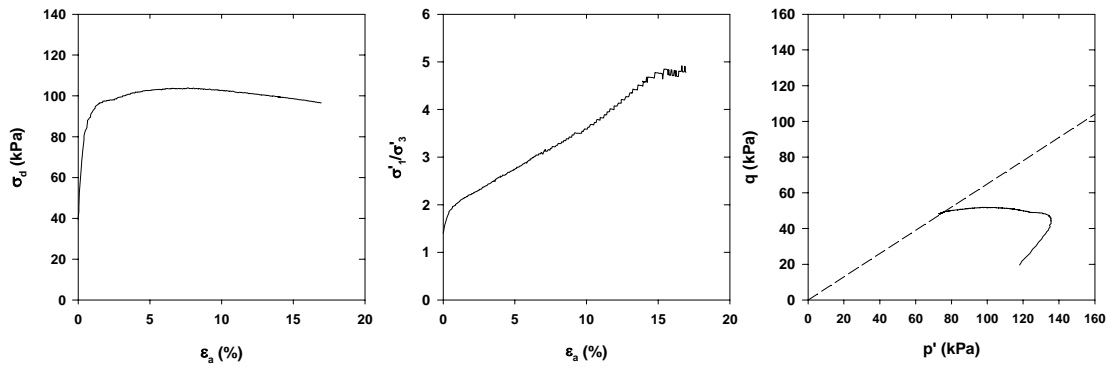
Figure B. 54. Presentation of STXT54
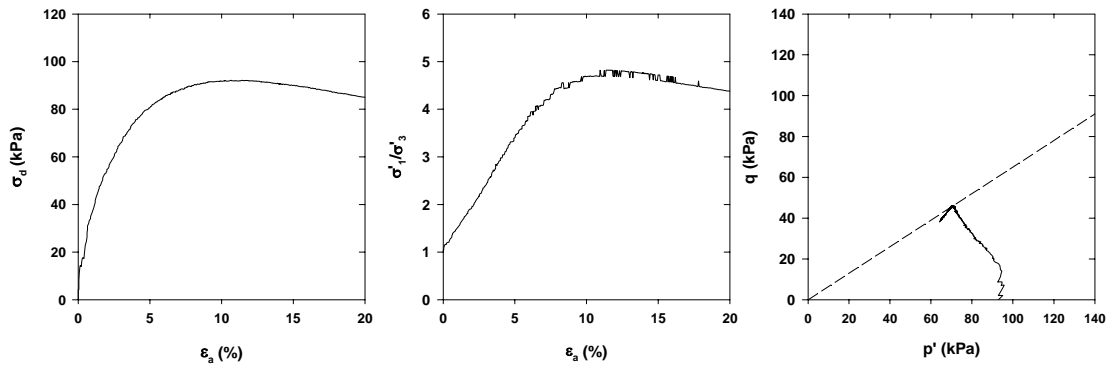
Figure B. 55. Presentation of STXT55
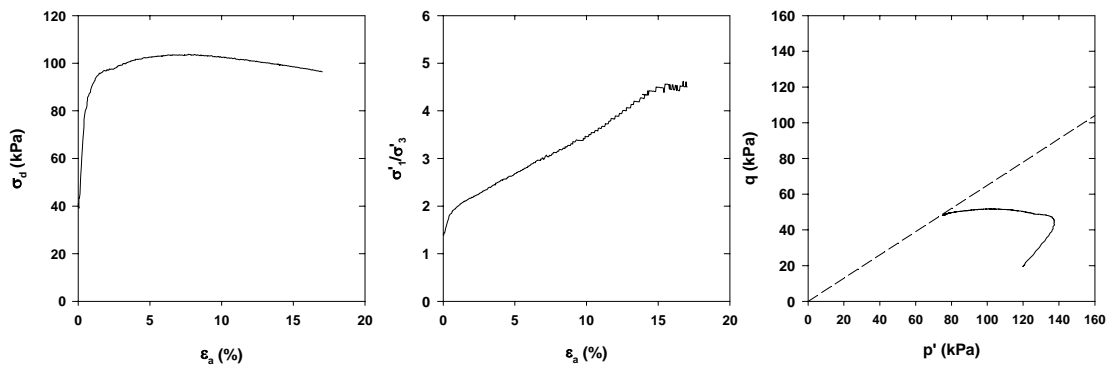
Figure B. 56. Presentation of STXT56
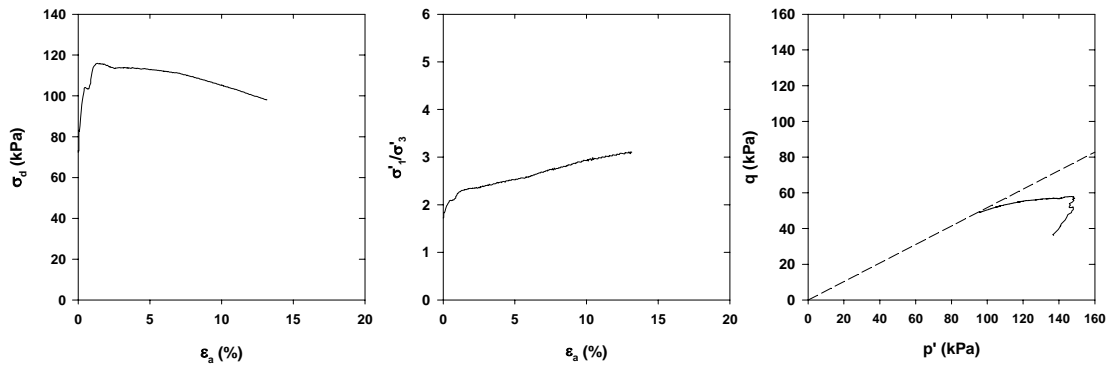
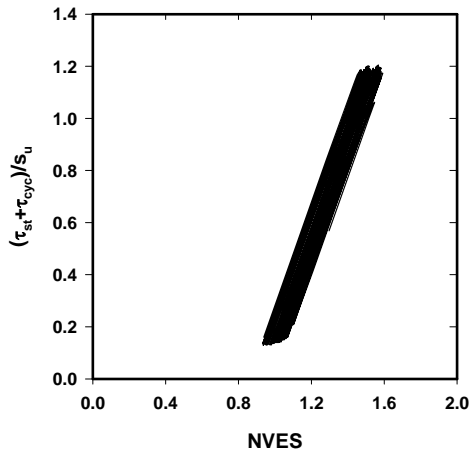**Figure B. 57. Presentation of STXT57**
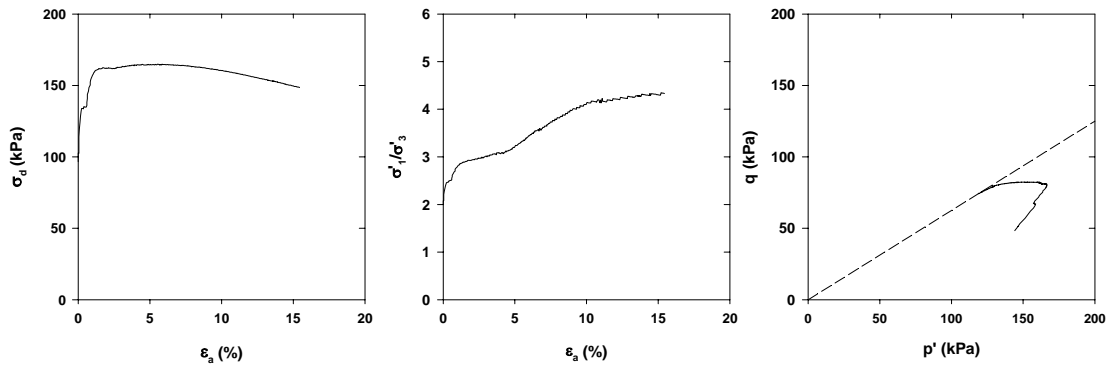
Figure B. 58. Presentation of STXT58
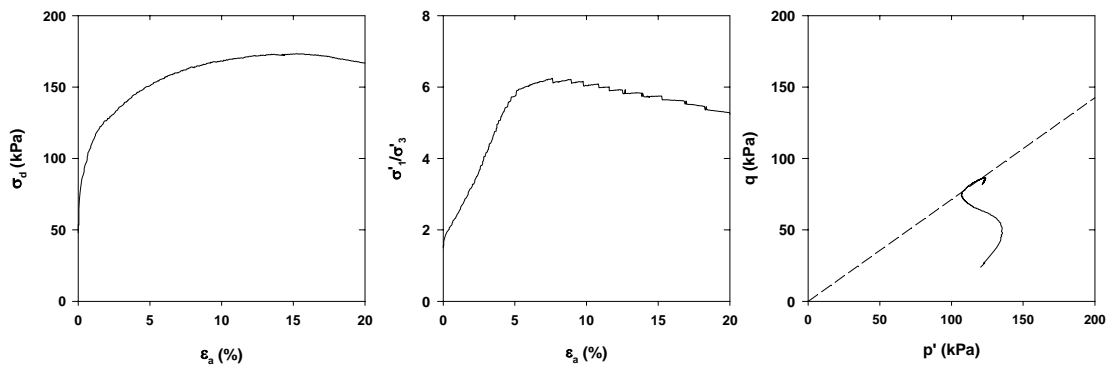
Figure B. 59. Presentation of STXT59

APPENDIX C

RESULTS OF CYCLIC TRIAXIAL TESTS
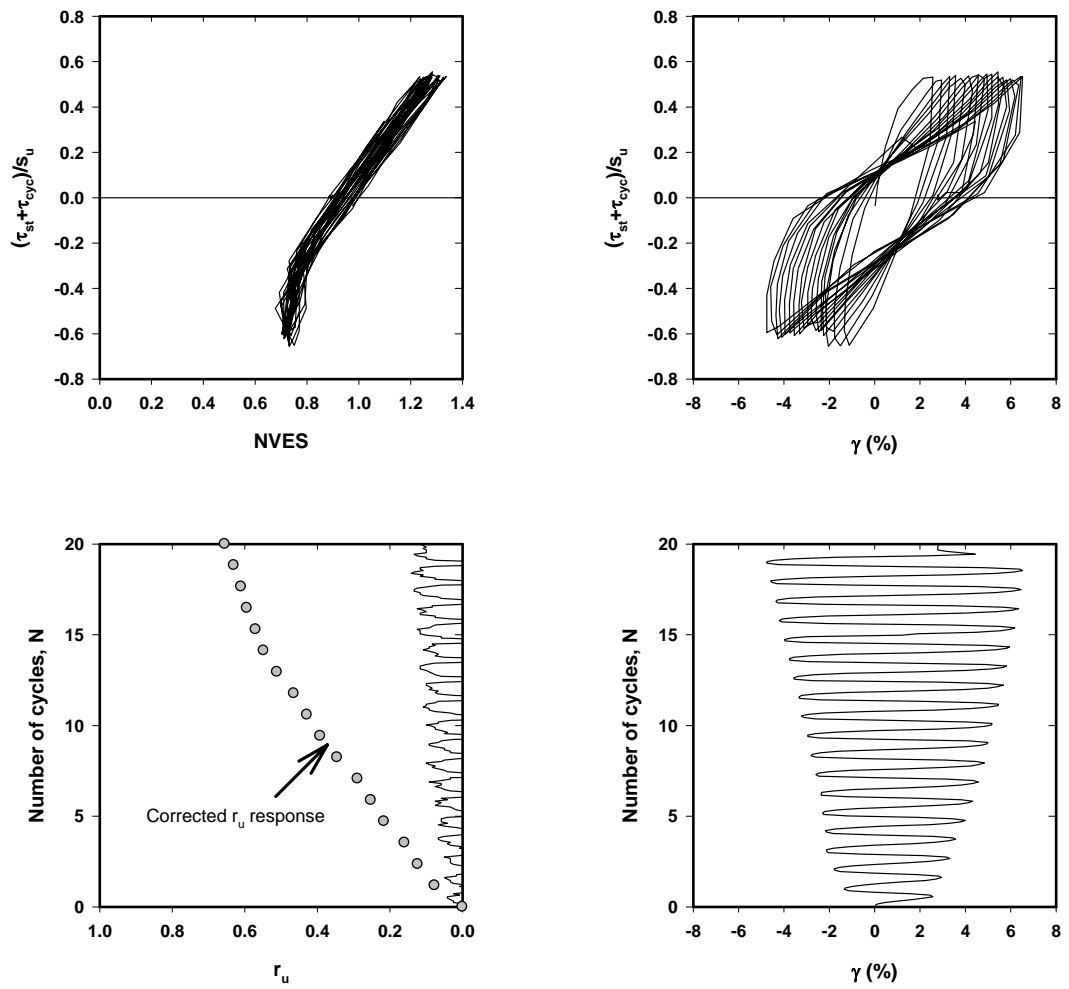
Figure C. 1. Presentation of CTXT1
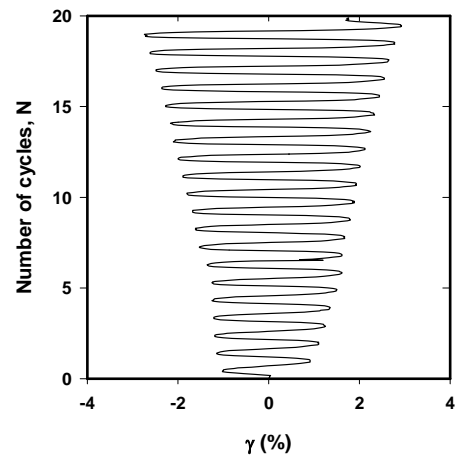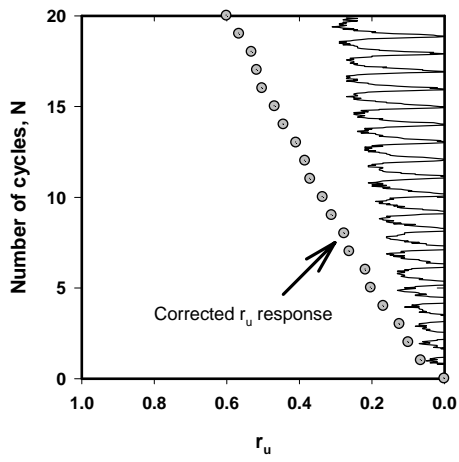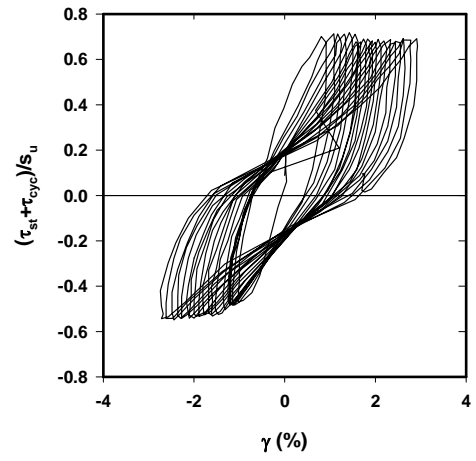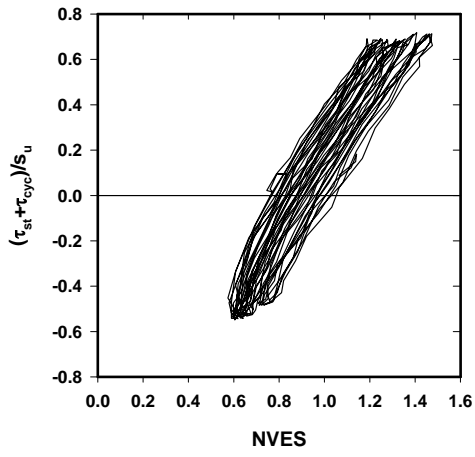
Figure C. 2. Presentation of CTXT2
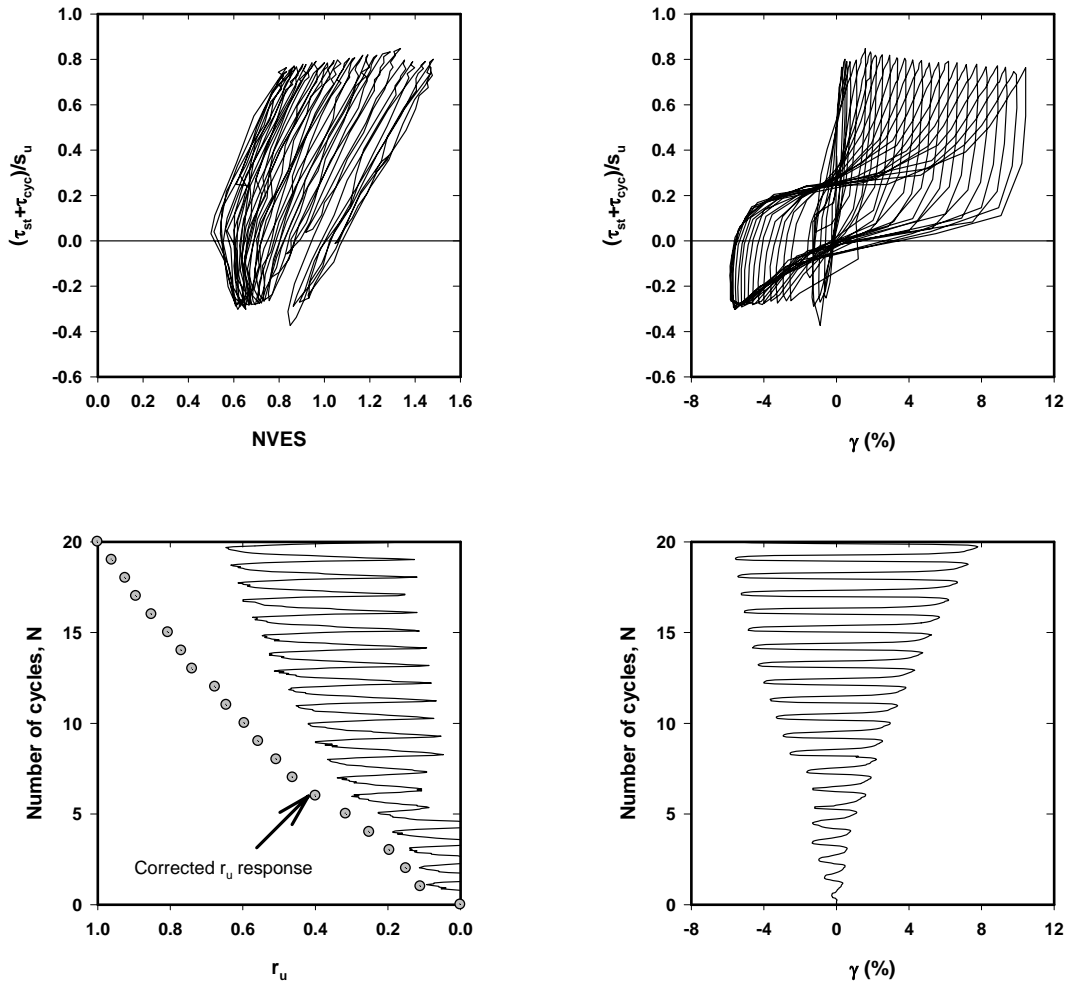
Figure C. 3. Presentation of CTXT3
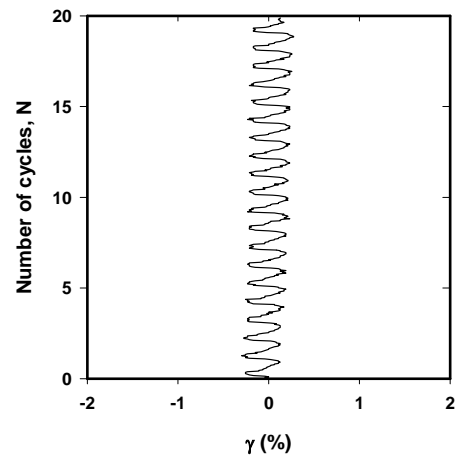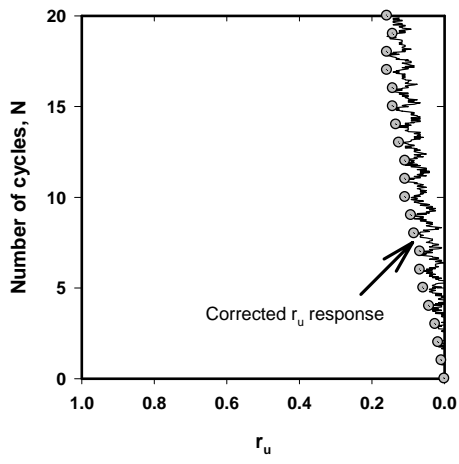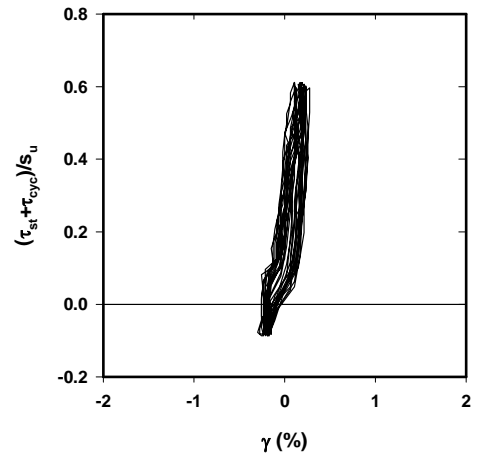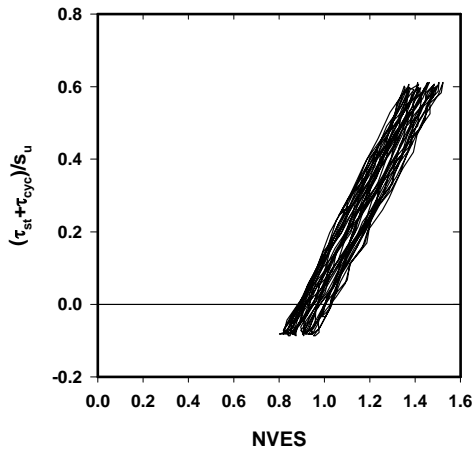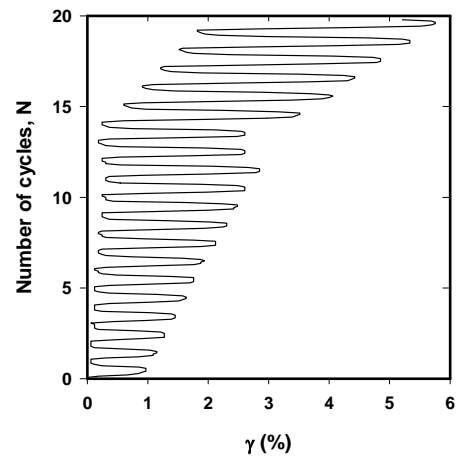
Figure C. 4. Presentation of CTXT4

211
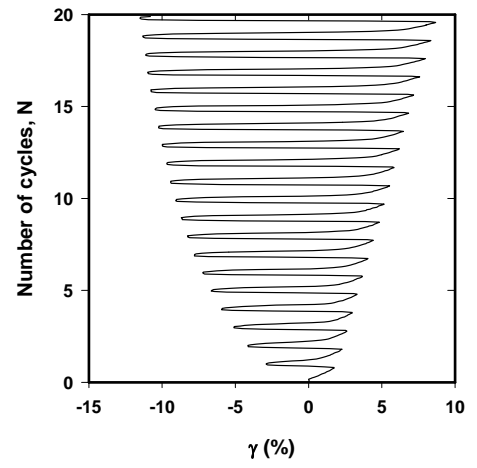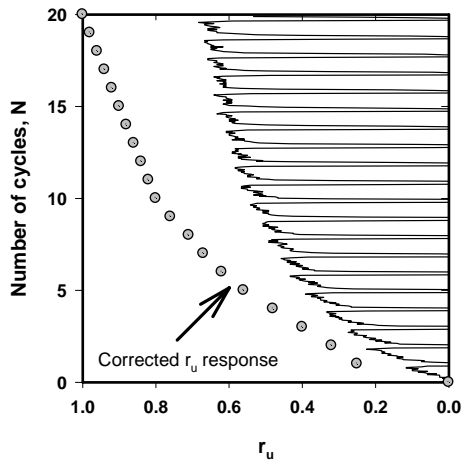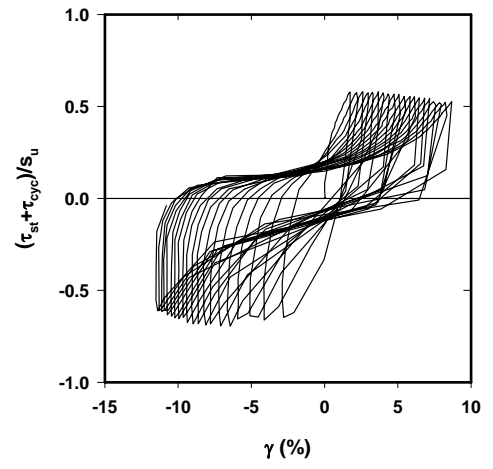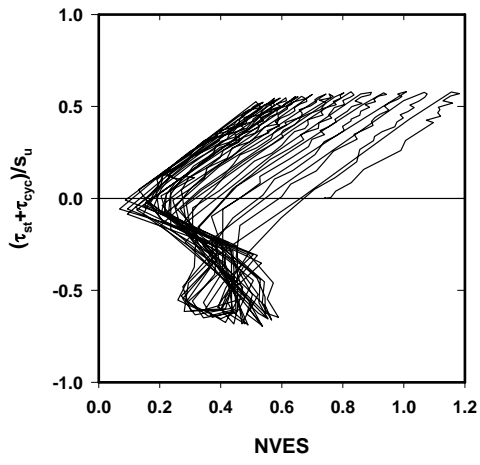
Figure C. 5. Presentation of CTXT5

212
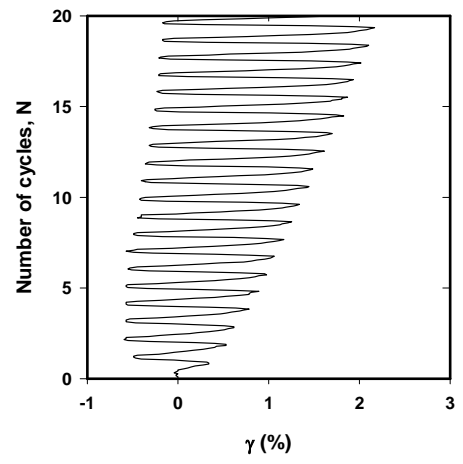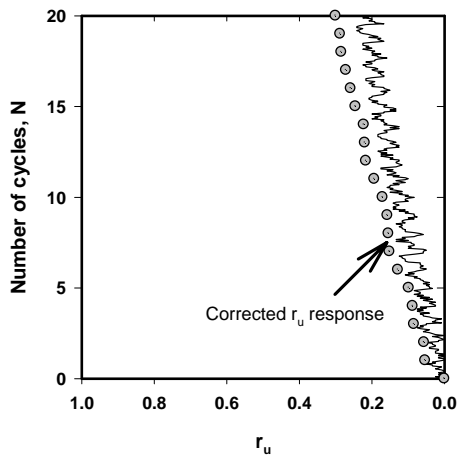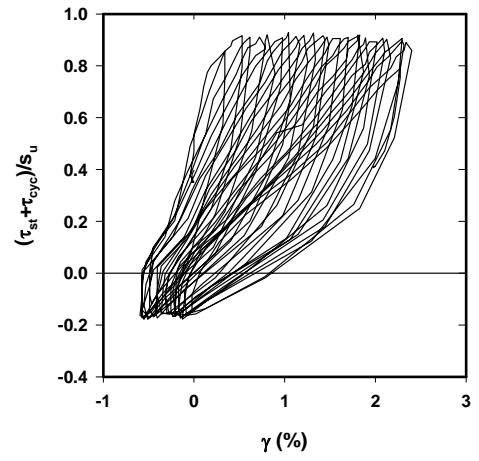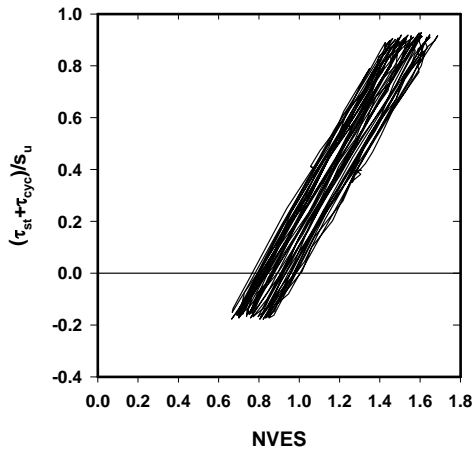
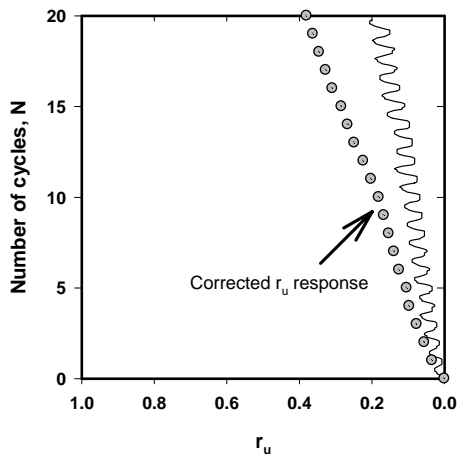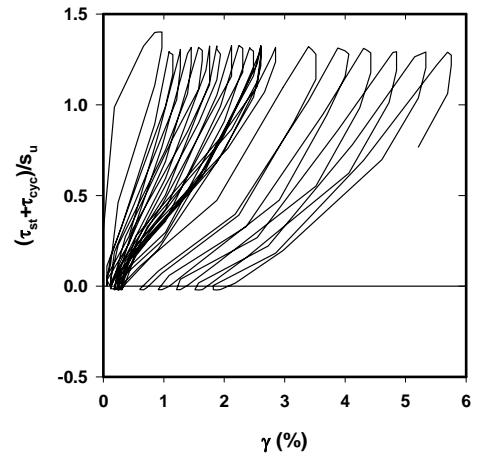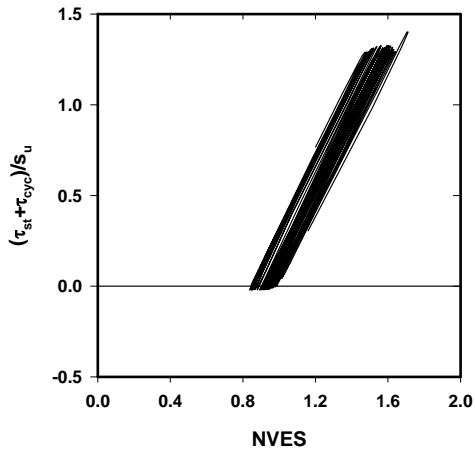**Figure C. 6. Presentation of CTXT6**
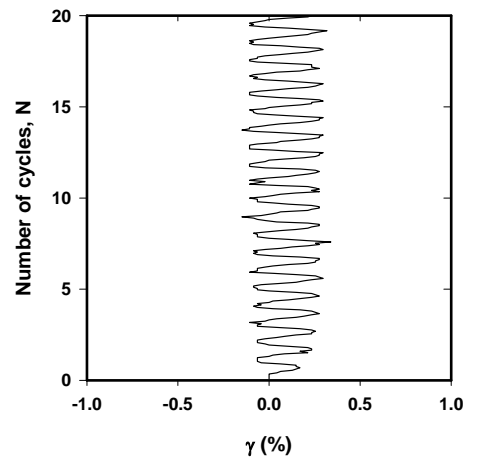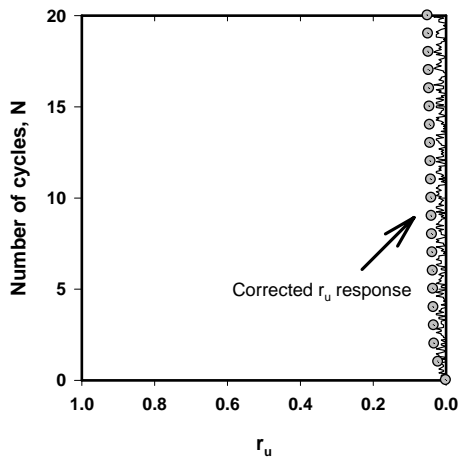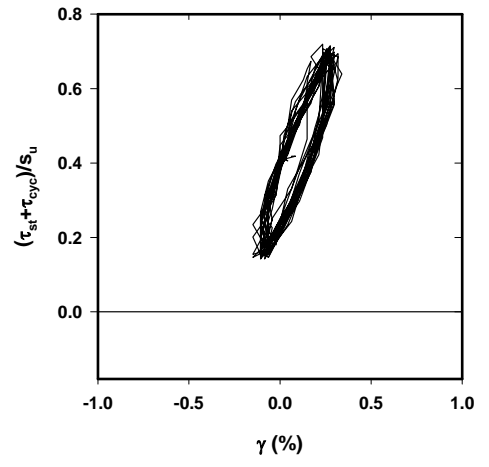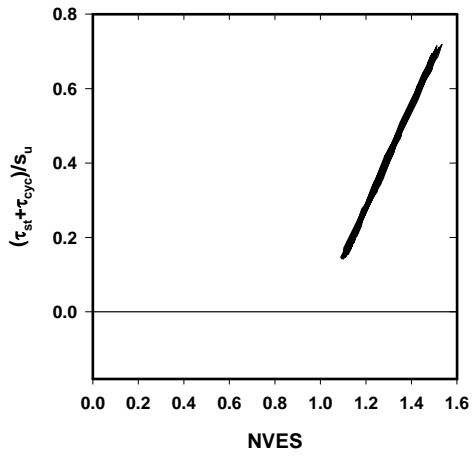
Figure C. 7. Presentation of CTXT7
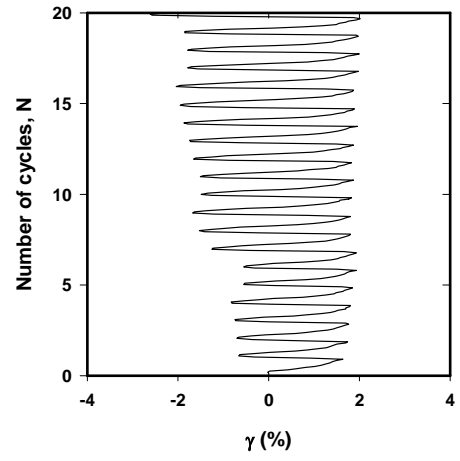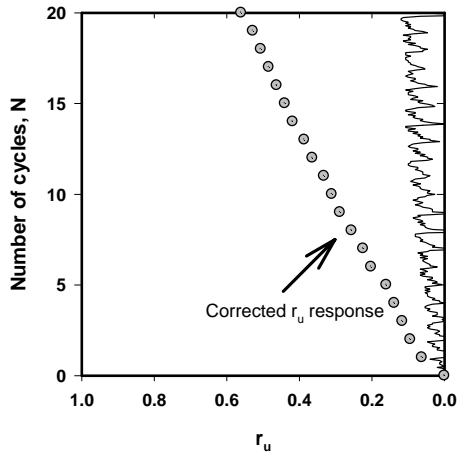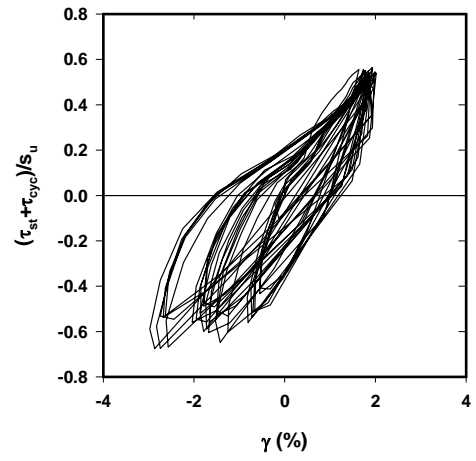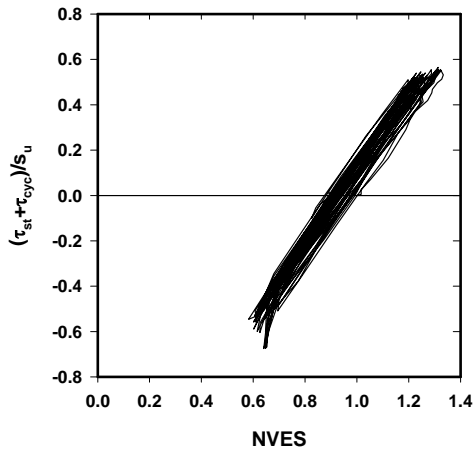
Figure C. 8. Presentation of CTXT9

215
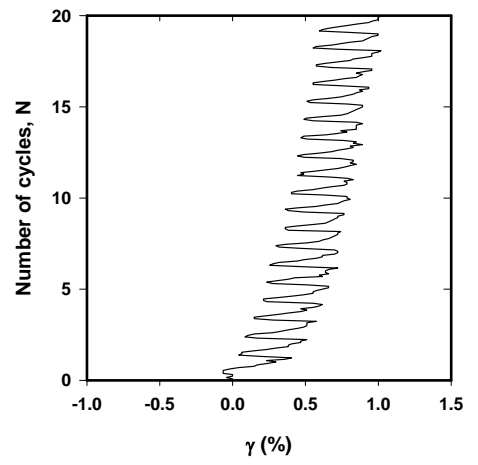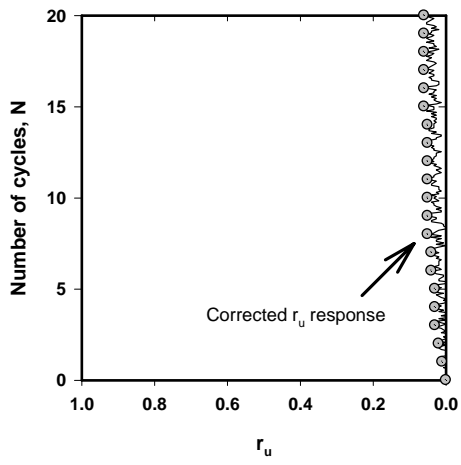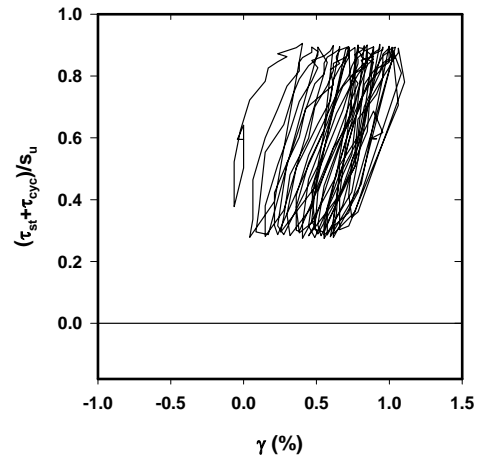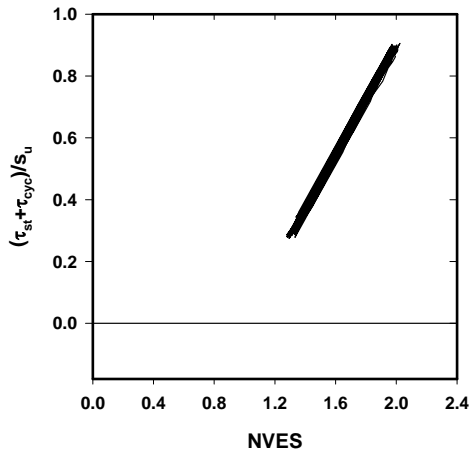
Figure C. 9. Presentation of CTXT10

216
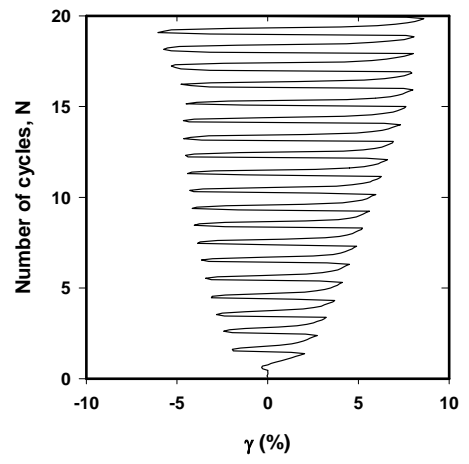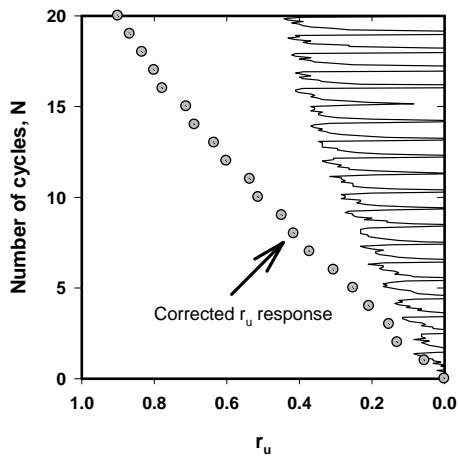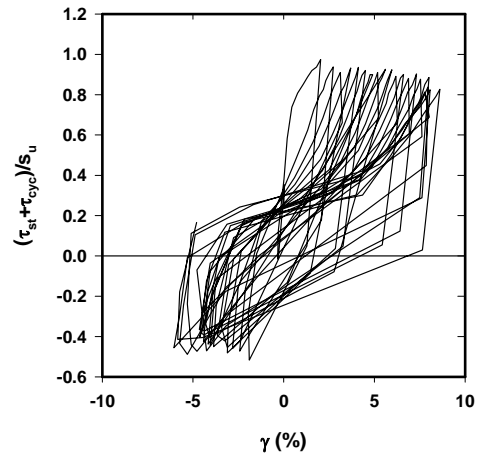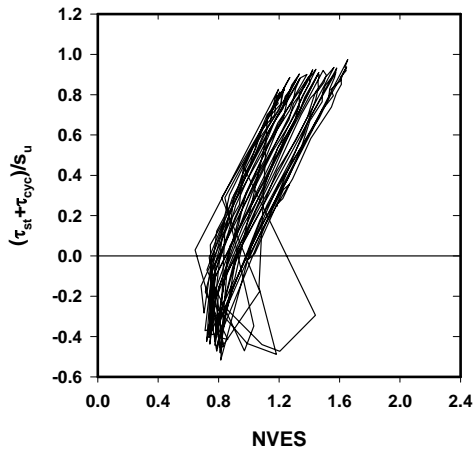
Figure C. 10. Presentation of CTXT11
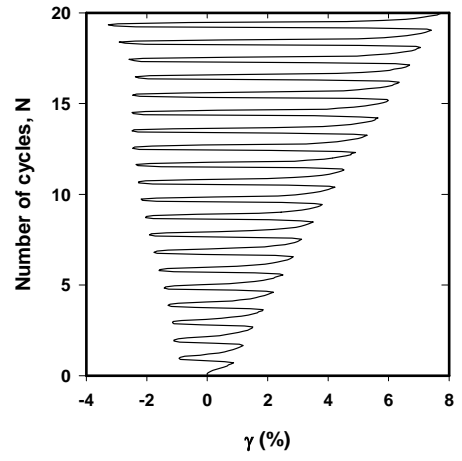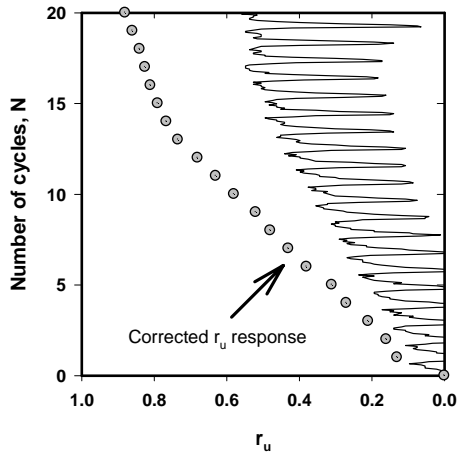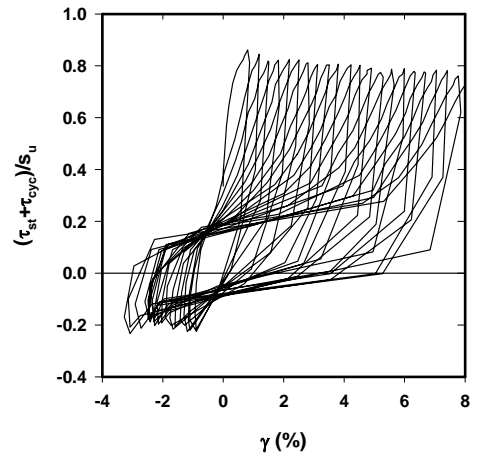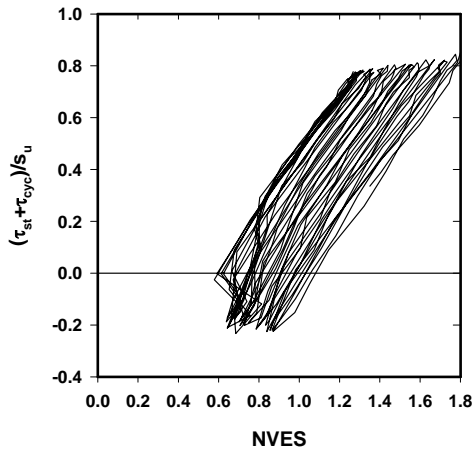
Figure C. 11. Presentation of CTXT12

218
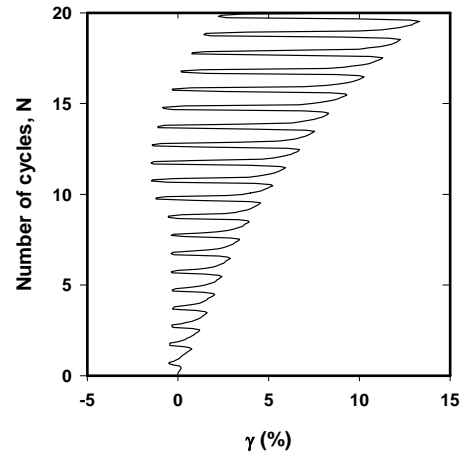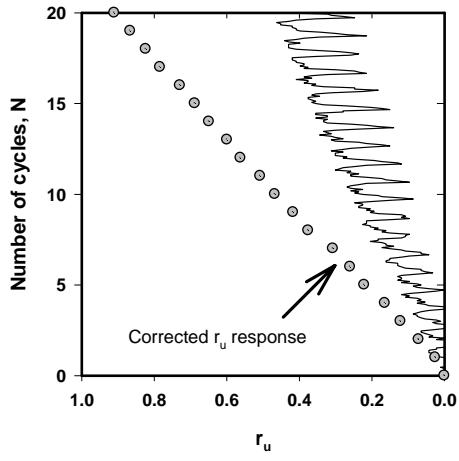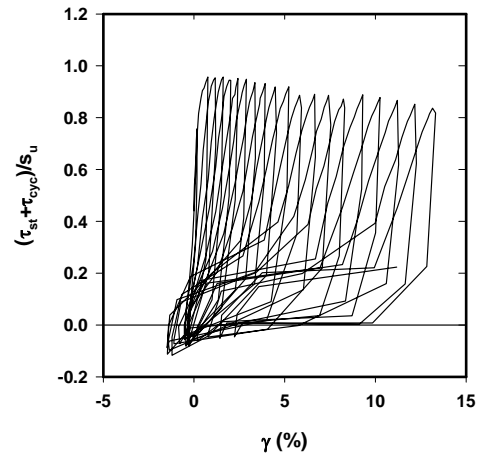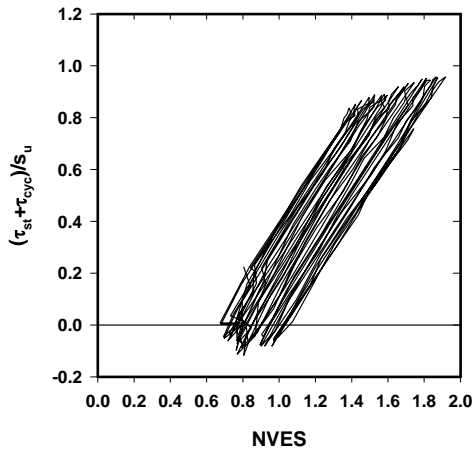
Figure C. 12. Presentation of CTXT13

219
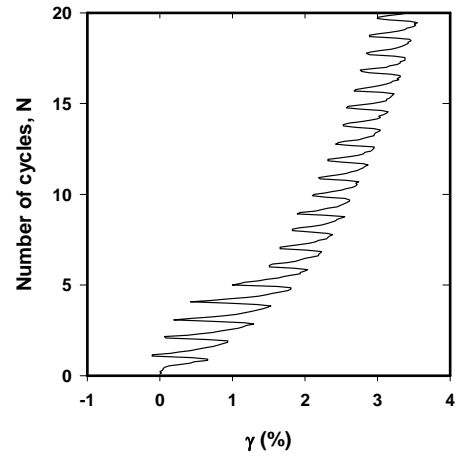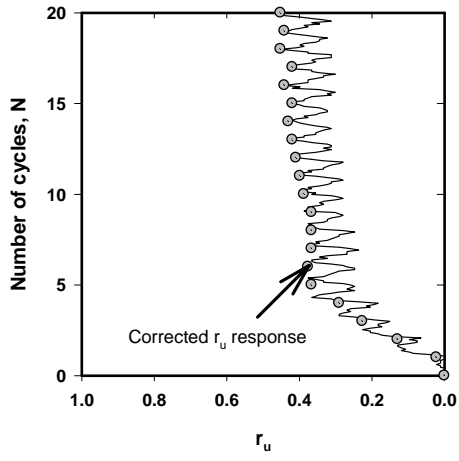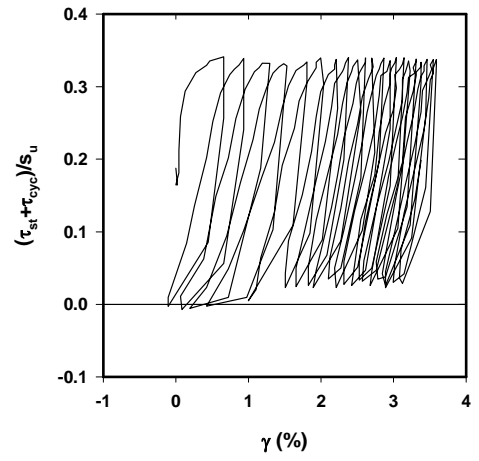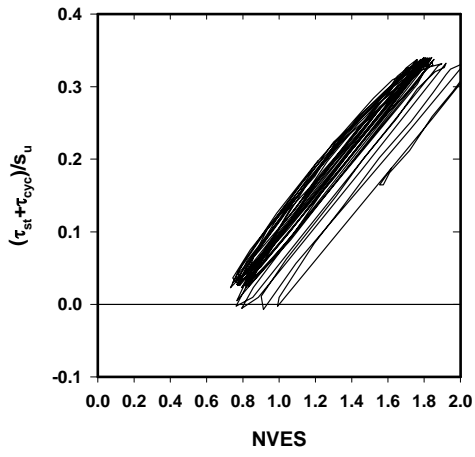
Figure C. 13. Presentation of CTXT14

220
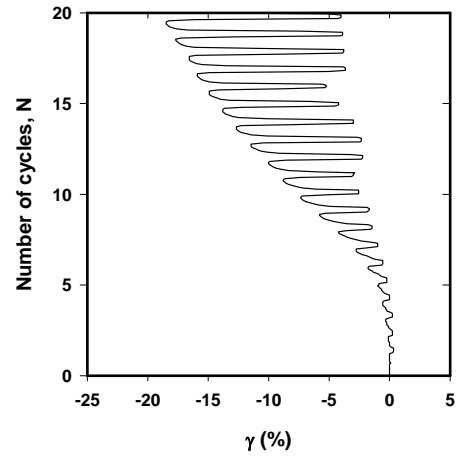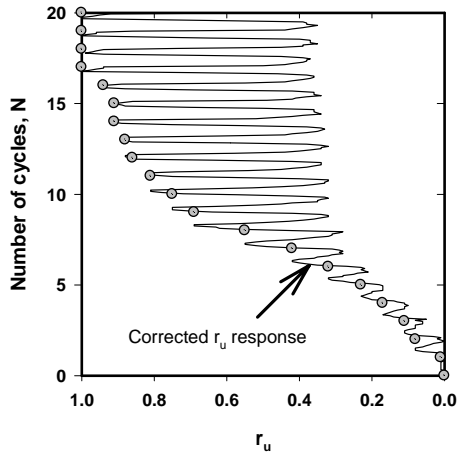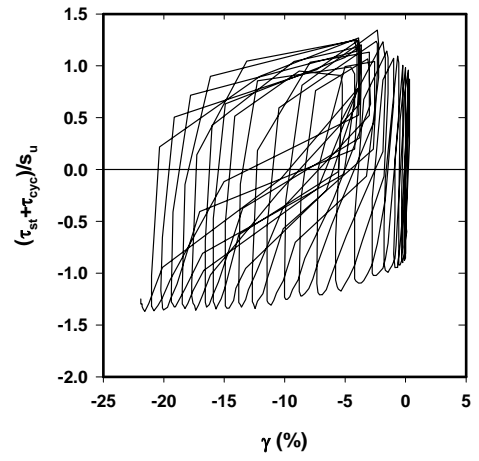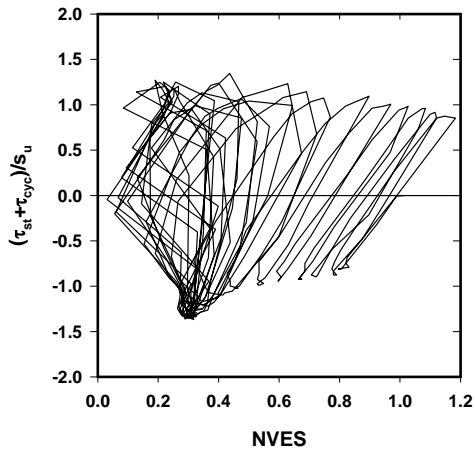
Figure C. 14. Presentation of CTXT15

221
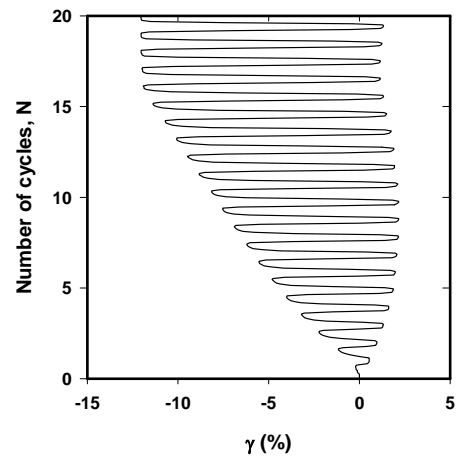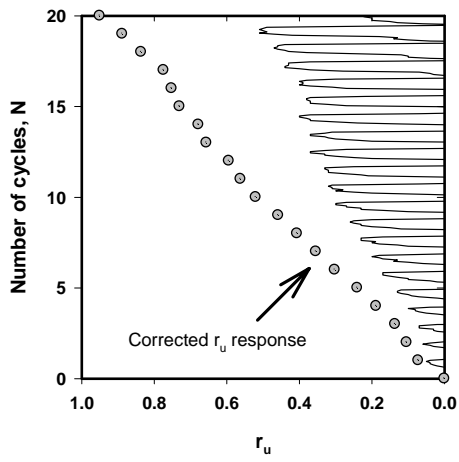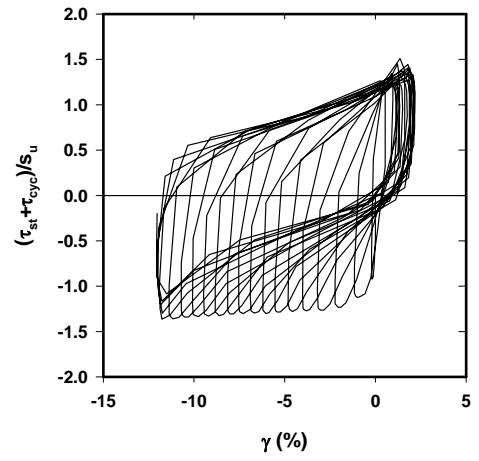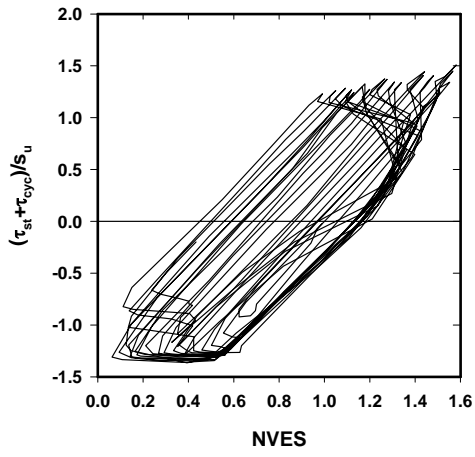
Figure C. 15. Presentation of CTXT16

222
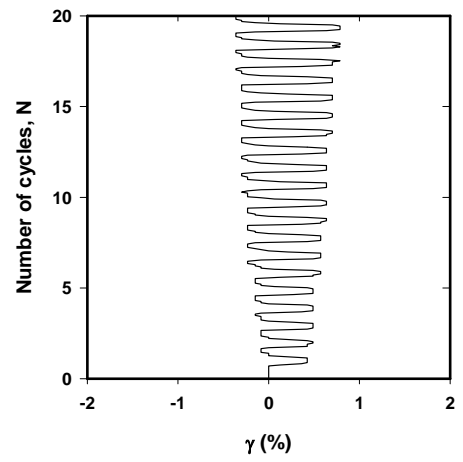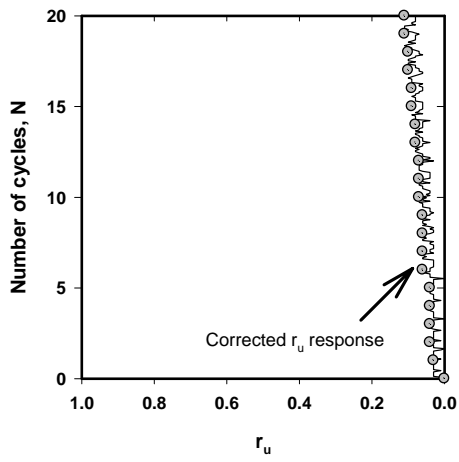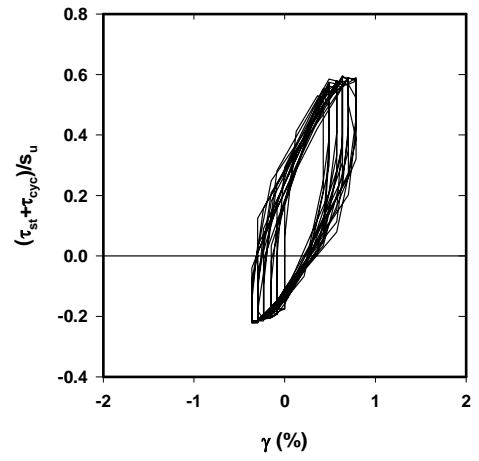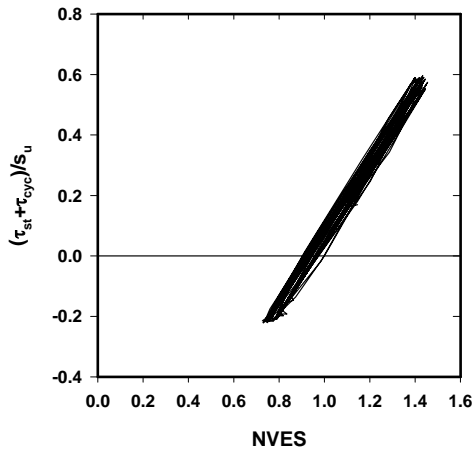
Figure C. 16. Presentation of CTXT18

223
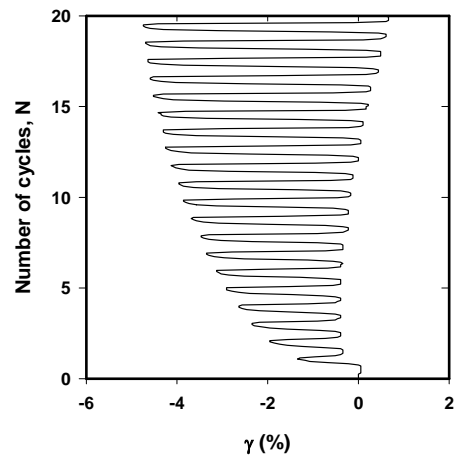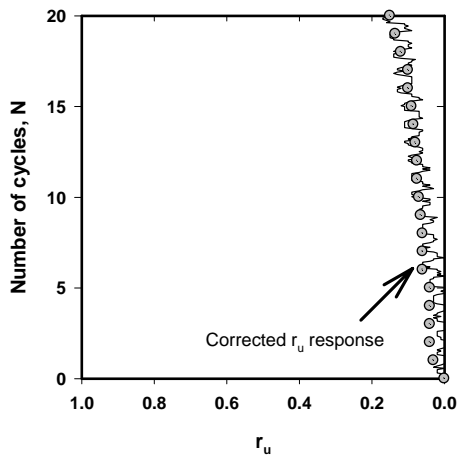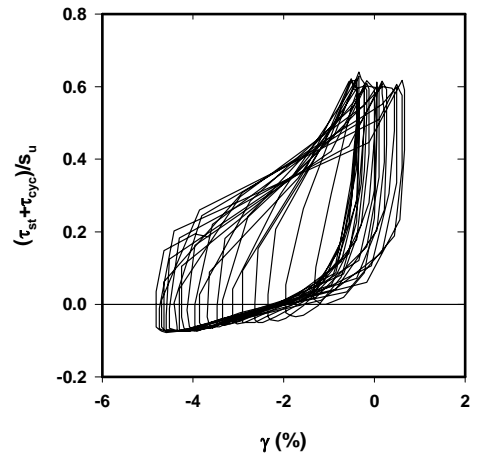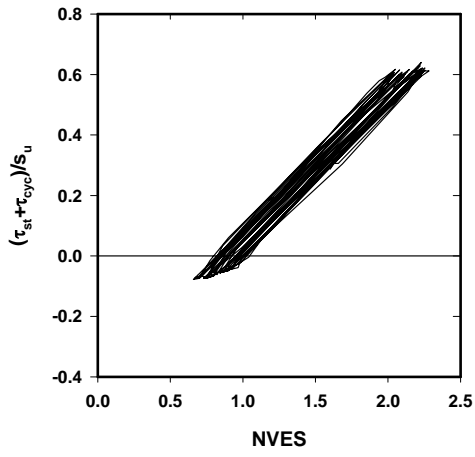
Figure C. 17. Presentation of CTXT19

224
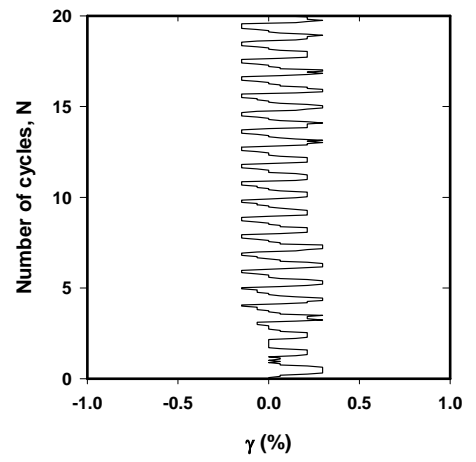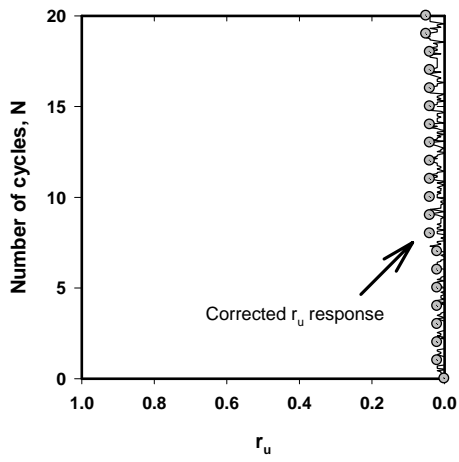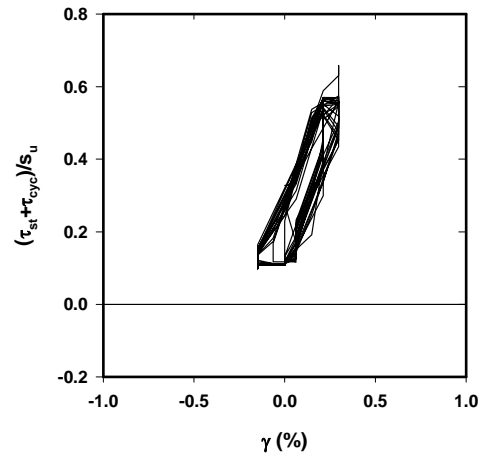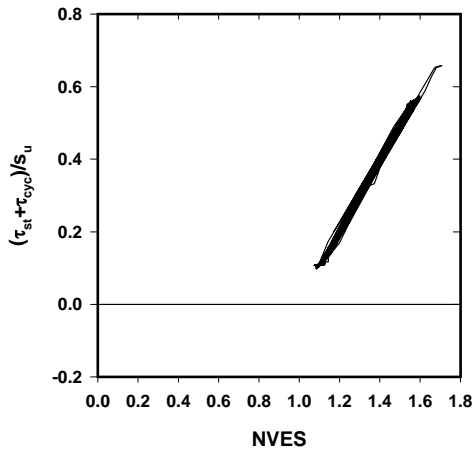
Figure C. 18. Presentation of CTXT20

225
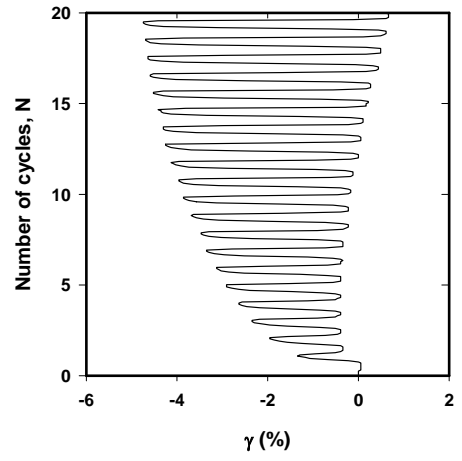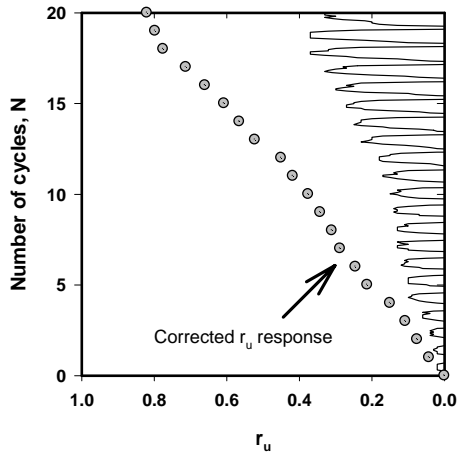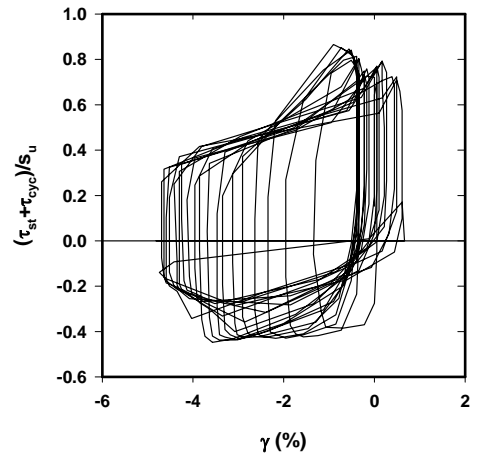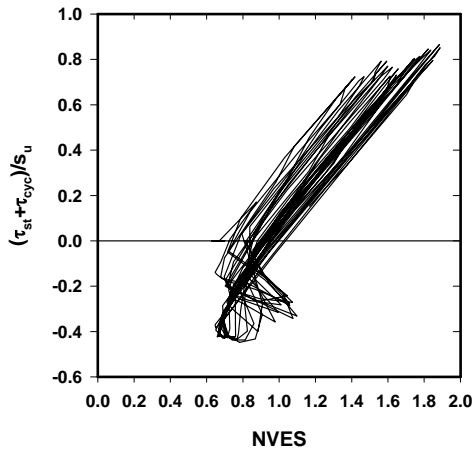
Figure C. 19. Presentation of CTXT21

226
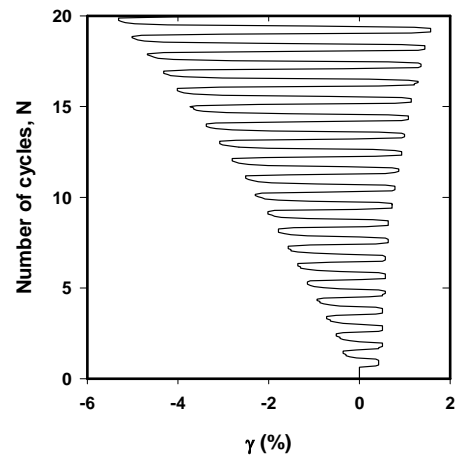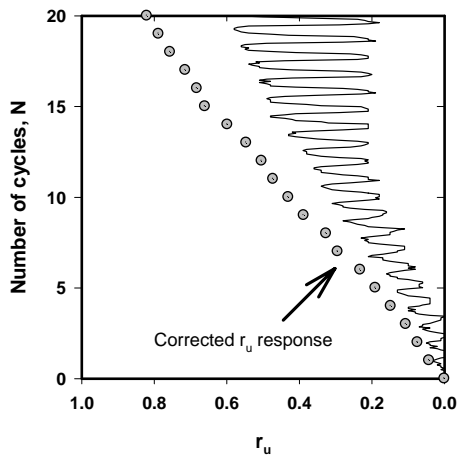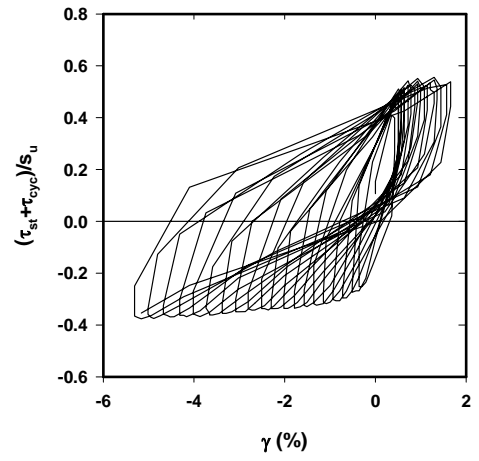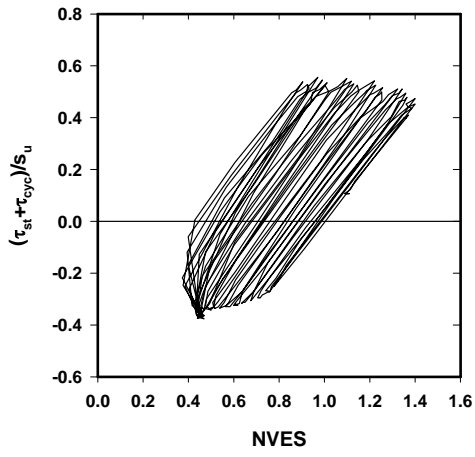
Figure C. 20. Presentation of CTXT22

227
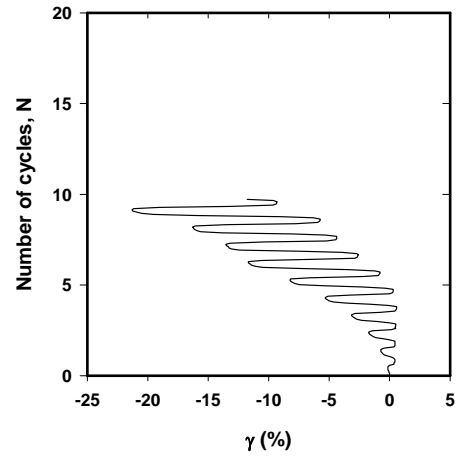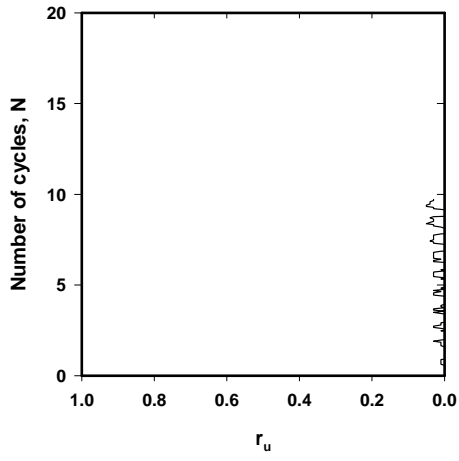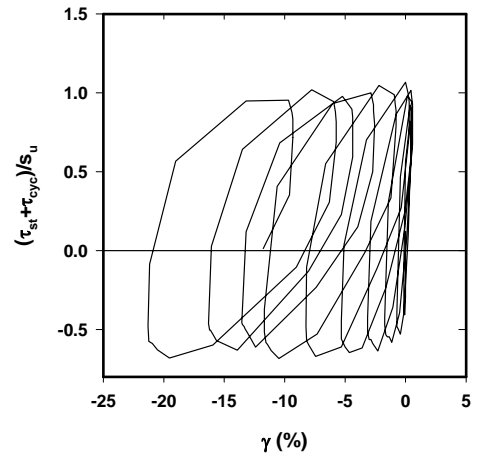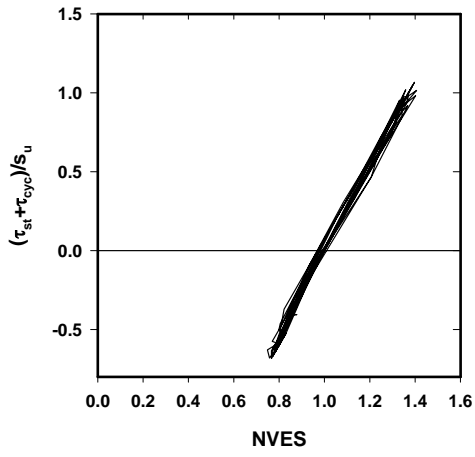
Figure C. 21. Presentation of CTXT23
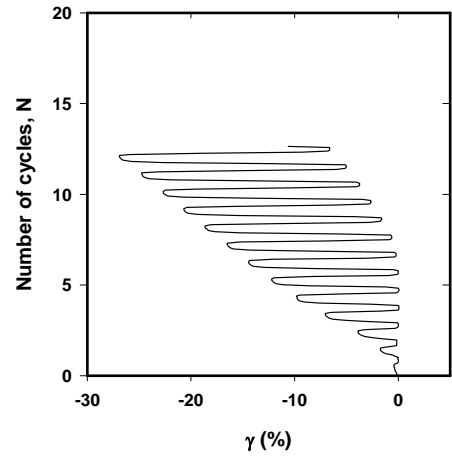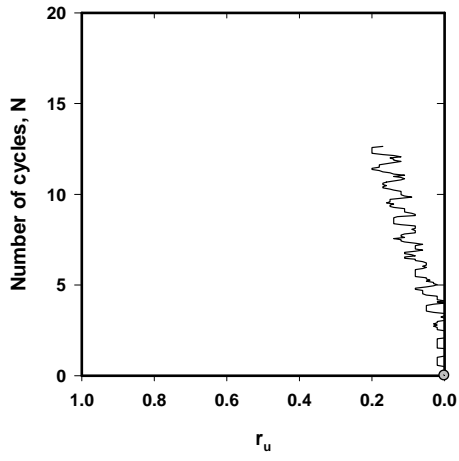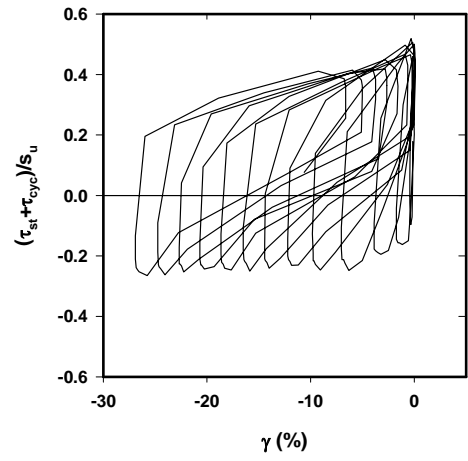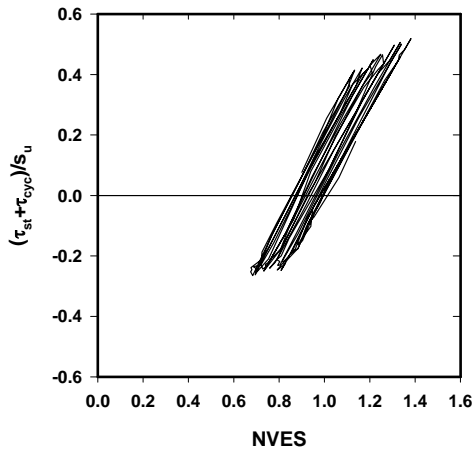
Figure C. 22. Presentation of CTXT24
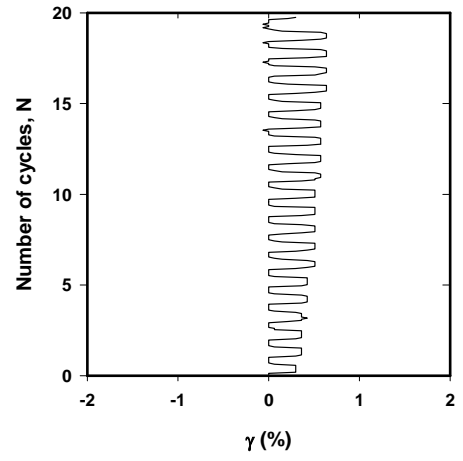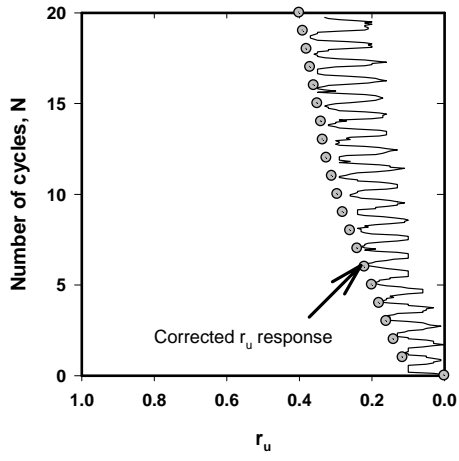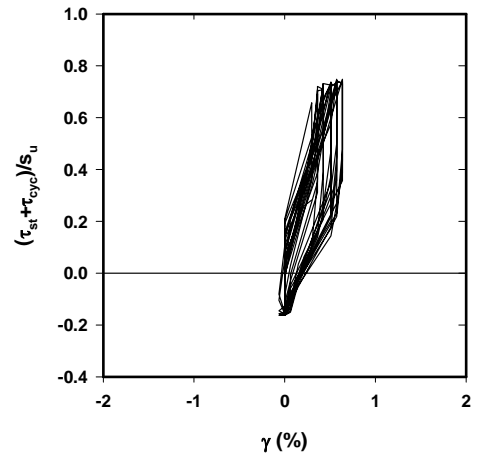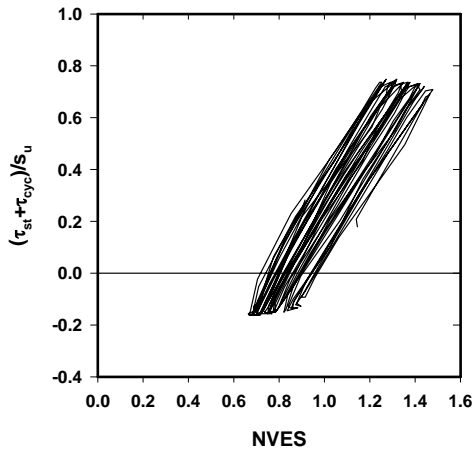
Figure C. 23. Presentation of CTXT25
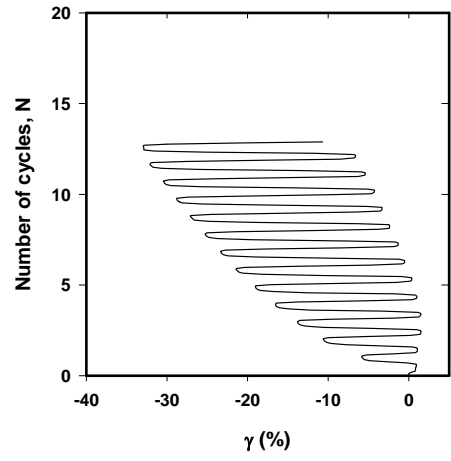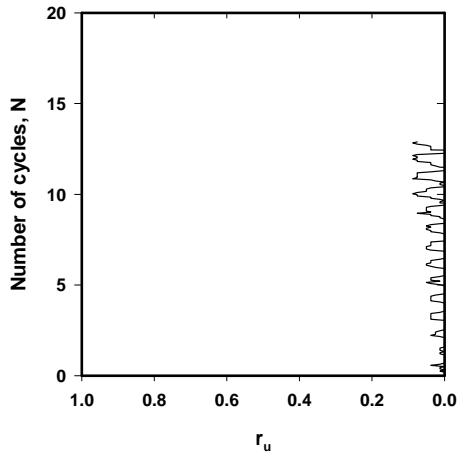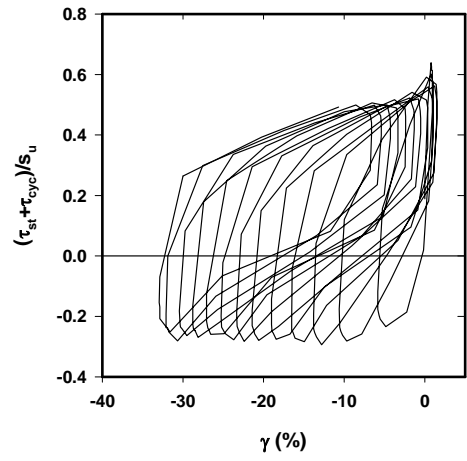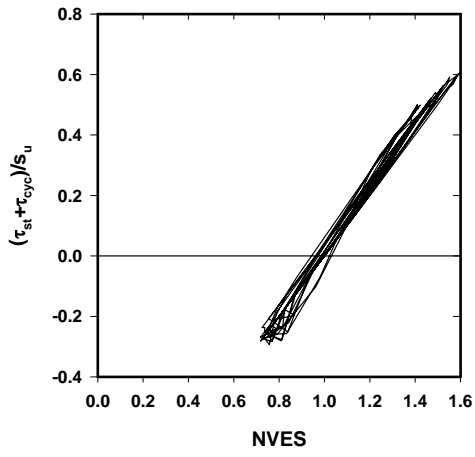
Figure C. 24. Presentation of CTXT26

231
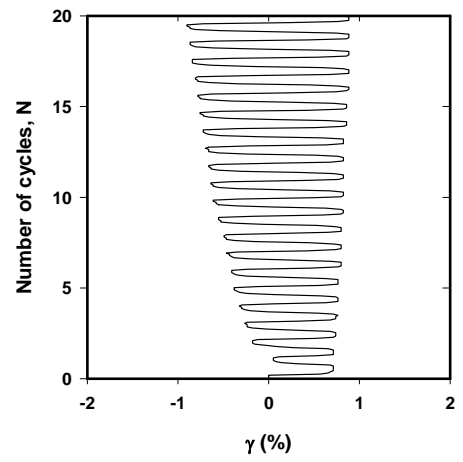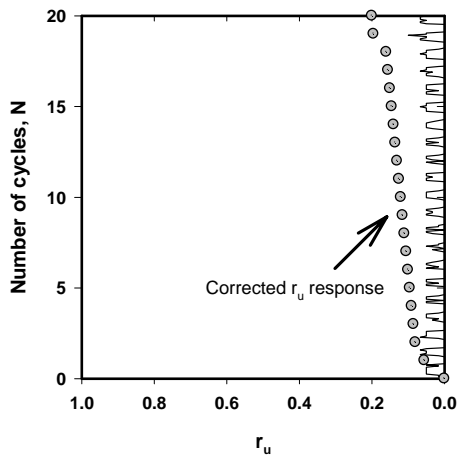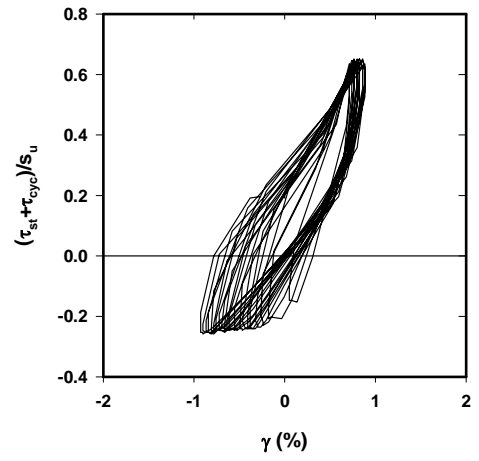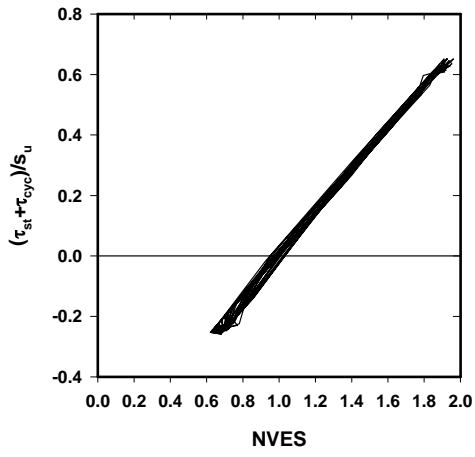
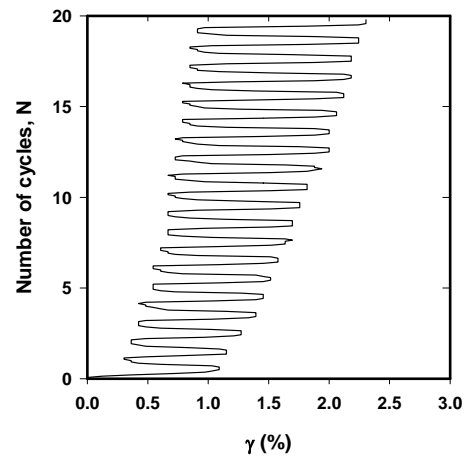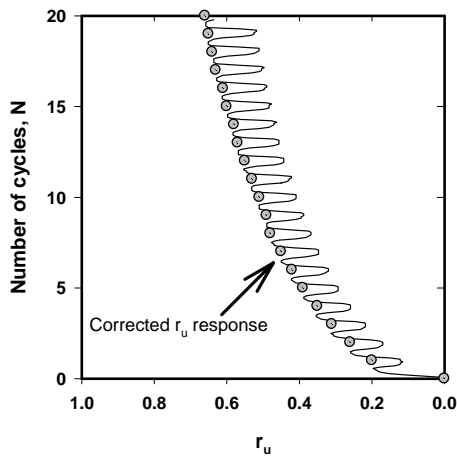**Figure C. 25. Presentation of CTXT27**

232
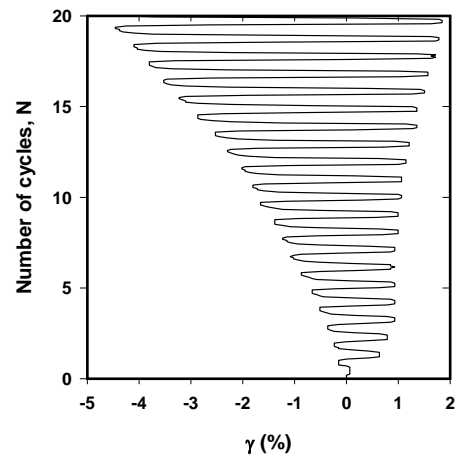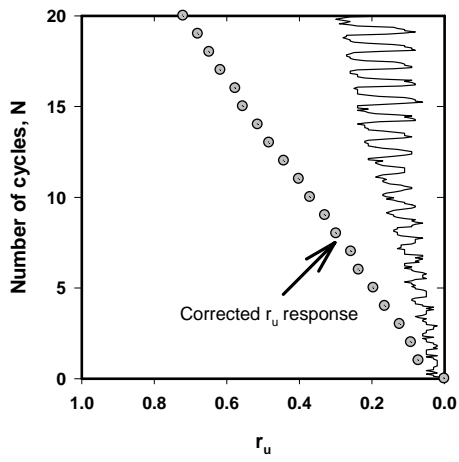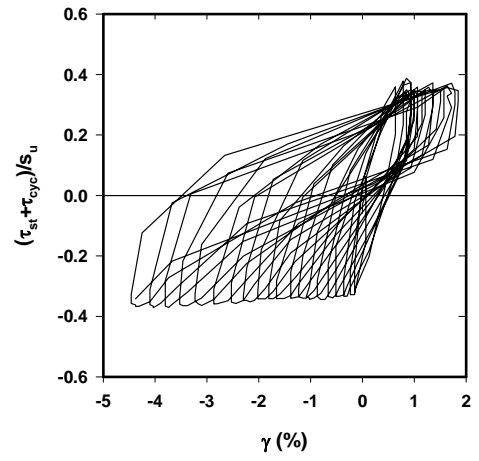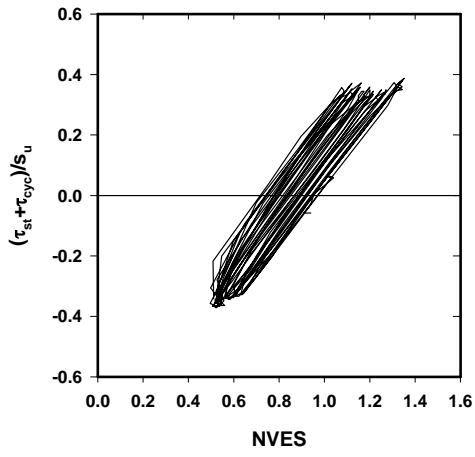
Figure C. 26. Presentation of CTXT28

233
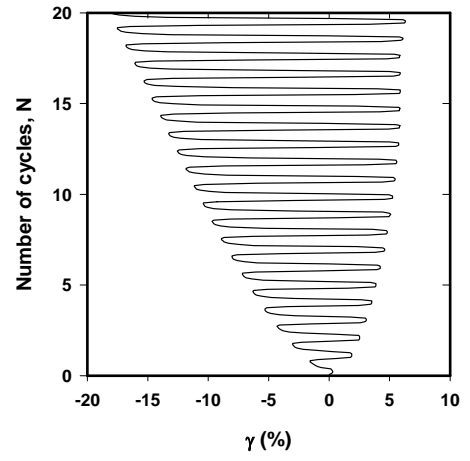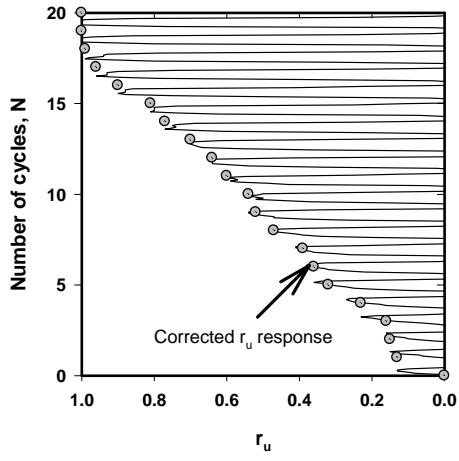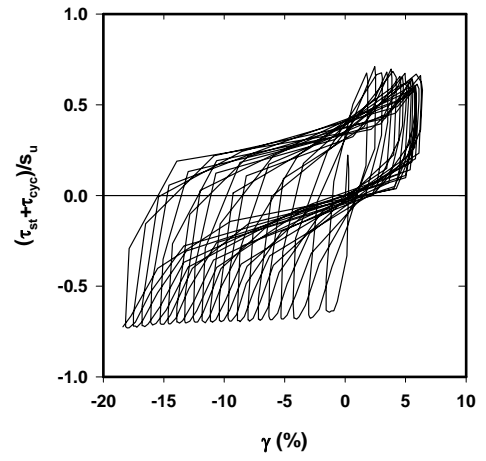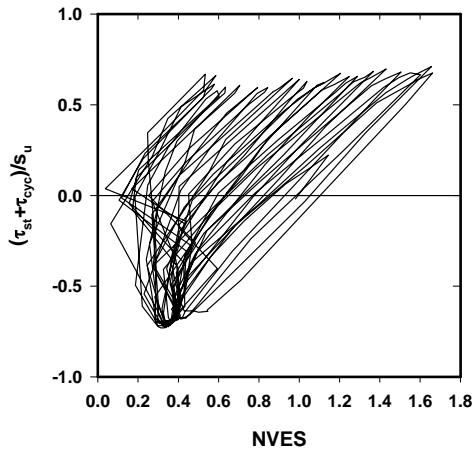
Figure C. 27. Presentation of CTXT29

234
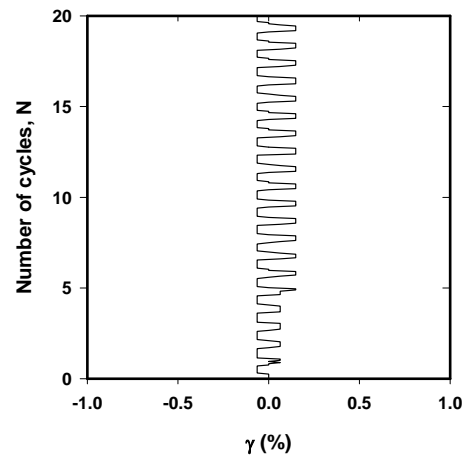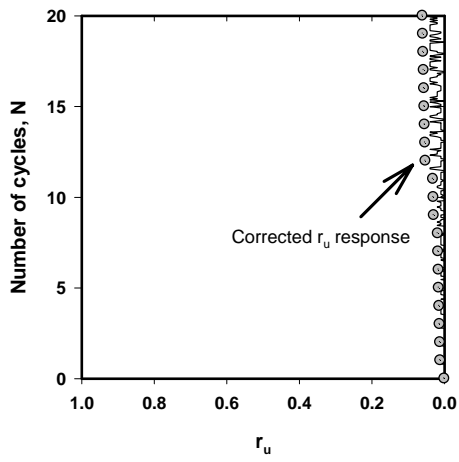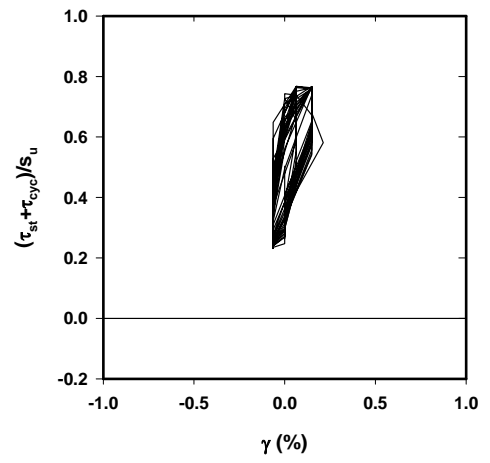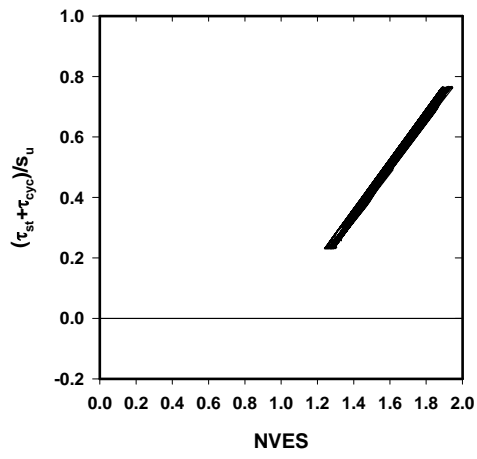
Figure C. 28. Presentation of CTXT30

235
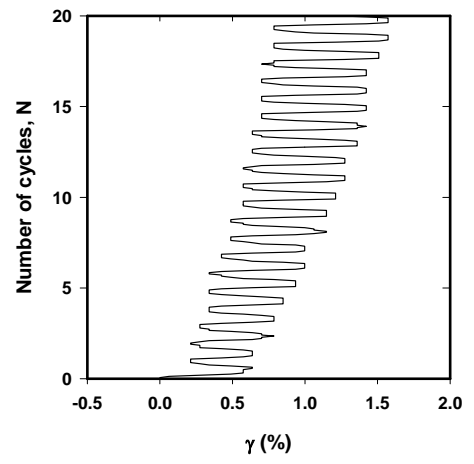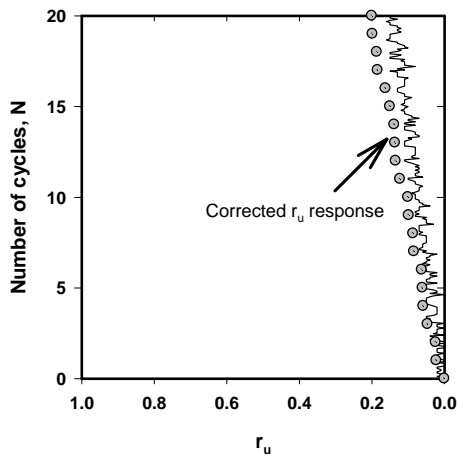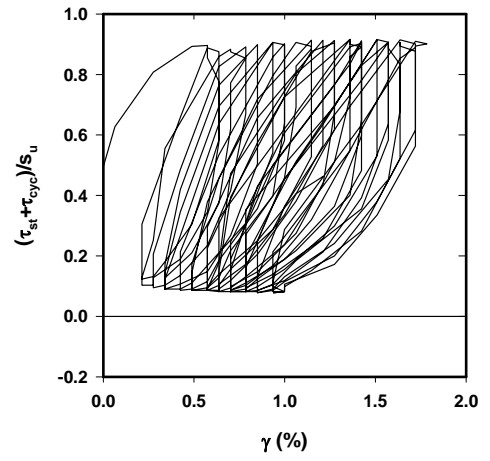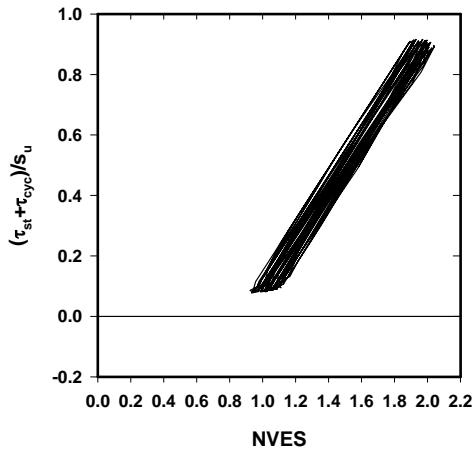
Figure C. 29. Presentation of CTXT31

236
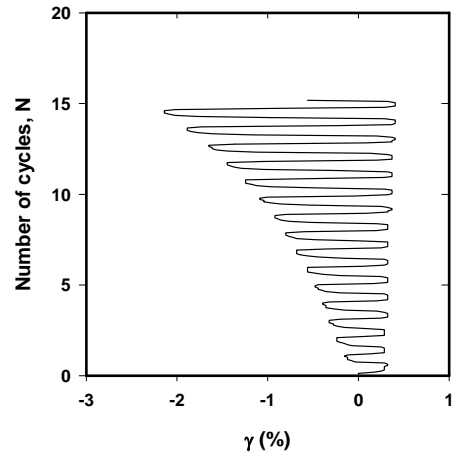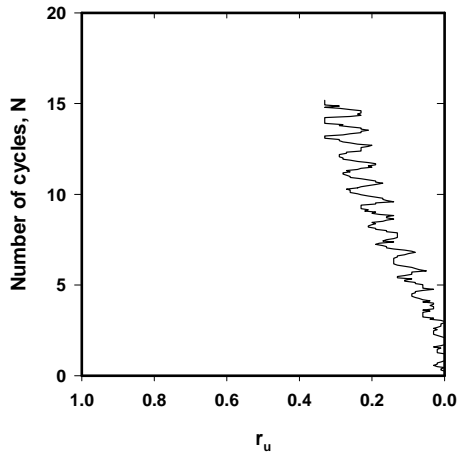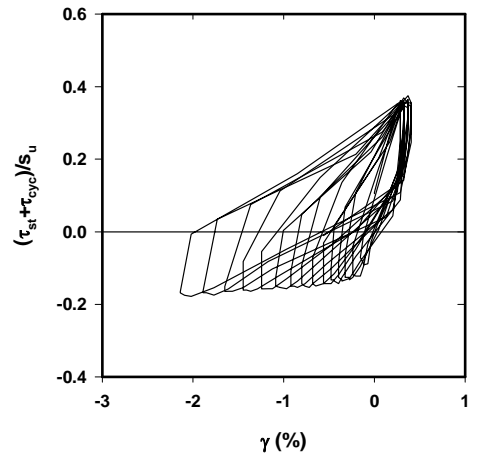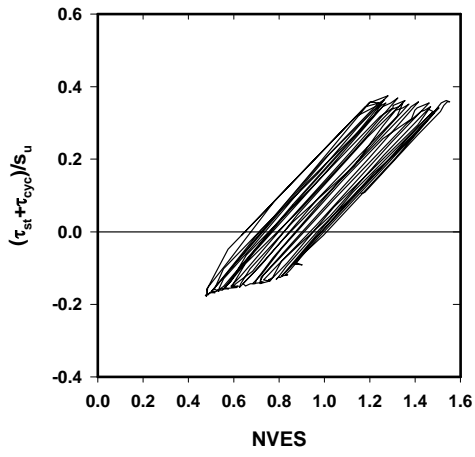
Figure C. 30. Presentation of CTXT32

237
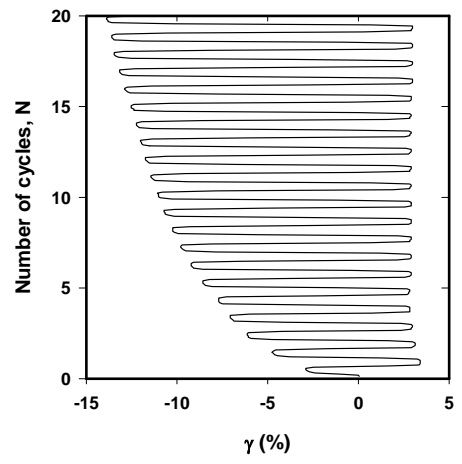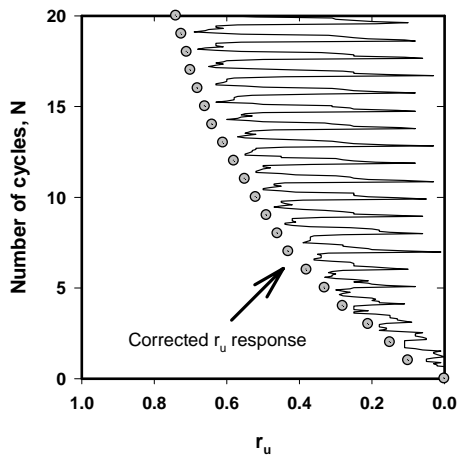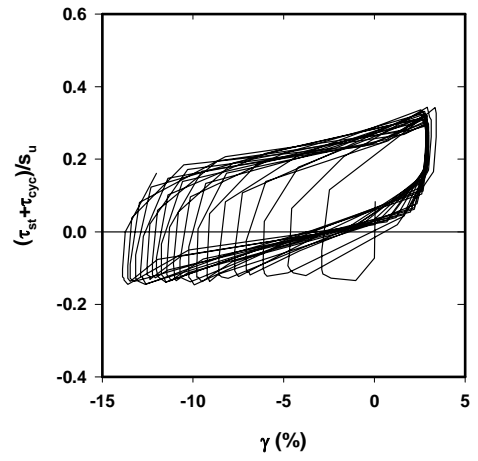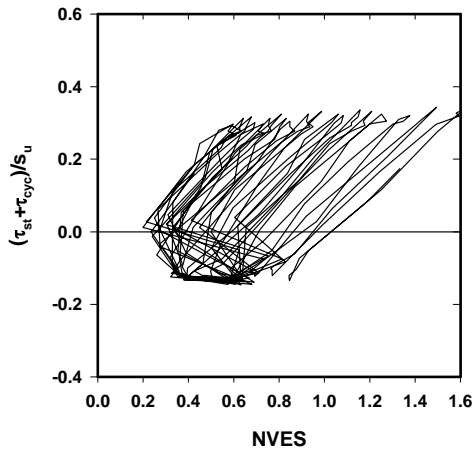
Figure C. 31. Presentation of CTXT33

238
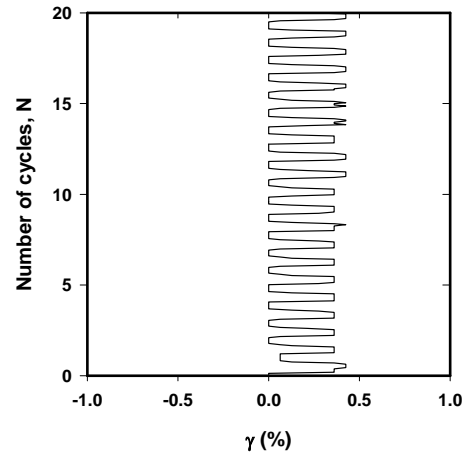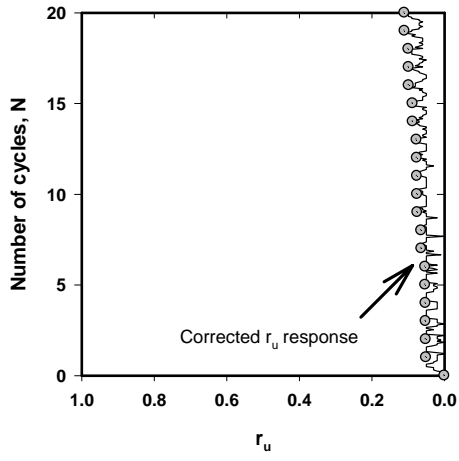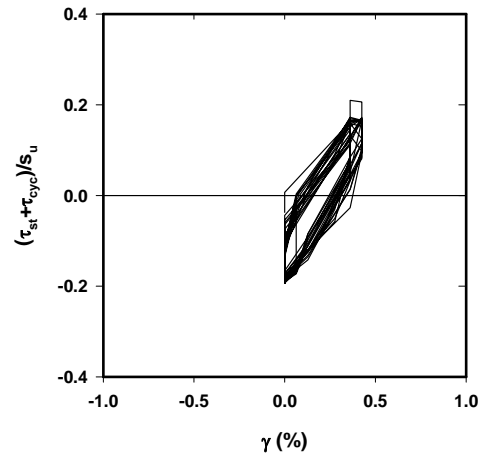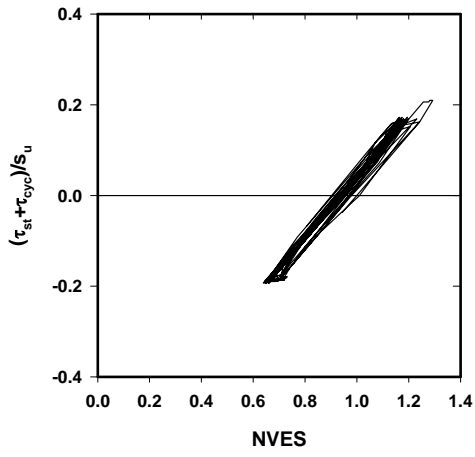
Figure C. 32. Presentation of CTXT34

239
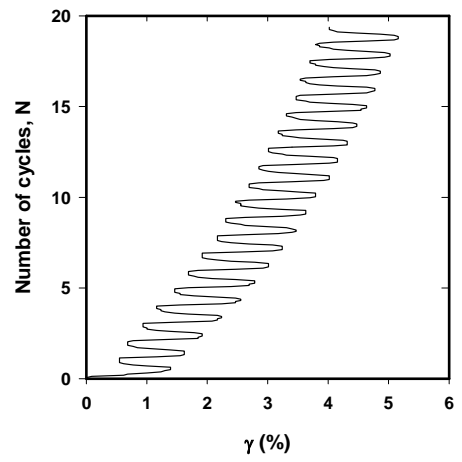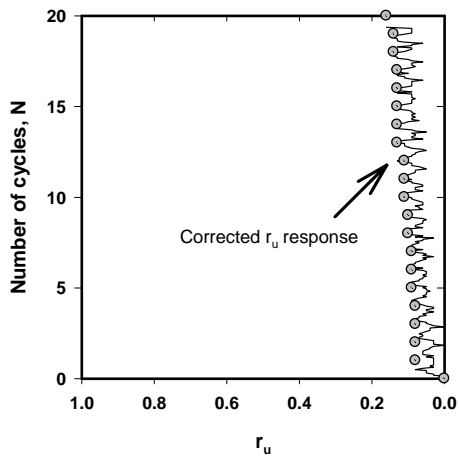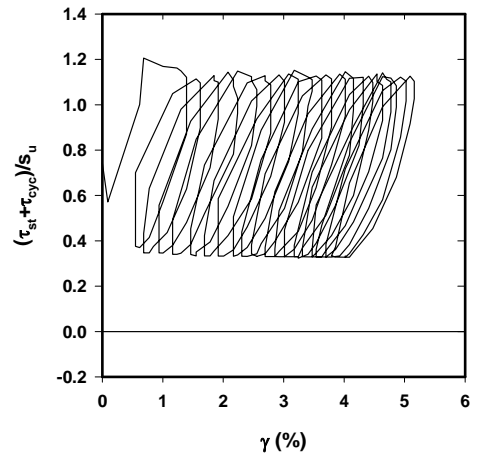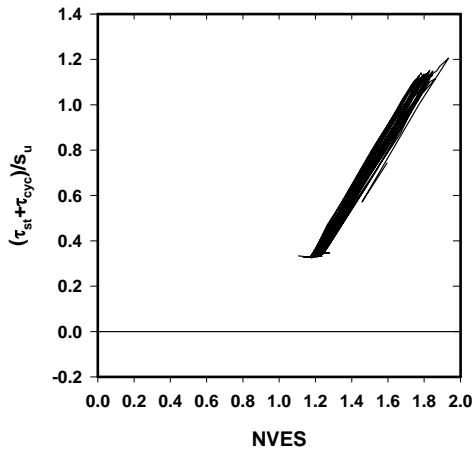
Figure C. 33. Presentation of CTXT35

240
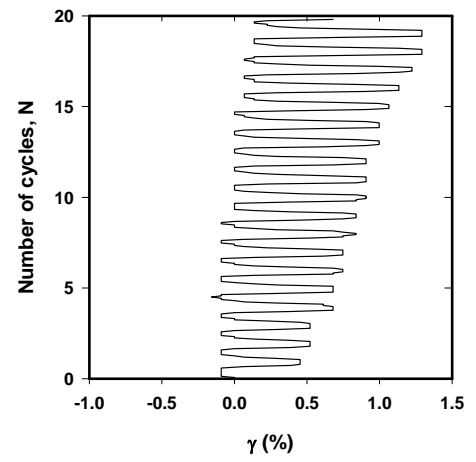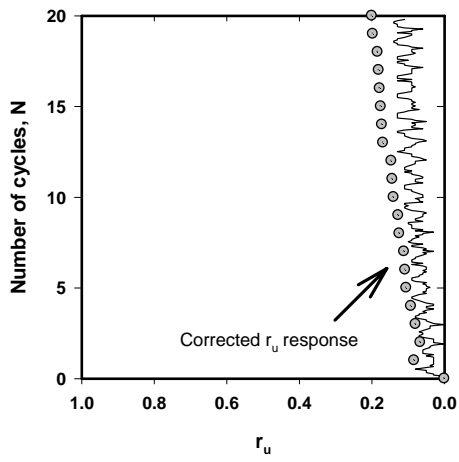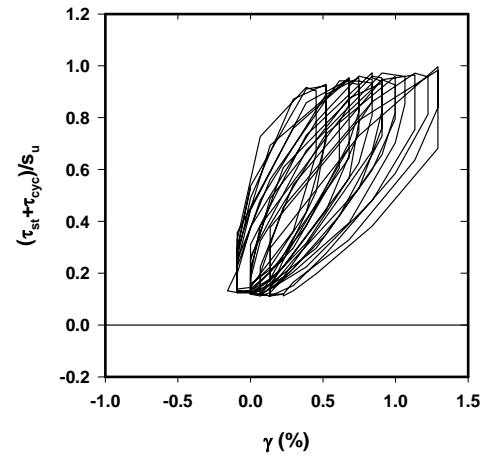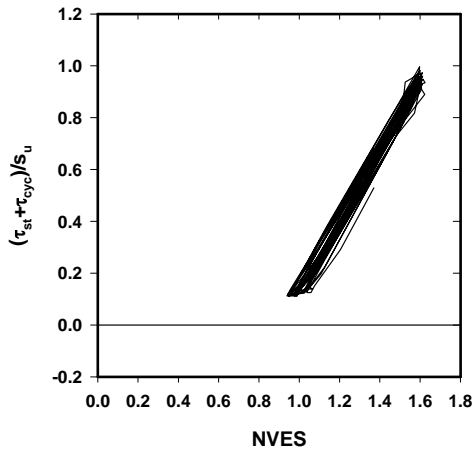
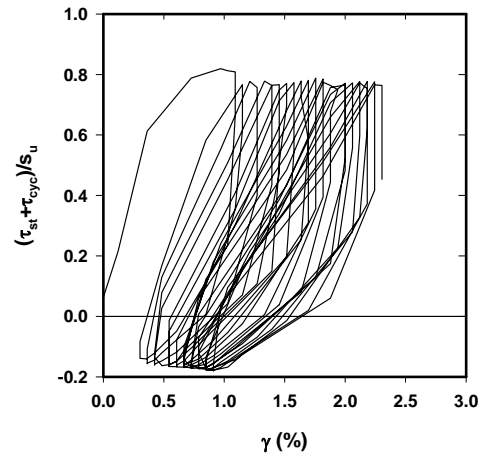**Figure C. 34. Presentation of CTXT36**

241
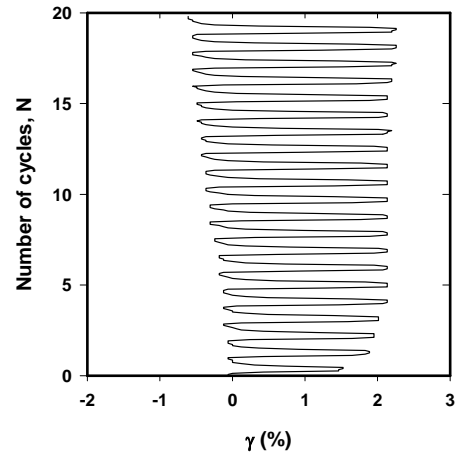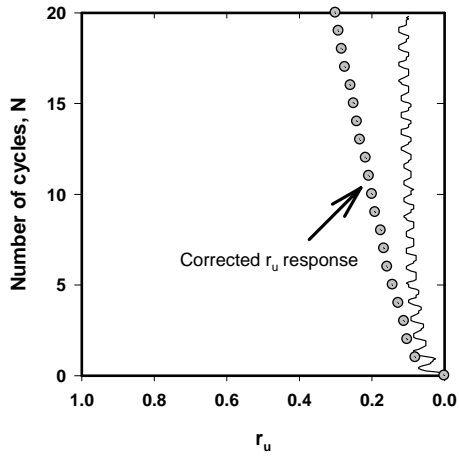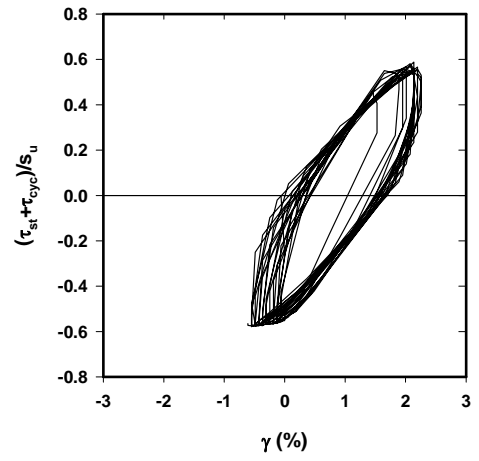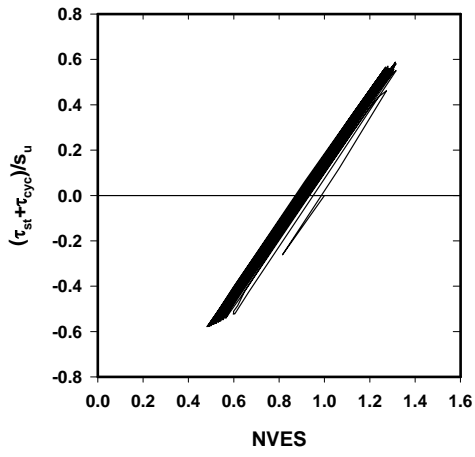
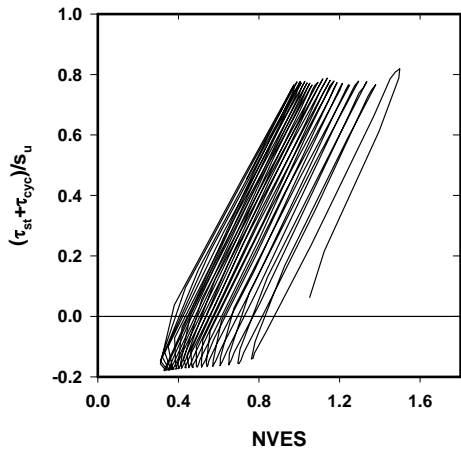**Figure C. 35. Presentation of CTXT37**
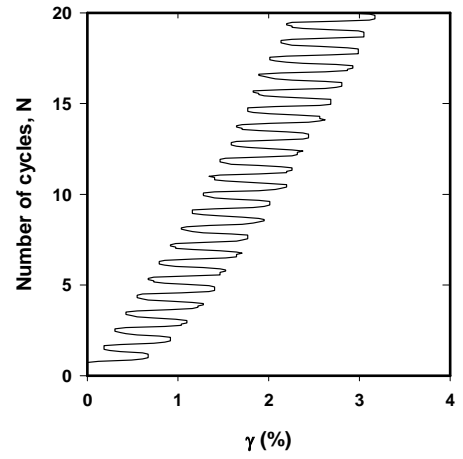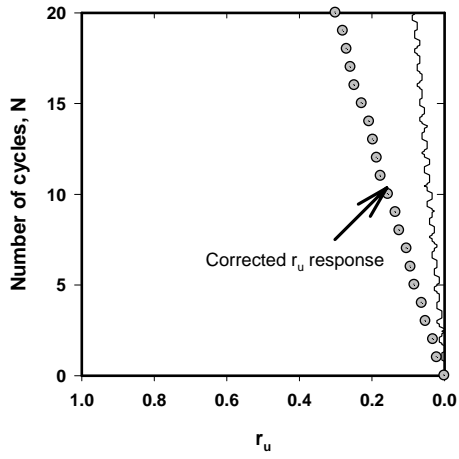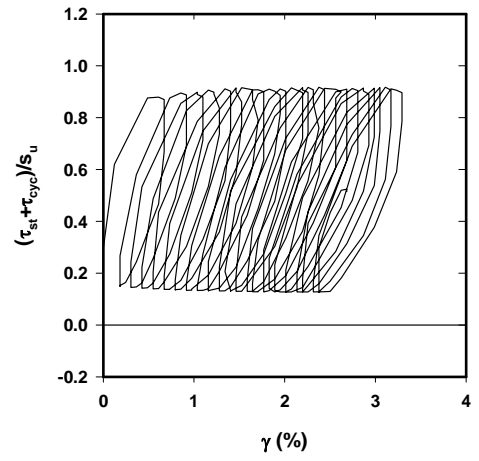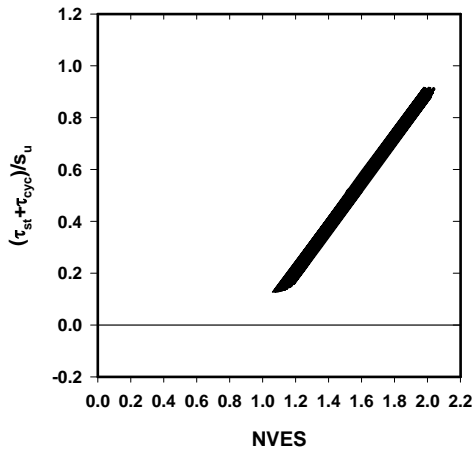
Figure C. 36. Presentation of CTXT38
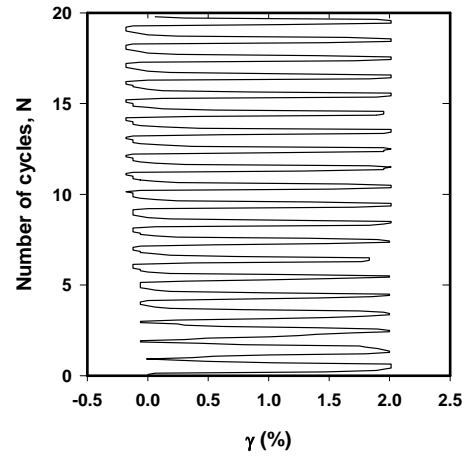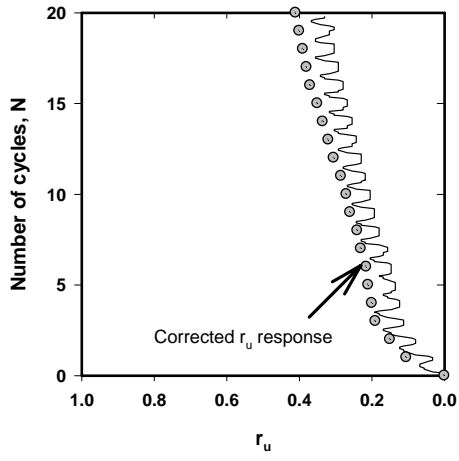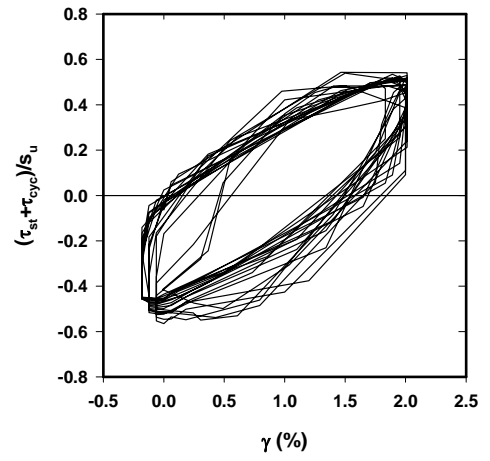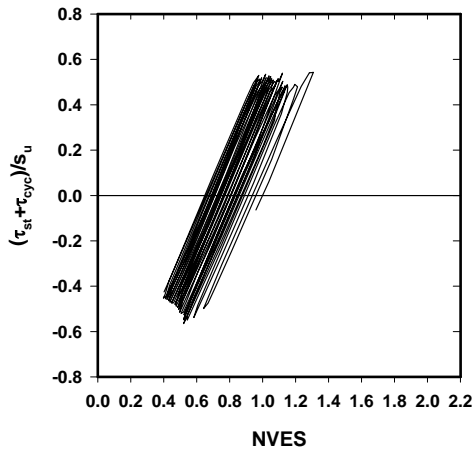
Figure C. 37. Presentation of CTXT40

244
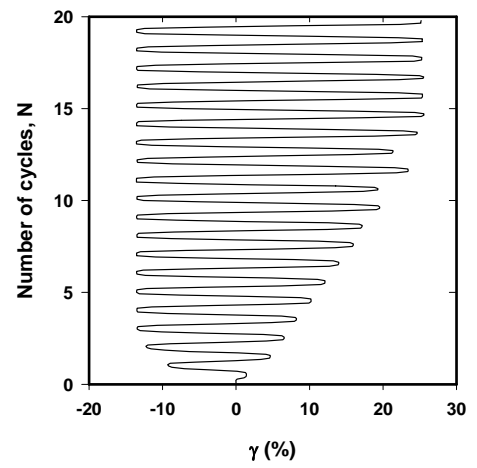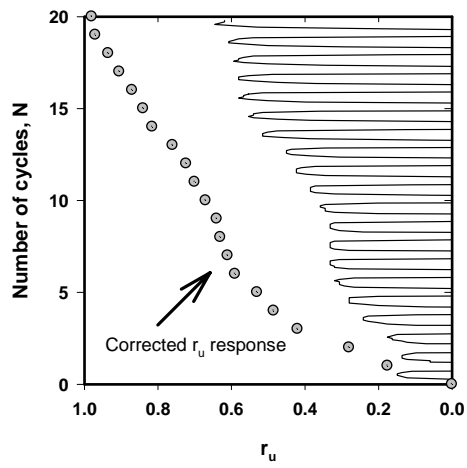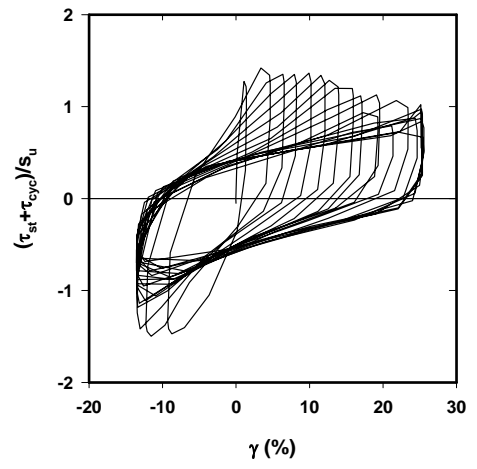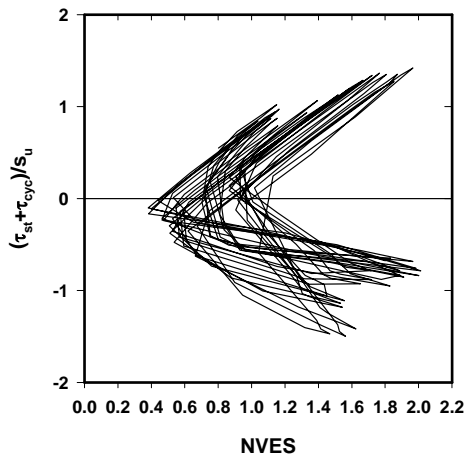
Figure C. 38. Presentation of CTXT42
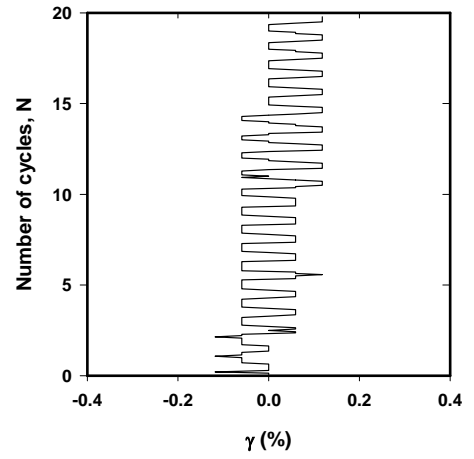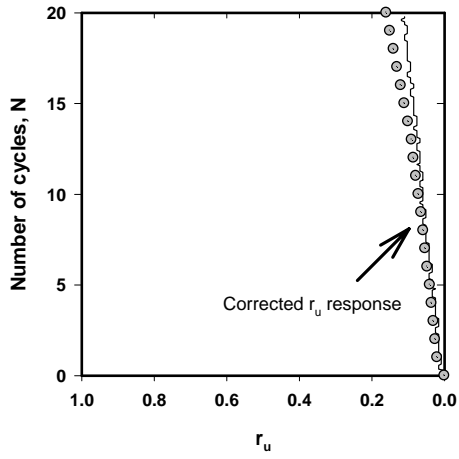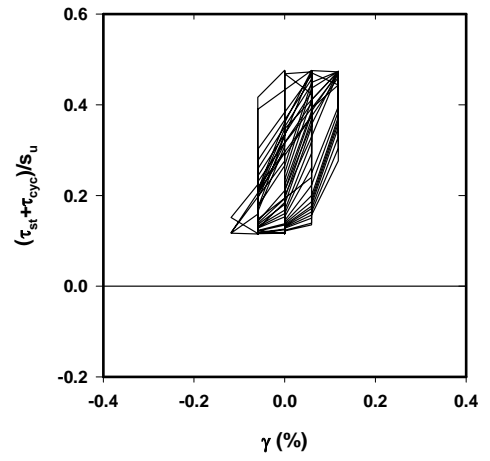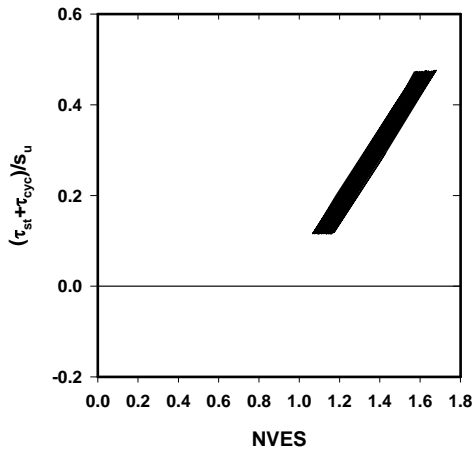
Figure C. 39. Presentation of CTXT43
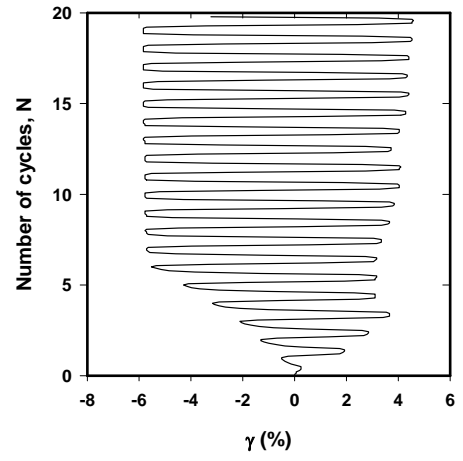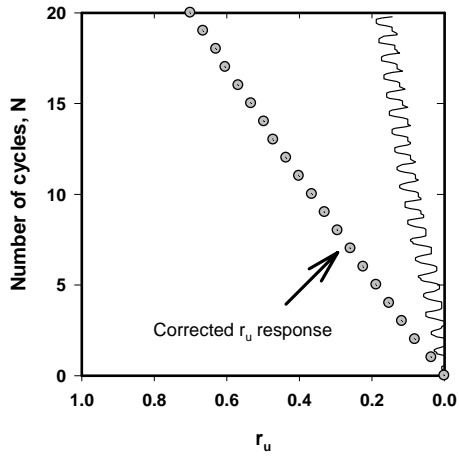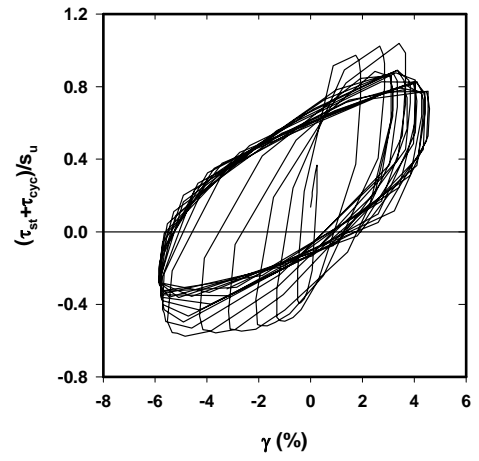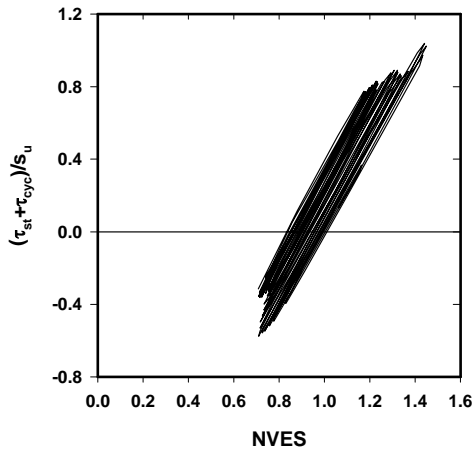
Figure C. 40. Presentation of CTXT44

247
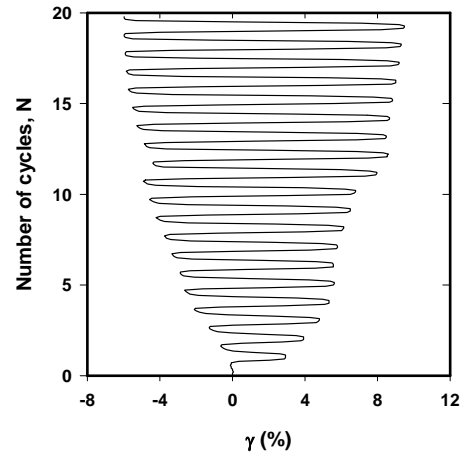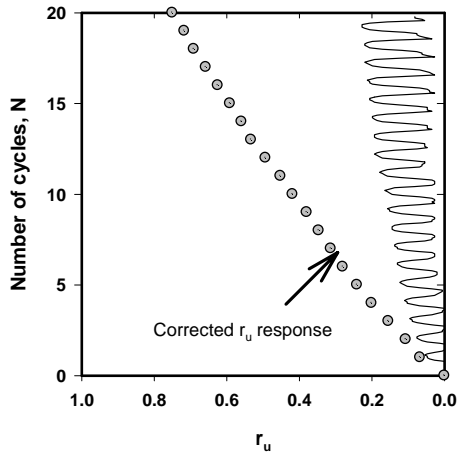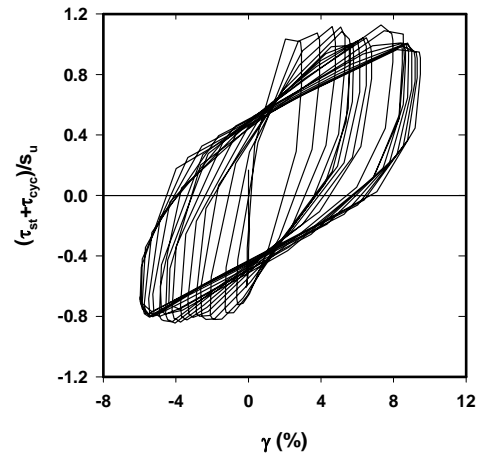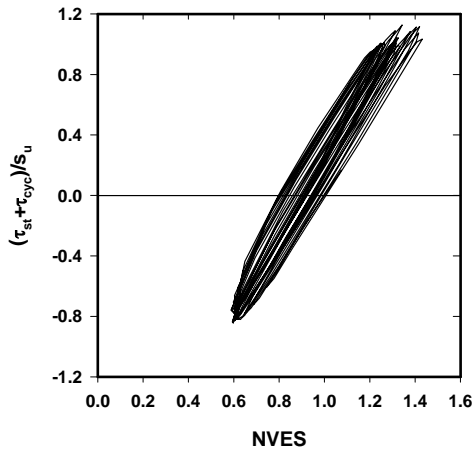
Figure C. 41. Presentation of CTXT45
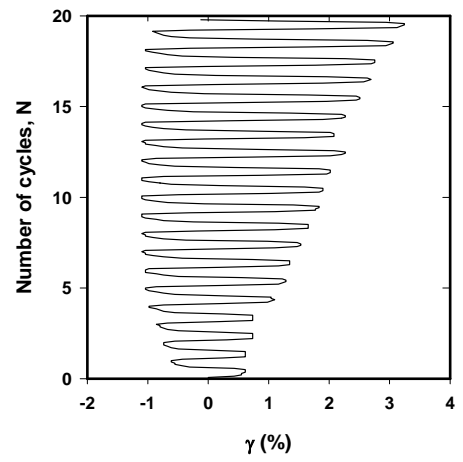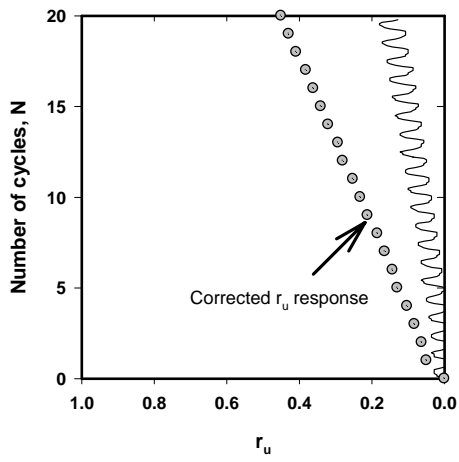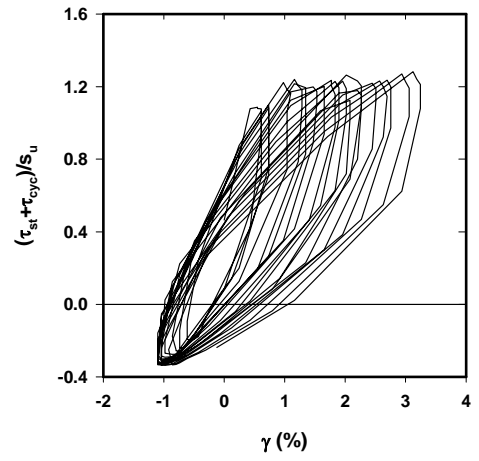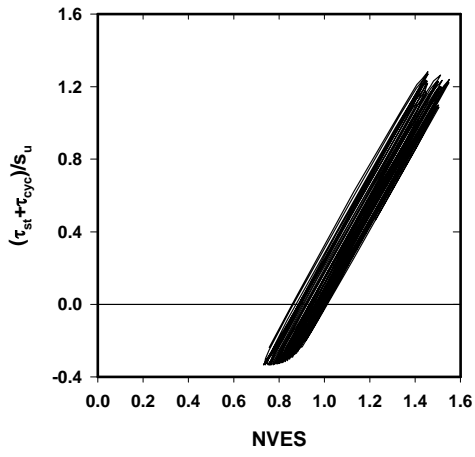
Figure C. 42. Presentation of CTXT46

249
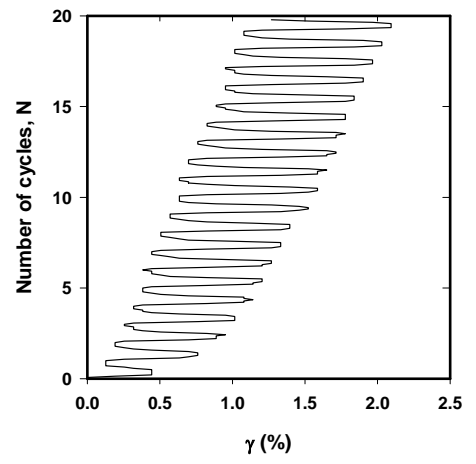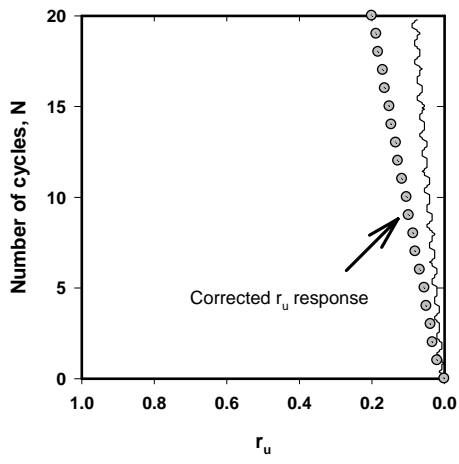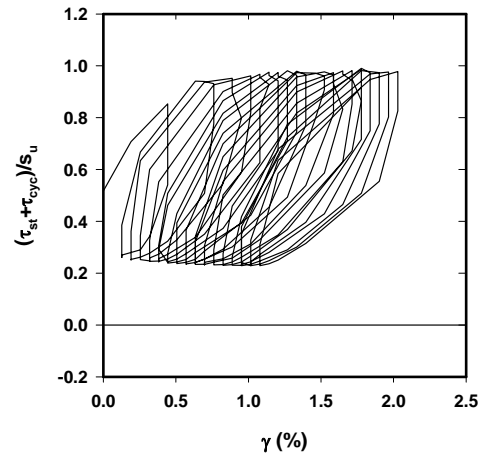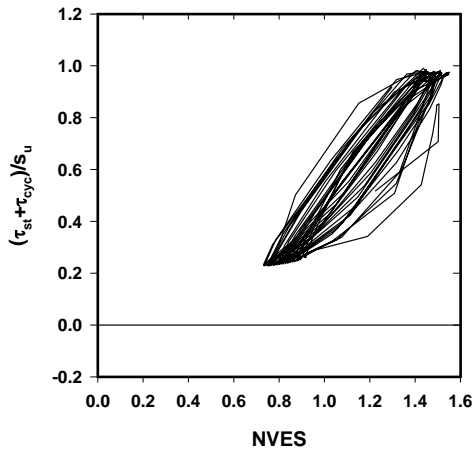
Figure C. 43. Presentation of CTXT47

250
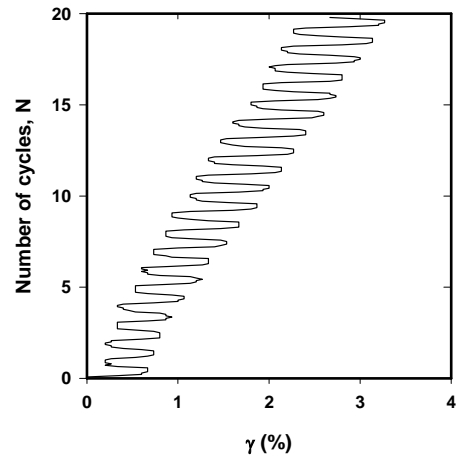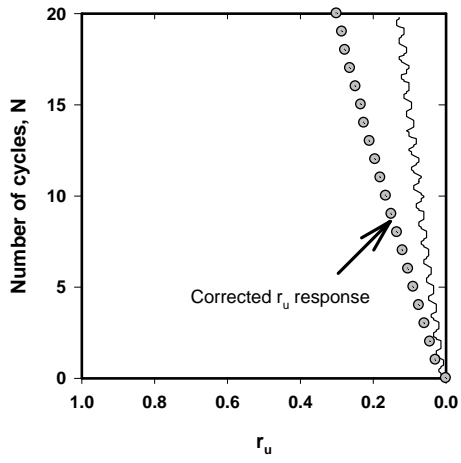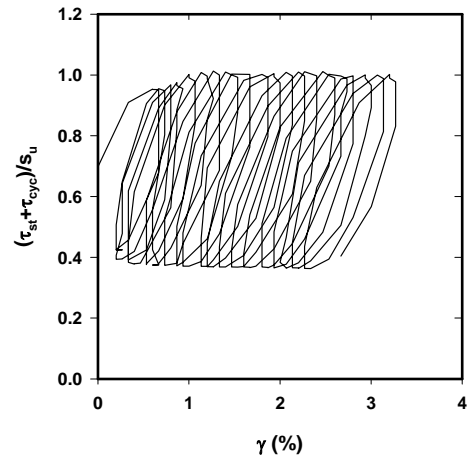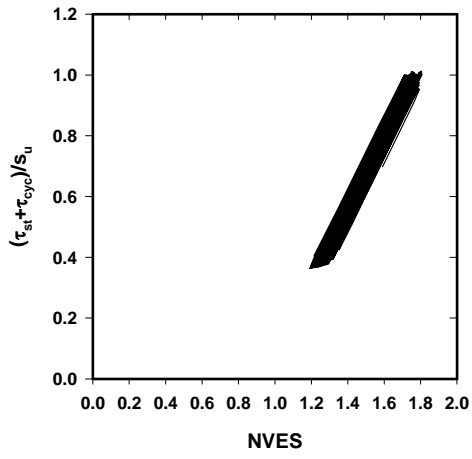
Figure C. 44. Presentation of CTXT48
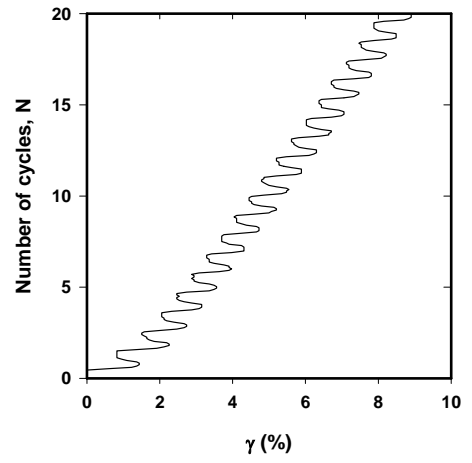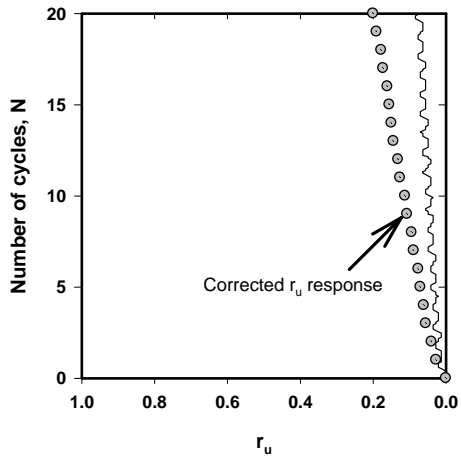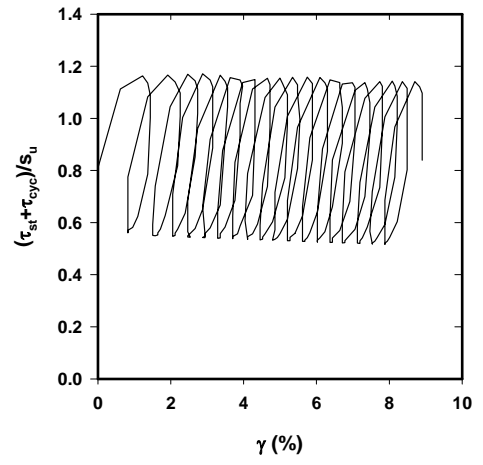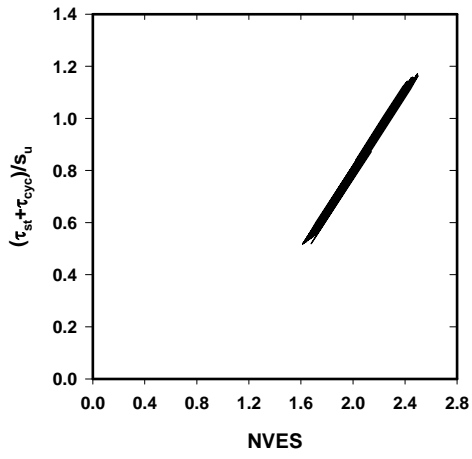
Figure C. 45. Presentation of CTXT49

252
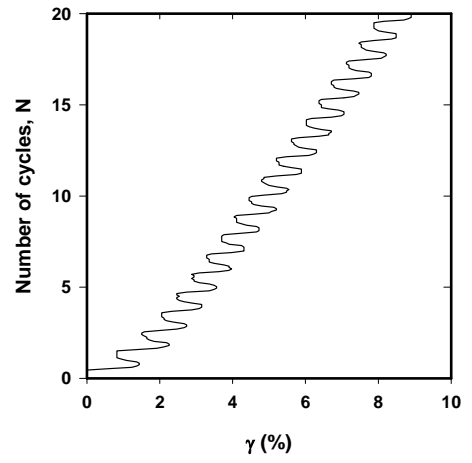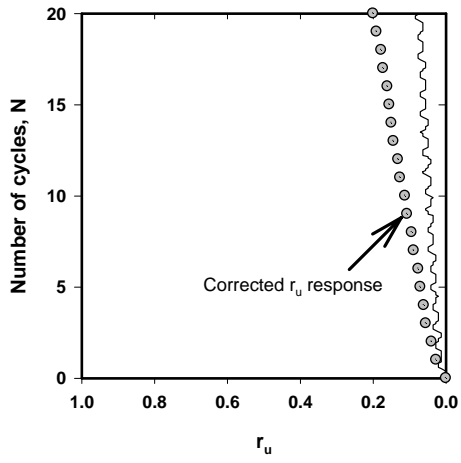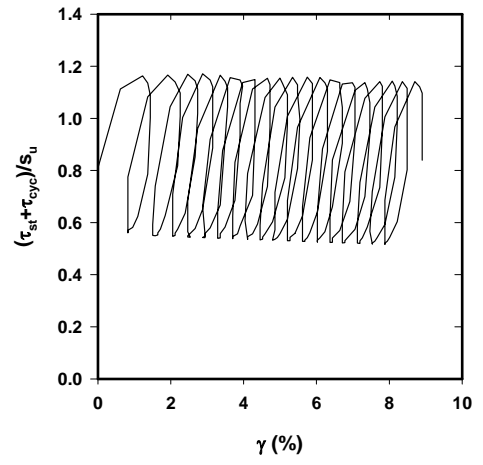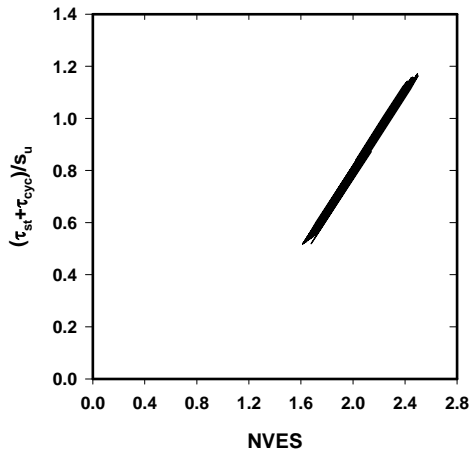
Figure C. 46. Presentation of CTXT50

253
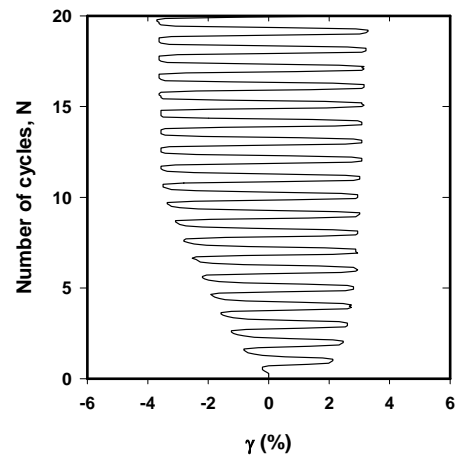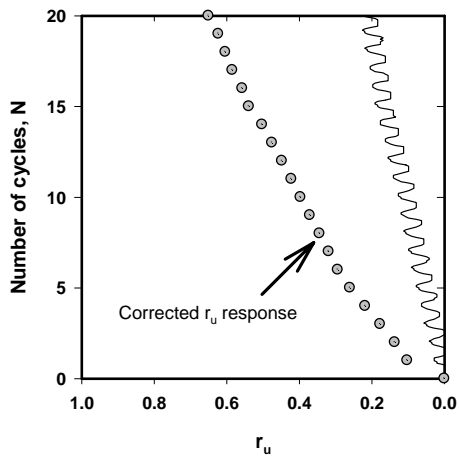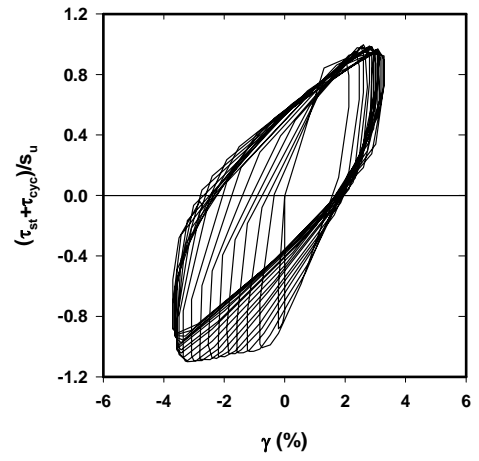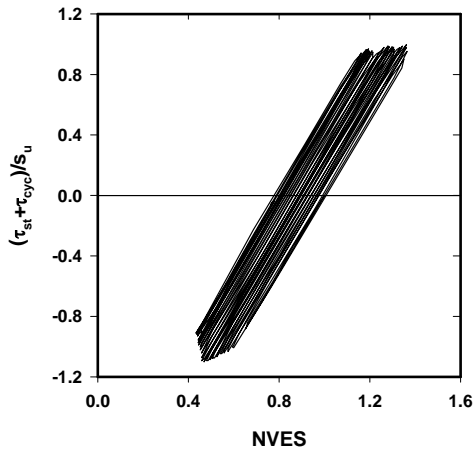
Figure C. 47. Presentation of CTXT51

254
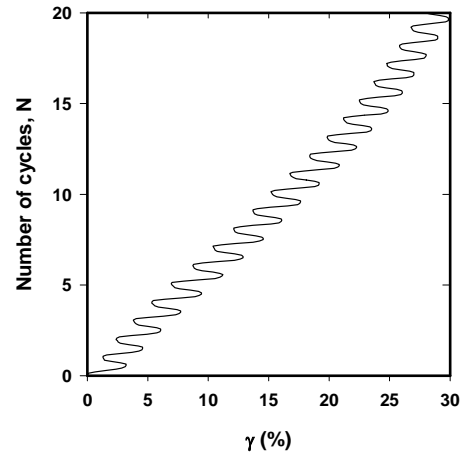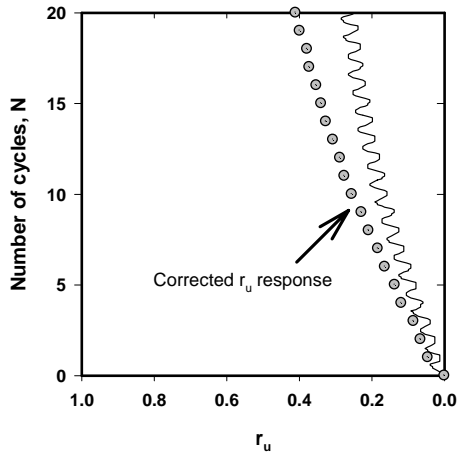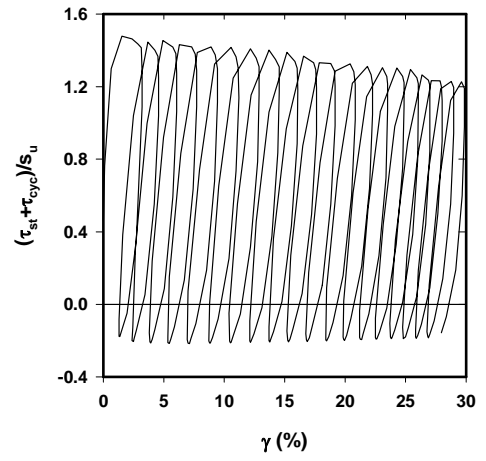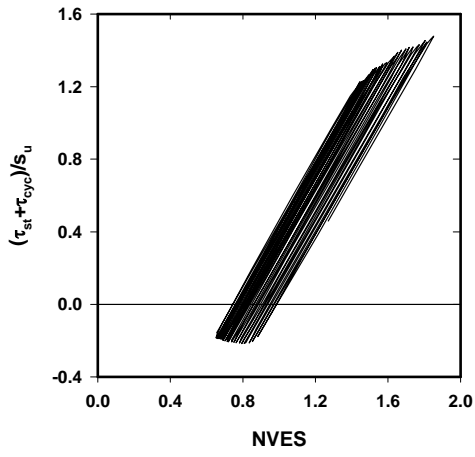
Figure C. 48. Presentation of CTXT52

255
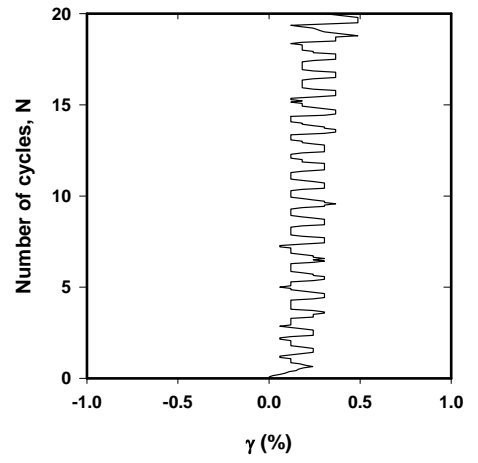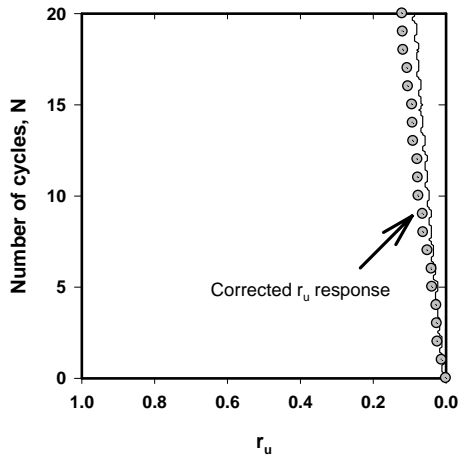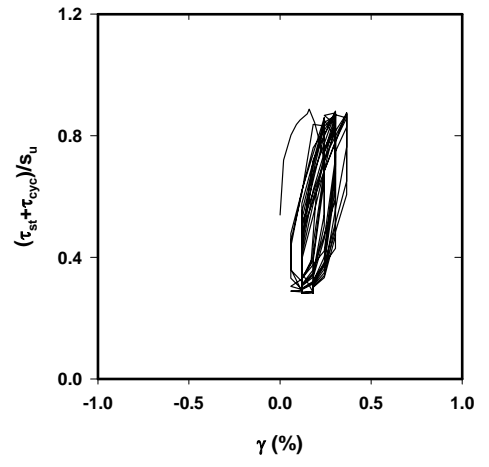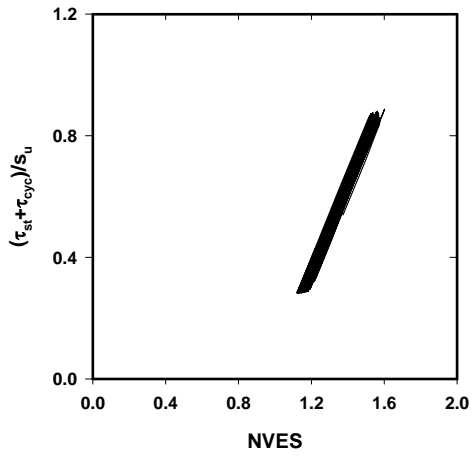
Figure C. 49. Presentation of CTXT53
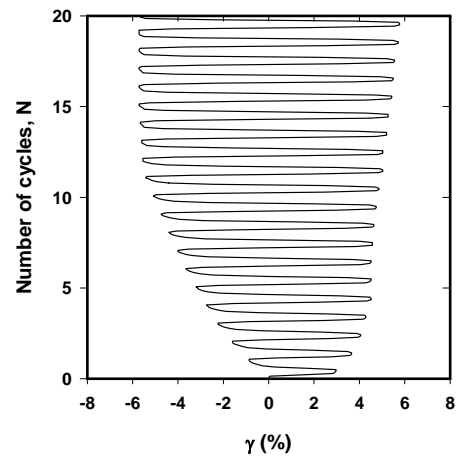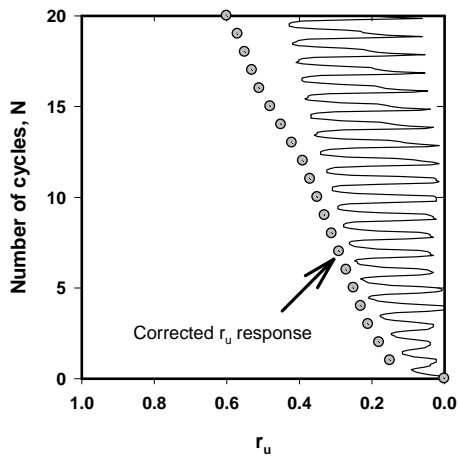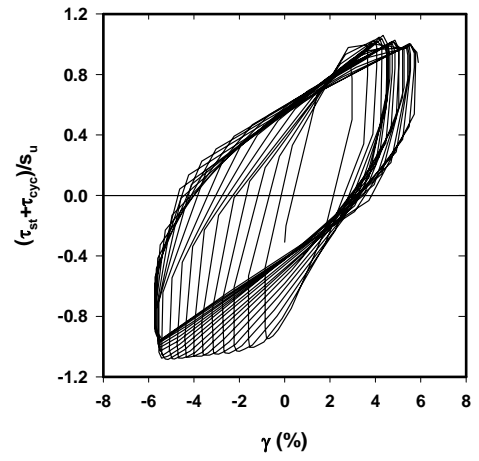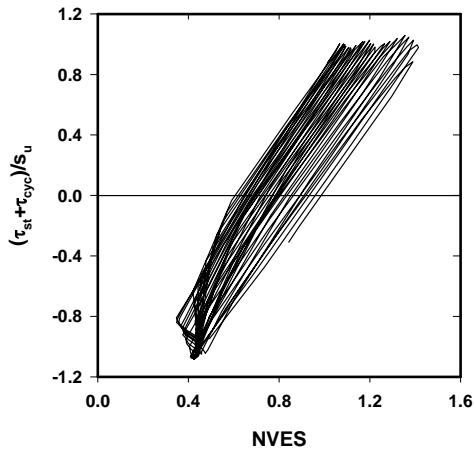
Figure C. 50. Presentation of CTXT54

257
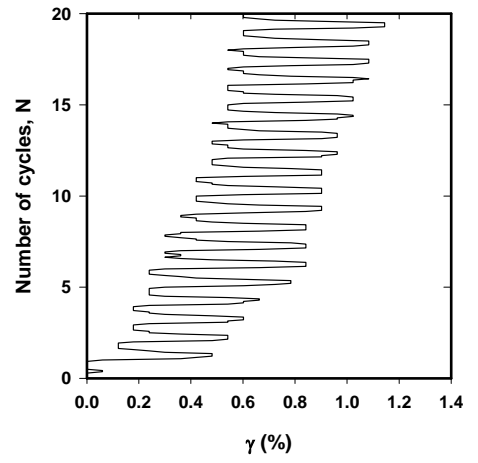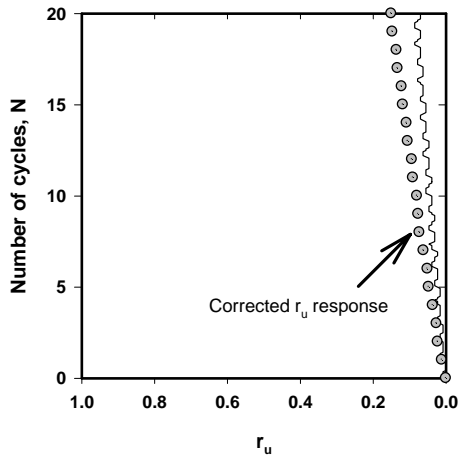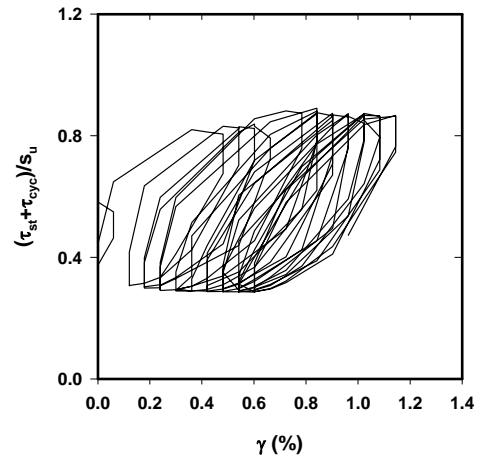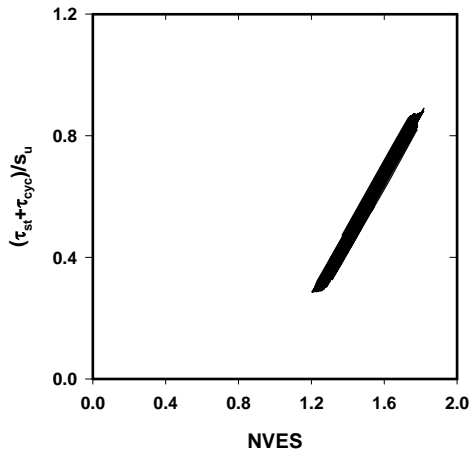
Figure C. 51. Presentation of CTXT55

258
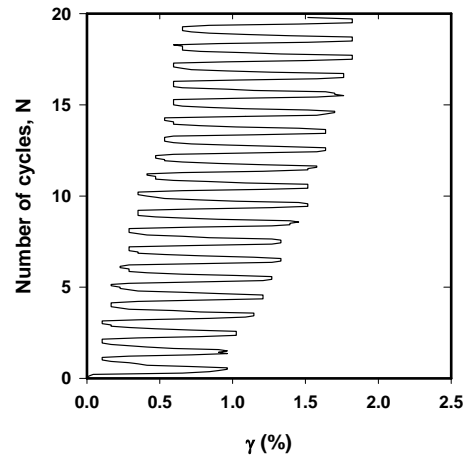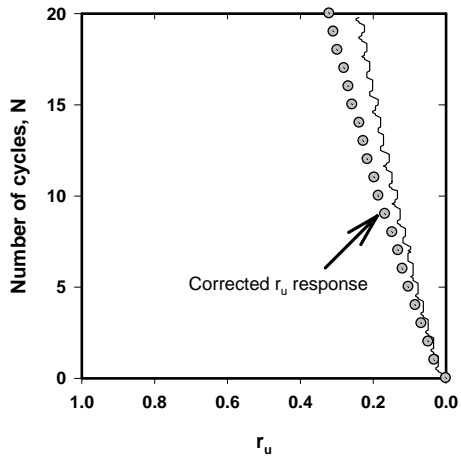
**Figure C. 52. Presentation of CTXT56**

259
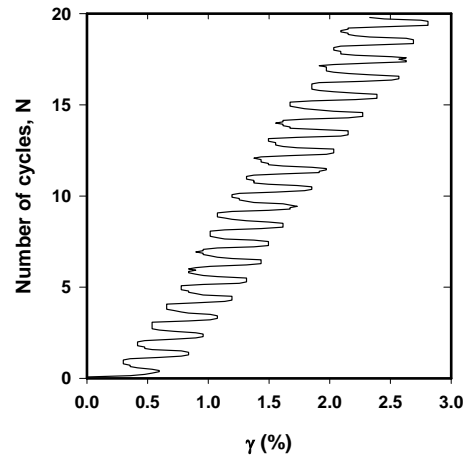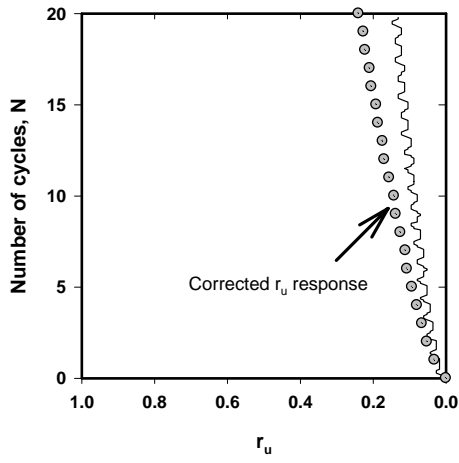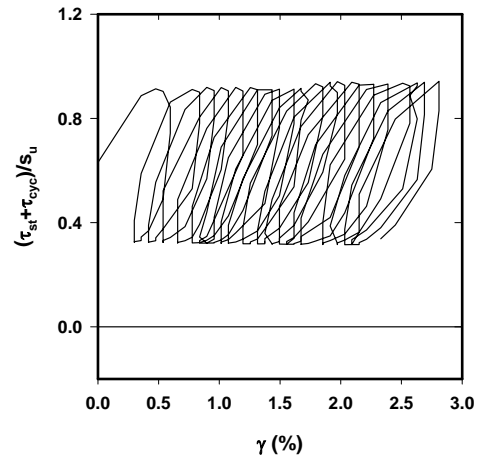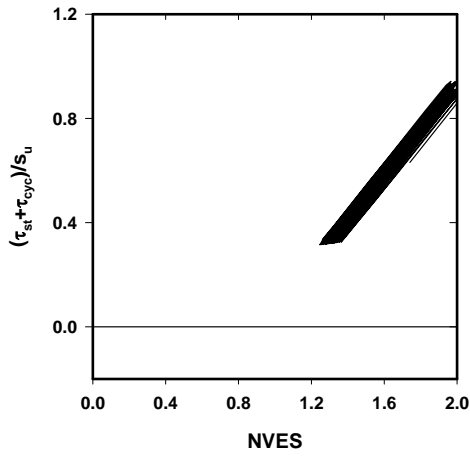
Figure C. 53. Presentation of CTXT58

260
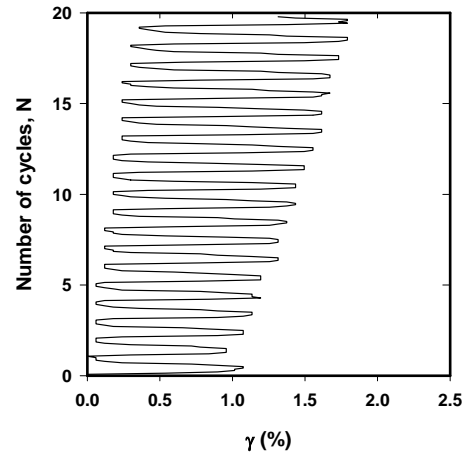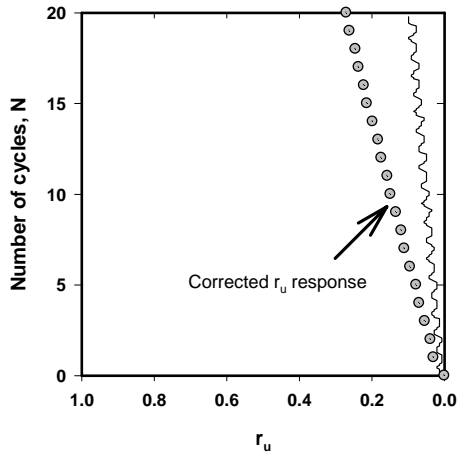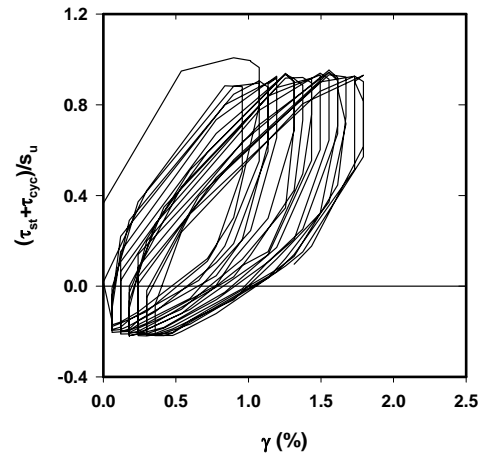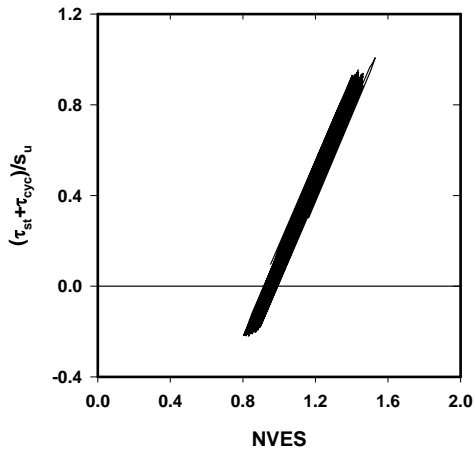
Figure C. 54. Presentation of CTXT59
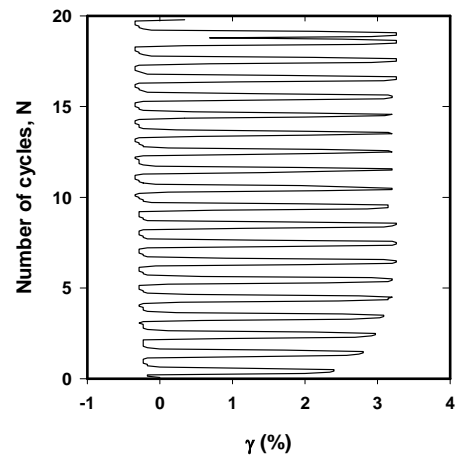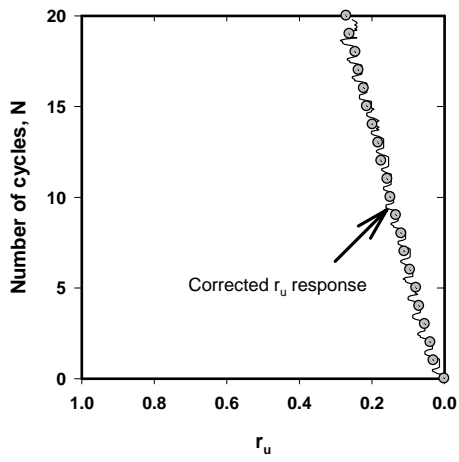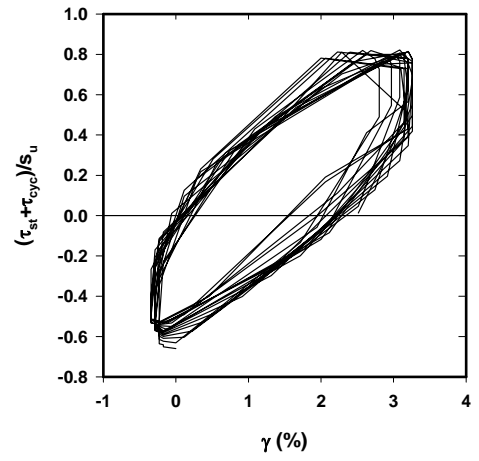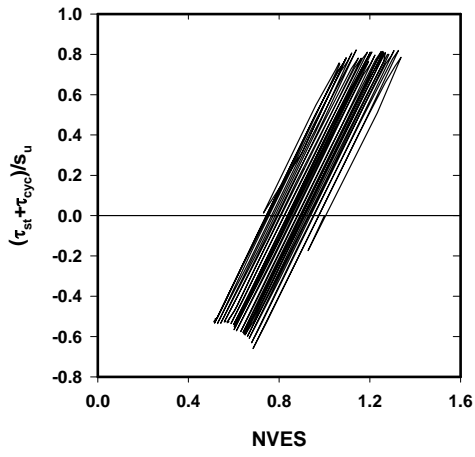
Figure C. 55. Presentation of CTXT60
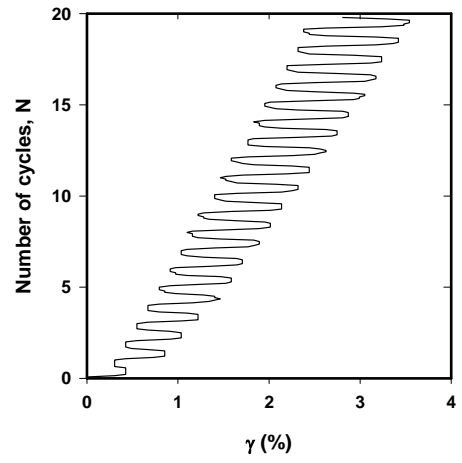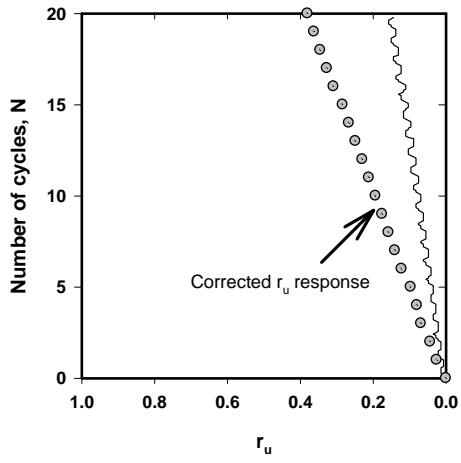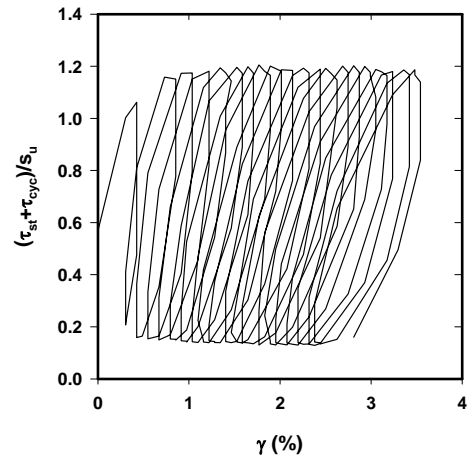
Figure C. 56. Presentation of CTXT61

Figure C. 57. Presentation of CTXT62
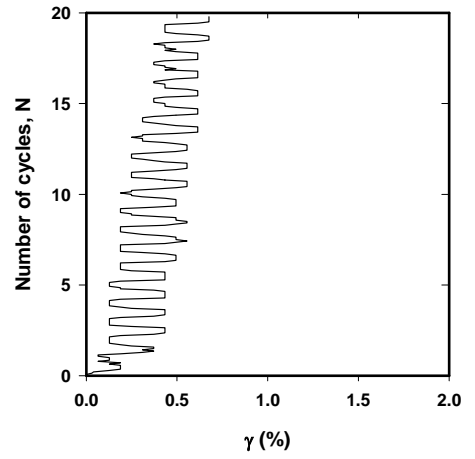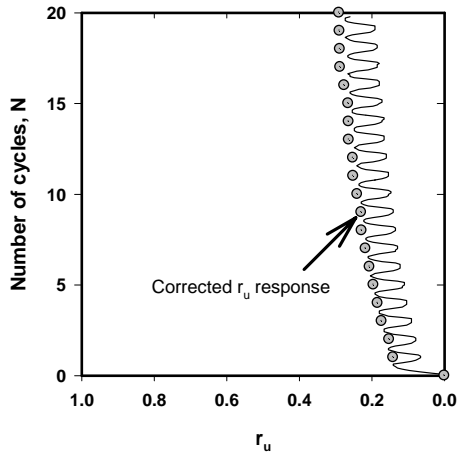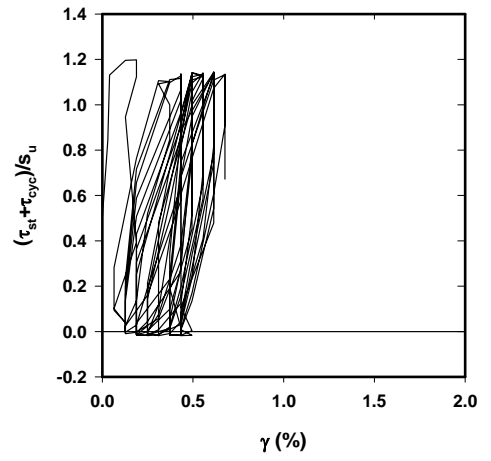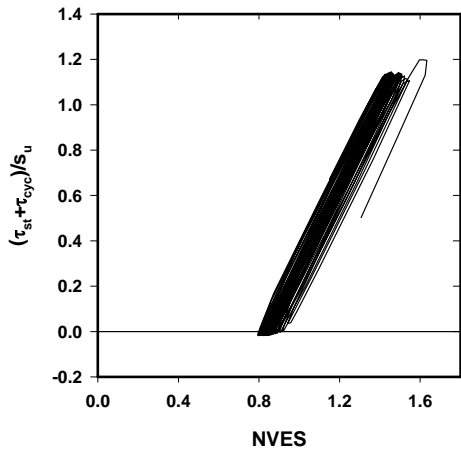
Figure C. 58. Presentation of CTXT63

265

Figure C. 59. Presentation of CTXT64
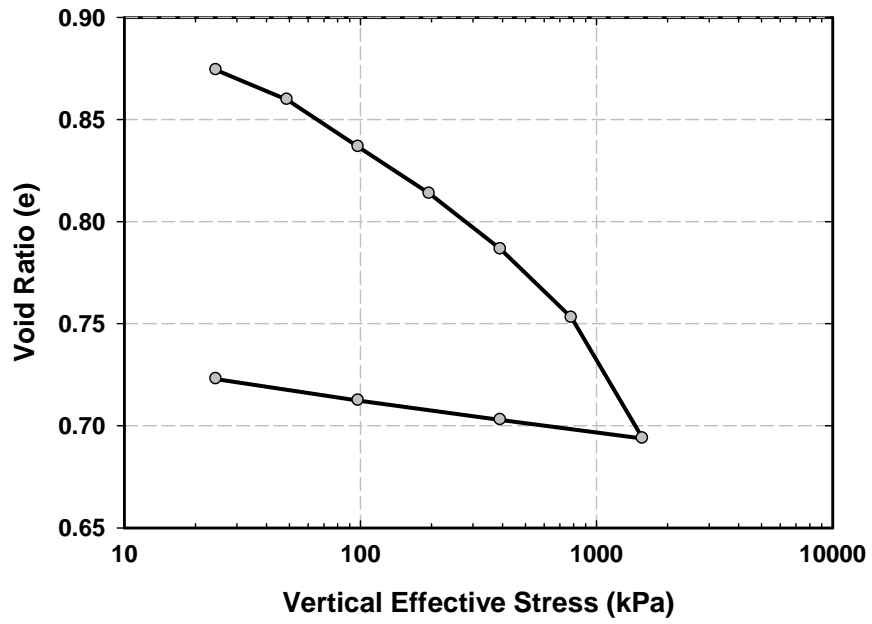
APPENDIX D

RESULTS OF OEDOMETER TESTS
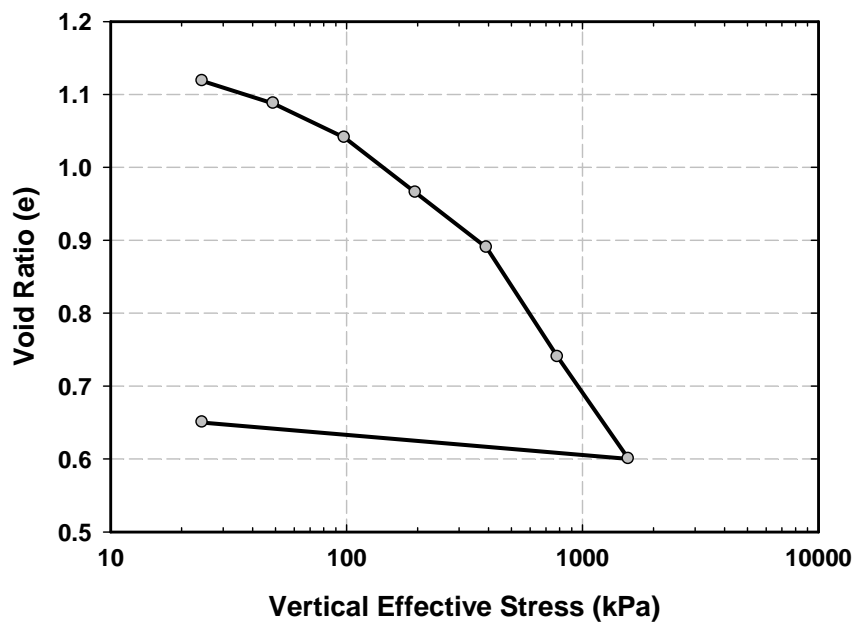
Figure D. 1. 1-D consolidation test data for sampling tube GD2-2
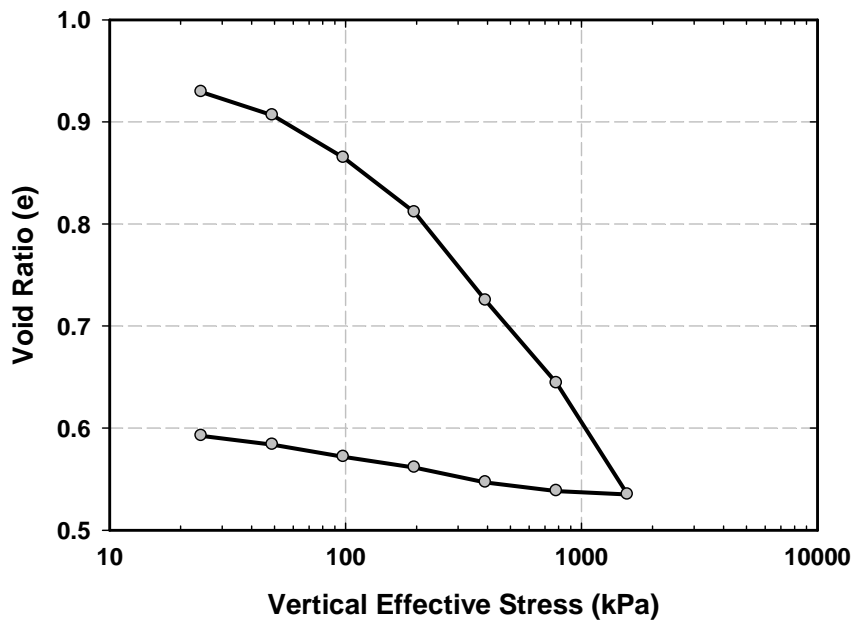**Related cyclic test: CTXT6**
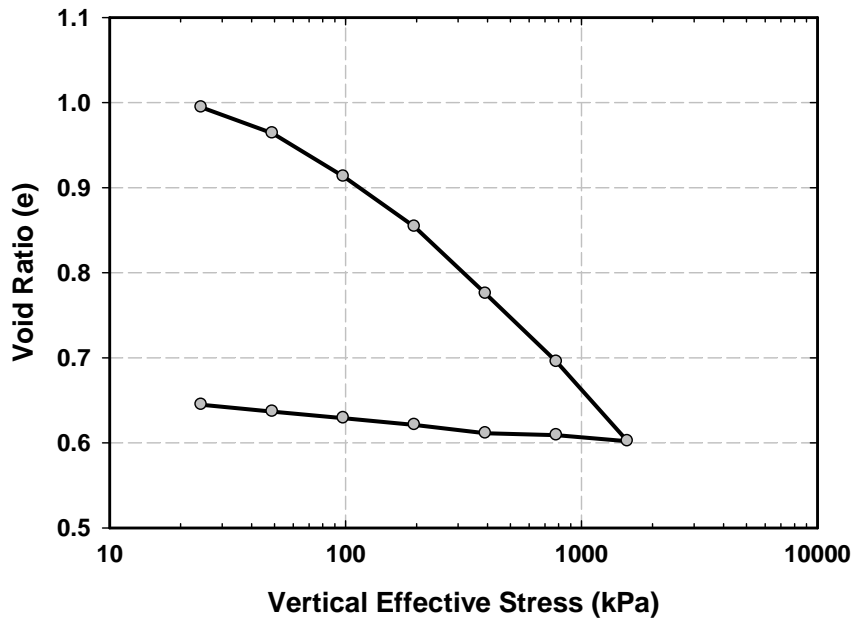
Figure D. 2. 1-D consolidation test data for sampling tube GB1-5
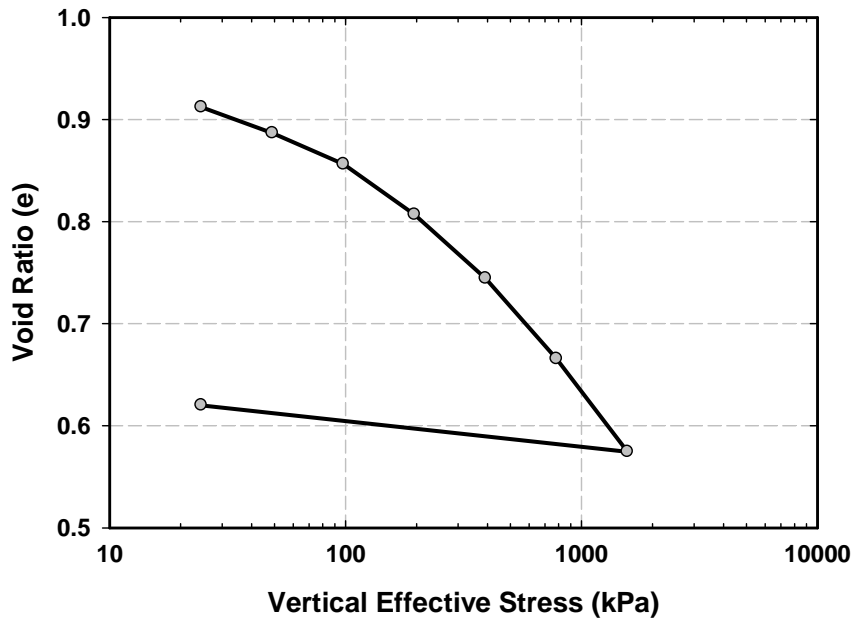**Related cyclic test: CTXT15, CTXT16**
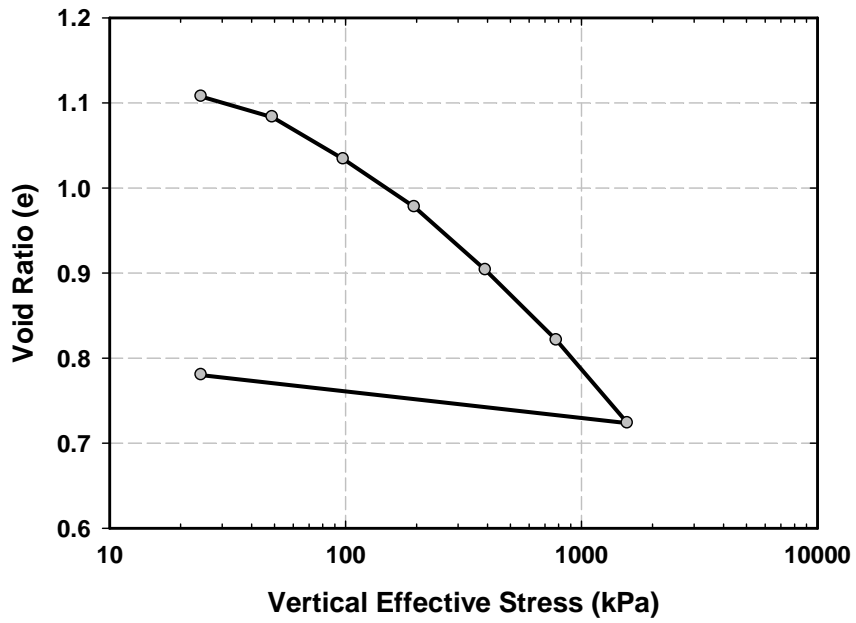
Figure D. 3. 1-D consolidation test data for sampling tube BF1-3
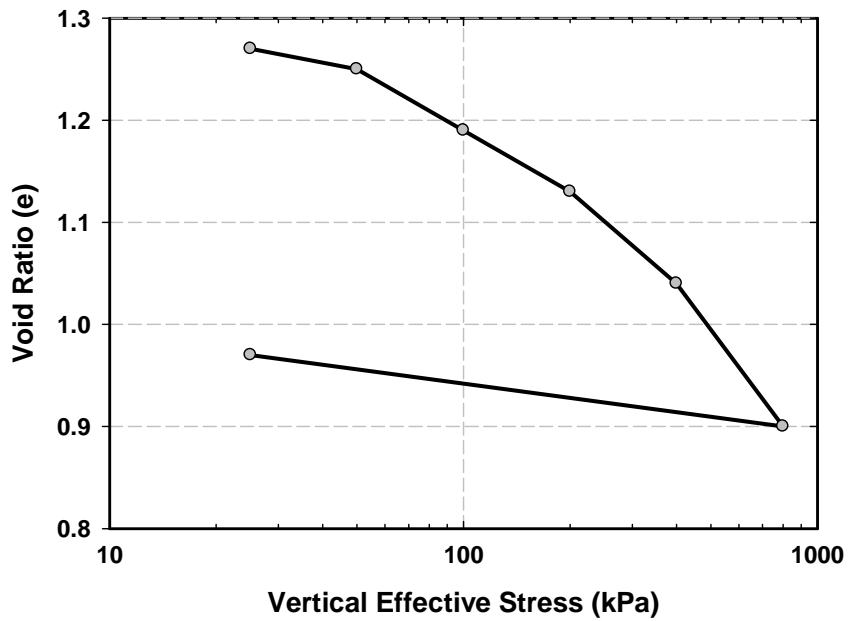**Related cyclic test: CTXT18, CTXT20**

**Figure D. 4. 1-D consolidation test data for sampling tube BH4-1
Related cyclic test: CTXT21, CTXT22**

**Figure D. 5. 1-D consolidation test data for sampling tube SK7-1
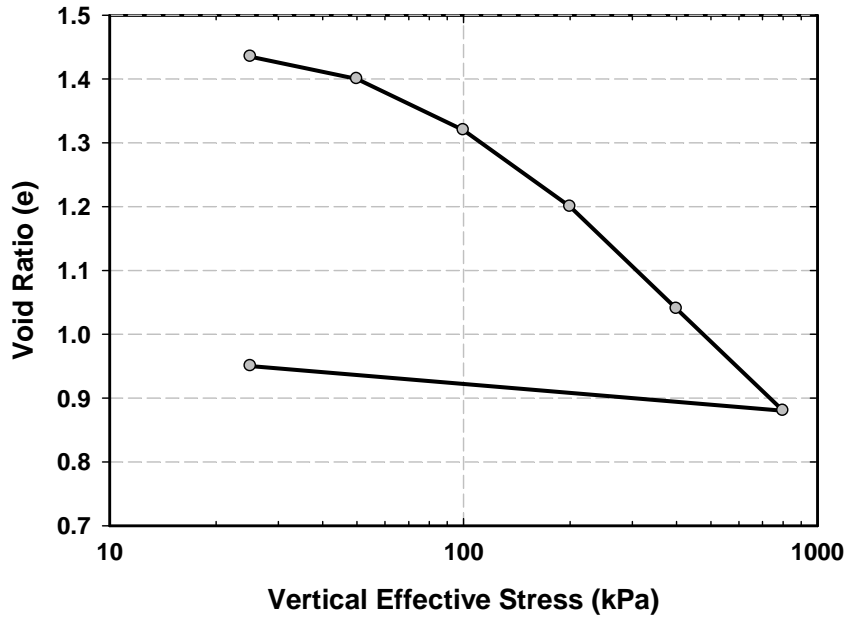Related cyclic test: CTXT25**

Figure D. 6. 1-D consolidation test data for sampling tube GA1-5
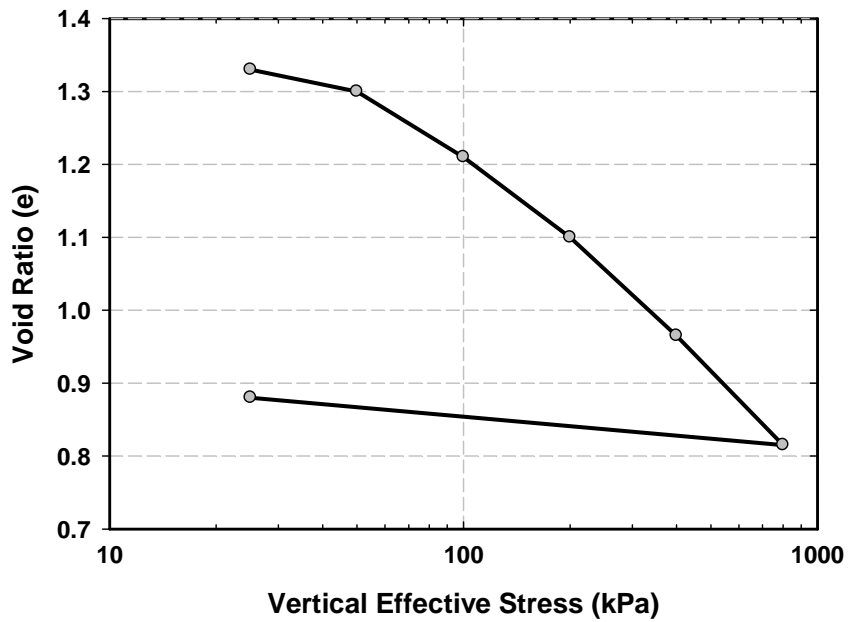**Related cyclic test: CTXT31**

Figure D. 7. 1-D consolidation test data for sampling tube BH6-3
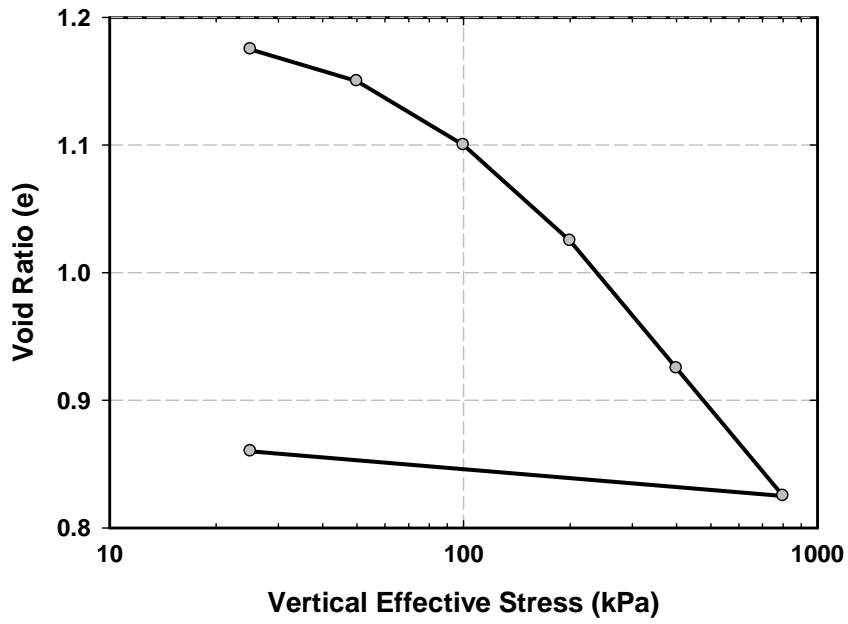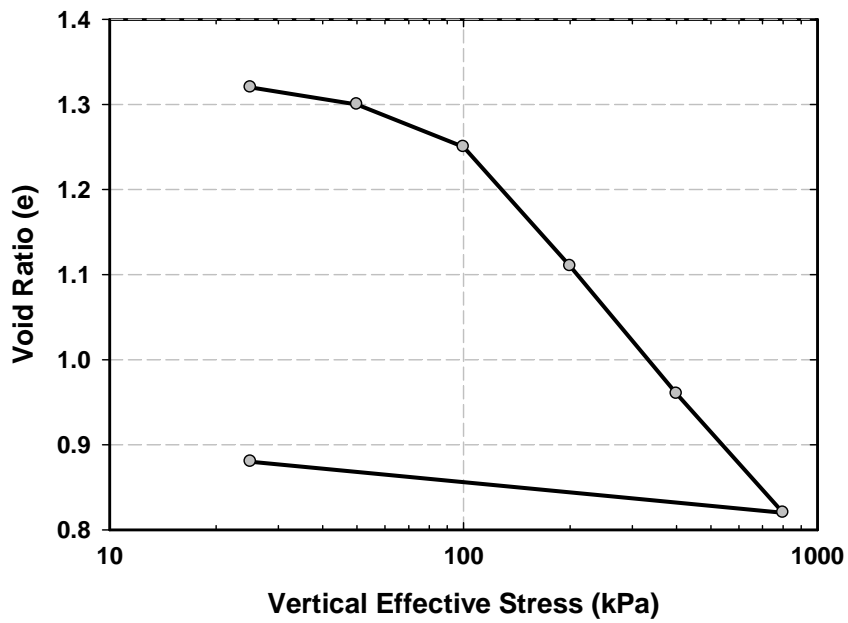**Related cyclic test: CTXT43, CTXT44, CTXT45**

Figure D. 8. 1-D consolidation test data for sampling tube BH4-3
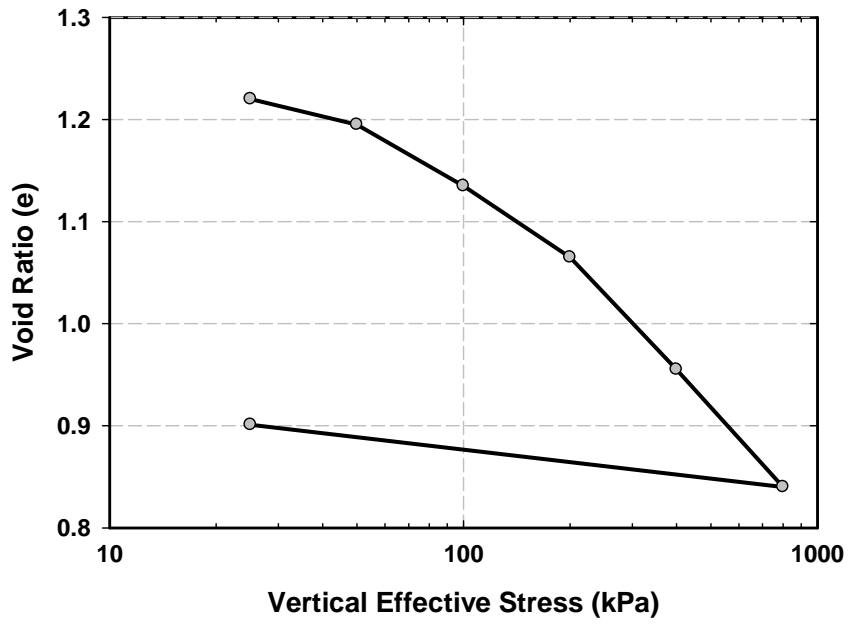**Related cyclic test: CTXT46, CTXT47, CTXT48**

Figure D. 9. 1-D consolidation test data for sampling tube BH1-5
Related cyclic test: CTXT51, CTXT52, CTXT53

**Figure D. 10. 1-D consolidation test data for sampling tube BH7-2
Related cyclic test: CTXT54, CTXT55, CTXT56**

**Figure D. 11. 1-D consolidation test data for sampling tube BH3-4
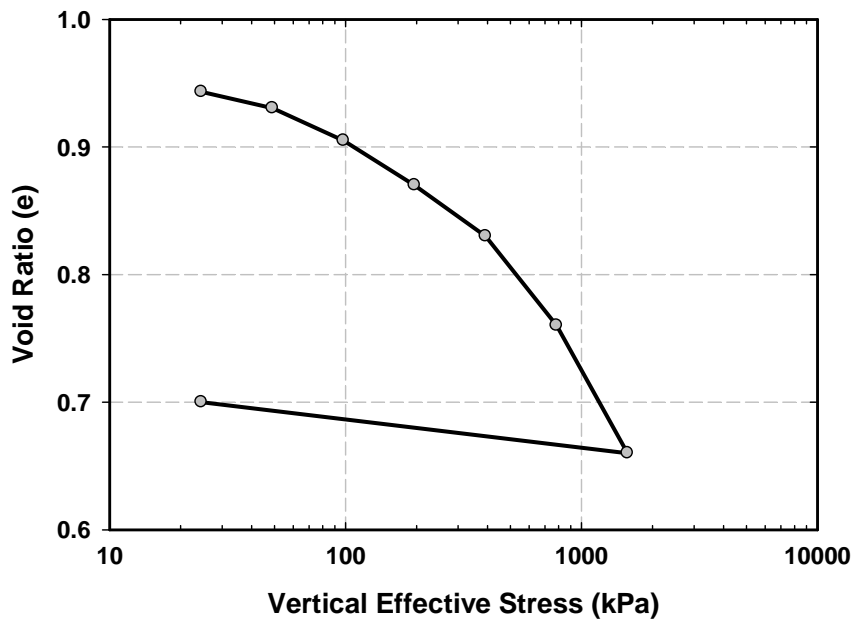Related cyclic test: CTXT58**

**Figure D. 12. 1-D consolidation test data for sampling tube BH7-4
Related cyclic test: CTXT59, CTXT60, CTXT61, CTXT62**

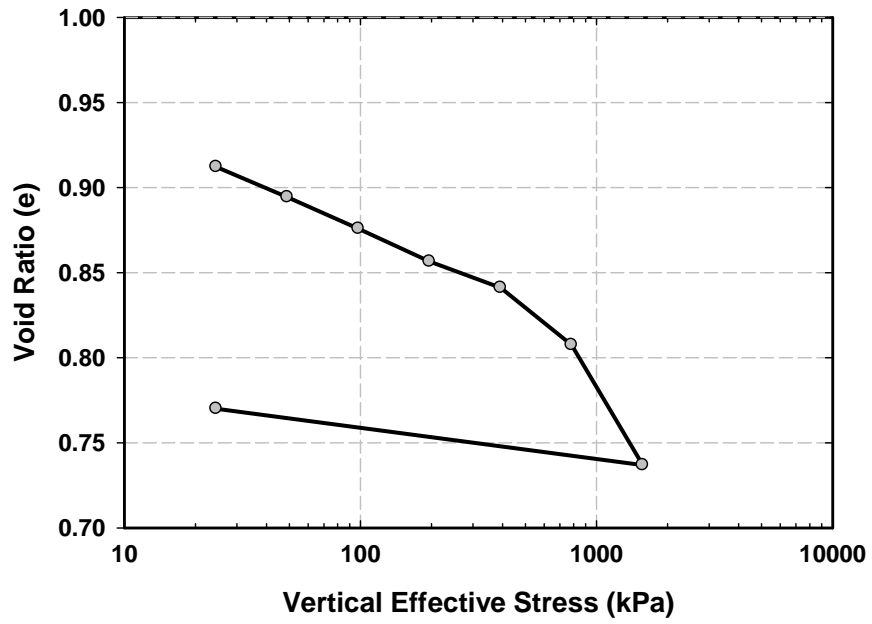**Figure D. 13. 1-D consolidation test data for sampling tube GE2-2**

273

Figure D. 14. 1-D consolidation test data for sampling tube GE3-1
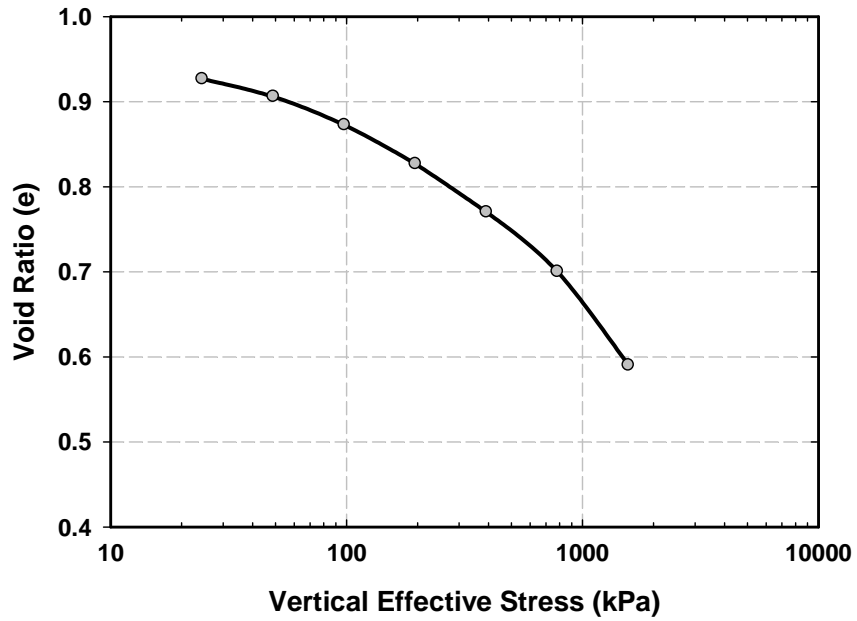

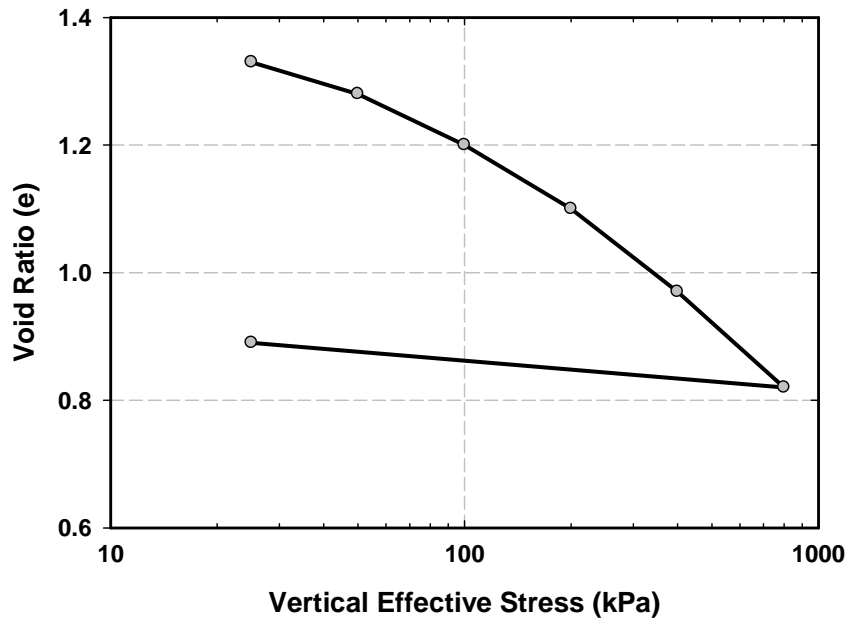**Figure D. 15. 1-D consolidation test data for sampling tube GD1-1**

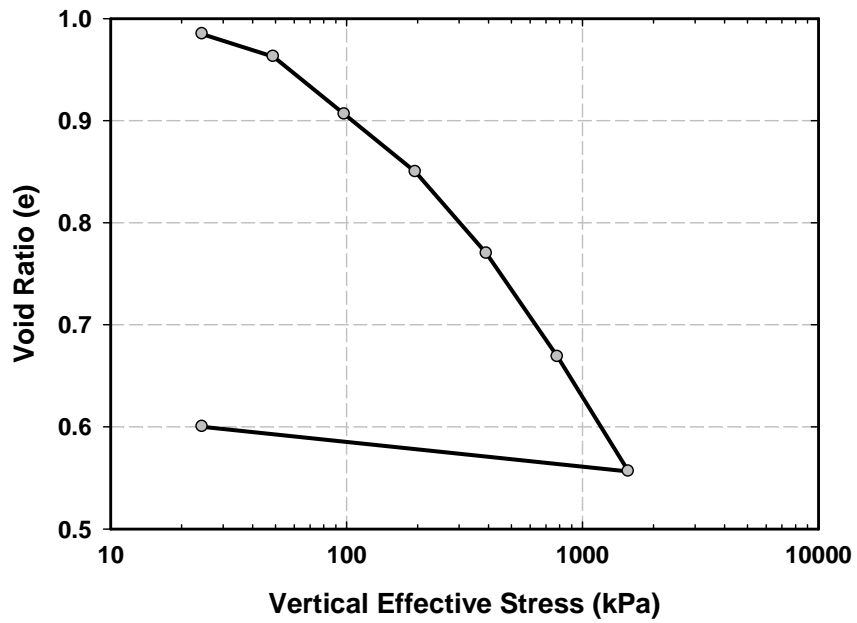**Figure D. 16. 1-D consolidation test data for sampling tube BH5-1**

Figure D. 17. 1-D consolidation test data for sampling tube V4

275

CURRICULUM VITAE

PERSONAL INFORMATION

Surname, Name	: Bilge, Habib Tolga
Nationality	: Turkish (TC)
Date and Place of Birth	: 11 December 1980, İstanbul
Marital Status	: Single
Phone	: +90 312 210 54 03
Fax	: +90 312 210 54 01
Email	: htbilge@gmail.com

EDUCATION

Degree	Institution	Year
MS	METU Civil Engineering (CGPA: 3.93/4.00)	2005
BS	METU Civil Engineering (CGPA: 3.39/4.00)	2002
High School	Alparslan High School (CGPA: 4.81/5.00)	1997

WORK EXPERIENCE

Year	Place	Enrollment
2002-Present	METU Department of Civil Engineering	Research Assistant
2006-Present	METU Department of Fine Arts and Music	Part Time Instructor
2007-2008	California Polytechnic State University, San Luis Obispo, CA	Research Associate
2000-2002	METU Department of Fine Arts and Music	Student Assistant
2001	Öztaş Construction Inc.	Intern Engineer
2000	Öztaş Construction Inc.	Intern Engineer

FOREIGN LANGUAGES

Advanced English, Intermediate French

PUBLICATIONS

1. Cetin, K. O., and Bilge, H. T. (2004). "Monitoring systems for earth fill dams" Proc. 1st National Symposium on Dams and Hydropower Plants, 351-361 (in Turkish).

2. Bilge, H. T., and Cetin, K. O. (2006). "Probabilistic models for the assessment of cyclic soil deformations" Proc. 8th U.S. National Conference on Earthquake Engineering, April 18-22, San Francisco, California, USA.

3. Bilge, H. T., and Cetin, K. O. (2007). "Field performance case histories for the assessment of cyclically-induced reconsolidation (volumetric) settlements" METU – EERC Report No. 07 – 01, Middle East Technical University Earthquake Engineering Research Center, Ankara.

4. Bilge, H. T., and Cetin, K. O. (2007). "Probabilistic models for the assessment of cyclic soil straining in fine-grained soils" 4th International Conference on Earthquake Geotechnical Engineering, 25-28 June, Thessaloniki, Greece.

5. Bilge, H. T., and Cetin, K. O. (2007). "Probabilistic models for the assessment of cyclic soil straining in fine-grained soils" 6th National Conference on Earthquake Engineering, 16- 20 October, Istanbul, Turkey (in Turkish).

6. Bilge, H. T., Yunatci, A., Unutmaz, B., Yunatci, I., and Cetin, K. O. (2007). "Liquefaction triggering under cyclic sea-wave loading" 6th National Symposium on Coastal Engineering, 25 – 28 October, Izmir, Turkey (in Turkish).

7. Bilge, H. T., and Cetin, K. O. (2008). "Probabilistic models for the assessment of cyclic soil straining in fine-grained soils" Geotechnical Earthquake Engineering and Soil Dynamics IV, 18 – 22 May, Sacramento, California, USA.

8. Cetin, K. O., Bilge, H. T., Wu, J., Kammerer, A. M., and Seed, R. B. (2008). "Probabilistic models for the assessment of cyclically-induced reconsolidation settlements" 12th National Conference of Soil Mechanics and Foundation Engineering, 16 – 17 October, Konya, Turkey.

9. Cetin, K. O., Bilge, H. T., Wu, J., Kammerer, A. M., and Seed, R. B. (2009). "Probabilistic models for cyclic straining of saturated clean sands" Journal of Geotechnical and Geoenvironmental Engineering, ASCE, 135(3), 371-386.

10. Cetin, K. O., Bilge, H. T., Wu, J., Kammerer, A. M., and Seed, R. B. (2009). "Probabilistic model for the assessment of cyclically-induced reconsolidation (volumetric) settlements" Journal of Geotechnical and Geoenvironmental Engineering, ASCE, 135(3), 387-398.

11. Unutmaz, B., Bilge, H. T., and Cetin, K. O. (2009). "Seismic response and liquefaction triggering analysis for earth embankment dams: A case study" 2nd International Conference on Long Term Behaviour of Dams, 12-13 October, Graz, Austria.

12. Bilge, H. T., and Cetin, K. O. (2009). "Cyclic large strain and induced pore pressure response of saturated clean sands" METU / GTENG 09/12-01, Middle East Technical University, Soil Mechanics and Foundation Engineering Research Center, Ankara.

13. Bilge, H. T., and Cetin, K. O. (2009). "Performance – based assessment of magnitude (duration) scaling factors" METU / GTENG 09/12-02, Middle East Technical University, Soil Mechanics and Foundation Engineering Research Center, Ankara.

14. Pehlivan, M., Bilge, H. T., and Cetin, K. O. (2010). "CPT-based evaluation of liquefaction potential for fine-grained soils" 2nd International Symposium on Cone Penetration Testing, 9-11 May, Huntington Beach, California, USA.

15. Cetin, K. O., Unutmaz B., and Bilge, H. T. (2010). "Assessment of liquefaction-induced foundation soil deformations" 5th International Conference on Recent Advances in Geotechnical Earthquake Engineering and Soil Dynamics, 24-29 May, San Diego, California, USA.

16. Cokca, E., Bilge, H. T., and Unutmaz, B. (2010). "Simulation of contaminant migration through a soil layer due to an instantaneous source" Computer Applications in Engineering Education Journal, Wiley InterScience, accepted for publication.

17. Cetin, K. O., and Bilge, H. T. "Cyclic large strain and induced pore pressure response of saturated clean sands" Journal of Geotechnical and Geoenvironmental Engineering, ASCE, submitted for publication.

18. Cetin, K. O., and Bilge, H. T. "Performance – based assessment of magnitude (duration) scaling factors" Journal of Geotechnical and Geoenvironmental Engineering, ASCE, submitted for publication.

AWARDS AND HONORS

Outstanding Research Assistant in Education Services, Middle East Technical University Civil Engineering Department and Turkish Chamber of Civil Engineers, for the academic year of 2008-2009.

Graduated with honors, Civil Engineering Department, Middle East Technical University, June 2002.

HOBBIES

Jazz, classical music, basketball, cinema.